IMPLEMENTATION AND IN-DEPTH ANALYSES OF A BATTERY-SUPERCAPACITOR POWERED ELECTRIC VEHICLE (E-KANCIL)

Manoj Embrandiri

Thesis submitted to the University of Nottingham for the Degree of Doctor of Philosophy

December 2013

ABSTRACT

This thesis contributes to the research issue pertaining to the management of multiple energy sources on-board a pure electric vehicle; particularly the energy dense traction battery and the power dense supercapacitor or ultracapacitor. This is achieved by analysing real world drive data on the interaction between lead acid battery pack and supercapacitor module connected in parallel while trying to fulfil the load demands of the vehicle.

The initial findings and performance of a prototype electric vehicle conversion of a famous Malaysian city car; the perodual kancil, is presented in this thesis. The 660 cc compact city car engine was replaced with a brushless DC motor rated at 8KW continuous and 20KW peak. The battery pack consists of eight T105 Trojan 6V, 225 Ah deep cycle lead acid battery which builds up a voltage of 48V. In addition to this, a supercapacitor module (165F, 48V) is connected in parallel using high power contactors in order to investigate the increase in performance criteria such as acceleration, range, battery life etc. which have been proven in various literatures via simulation studies. A data acquisition system is setup in order to collect real world driving data from the electric vehicle on the fly along a fixed route. Analysis of collected driving data is done using MATLAB software and comparison of performance of the electric vehicle with and without supercapacitor module is made.

Results show that with a parallel connection, battery life and health is enhanced by reduction in peak currents of up to 49%. Peak power capabilities of the entire

hybrid source increased from 9.5KW to 12.5KW. A 41% increase in range per charge was recorded. The author of this work hopes that by capitalizing on the natural peak power buffering capabilities of the supercapacitor, a cost effective energy management system can be designed in order to utilize more than 23.6% of the supercapacitor energy.

PUBLICATIONS

During the course of this research work, the following papers were accepted for publication in international conferences and journals:

1. Manoj.E, Dino Isa, Roselina Arelhi, “Supercapacitor/Battery hybrid Powered Electric Bicycle via a Smart Boost Converter” © EVS-25 Shenzhen, China, Nov. 5-9, 2010 The 25th World Battery, Hybrid and Fuel Cell Electric Vehicle Symposium & Exhibition.
2. Manoj.E, Dino Isa, Roselina Arelhi, “Performance of an Electric Vehicle Conversion at the University of Nottingham, Malaysia” presented at world conference of fuel economy and sustainable road transport, Institution of Mechanical Engineers (IMechE), Pune India.
3. Embrandiri, Manoj, Dino Isa, and Roselina Arehli. "An Electric Vehicle Conversion using Batteries and Ultracapacitors." Journal of Asian Electric Vehicles 9.2 (2011): 1521-1527.
4. Manoj.E, Dino Isa, Roselina Arelhi, “Supercapacitor/Battery hybrid Powered Electric Bicycle via a Smart Boost Converter” World Electric Vehicle Journal Vol. 4 - ISSN 2032-6653 - © 2010 WEVA page 280.

ACKNOWLEDGEMENTS

I would like to express my sincere gratitude to Prof. Dino Isa, firstly for giving me this opportunity and secondly for his constant support, guidance and friendship throughout the course of this research work. It has come a long way.

Special thanks to my dad, mom and sisters for their much needed moral and financial support over the years. Thank you for believing in me. To the Indrans, thank you for being my family in Malaysia. The amount of support I have received from you guys over the years is overwhelming and definitely not quantifiable. To my fellow PhD colleagues Ahmida and Zhen Wei, we have had some good laughs over the years. I wish you all the best in the future.

The equipment that was used to carry out this research work was funded by a research grant e-Science from the ministry of science Malaysia (MOSTI) and the facilities at the University of Nottingham Malaysia campus. Several aspects of this project would not have been achieved without inputs from people like Mr. K. Parthipan and Mr. Joseph Koh etc.

Finally and most importantly, you, yes you; Shanu Indran, the love of my life, thank you for tolerating me and for being there through thick and thin.

TABLE OF CONTENTS

LIST OF FIGURES

CHAPTER 2

CHAPTER 3

CHAPTER 4

LIST OF TABLES

CHAPTER 1: INTRODUCTION

1.1 INTRODUCTION TO THE THESIS

This thesis is dedicated to the research, modelling and eventual implementation of a battery-supercapacitor hybrid energy source in order to power an electric vehicle. This is in recognition of the assertion that the electric vehicle will be a significant stakeholder in future transportation systems.

A growing concern in today's world is environmental protection and energy conservation. Automotive manufacturers are developing alternatives to existing fossil fuel-driven vehicles. This has paved way for the development of Electric Vehicles (EV) and Hybrid Electric Vehicles (HEV). While HEVs tend to reduce the emissions from internal combustion vehicles as a result of greater fuel efficiency, they do not completely solve the problem. Electric vehicles on the other hand are much more energy efficient, produce absolutely no tail pipe emissions and requires less maintenance as compared to the conventional internal combustion engine (ICE) vehicles [2]. However, the reason the automotive industry has not gone pure electric or able to compete favourably with existing gasoline cars, lies in the inherent problem of existing battery technologies. Even with ICE energy conversion efficiency figures of below 20%, the energy density (Joules/kg) of petroleum far surpasses the energy density of any known battery technology [2]. Batteries are the weak link in EVs at the moment [6]. The lack of a single reasonably priced energy storage device that can simultaneously provide high power density and high energy

density for EVs has been the main stumbling block to the acceptance of EVs as the main form of private and public transportation.

Presently the only viable solution to this problem is to combine a high energy storage device such as an electrochemical battery or fuel cell with a high power device such as an Electric Double Layer Capacitor (EDLC) or ultracapacitor or more often called a supercapacitor [8]. In this work, we investigate the effect of integrating the supercapacitor with the main power source (deep cycle lead acid batteries) of an EV conversion. More so, at the University of Nottingham Malaysia Campus, we have a supercapacitor pilot production plant which is dedicated to the research and development of home grown supercapacitors and extensive materials research. Concerted efforts have been made by the research group to investigate the viable areas of application of supercapacitors such as consumer electronics, mobile phones, solar and of course, the electric vehicle. The latter forms the basis and also the genesis of the electric vehicle adventure at the University of Nottingham Malaysia.

1.2 RESEARCH ISSUES ADDRESSED BY THIS WORK

The aim of this project is to address key issues that prevent electric vehicles from being widely accepted and adopted by public and private transportation system. Some of the research issues which may be regarded as problem statements are as follows:

- The low power density of EV batteries. In order for the EV to approach, or try to approach, the performance of its conventional counterpart (ICE), the battery or energy storage system should have similar or equivalent power density as the ICE. The limitation of energy storage devices (batteries) to deliver energy at high power rates during acceleration and also accept energy during regenerative braking schemes. This is not to say that high power density batteries do not exist, but at what cost and complexity for practical use in a consumer electric vehicle.
- Due to the haphazard nature of the load profile of an EV (traffic condition, driver behaviour, etc), the battery suffers from inherent random high discharge and charge (regenerative braking) rates as well. This is detrimental to the shelf life of the battery
- This led to the hybridization of batteries with supercapacitors as it becomes impractical and cost ineffective to size a single energy storage system (battery) for peak power demands several times higher than the mean power demand. However, effective control strategies are still being developed and redeveloped for energy management in a battery-supercapacitor vehicle using various methods ranging from heuristics to

artificial neural networks to various learning algorithms. This power and energy management poses as the most challenging task as it is to be done without compromising the vehicles target performance.

- The forecasting/prediction of driving load condition in advance is key to efficient energy management systems for electric vehicles. An energy management system for electric vehicles with multiple energy sources based on the prediction of driving conditions or by analysing drive cycles.

1.3 RESEARCH OBJECTIVES

Based on the research issues highlighted above, the objectives of this research work include the following:

- To design and implement a small electric vehicle which will be solely powered by a combination of deep cycle lead acid batteries and a supercapacitor module. This will serve as a foundation for future research work on electric vehicles at the university.
- To design and implement an onboard data acquisition system to monitor and log critical data from the electric vehicle.
- To provide first hand insight into the interaction between lead acid battery pack and supercapacitor module connected in parallel. This is achieved by analysing novel real world drive data obtained by driving the vehicle in the university's premises.
- To investigate and justify the reported increase in battery life, range per charge and vehicle acceleration by augmenting the battery pack with a supercapacitor module. This is also achieved using real world drive data and results.

1.4 RESEARCH SCOPE

When the initial research objectives for this project were conceived, the main aim was to identify and propose an intelligent energy management system for electric vehicles powered by a battery and supercapacitor combination. Emphasis was on the optimum management of power and energy flow of multiple energy sources in order to meet the demand of the vehicle's propulsion as well as its requirement for accessory loads. However, being the pioneer of the EV research team within the research division, we had to create a solid platform or basis on which testing, research and development can be carried out.

Due to inherent cost constraints, an ideal Hardware-In-the-Loop, (HIL) based EV test bench could not be implemented. An experimental test vehicle would be constructed; basically a conversion from a conventional ICE to electric. It would be fitted with state of the art data acquisition system which monitors the interaction between the energy and power sources as it tries to fulfil the load requirements of the vehicle. In this case, the load on the propulsion system comes from 100% real world driving. The only downside envisaged from this setup is the inability to replicate the exact same driving pattern over a fixed route.

Experimental data obtained from this work is limited to the fixed driving route within the university campus. Also the driving style of the driver could not be controlled. However, the same driver was used in all experiments. Starting form a pure battery driven vehicle, the energy system was then augmented with the addition of a supercapacitor bank. Apart from manufacturer's information, there is very limited experimental data on supercapacitor field testing. As such, the vehicle

provided a means to obtain unbiased empirical data to substantiate research claims and also to serve as a test platform for further work.

1.5 THESIS CONTRIBUTION

This dissertation contributes to the emerging field of pure electric vehicles that are powered by hybrid energy sources. This is achieved by providing first hand insight into the interaction between lead acid battery pack and supercapacitor module connected in parallel which is used to power a compact city car. Real world driving data along with instantaneous voltages and currents from the energy sources provide a novel and unique approach to obtaining unbiased empirical data to substantiate research claims and also to serve as a test platform for further work.

The problems or challenges with having hybrid energy sources on-board a purely electric vehicle rests heavily on the successful management of these sources in order to meet the propulsion demand of the vehicle. As opposed to the general consensus of designing and implementing complex control systems, this work takes the basic parallel connection between battery and supercapacitor and investigates the reported increase in battery life, range per charge and vehicle acceleration. This is done with the hope that by analysing the natural power split between these two devices in parallel, a practical, cost effective energy management system can be developed in the future. Optimistically, several novel ideas will emerge from the collaborative efforts of many small but progressive research contributions such as this one.

1.6 THESIS ORGANIZATION

Chapter 2: Background and Literature Review – This chapter provides a brief background on electric vehicles in terms of basic configurations, advantages and disadvantages and also the hybrid vehicle configurations as well as related battery chemistries. The basic structure and characteristics of the supercapacitor is tabled out as well as its inherent pros and cons. A thorough literature review is presented on multiple/hybrid energy sources for powering electric/hybrid vehicles with particular emphasis on supercapacitors.

Chapter 3: Methodology – This chapter is divided into two parts. The first part describes the equations governing the movement of an electric vehicle on a level or inclined road surface. Using these equations, various software models were developed in MATLAB Simulink © environment in order to simulate the performance of the proposed experimental test electric vehicle conversion. The second part describes the step by step design and construction of the experimental test vehicle. Also, the traction and control wiring, sensor setup, data acquisition system, on-board real time display of circuit parameters were laid out in detail.

Chapter 4: Results and Discussion – The results of the hardware implementation of the battery supercapacitor combination are described and analysed. First hand insight into the interaction between lead acid battery pack and supercapacitor module connected in parallel was provided. Investigation and justification of the reported increase in battery life, range per charge and vehicle acceleration by augmenting the battery pack with a supercapacitor module was done.

Chapter 5: Conclusion and future work – Conclusion is presented here where major accomplishments and research objectives achieved are summarised. The possibilities for future work and improvements to be carried out will also be discussed.

CHAPTER 2: BACKGROUND AND LITERATURE REVIEW

This chapter begins by providing a brief background on electric vehicles in terms of basic configurations, advantages and disadvantages and also the hybrid vehicle configurations. It proceeds to describe various battery chemistries that are used in today's electric vehicle and also the technical jargon associated with battery technologies. An important term called state of charge (SOC) of a battery is described as well as some methods to calculate it.

A huge portion of this research is dedicated towards investigating a certain device's use or relevance in the ever growing electric/hybrid vehicle industry; the supercapacitor or ultracapacitor or electric-double-layer capacitor (EDLC). The basic structure and characteristics of the supercapacitor is tabled out as well as its inherent pros and cons. One feature which sticks out is its high power density which is very complimentary to present day battery technologies.

A thorough literature review is presented on multiple/hybrid energy sources for powering electric/hybrid vehicles with particular emphasis on supercapacitors. The challenges faced by various researchers in this field are outlined which are associated with energy management of the multiple energy and power sources. Various combination algorithms have been proposed and results shown ranging from fuzzy logic, neural networks, genetic algorithms to support vector machines.

Finally, the support vector machine (SVM) which has been identified as one of the leading classifiers in machine learning is described.

2.1 BACKGROUND

2.1.1 Electric Vehicles

Electric vehicles (EV) are propelled by an electric motor (or motors) powered by a stack of rechargeable batteries. In EV's, the internal combustion engine (ICE) is replaced by an electric motor which gets its power from a controller circuit.

The first EVs of the 18th century used non-rechargeable batteries and by the end of the 19th century, mass production of rechargeable batteries made EV's fairly common[1]. At the start of the 20th century, EV's seemed to be a strong contender for future road transport as ICE vehicles were at the time unreliable, extremely pollutive, and needed to be cranked manually to start.

Hope for EV was dashed when in the early 1900's, cheap oil was widely available and a self starter for ICE's was developed. IC engines proved a more attractive option for powering vehicles and rechargeable batteries were ironically adopted for starting ICE's [2].

Despite the above problems, electric vehicles always found its use in delivery vans, warehouse vehicles and golf carts etc. [2]. Environmental issues may well be the deciding factor in the adoption of EVs for town and highway uses coupled with the fact that tremendous technological developments have taken place in vehicle design, improvement to rechargeable batteries, motors and controllers. It is evident that electric vehicles have come to stay this time around.

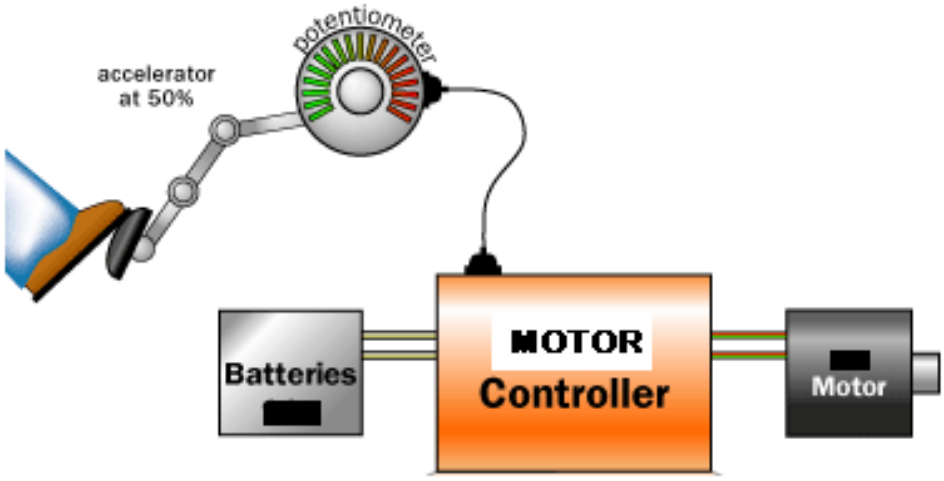

FIG 1: The Basic Electric Vehicle Configuration (Source: HowStuffWorks[79])

Figure 1 represents the basic principle of operation of an electric vehicle. The accelerator pedal is connected to a potentiometer which determines how much power the controller must deliver to the motor. The electric motor can be either ac or dc type.

A dc motor and controller system tends to be simpler and less expensive to install. They can also be overdriven i.e. accept up to ten times its rated power for a few seconds. This is useful for providing short bursts of acceleration. However the motor is bound to heat up [3].

On the other hand ac systems allow for the use of any industrial 240V three phase motor which is readily available. Also, regenerative braking is possible as ac motors can be turned into generators to recover braking energy. It is without doubt that ac controllers are more complicated due to the fact that dc has to be converted to three phase ac using inverters.

Advantages over ICEs

I. They are more energy efficient; more than 50% of the chemical energy in a battery is converted to electrical energy which is used to power the wheels whereas only around 20% of the energy in petrol/diesel is converted to electrical energy
II. Since no combustion takes place, there are no tail pipe emissions
III. Electricity is a domestic source of energy; thus EVs can be recharged easily and conveniently.
IV. Quiet smooth operation and requires less maintenance as compared to ICE counterpart

The downside of EVs is usually battery related. Batteries are the weak link in EVs at the moment.

I. The driving range is much less ; the battery needs to be recharged more often
II. Usually recharge time for the batteries is too long (4-8 hours).
III. Battery packs are expensive and need to be replaced more number of times
IV. Battery packs are heavy, heavy and take up a lot of space.

Researchers all over the world are working on improved battery technologies to make up for the disadvantages mentioned above. The results of this research will go a long way in determining whether EVs are fully adopted in the future.

Electric cars are mechanically much simpler than both gasoline cars and fuel-cell cars. There is no motor oil, no filters, no spark plugs, and no oxygen sensors. The motor has one moving part, there is no clutch, and the transmission is much

simpler. Due to regenerative braking, even the friction brakes will encounter little wear. The only service that a well-designed electric car will need for the first 100,000 miles is tire service and inspection [3].

Until an electric car manufacturer achieves high enough sales to approach a gasoline car manufacturer's volume efficiencies, electric cars will need to compete on other grounds besides price. Aside from the obvious emissions advantage, there is another way that an electric car can vastly outperform a gasoline car – in a word, torque. A gasoline engine has very little torque at low rpm's and only delivers reasonable horsepower in a narrow rpm range. On the other hand, an electric motor has high torque at zero rpm, and delivers almost constant torque up to about 6,000 rpm, and continues to deliver high power beyond 13,500 rpm. This means that a performance electric car can be very quick without any transmission or clutch, and the performance of the car is available to a driver without special driving skills [3].

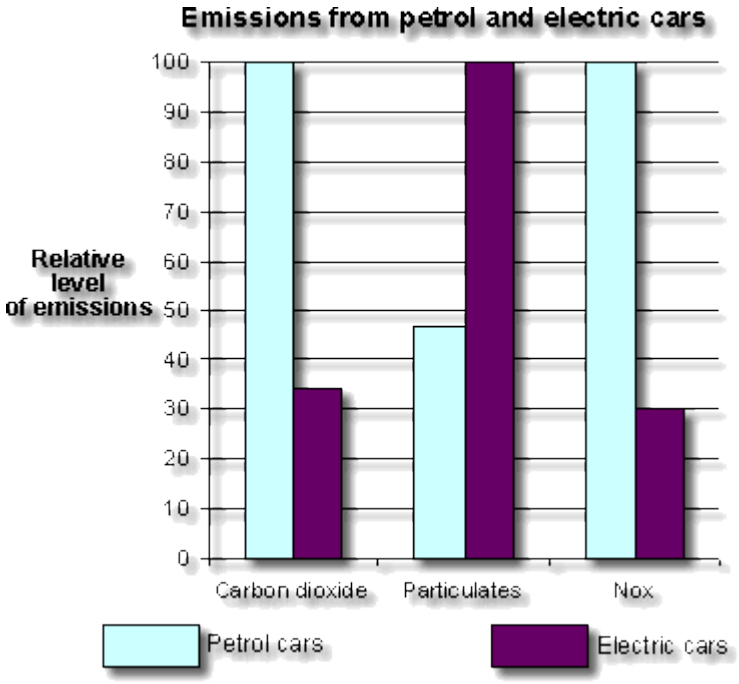

Fig 2: Emissions: EV vs. ICE (Source: Sustainability-ed.org.uk [80])

The graph in the figure 2 compares the emissions from petrol cars and electric cars using electricity generated in conventional power stations. Overall, there are fewer emissions from electric cars. This could help to reduce global warming and also improve the air quality in our cities. According to the U.S. Environmental Protection Agency (EPA), vehicle emissions currently contribute between one third and one half of the total U.S. atmospheric burden of three major pollutants: carbon monoxide (CO), nitrogen oxides (NOx), and hydrocarbons (HC) [4]. Their impact is even greater in many U.S. urban areas. This comparison does not include emissions from ICEs due to lack of maintenance. One school of thought argues that even though EVs do not produce tailpipe emissions, the electricity which is used to charge them comes from a power plant that burns fuel. Many researchers have studied this problem, and the general conclusion is that, including the power plant emissions, the electric vehicle is much less polluting. How much cleaner it is, depends on what energy source the power plant uses, coal being the dirtiest. But if you can transform the grid to run from a renewable source, then we may have something exciting to talk about. However, we're not there yet.

Although this report is focused on the pure electric vehicle or sometimes called battery electric vehicle (BEV), it was mandatory to study about HEV's which a trade-off between EV's and ICE engines. Also a lot of research literature has been published on energy management strategies for HEV's which could be applicable to multiple energy sources on board an electric vehicle.

2.1.2 HEV drive configuration

HEV's capability of reducing fuel consumption and emissions while maintaining the same high performance as conventional vehicles lies in a key factor. This factor is being able to operate the ICE under near optimal conditions [5].

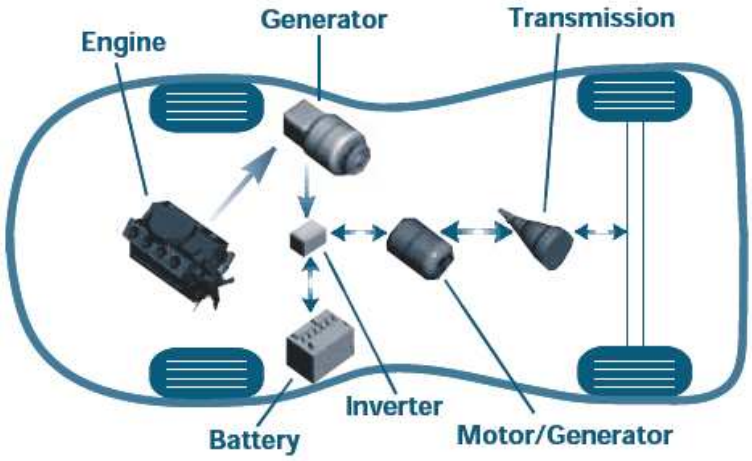

Fig. 3: Series Hybrid Drive (Adapted from US DoE Office of Transport [5])

Series Hybrid Drive

The internal combustion engine drives an alternator to generate electricity that drives the traction motor (wheels) directly or it can be stored in a battery. The traction motor can be supplied solely from the battery (zero emissions mode), from the engine or from a combination of both. In the event that the battery discharges below a certain level, the engine turns on and recharges the battery. It should be noted that the internal combustion engine is not mechanically connected to the wheels thus less dependent on the vehicles changing power demands. In this drive configuration, the ICE can operate at optimum conditions but the efficiency of the electrical system suffers due to series connected components.

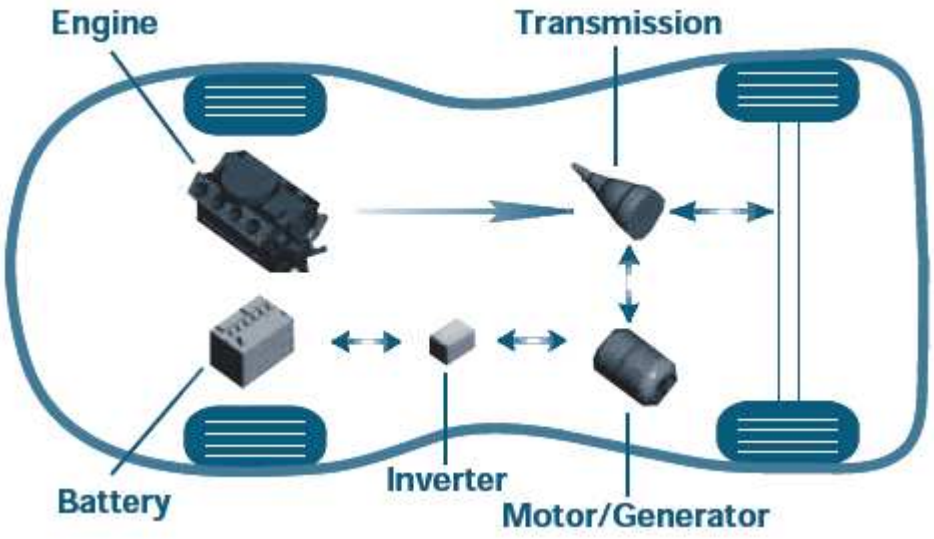

Fig.4: Parallel Hybrid Drive (Adapted from US DoE office of Transport [5])

Parallel Hybrid Drive

In parallel hybrid drive configuration, both the internal combustion engine and the electric motor are mechanically connected to the transmission system i.e. the wheels. A parallel HEV typically has two power paths; either the ICE or the electric motor or both can be used to provide the power to turn the wheels. A computer controls the electric motor depending on the power needs of the vehicle. For example, the electric system may be used for short trips while for longer trips the ICE would provide the vehicle's main power with the electric system supporting in periods of sudden acceleration or other peak power demands. A drawback however is that the ICE load is more dependent on the actual driving situation.

Combined Switched Hybrid drive

The combined switched drive allows for a purely series or parallel drive by the activation of the clutch. When driving at low speeds i.e. within the city, the series regime can be used and the ICE operated at optimum condition. For inter-city driving which requires higher output from the ICE, the parallel regime can be employed.

Power Splitting Systems

Propulsions with electric power splitting are based on ICE power splitting into two parts. One part is converted in electric power in generator, which supplies traction motor mechanically connected to drive wheels and remaining part is transmitted by electromagnetic forces in the air gap to the wheels mechanically without losses in electric machines. The splitting device can be realized mechanically by planetary gear or electrically by a special electric generator.

Although HEVs are by now an industrial standard in the automotive industry experiencing an exponential growth, they will be no further discussion on them in this report. The sole focus will instead be on pure electric vehicles (no IC engine at all), which consists of the use of more than one type of electrical energy storage device. Fuel cell vehicles (FCV) and the related problems of hydrogen production and storage, although recognized as being an extremely interesting technology, are also beyond the scope of this thesis. However, it is pointed out that most of the concepts related to hybridization discussed in the following will readily apply to fuel cell vehicles, since in virtually every implementation the slow dynamics of the fuel

cell require the use of some kind of additional power source, like a battery or a supercapacitor bank.

2.1.3 Battery Technologies for the Electric Vehicle

Technological advances in the automotive industry have led to the demand for more power in today's automobile. This has heaped a lot of pressure on battery manufacturers to produce batteries which can meet the demands of power hungry applications (anti-lock braking system, air conditioning, power steering, etc.) as well as improve fuel efficiency.

The classic electric vehicle has only one energy storage unit; the battery. It is usually that component with the highest cost, weight and volume. Likewise, in hybrid vehicles the battery must continually supply or store electrical energy. The battery is of utmost importance; the key and enabling technology to the electric vehicle revolution. The basic requirements for a battery used in electric vehicles are as follows:

(i) Low cost: the ultimate aim of the automotive industry

(ii) Lowest possible weight to reduce load on drive train

(iii) High cycle-life: ideally to last the lifetime of the vehicle, practically for a reasonably long period of time.

(iv) High-energy density can be attained with one charge to provide a long range or mileage

(v) High power delivery and fast recharge capability: this is a very desirable requirement as batteries could be fully recharged in 5-10mins; the time

it takes to refill a gas tank. Also, energy saving schemes such as regenerative braking can be easily incorporated. Energy can be captured, stored and delivered as soon as required.

(vi) Safety is also a big concern in terms of overcharging, over heating etc.

(vii) Wide acceptance as a recyclable battery from the environmental standpoint

At the present time, the battery types being considered and developed for electric vehicles are relatively few, namely lead-acid, nickel metal hydride, lithium-ion and lithium polymer, and sodium nickel metal chloride (ZEBRA). Each of these battery types has some advantages and disadvantages and unfortunately none of them are attractive in all respects for electric vehicles. The main parameters that specify the behaviour and performance of a battery are given in the following section:

Some Common Battery Parameters

Ampere-hour Capacity: This parameter, measured in coulombs (C) but usually expressed in Ampere-hour (Ah) capacity, is the total charge that can be discharged from a fully charged battery under specified conditions. The rated Ah capacity is for a new battery under the conditions predefined by the manufacturer. Watt-hour (Wh) or kWh is also used to represent battery capacity.

$$\text{Rated Wh Capacity} = \text{Rated Ah Capacity} \times \text{Rated Battery Voltage}$$

For example, a 48V 225 Ah pack will have a rate capacity of 10.8 Kwh.

C-rate: The charge and discharge of a battery is measured in C-rate. The nominal C-rate is used to represent a charge or discharge rate equal to the capacity of a

battery in one hour i.e. 1C. Most portable batteries, with the exception of the lead acid, are rated at 1C. A 6V, 225Ah Trojan T105 lead acid battery is rated for 20hour discharge i.e. C20 or C/20 or 0.05C. This means that if the battery were to be discharged over a period of 20hours, then a current draw of 11.25A is approximately expected.

Specific Energy (W/kg): This is the nominal battery energy per unit mass; a characteristic of the battery chemistry and packaging. Along with the energy consumption of the vehicle, it determines the battery weight required to achieve a given electric range.

Specific Power (W/kg): This is the maximum power per unit mass which is available. It determines the battery weight required to achieve a given performance target.

Internal Resistance: Internal resistance is the overall equivalent resistance within the battery. It is different for charging and discharging and may vary as the operating condition changes. As internal resistance increases, the battery efficiency decreases and thermal stability is reduced as more of the charging energy is converted into heat.

State of Charge (SOC): It is a dimensionless parameter defined as the remaining capacity of a battery and it is affected by its operating conditions such as load current and temperature. For battery electric vehicles, it is synonymous to the fuel gauge in a conventional vehicle [6]. There are several methods of estimating the SOC of a battery such as voltage method, specific gravity, coulomb counting or current integration, impedance spectroscopy and newer methods like quantum magnetism. The SOC in simple terms is defined as:

$$\mathrm{SOC} = \frac{Remaining\ Capacity}{Rated\ Capacity}$$

SOC is a critical condition parameter for battery or energy management. Accurate gauging of SOC is very challenging, but the key to the healthy and safe operation of batteries. In the sections to come, various techniques from literature have been proposed on estimating this parameter. SOC is generally calculated using current integration to determine the change in battery capacity over time as described in the equation below:

$$\Delta\mathrm{SOC} = \mathrm{SOC(t)} - \mathrm{SOC}(t_0) = \frac{1}{Ah\ Capacity}\int_{t0}^{t} i(\tau)d\tau$$

Depth of Discharge (DOD): DOD is used to indicate the percentage of the total battery capacity that has been discharged. For deep-cycle batteries, they can be discharged to 80% or higher of DOD. Typically, it is desired that the DOD of a battery is kept within appropriate safe limits as specified by the manufacturers.

$$\mathrm{DOD} = 1 - \mathrm{SOC}$$

State of Health (SOH): This gives an indication of the battery's present condition in terms of its present energy capacity as compared to the rated energy capacity when it was new [7].SOH is an important parameter for indicating the degree of performance degradation of a battery and for estimating the battery remaining lifetime.

$$\mathrm{SOH} = \frac{Aged\ Energy\ Capacity}{Rated\ Energy\ Capacity}$$

Cycle Life (number of cycles): Cycle life is the number of discharge–charge cycles the battery can handle at a specific DOD (normally 80%) before it fails to meet specific performance criteria.

Battery Management System (BMS).: It is a network of sensors, controller, communication, and computation hardware with software algorithms designed to decide the maximum charge/discharge current and duration from the estimation of SOC and SOH of the battery pack.

A summary of the main battery technologies used in electric vehicles available today are as follows [8]:

Lead-acid

I. Lead as negative electrode, lead oxide as positive electrode and dilute sulphuric acid as electrolyte or in more advanced forms as gels
II. Ruggedness, low cost, inherent safety, and temperature tolerance
III. It is a mature technology
IV. It reached the mass production stage a very long time ago
V. The valve regulated lead-acid (VRLA) battery is maintenance-free and has good cyclability even at deep discharge; two types absorbed glass mat (AGM) based and gel based batteries
VI. Limited depth of discharge DOD
VII. Limited life cycle when deep discharged
VIII. Low specific energy and power due to heavy lead collectors
IX. Not environmentally friendly to dispose

Ni-MH (Nickel-Metal Hydride)

I. Nickel Hydroxide as positive electrode, alloy as a negative electrode and an alkaline solution as electrolyte
II. Most currently available hybrid electric vehicles use this chemistry as energy storage system
III. High volumetric energy and power as this technology has experienced great advances in the past 15yrs
IV. Safe operation at high voltages
V. Environmentally friendly and recyclable
VI. Longer cycle life when compared to lead acid as it has a reasonable tolerance over abusive overcharge and discharge
VII. Wider Operating temperature due to better thermal properties
VIII. The cost is a huge problem as the high price of the raw material, mainly nickel, will not come down in mass production

Nickel Zinc (NiZn)

I. Anode is Zinc, cathode is from Nickel and electrolyte is an alkaline solution
II. Specific energy and power greater than lead acid chemistry
III. NiZn batteries do not use mercury, lead, or cadmium, or metal hydrides that are difficult to recycle. Both nickel and zinc are commonly occurring elements in nature, and can be fully recycled.
IV. suffer from poor lifetime due to the fast growth of dendrites

Nickel Cadmium (NiCd)

I. Nickel oxide as positive electrode (cathode), cadmium compound as negative electrode (anode) and potassium hydroxide as electrolyte

II. Where energy density is important, Ni–Cd batteries are now at a disadvantage compared with nickel–metal hydride and lithium-ion batteries
III. Smaller and lighter than lead acid equivalents
IV. Can endure high discharge rates without any significant loss of capacity or damage
V. High cost of cadmium and nickel
VI. Cadmium is an environmental hazard, and it is highly toxic to all higher forms of life hence requires special care during disposal

Lithium Ion Batteries; Next Generation of Electric Vehicles

Lithium is the lightest of all metals, has the greatest electrochemical potential and provides the largest energy density for weight. In 1991, the Sony Corporation commercialized the first lithium-ion battery. Lithium-ion batteries are incredibly popular these days. You can find them in laptops, PDAs, cell phones and iPods [9].

Lithium-ion is a low maintenance battery, an advantage that most other chemistries cannot claim. There is no memory effect and no scheduled cycling is required to prolong the battery's life. In addition, the self-discharge is less than half compared to nickel-cadmium, making lithium-ion well suited for modern fuel gauge applications. Lithium-ion cells cause little harm when disposed [10].

Despite its overall advantages, lithium-ion has its drawbacks. It is fragile and requires a protection circuit to maintain safe operation. Built into each pack, the protection circuit limits the peak voltage of each cell during charge and prevents the cell voltage from dropping too low on discharge. This is because a total discharge of the Li-ion battery can irreversible as it may not be able to be recharged anymore.

Thus what will happen if a vehicle with a Li-ion battery pack is unused for say one month?

In addition, the cell temperature is monitored to prevent temperature extremes. Li-on does not fare well in very cold climates. Below zero temperature seriously impairs its battery capacity, or ability to provide its full discharge capacity at lower temperatures. Aging is a concern with most lithium-ion batteries and many manufacturers remain silent about this issue. Some capacity deterioration is noticeable after one year, whether the battery is in use or not. It should be noted that other chemistries also have age-related degenerative effects. Manufacturers are constantly improving lithium-ion. New and enhanced chemical combinations are introduced every six months or so. With such rapid progress, it is difficult to assess how well the revised battery will age.

Lithium Iron Phosphate (LiFePO4) is proving to be a breakthrough for EV batteries. Based upon lithium ion technology, LiFePO4 batteries offer many advantages over lithium cobalt dioxide (LiCoO2) batteries which are commonly used in laptops, mp3 players and cell phones. In EVs, LiFePO4 batteries offer greater range, power and safety. They provide full power until they are completely discharged, and recharge in just 2.5 hours. LiFePO4 chemistry is also environmentally friendly — it's the least toxic of all the battery types. Lithium Nickel Manganese Cobalt Oxide technology is the preferred candidate for EVs [11], as it provides an excellent trade-off between specific energy and power, cost, performance, life span and cost.

The figure 5 below shows the energy densities in Wh/kg of various battery technologies.

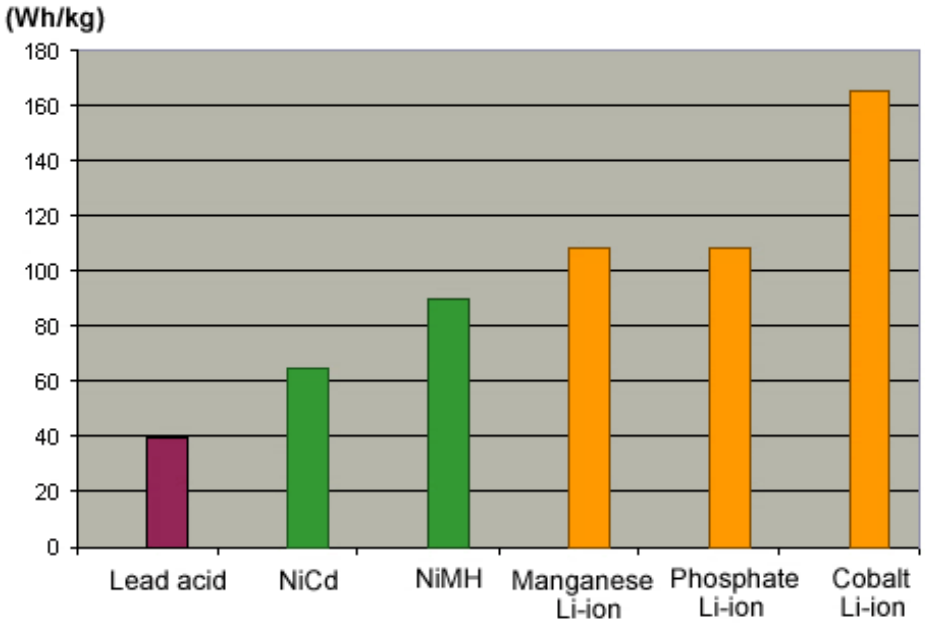

Fig. 5: A Comparison of Energy densities of various batteries (Source: Battery University [81])

2.1.4 Supercapacitors/ Ultracapacitors/ Electric Double Layered Capacitors (EDLC)

As the name implies, a supercapacitor/ultracapacitor/EDLC (names used interchangeably) is a capacitor with capacitance greater than any other, usually in excess of up to 4000 Farad. They possess a greater specific energy density (Wh/kg) than conventional electrolytic capacitors and a higher specific power density (W/kg) than most battery technologies. Supercapacitors do not have a traditional dielectric material like ceramic, polymer films or aluminum oxide to separate the electrodes instead a physical barrier made of activated carbon [12]. A double electric field which is generated when charged, acts as a dielectric. The surface area of the activated carbon is large thus allowing for the absorption of large amount of ions [13]. Figure 3 below is the basic structure of a supercapacitor.

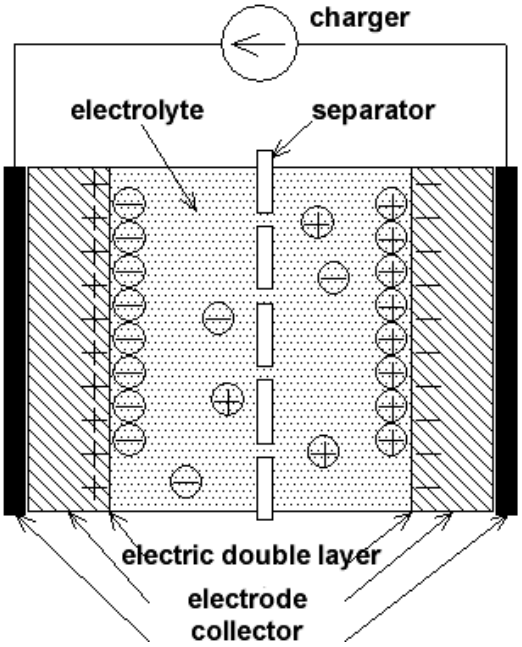

Fig 6: Electric Double Layer Capacitor Structure (Source: EAMEX Capacitor [82])

Activated carbon is impregnated with electrolyte. Positive and negative charges are formed between the electrodes and the impregnate. The magnitude of voltage where charges begin to flow is where the electrolyte begins to break down. This is called the decomposition voltage. Supercapacitors have a low energy density of less than 15Wh/kg but a very high power density of up to 4000W/kg and capacitance values of thousands of Farads are possible [14].

As with conventional capacitors, the capacitance (C) of a supercapacitor is simply the ratio of the stored charge (Q) to the applied voltage (V). Also C is directly proportional to the surface area A of each electrode and inversely proportional to the distance D between the electrodes. This is described in the equation below:

$$C = \epsilon_o \varepsilon_r \frac{A}{D}$$

ϵ_o is the dielectric constant of free space and ϵ_r is the dielectric constant of the insulating material between the electrodes or the electrically non permeable separator. They are constants which depend on the type of material being used. Since the surface area of the activated carbon electrodes is very high; 1000-2300 m^2/g, as compared to the distance between them; 10 Angstroms or less, the capacitance can be potentially very high [15]. Their voltage ratings are typically low (2.5V to avoid electrolysis of the electrolyte) thus they are combined in modules/banks (series connection) to handle higher voltages.

The energy, E stored in a supercapacitor is directly proportional to its capacitance:

$$E = \frac{1}{2} C V^2$$

The greatest factor in determining the supercapacitor performance is the energy lost through internal resistance, represented by an ESR (equivalent series resistance). Thus reducing ESR increases the power density [16].

Variations in individual cell resistance and capacitance result in uneven voltage distribution in a bank causing destruction of the cell. A circuitry which is able to spread the available charge evenly between the capacitors is necessary for a supercapacitor bank. This is called a voltage balancing or equalization circuit. There are two reasons for an imbalance of voltages in a serial string of supercapacitors: (i) deviations from the nominal capacitance of the capacitors and (ii) deviations in self discharge performance i.e. deviations in the leakage current.

Advantages of Supercapacitors

I. Cell voltage determined by the circuit application not limited by cell chemistry
II. Very high cell voltages possible
III. High power density
IV. Can withstand extreme temperatures
V. Simple charging methods
VI. Very fast charge and discharge
VII. Long life cycle
VIII. Low impedance

Disadvantages/Shortcomings

I. Linear discharge voltage characteristic prevents use in some applications
II. Power only available for very short duration (short bursts of power)
III. Low capacity
IV. Low energy density
V. Voltage balancing required when banking
VI. High self discharge rate

The EDLC stores charges in a different way as compared to the conventional electrolytic capacitor [17]. Thus traditional models are inadequate to describe the EDLC although the basic equations for capacitors still apply. The double layers formed on the activated carbon surfaces of a supercapacitor can be modeled as a series of parallel RC circuits as shown in the figure below.

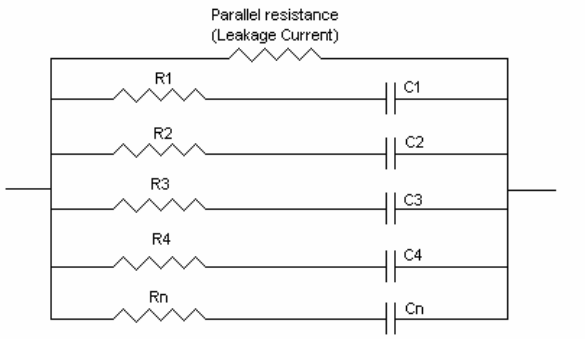

Fig 7: Electric Double Layer Modeled as Series of Parallel RC Circuits

Where R1, R2, R3 … Rn represent the series resistance and C1, C2..., Cn are the electrostatic capacitances of the activated carbons. When voltage is applied, current flows through each of the RC circuits.

Figure 8 below represents the first order model of the supercapacitor which comprises of four ideal circuit elements: a capacitance C, a series resistor Rs, a parallel resistor Rp, and a series inductor L. Rs is called the equivalent series resistance (ESR) and contributes to energy loss during capacitor charging and discharging i.e. current flow. Rp simulates energy loss due to capacitor self-discharge, and is often referred to as the leakage current resistance. Inductor L results primarily from the physical construction of the capacitor and is usually small.

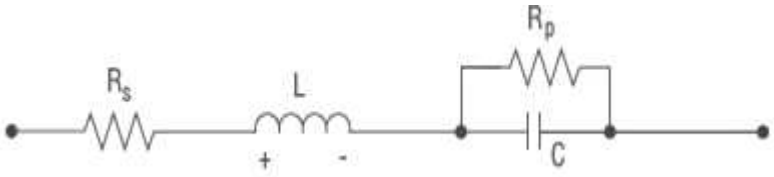

Fig 8: 1st Order Model of the Supercapacitor

In actuality, Supercapacitors exhibit a non-ideal behaviour due to the porous material used to form the electrodes that cause the resistance and capacitance to

be distributed such that the electrical response mimics transmission line behaviour. This is shown in the figure below.

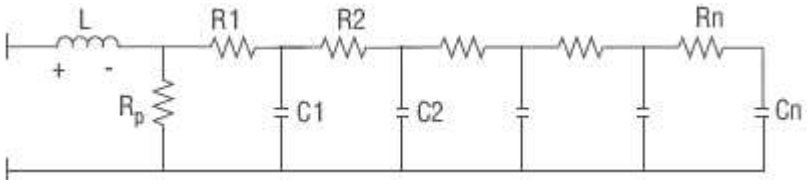

Fig 9: Non Ideal (transmission line) Model of the Supercapacitor

The most common supercapacitor applications are memory backup and standby power. In some special applications, the supercapacitor can be used as a direct replacement of the electrochemical battery. Additional uses are filtering and smoothing of pulsed load currents [18]. A supercapacitor can, for example, improve the current handling of a battery. During low load current, the battery charges the supercapacitor. The stored energy then kicks in when a high load current is requested [19]. This enhances the battery's performance, prolongs the runtime and even extends the longevity of the battery. The shortcomings of a supercapacitor may render them unsuitable as the primary source of power in an EV or HEV. However their unique features make them ideal for temporary energy storage such as storing energy via regenerative braking and also for providing a booster charge in response to sudden power demands in vehicles [20]. Thus the idea of combining the high power density features of a supercapacitor with the existing high energy density of a battery is very promising and thus a subject of intense research nowadays.

The best way to compare the capabilities of the storage devices mentioned above is by a Ragone chart. The values of energy density (in Wh/kg) are plotted versus power density (in W/kg). Both axes are logarithmic, which allows comparing performance of very different devices (for example extremely high, and extremely low power). From the chart below, it will be observed that the batteries are in the region of high energy density, low power density and longer discharge time while the ultracapacitor is in the region of high power density, low energy density and very fast discharge time. It should be noted that the diagonal lines across the chart represents discharge time.

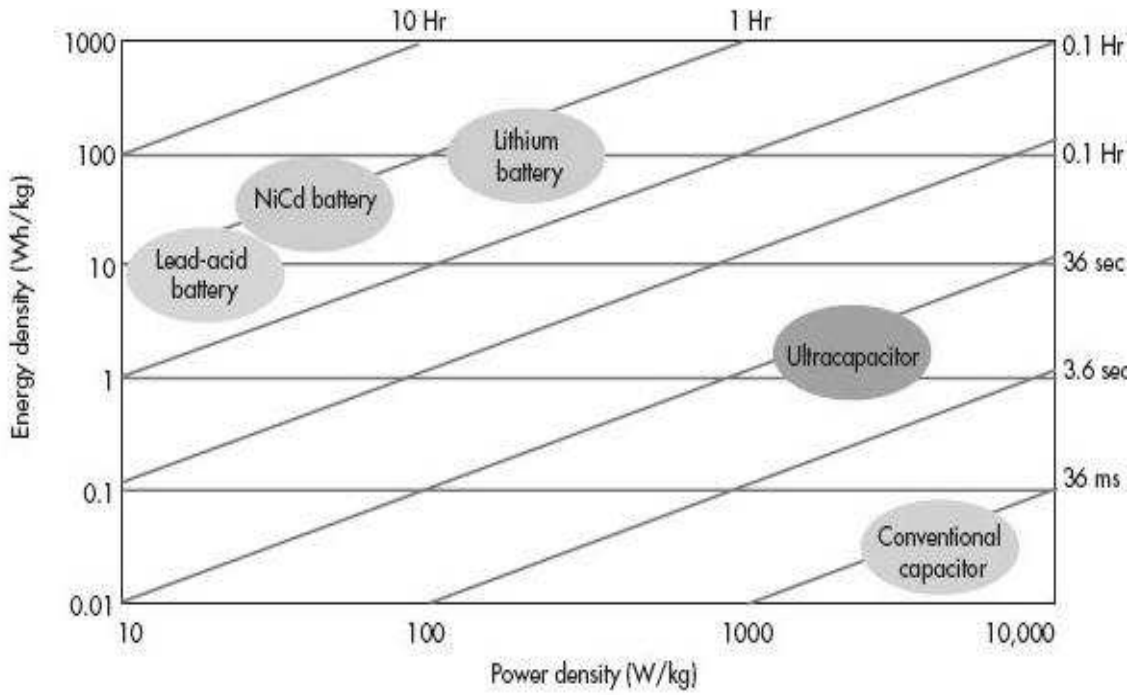

Fig 10: A Ragone Chart (Source: Don Tuite [83])

Chemistry	Nom. Voltage (V)	Energy Density (Wh/kg)	Power Density (W/kg)	Cycle life
Lead-acid	**2**	**30-40**	**180**	**≤800**
Ni-Cd	**1.2**	**~50**	**150**	**≤500**
Ni-Mh	**1.2**	**55-80**	**400-1200**	**≤1000**
Li-Phosphate	**3.2~3.3**	**80-125**	**1300-3500**	**≤2500**
Li-ion	**3.6**	**80-170**	**800-2000**	**≤1500**
Li-Manganese	**3.7**	**110-130**		**≤2000**
Li-polymer	**3.7**	**130-200**	**1000-2800**	**≤1500**
Supercapacitor	**2.5 or 2.7**	**5-10**	**4000-10,000**	**≥1,000,000**

Table 1: Specific battery figures in comparison with supercapacitor figures (Sources: [21]-[28]).

The table above clearly shows the disparity between batteries (all chemistries) and the supercapacitor. Batteries have an energy density varying from 30-200 Wh/kg while the supercapacitor has only 5% of that energy density. On the other hand, the power density of the supercapacitor is 4 to 10 times greater than that of any known battery chemistry to date. Also it can boast of 500 times more calendar life than its battery counterparts. Researchers have typically classified batteries and supercapacitors as electrochemical devices. However operating principles of both these devices are different which make their characteristics highly different. It becomes very obvious that a synergy between these two devices (battery and supercapacitor) will bring about an overall increase in efficiency and power delivery. It should be noted that this hybrid combination is not limited to electric or hybrid vehicles as it can be substituted for any conventional energy storage system which has a fluctuating load profile. However the aim of this research work is to be centred around battery electric vehicles only.

2.2 STATE-OF-THE-ART ON HYBRID/MULTIPLE ENERGY STORAGE SYSTEMS FOR ELECTRIC VEHICLES

Usually when two or more energy sources are involved in a hybrid energy storage system for an electric vehicle, these sources can be distinguished by their energy storage and power delivery capacities respectively. For a pure electric vehicle, sources with high energy density would be considered as the main energy source such as battery packs and fuel cells. As such, they can solely power a vehicle from point A to point B even though the efficiency figures could be low. To boost these figures to a reasonable level, an auxiliary energy source synonymous with high power density or delivery is usually utilized. Popular choices for this source include high power batteries and supercapacitors. It should be noted that a vehicle may not be able to run solely on this auxiliary source albeit for a few kilometres only. Due to today's requirement of maximum regenerative braking energy recapture, power batteries being a chemical energy conversion process are not as dynamic enough for this purpose. Supercapacitors on the other hand remain the only viable alternative for a powerful yet dynamic auxiliary source which is able to compliment the already stable main energy source. This provided a good motivation for this research work which aims to integrate and analyse the effects of supercapacitors as peak power buffer system for electric vehicles.

Engineers generally address peak power needs by designing the primary energy source to the size needed to satisfy peak demands, even if those demands occur for only a few seconds. Sizing an entire system for peak power needs, rather than for the average power requirement may prove costly and inefficient. Such systems can

be significantly improved by storing electrical energy from a primary energy source such as a battery in a secondary energy storage device, and then delivering that energy in controlled high power bursts when required. Such high power delivery provides electrical systems with dynamic power range to meet peak power demands for periods of time ranging from fractions of a second to several minutes. Batteries are not designed to provide bursts of power over many hundreds of thousands of cycles. Supercapacitors perfectly meet this requirement. The general scope of an energy management system for multiple sources is described in the figure below.

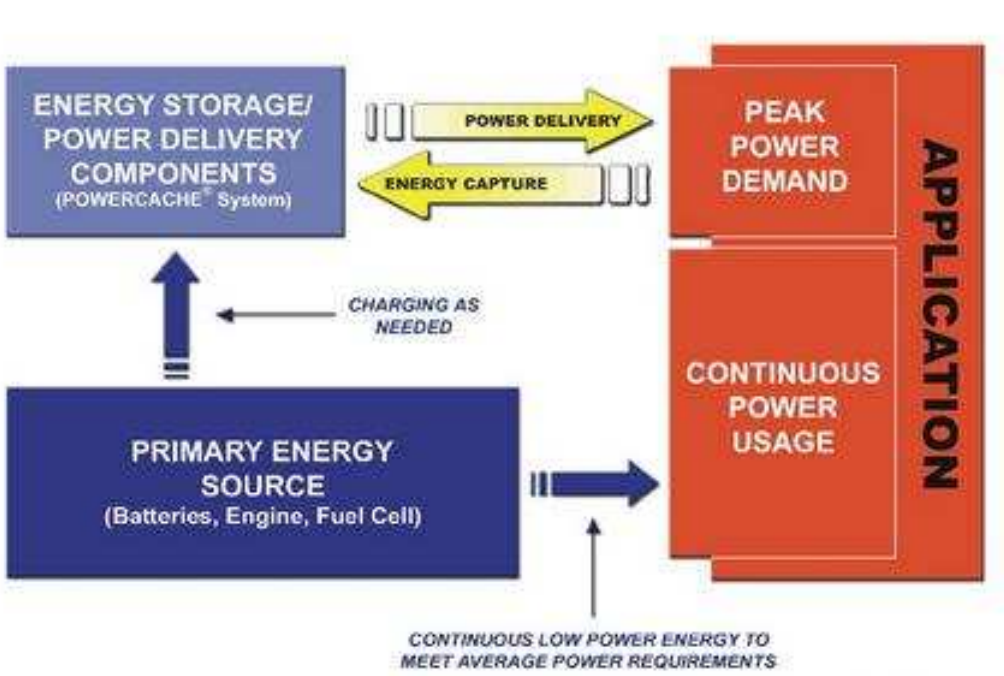

Fig 11: General Overview of an Energy Management System (Source: EEtimes Design [84])

The figure above represents what the EMS of an electric vehicle should effectively do i.e. main energy source (battery) for average power demand, auxiliary energy

source (supercap) for peak power demand and energy capture (regenerative braking) schemes.

The issue of power arbitration or sharing between multiple sources to satisfy the load requirement may be seen in another light as in the figure below which was explained in L.C Rosario's PhD thesis [54]

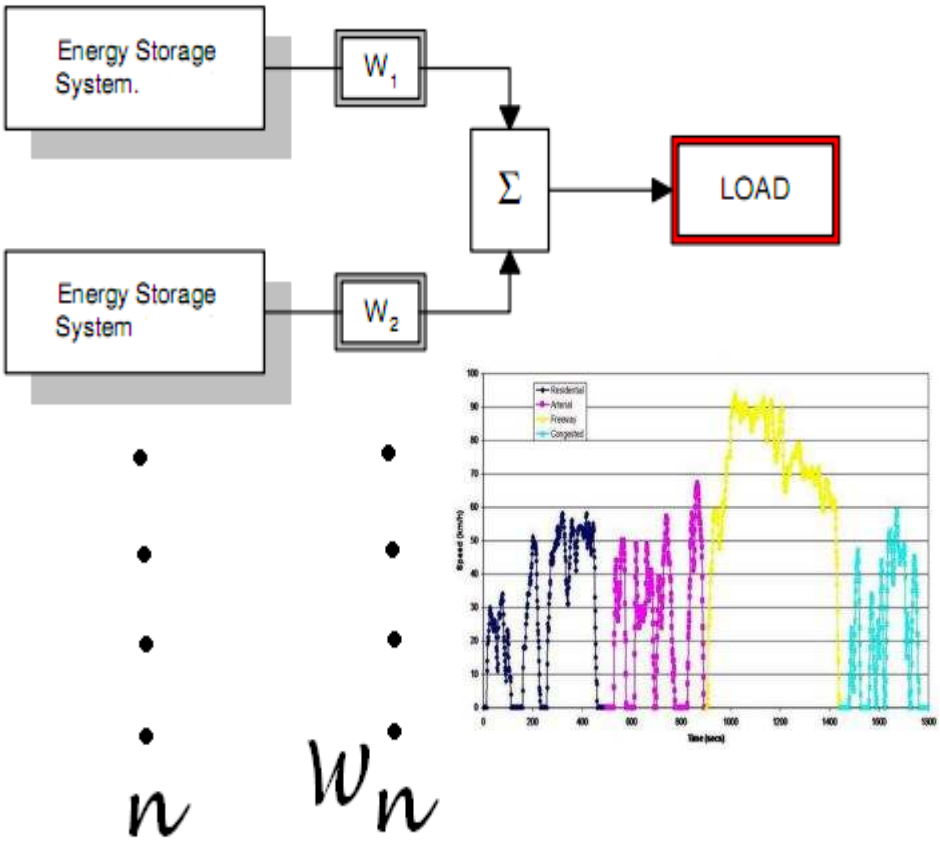

Fig 12: Power arbitration concept for multiple energy sources (Source: L.C Rosario [54])

The figure above can be explained in very simple terms as follows:

- There are usually N storage devices

- W: weight factor for adjusting the rate at which energy is being drawn (power) from each source.

- ∑: algorithm to coordinate the power flow by dynamically varying the weight factors in response to the ever dynamic driving load. Also taking into consideration the system constraints such as depletion levels or limits of the energy storage systems

- The load requests fluctuate through a drive cycle in the case of an electric vehicle

During the course of this research project, a few hundred literatures was collected including textbooks, journal papers, conference papers, application notes, patents and standards. A summary of work conducted by research groups in the area of energy/power management for electric vehicles with hybrid energy sources is presented in the sections below. The works presented range from a simple parallel connection, series configurations to complicated intelligent energy management systems using some sort of machine learning theory. It should be noted that in all literature surveyed, the supercapacitor was acting as the auxiliary source while a battery pack or fuel cell, as the case may be, was the main energy source.

The most basic method of combining a supercapacitor with a battery pack is a simple parallel configuration. The performance of a battery–supercapacitor hybrid power source under pulsed load conditions was analytically described using simplified models in this work [29], to reveal potential gains in peak power, reduction of internal losses and extension of discharge life. A basic circuit shown in

the figure below, and its thevenin equivalent in frequency domain was used to perform a theoretical analysis.

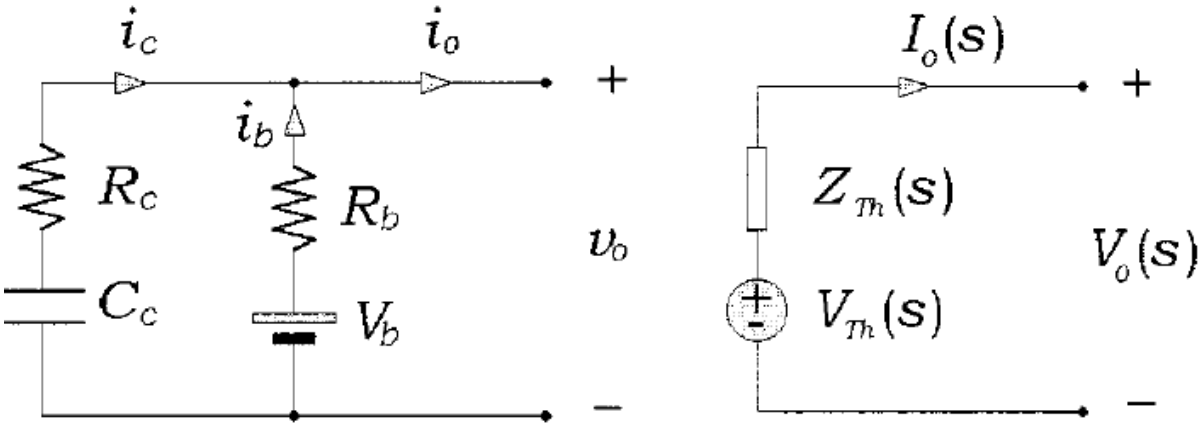

Fig 13: Supercapacitor-battery parallel circuit and its Thevenin equivalent in frequency domain (Source: Dougal et al [29])

C_C is the supercapacitor nominal capacitance and R_C, its equivalent series resistance or ESR. V_b is the battery's ideal voltage and internal resistance is R_b. Based on the circuits above, the load, battery and supercapacitor currents were simulated with particular values of resistance and capacitance with pulse frequency of 0.1 Hz and load duty ratio of 0.1. It was observed that the current supplied by the capacitor during the load, on-state relieves peak stresses on the battery and therefore influences the performance of the entire system is a positive way. A number of factors affecting the amount of current supplied by the supercapacitor were identified as bank size and configuration, pulse rate and duty ratio of the load. The peak power enhancement capability of the supercapacitor was theoretically analysed as the direct result of its current sharing capability; small series resistance which can be obtained cascading more capacitors in parallel than in series. This relates to the supercapacitor bank size and configuration. The result of this analysis

was used to optimize a system design case study and it resulted in a power loss saving of 74% from the battery and also an increase in run time of the entire system by 8.4 minutes.

An insightful piece of practical research case study on the integration of batteries and supercapacitors for electric vehicle propulsion would be [30], carried out at Massachusetts Institute of Technology, MIT. It was a student driven project aimed at powering a go-kart with a combination of lead acid batteries and supercapacitor module in a series configuration. Figure [13] below describes this configuration.

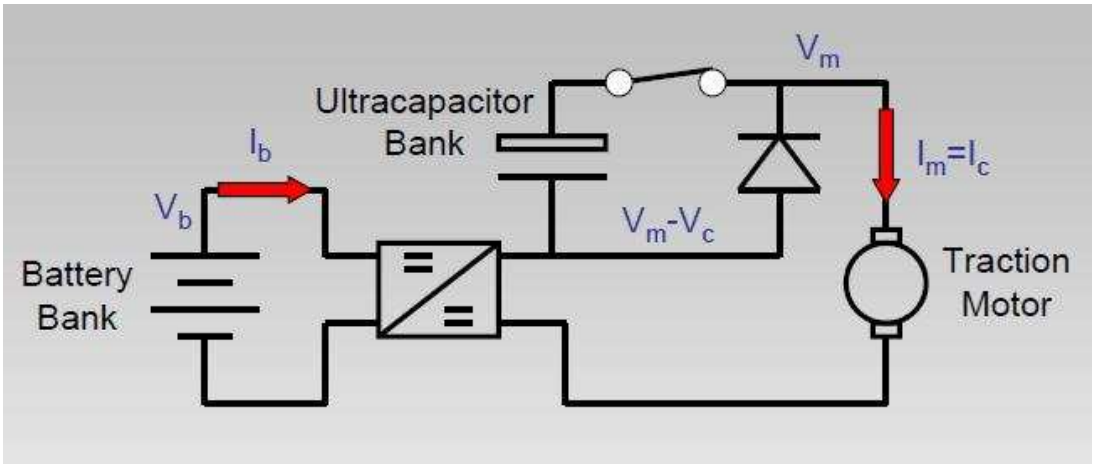

Fig 14: Battery + Supercapacitor Series Configuration (Source Colton.S [30])

In this configuration, the voltage present on the supercapacitor reduces the current demand from the battery at a given load current. The battery pack is connected to the traction motor via a half bridge converter which essentially acts as an isolation switch; pulse width modulation to turn on and off the switching circuit. A high power by-pass diode enables the go-kart to be powered solely by the battery pack while the capacitor contactor switch enables a boost mode whereby the supercapacitor is in series with the motor and contributes to the load demand. Also, regenerative braking is solely channelled into the supercapacitor. Positive attributes

of this configuration as observed on the go-kart implementation included the following:

- Small supercapacitor and its entire voltage range utilized at a lower cost when compared to the traditional parallel configuration
- No need for external inductors as all the switched current passed through the motor windings
- Off-the-shelf dc to dc unidirectional converters may be used to connect the battery to the traction motor.

The disadvantages highlighted in this work being no direct power transfer between the two power sources i.e. the battery cannot charge the supercapacitor and vice versa. Also the regenerative braking energy cannot be used to charge the battery pack.

A direct parallel connection of the supercapacitor across the battery terminals does reduce transient currents in and out of the battery according to Pay et al. Figure 15 below describes the direct parallel connection in which the supercapacitor has to be precharged to the battery's terminal voltage first. This makes it impossible to control the power flow in and out of the supercapacitor bank because its terminal voltage is tied to that of the battery at all times. In effect, current division between these two devices solely rests on the value of their internal resistances [31]. An Experimental setup consisting of valve-regulated lead acid (VRLA) batteries to make up a total of 336VDC, 170Ah and a string of supercapacitors each 2.5V 2500F totalling 375VDC 16.67F were used for validation. Results such as a 40% reduction in battery pack current and 30% improvement in dc bus voltage regulation were

obtained. However, it was observed that the state of charge (SOC) of the supercapacitor dropped considerably after an acceleration.

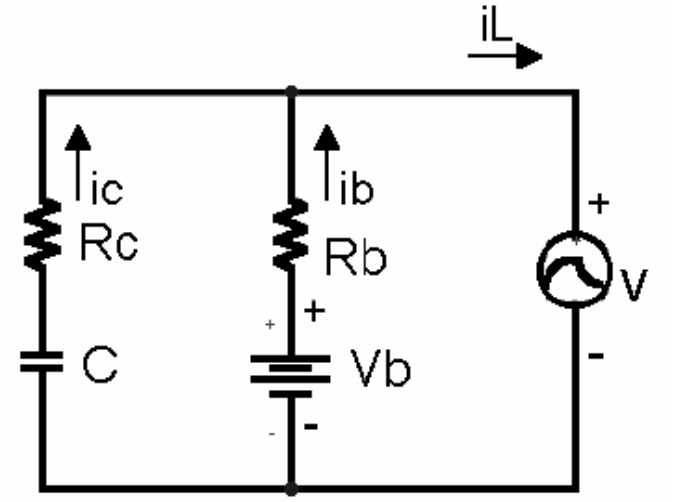

Fig 15: Direct Parallel Connection of Battery bank (b) with Supercapacitor Bank (c) supplying a load. (Source Pay.S et al [31])

Authors Gao, Dougal and Liu, went a step further with their original work [29], to produce a comparison between passive (direct paralleling) and active (via a converter) configurations between a battery and supercapacitor (see figure 15 below) using a software simulation package called the Virtual Test Bench (VTB) [55]. A hardware implementation was also carried out using real time dSPACE controller, SonyUS18650 lithium ion battery pack, Maxwell PC100 supercapacitor and a programmable pulsed load.

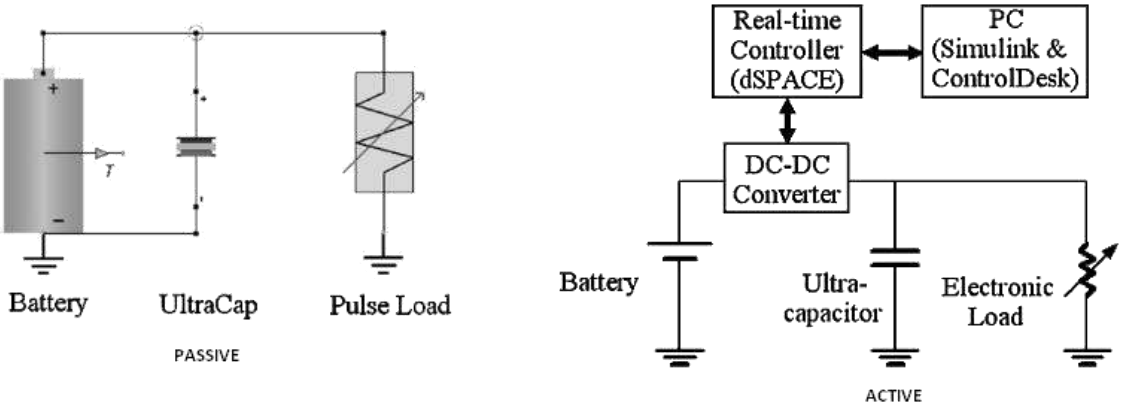

Fig 16: Passive (left) and Active (right) Configurations (Source Gao et al [55])

Simulation results of both passive and active connections with respect to the current waveforms under the same pulsed load conditions. These are shown in the figure below to give a better picture of the difference in power delivery.

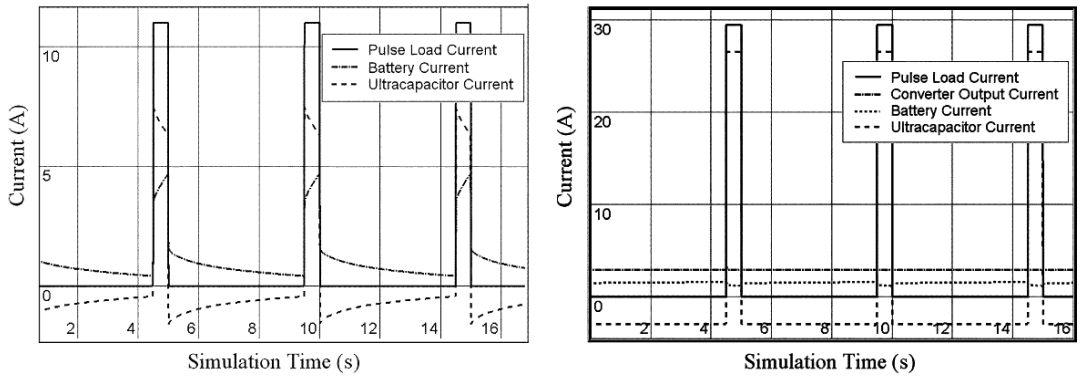

Fig 17: Passive (left) and Active (right) Current waveforms (Source Gao et al [55])

In the passive configuration, the battery delivered power to the load during the pulse-on time and recharged the supercapacitor during pulse-off. The passive system was capable of delivering a power 2.3 times greater than the battery alone would have been able to supply. It was observed that battery current spikes were drastically reduced by the hybrid system but not entirely. The battery's safe limit

was 2.4A but peak values of almost 5A were recorded. This could be detrimental to the battery life.

In the active configuration, a higher battery voltage was used via a step down converter whose output was more or less the same as the supercapacitor voltage. The converter was made to output current at a constant rate throughout the load cycle which would either top off the supercapacitor (during pulse-off), or contribute towards the load current (pulse-on). The deliverable peak power capacity recorded was said to be 3 times greater than the passive configuration, and a whopping 7 times greater than the battery alone. As great as these figures sound, it came at a cost. The total discharge time for the battery, i.e. the time it would take for the battery to discharge from 100% SOC to the rated cut-off voltage, was 14.4 minutes less than when the passive configuration was used. This was attributed to converter losses. In the electric vehicle world, this could result in a decrease in range. A comprise will have to be reached to get a right balance.

D. Shin et al [32], describes the parallel connection as an intuitive way of reducing the load fluctuation effect on the voltage supply or dc bus. The supercapacitor in parallel is essentially a low pass filter that prunes out rapid voltage surges; the higher the capacitance, the better the filtering effect. To improve on this configuration, one involving a constant current regulator that separates the battery pack from the supercapacitor was proposed. This is shown in the figure below. Issues associated with this arrangement include the supercapacitor charging current control and terminal voltage control. With fixed charging current, the amount of delivered power from the battery to the load will depend on the terminal voltage of

the supercapacitor which must be maintained within an appropriate or optimal range in order to meet the load power demand.

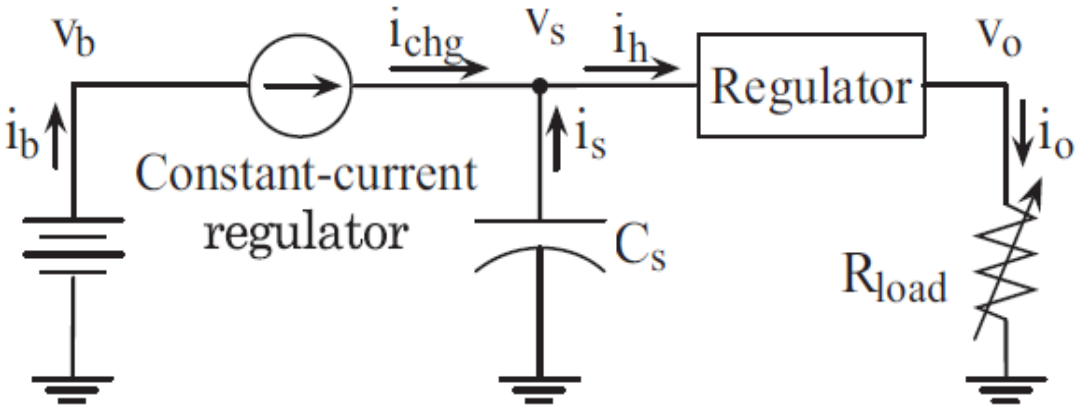

Fig 18: Constant Current Regulator based Configuration. (Source D.Shin et al [32])

ATT R&D Co. and Ness Capacitor Co. Ltd conducted tests on a neighbourhood electric vehicle (NEV); the Invita, to demonstrate the advantages of using supercapacitors alongside batteries [34]. With the aid of a high power contactor, a direct parallel connection between the battery pack (72V sealed lead acid) and supercapacitor module (92V, 50F) was achieved. The latter electronically limited to 72V by a charge balancing circuit to match the dc bus voltage. The curb weight for the NEV was 545Kg and a data acquisition device was setup to log vehicle speed, battery voltage and current, supercapacitor voltage and current in real time. A fixed 15km route with light traffic congestion and frequent stop-and-go situations was chosen to test the Invita. In each case (with and without supercapacitor), the vehicle was driven until the battery's state of charge indicated a complete depletion. Results reported that on a full charge, energy consumption in Kwh/km

was 0.161 with supercapacitor on and 0.186 when off. This translated to a 15.4% increase in range per charge.

Researchers in [35] have also attempted a parallel combination of a valve regulated lead acid (VRLA) cell with a string of supercapacitors to improve the former's performance under realistic hybrid vehicle power demands. By logging voltage and current data from a Honda insight driven on a test track, a power demand profile was created and scaled down to represent the power profile experienced by a single cell within the battery pack. Hawker Cyclon 8Ah cells were used along with both EPCOS and MAXWELL supercapacitor cells. They were subjected to the same power demand profile on a purpose built test bench over 2400 seconds. Results show that cell current drawn was significantly reduced as the supercapacitor sources and sinks most of the transient current. The VRLA cell acted as bulk energy reservoir and supported the low energy storage deficiency of the supercapacitor. A comparison of rms and maximum cell current was done with and without supercapacitor combination. A 10% reduction was recorded with a 100F supercapacitor, 50% reduction with 1250F and 60% reduction with 2500F as compared to when the cell was used alone to fulfil the power demand profile. Ohmic losses which are effectively I^2R losses are the major culprit of cell heating. By reducing the rms current from the cell i.e. heating effect, beneficial effects on cell lifetime, electrolyte loss, gassing and corrosion are obtained as they are all temperature dependent.

Control System and Energy Management Algorithms

Researchers in [33] successfully developed a prototype EV powered by a combination of high energy sodium nickel chloride (ZEBRA) batteries (28Kwh) and supercapacitors. ZEBRA battery was chosen due to lower costs and safety factor even though it is known to have a low specific power density [16]. To solve this power problem, a supercapacitor bank (20F, 300V) was installed to provide peak power for driving the 53KW brushless dc motor, better acceleration and also improved regenerative braking capabilities. To manage the energy flow between the ZEBRA battery and supercapacitor bank, a buck boost type dc to dc converter which is implementing an energy management algorithm was used. Figure X below shows the block diagram and also the control scheme of the system. The algorithm is based on input parameters from sensors mounted in the vehicle such as battery voltage and current, drive current, supercapacitor voltage and current, input and output currents of the dc to dc converter, battery state-of-charge (SOC) and vehicle speed. The platform used is a TMS320F241 DSP from Texas Instruments which sends corresponding gating signals to the converter. Speed provides a useful insight into the vehicle's energy requirement; low speeds means more energy required for an impending acceleration (i.e. keep the supercapacitor fully charged) while high speeds translate to more space for storing regenerative braking energy (i.e. empty out the supercapacitor). Predetermined charge curves for the supercapacitor bank based on the conditions mentioned above were also estimated using neural networks. Results from this work show that an improvement in acceleration was achieved as a result of the supercapacitors; 16.1% higher for 0-40 km/h acceleration, 31.3% for 0-60km/h and 38.5% for 0-80km/h. In terms of range, a

10.76% improvement was recorded on a fast track and a 16.67% improvement on a slow track. Fast track in this context refers to highway speeds with longer periods of acceleration with little or no stops (i.e. supercapacitor has little or no chance of recharging via regenerative braking). Slow track refers to city speeds; short bursts of acceleration as well as braking (i.e. the supercapacitor is constantly being topped off).

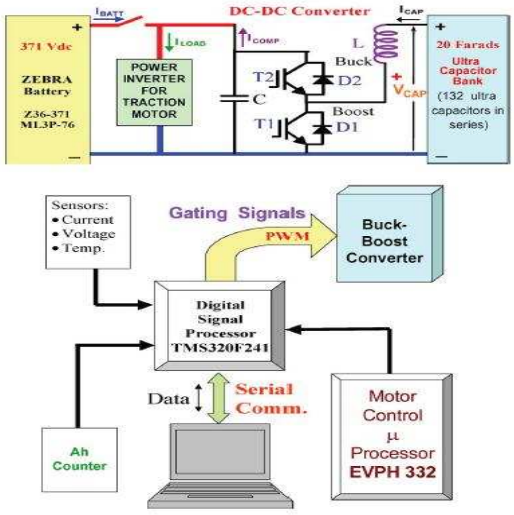

Fig 19: Block Diagram and Control Scheme of Dixon et al ZEBRA + Supercapacitor [33]

Researchers at the University of Strathclyde developed some control strategies based on some simple rules for a battery-supercapacitor power pack implementation in a Shelby cobra [56]. However, only a simulation was done using ADVISOR software which was developed by National Renewable Energy Labs (NREL). A 78V, 70Ah gel-type lead acid battery pack and a supercapacitor series pack of the same voltage, 83F were modelled. Two half-bridge DC to DC converters controlled the power flow from the battery and supercapacitor respectively with a by-pass option for when the battery solely powers the motor. This was to avoid the

losses associated with the converter usage. The control strategy was summarized in the figure below.

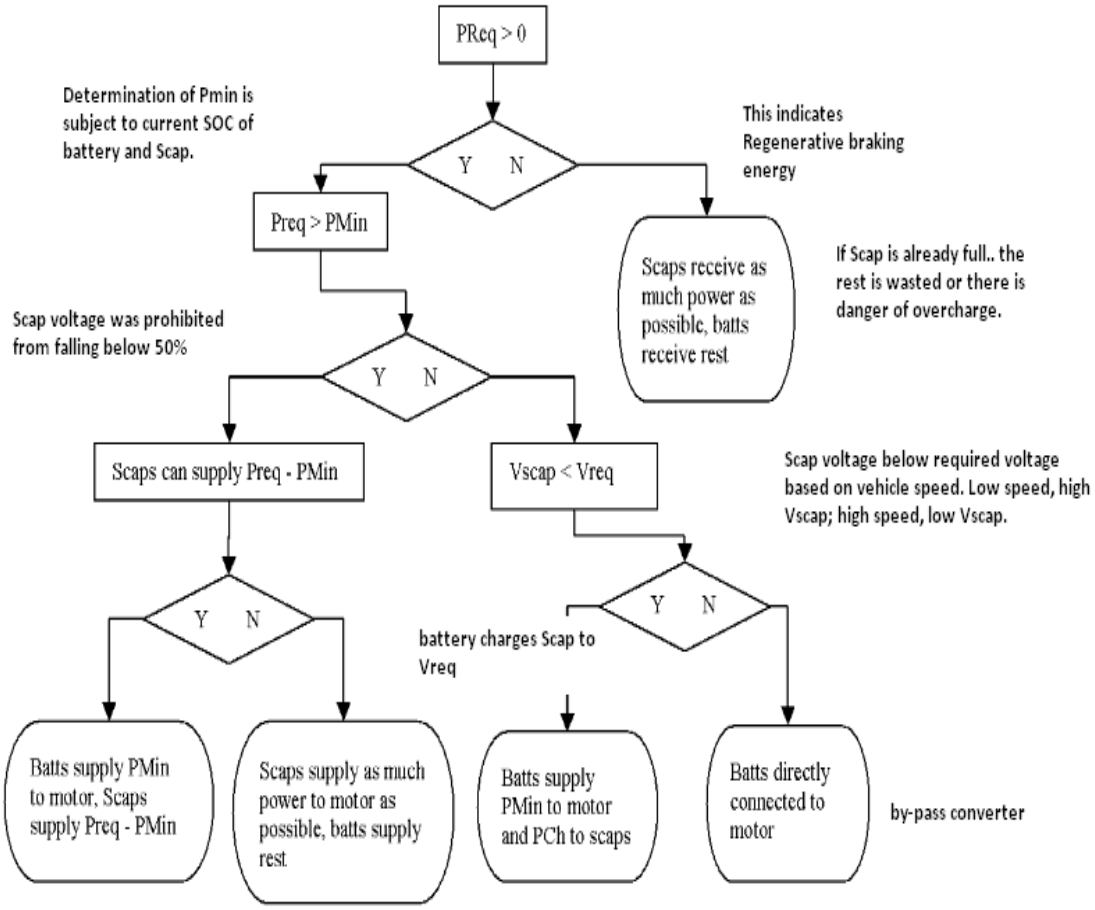

Fig 20: Flow chart of Control developed for battery supercapacitor Shelby cobra (Source Carter et al [56])

Two control strategies were tested over simulated drive cycles (the New European Driving Cycle ECE); one for maximising system efficiency and the other intended to minimise peak battery currents. The results obtained were compared with the same simulation but using the battery as the sole power source which recorded a peak battery current of 240A and a yield of 6.26 km/kwh. It is tabulated below:

Strategy	Pmin	Pch	Peak Battery Current	Yield
Max. system efficiency	6800W	0W (Supercap only charged during Regen.	105A (56.25% reduction)	6.38 km/Kwh (3% increase)
Optimised battery life	4200W	1600W	66A (72.5% reduction	6.11 km/Kwh (3% loss)

Table 2: Comparing the two control strategies developed by Carter et al [56].

The tabulated results showed that it is not usually possible to simultaneously optimise the hybrid system for both efficiency and battery life; one must be prioritized over the other. Both strategies improve the vehicles ability to meet power demands.

The current state-of-the-art of energy management algorithms for hybrid and electric vehicles is based on heuristics and gradually progressing towards artificial intelligence methods such as neural networks etc. [36]. The control strategy for battery + supercapacitor combination is largely a function of the supercapacitor capacity [37]. Cost constraint of large super-capacitors creates the need for advanced energy control strategies. Control strategies usually based on heuristics or an optimization model are translated into algorithms and implemented on an embedded system (microcontroller or digital signal processor). The embedded system acquires all relevant signals, processes data, and generates the PWM signals to commutate IGBTs in the DC-DC converter. Input signals include motor/vehicle speed and power, battery voltage and current, battery and supercapacitor State-of-charge (SOC), system temperature among others.

A heuristic energy management algorithm is based on the fact that the energy content of the supercapacitor must have an inverse relation to vehicle speed [38].

Thus, when the vehicle runs at low speeds, energy is reserved to accelerate. On the other hand, when the vehicle runs at high speeds, space to store energy from braking is made available. This is achieved by injecting or extracting current from the ultracapacitors to reach a predefined state-of-charge reference, which depends on the vehicle speed. By limiting the current extracted from (or injected to) the battery pack, its lifecycle is effectively increased. The supercapacitor array supplies the currents whose limits are outside that of the battery pack.

Optimal control energy management algorithm is based on the application of optimal control techniques to determine the optimal power support for a real-life power-demand-profile [38] i.e. minimizing the energy extracted from the battery and providing a power buffer from the supercapacitor in order to maximize system efficiency for a particular drive cycle. Power demand data series is obtained experimentally from driving an EV or a test bench under real driving conditions. This data series is used as a knowledge base to train an Artificial Neural Network (ANN).

A neural network is a computer architecture modeled upon the human brain's interconnected system of neurons which mimics its information processing, memory and learning processes. It imitates the brains ability to sort out patterns and learn from trial and error, discerning and extracting the relationships that underlie the data with which it is presented. As a result of this training, the network acquires the "knowledge" necessary to determine the most efficient supercapacitor current under different conditions. The optimality will depend on how many sets of data (or the driving conditions) are used to train the network.

Research work [39], combines a heterogeneous energy storage system consisting of low power; high capacity batteries and high power supercapacitors with a predictive control system that optimizes power flow. The “ChargeCar” project, which authors of this work have pioneered, was aimed at achieving optimized power management between the energy sources by utilizing information such as vehicle state, driver history, GPS coordinates and even information available on the web like traffic data, weather reports etc. Variables that significantly impact the energy demands of a commuter electric vehicle (or any other vehicle) are highly variable speeds and traffic conditions, unique individual human driving style and elevation changes through the course of travel. Each one of these factors would affect the design of an optimal control system for a battery-supercapacitor combination.

The ChargeCar project has collected driving data from normal petrol volunteer vehicles borne with GPS units and elevation data for the entire United States. This large repository was used to test various energy management algorithms rather than using standard drive cycles such as FUDS, UDDS etc. A robust physics-based electric vehicle model was created which takes input GPS coordinates from the data repository and translates it into accurate power demand for equivalent electric vehicles. This power demand data along with vehicle, battery and supercapacitor state was used to test out algorithms which control power flow. The physics-based model described in this work is similar to the modelling done in chapter 3 of this thesis where the total tractive force required by the vehicle is equal to the sum of the acceleration force and the resistive forces due to air, rolling and gravitational resistance. The power required by the motor to propel the vehicle was thus

calculated by taking into account 85% drivetrain efficiency during forward movement and a 35% energy recovery during braking. The model for predicting the power required by the load was verified and validated by comparing data with 2002 Toyota Rav4 EV, and using Bombardier's large scale people mover vehicles.

Various algorithms were tested out starting from an ideal case to predictive algorithms. In each case, current-squared (I^2) demand on the battery as an indicator of efficiency was used as it is closely related to both internal efficiency as well as overall battery longevity. The ideal case algorithm or optimal bound as it was referred to, assumes, or provides the power demand profile of the particular vehicle for the entire trip beforehand thus serving as a benchmark to subsequent predictive algorithms. The energy management system uses rules to force the power flow to certain levels according to the demand profile and keeping the I^2 losses to the minimum. A 70.06% reduction in current-squared was recorded which suggested a significant amount of battery life savings; however the exact savings figure calculation was beyond the scope of this work. Also a 15.56% increase in range was recorded. The second algorithm tested could be referred to as a naïve buffer as it only utilizes the supercapacitor when necessary; for acceleration and it is recharged by regenerative braking only. There is no interaction between the battery and supercapacitor. In this scenario if the supercapacitor is completely depleted during a discharge or acceleration, the battery takes over the remaining responsibility. The results of this experiment were a 9.05% reduction in current-squared on the battery, and the 6.27% increase in range. This provided some insight as to what an "intelligent" energy management algorithm can achieve given the degree of

freedom of approximately 9% to 70% in current-squared and 6% to 15% increase in range.

An improvement to the naïve buffer was developed and it was aimed at charging the supercapacitor at a constant rate whenever the load demand was low; during idle or stop conditions, to a maximum charge limit. This limit could be shifted based on the speed of the vehicle. For example, based on the present speed, leave enough room in the supercapacitor to store regenerative braking energy should the vehicle come to a stop. At the same time, let the energy present in the supercapacitor be sufficient for an acceleration, while at complete stop conditions, charge the supercapacitor fully for an impending acceleration. The algorithm was built around these rules and the results obtained came much closer to the optimal bound; 40.15% reduction in I^2 and 9.55% increase in battery pack range.

In a bid to utilize the knowledge obtained from maps, routes, traffic signals and GPS coordinates, machine learning techniques were incorporated into an algorithm which uses the K-Nearest Neighbour (KNN) search to predict the upcoming duty of the vehicle. At each time-step in a trip, the algorithm searches for k, in this case,7, nearest, most similar data points in a particular driver's history which consists of 55hours of driving data for each driver. The nearest-neighbour search finds the most similar neighbours and then averages these upcoming duty curves with each other at each time slice into the future, discretized to one second. This yields an average future duty for seven points in a driver's history most similar to his current state. This is used as the predicted duty for the energy management algorithm, which then simply assumes that this upcoming duty is absolute truth and calculates

the same brute force solution as in the optimal bound. Therefore, the gap between the optimal bound and the performance of this algorithm hinges simply on the accuracy of the predictions. The k-Nearest Neighbor search, which has very little semantic knowledge of the problem, nevertheless yields decent results: a 57.69% reduction in battery current-squared, and a 12.53% increase in range.

Electric vehicles cannot compete with ICE's yet in terms of driving range. An intelligent EMS needs to be adopted to maximize the utilization of the energy source. According to [40], making use of sensory inputs like current, voltage, speed as well as external factors like climate and environment, the EMS can realize many functions. Optimize system energy flow, predict the remaining energy and hence the residual driving range, suggest more efficient driving behavior, more efficient regenerative braking among others. In order to increase the driving range, multiple energy sources may be adopted for modern EVs. The corresponding combination and hybridization ratio should be optimized on the basis of the vehicle performance and cost.

The current state-of-the-art of energy management algorithms for hybrid and electric vehicles is based on heuristics and progressing rather rapidly towards artificial intelligence methods such as neural networks etc [38]. In this work both a heuristic based algorithm and optimal control technique applied to neural networks were implemented on a battery – ultracapacitor hybrid energy storage system. The vehicle's yield (km/kWh) was increased in 5.2% and 8.9% with the first and second algorithms, respectively. An economic analysis of costs only was carried out and it showed that the present high cost of ultracapacitor energy storage

systems can only be compensated for, if it contributes to a 50% or more extension of battery life.

Even though the cost of ultracapacitor cells are projected to fall in coming years, the challenge of this research project would be to justify the incorporation of ultracapacitors in an electric vehicle by showing at least a 50% increase in battery life.

Real time control strategies and energy management system requirements of battery supercapacitor combination proposed in [37] include a current and speed restrained control strategy. The former ensures that the current drawn from the main battery pack is within a certain safe limit and extra current is drawn from the supercapacitor while the latter control strategy is based on the speed of the vehicle i.e. at high speed, the supercapacitor should be discharged and prepared for imminent regenerative braking while at low speeds the supercapacitor should be fully charged in anticipation of acceleration. The results of implementing the control strategies showed an increase in maximum speed of 68km/h without supercapacitor to 96km/h with supercapacitor. An important observation from this work is that the average energy consumption of the vehicle with auxiliary supercapacitor source is reduced in city driving conditions due to constant stop-and-go regenerative braking while in highway driving, the energy consumption does not reduce as the speed is fairly constant.

Machine learning algorithm combined with fuzzy logic for online power management of a multi powered source HEV based on minimizing the power loss from each source and placing system constraints to ensure good quality power

service [41]. This algorithm learns about the optimal combination of power sources (e.g. battery, fuel cell, supercapacitor etc) best suited for a given driver load request (drive cycle) and a fuzzy controller acts on this knowledge by delivering power as soon as the load request is made, bearing in mind all the system constraints like state of charge of battery, ultracapacitor etc. Each power source combination is associated with a power loss function at any time *t* during the load request.

According to Y.L Murphey et al [42], driving patterns exhibited in a real world driver are the product of the instantaneous decisions of the driver to cope with the driving environment (road type, traffic congestion, driving style, vehicle operation mode). A neural network model was developed for predicting online driving patterns in the near future based on the short term history of the driver during a trip. A quasi optimal set of 14 statistical features (after a rigorous feature selection process involving the facility specific driving cycles) was used to characterize the speed profile of a vehicle (see table below).

Name of selected features:
Trip distance;
Maximum speed;
Maximum acceleration;
Maximum deceleration
Average speed
Average acceleration
S. D. of acceleration
Average deceleration
% of time in speed interval 0-15 km/h
% of time in speed interval 15-30 km/h
% of time in speed interval >110 km/h
% of time in deceleration interval (-10)-(-2.5) m/s2
% of time in deceleration interval (-2.5)-(-1.5) m/s2
Number of acceleration/deceleration shifts per 100m where the difference between adjacent local max-speed and min-speed was >2 km/h

Fig 21: 14 features selected for roadway prediction (Source Y.L. Murphey [42])

To realize real-time control, the historical data should be acquired online in a certain time window. If the time window is too short, the historical data may not reflect the driving cycle correctly; if the time window is too large, the computational burden may be too heavy for real-time control. An optimal window size and time step was proposed to divide the speed profile into segments. The figure 22 below illustrates a segmented speed profile of the UDDS (Urban Dynamometer Driving Schedule) with a window size (ΔW) of 150s and a time step (Δt) of 100s (in reality Δt is much smaller).

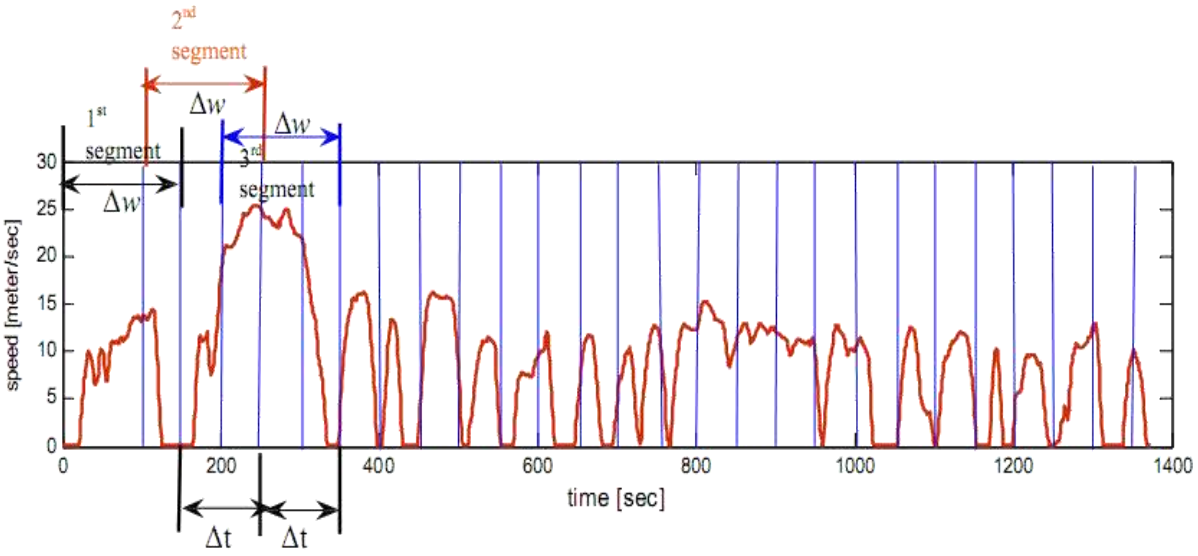

Fig. 22: UDDS cycle segmented by a window size and a time step. Source Y.L Murphey [42]

11 standard drive cycles were segmented as describes above for use as training and test data. PSAT©; a simulation software was used to simulate the drive cycles. Each segment contained a vector of 14 features which were randomly sampled into a training and test data sets. A multi layered, multiclass neural network of 14 input nodes, 11 output nodes with a hidden layer of 20 nodes was trained for the roadway type prediction. An intelligent vehicle power controller that incorporates the knowledge about the roadway type and traffic congestion level predicted by the neural network is used to make power management decisions in a conventional car. Significant reduction in fuel consumption was obtained even though an offline dynamic programming algorithm was used to optimize the power management strategy.

Y.L Murphey et al [64] also did some work on driver style classification using jerk analysis. Jerk may be defined as the rate of change of acceleration or deceleration.

Mathematically, it is calculated as the derivative of acceleration/deceleration or the second derivative of the velocity. A true indication of a driver's aggressiveness (which is directly related to power demand in electric vehicles) is its jerk profile rather than its acceleration profile. Appropriate feature extraction of jerk data can be utilised to develop a robust algorithm to classify drivers' style. Fuel rate in conventional vehicles was compared with its respective jerk profile using software simulation packages; variation in jerk results in change in fuel rate. Mathematically, if a drive cycle is represented by DC (t), the jerk function J (t) is given as:

$$DC(t) = \frac{d^2DC(t)}{dt^2}$$

A jerk feature was defined as:

$$\gamma = \frac{S.D_J}{\bar{J}}$$

Where $S.D_J$, is the standard deviation of the jerk over certain specified window size and $\bar{J}$ is the mean jerk of the current road-type which the driver is on at that moment. The ratio mean used is statistically called the coefficient of variation and it is often used to depict the amount of variance between populations with different average values. In this case different road types have different average jerk values.

Courtesy of sierra research [65], [66], 11 standard drive cycles were developed depicting driving style on different roadway types and traffic congestion levels. The 11 cycles are divided into 4 categories; freeway, freeway ramp, arterial or urban

road and local roadways. A qualitative measure called the level of service (LOS) was introduced to further classify the freeway and arterial categories based on speed and travel time, freedom to manoeuvre, traffic interruptions, comfort and convenience. $\bar{J}$ was calculated for each of the 11 drive cycles and used in a driver style classification algorithm on a window by window basis. The algorithm is described in the figure 22 with the thresholds for normal and aggressive being 0.5 and 1.0 respectively.

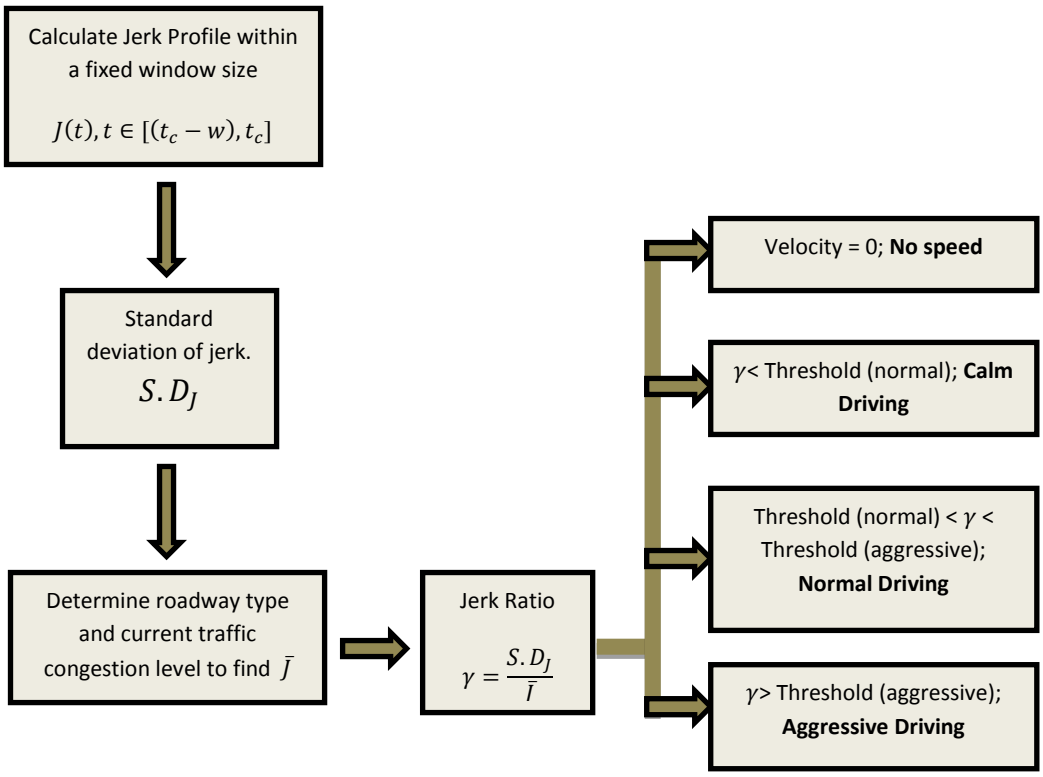

Fig 23: Driver Style (DS) Classification Algorithm Proposed by Y.L. Murphey et al [64]

The significance of determining a driver's level of aggressiveness or calmness based on jerk feature may be used as a key feature in energy management algorithms for electric vehicles. Choosing the appropriate window size allows for accurate capture of transient behaviours or jerks. If the window size is too small, it may not be

enough time to capture the entire acceleration or deceleration event. On the other hand, if the window size is too big, it may capture multiple events which would lead to misclassification.

Langari and Won [43] proposed a conceptual intelligent energy management agent (IEMA) to enable a hybrid vehicle to be driven in an economical and environmental friendly way while still satisfying the driver's power requirement and also charge sustenance over the entire range of driving. This system incorporates a number of subsystems such as a driving information extractor (DIE) of driving patterns for characterizing the driving situation as well as developing a knowledge base for torque distribution. The driving situation identifier (DSII) consists of the roadway type identifier (RTI), driver style identifier (DSI), driving trend identifier (DTI) and driving mode identifier (DMI). Fuzzy torque distributor (FTD) effectively splits torque between the motor and the engine. A state-of-charge compensator was implemented to address the issue of charge sustenance over a prescribed range. The figure 24 below extracted from J.S Won's PhD Thesis [44], gives a graphic explanation of the architecture of the IEMA.

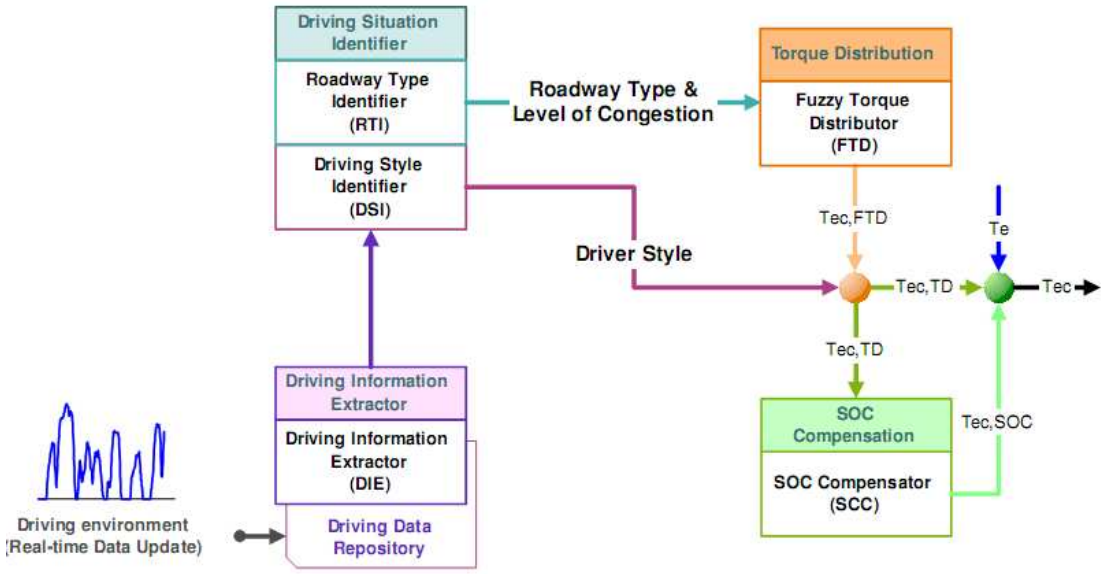

Fig. 24: Architecture of the Intelligent Energy Management Agent (IEMA). Source J.S Won Thesis [44]

An interesting algorithm used in this work is the Learning Vector Quantization (LVQ) network; a prototype based supervised classification algorithm for roadway type classification. Compared to other neural networks, the main feature of the LVQ network is to classify input vectors into target class through a competitive layer for identifying subclasses of input vectors and a linear layer for combining them into the target classes. The LVQ network was trained using the statistics from 9 facility specific driving cycles [65] to recognize driving patterns. Results were able to show that most of the patterns were correctly classified and even the misclassified ones were classified as the neighbour class or one with similar statistics.

The DTI assesses short term/transient features of driving cycles such as low speed cruise, high speed cruise, and acceleration/deceleration. These features were described by magnitudes of the average speed and acceleration values. DMI

classifies the drivers operating mode into startup, acceleration, cruise, deceleration and stop or idling. FTD takes input from RTI, DTI, DMI and the current state of charge of the energy storage device to compute an appropriate engine torque command. Also a fuzzy driver style identifier was implemented to study the effect of driver variability (calm, normal and aggressive driving) in the IEMA; average acceleration and ratio of standard deviation to average acceleration as inputs and a weight factor which compensates the torque distributor as output. A simulation study was carried out on a typical parallel hybrid power train to evaluate the performance of the IEMA and it was concluded that the length of window time for each of the subsystems was critical for proper classification.

A multiple input power electronic converter (MIPEC) for interconnection among three power sources; fuel cell (FC), battery (BT) and ultra-capacitor (UC) to power a road electric vehicle was proposed by [45]. The control strategy of the MIPEC includes linear control of single bidirectional boost subconverters for each source and a supervisory system that coordinates the power flow among the power sources to the load. The 3 sources are all below the dc-link voltage of 320V dc; FC at 150V, BT at 144V and UC at 116V. An efficiency analysis was carried out to determine the desired operating region of each device. The converter for FC and BT limits sudden/fast variations in charge/discharge currents. The energy management and fuzzy supervisory system proposed by the authors of this work is shown in the figure 25:

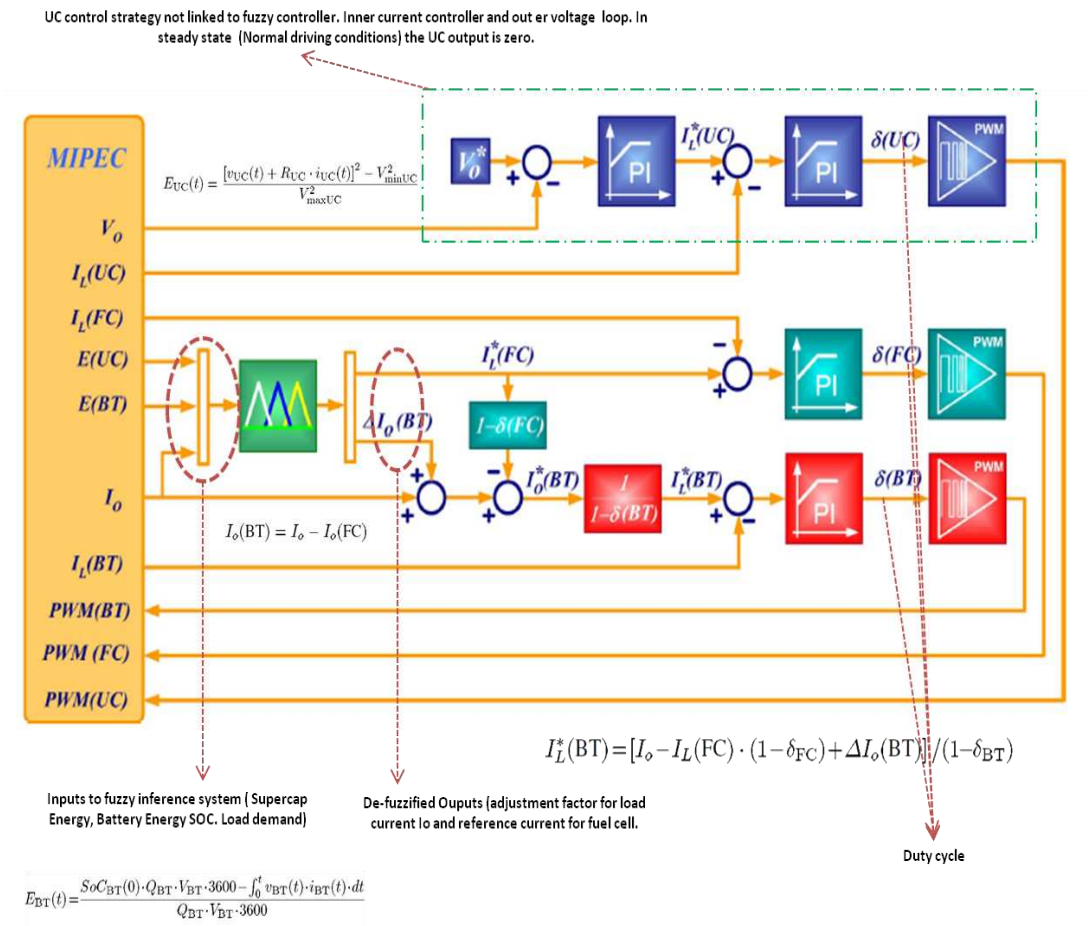

Fig. 25: Block diagram of Fuzzy Logic Supervisory Controller by A.A Ferreira et al [45]

The fuzzy logic controller has three input variables (load current, battery energy and ultracapacitor energy) and two output variables (output correction term and fuel cell current reference). The rule base specification depends on the designer (expert) knowledge about the power sources and traction constraints. The rules developed were based on successive experiments to ensure the process's robustness and reliability. A summary of the rule based is described below as this will give an insight to control algorithms which may be proposed by this thesis in future chapters:

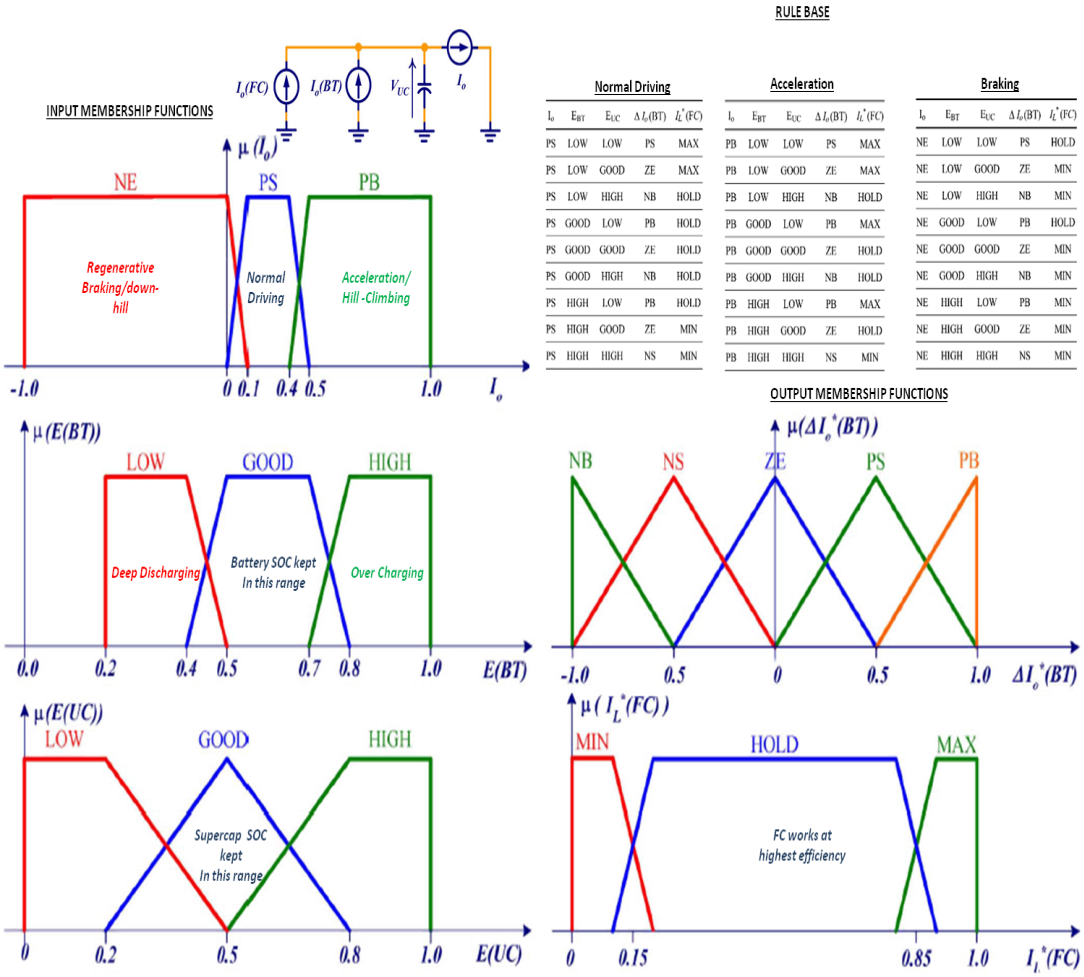

Fig. 26: Fuzzy Membership Functions and Rule Base by A.A Ferreira et al [45]

Detailed information regarding the fuzzy rules can be obtained from [45]. It was acknowledged that fuzzy logic does not guarantee optimal results in all situations, but provides a satisfactory solution to control the overall system, allowing easy modifications for adding on more rules to improve the performance.

An interesting work was presented by Jian Yang et al [46]; the estimation of the driving load of a HEV by a predicition model using discrete cosine transform (DCT) and support vector machines (SVM). The DCT was used to compress the data for reduction of dimensionality and filtering noise. It reduced the dimensionality of the drive cycle (historical part) data from 150 to 9 in this work. This not only

significantly reduced computational complexity, but also reduced the standard deviation and slightly improved the prediction accuracy. DCT uses fewer bases to transform the data than the FFT. Again Fuzzy logic approach was used to determine the average driving load levels during the forecasting period. This time the input membership functions were the vehicle speed and acceleration while the output is the driving load. In the step of de-fuzzification, centre of gravity method is adopted to convert the fuzzy value into numerical value.

The SVM with a radial basis function (RBF) kernel was adopted to classify the driving load sequence into five levels of driving load (VL=very low, L=low, M=medium, H=high, VH=very high) defined by fuzzy logic. LIBSVM [77], was utilized as an off-the-shelf software package for the implementation. To optimize the parameters of the SVM, a stochastic global optimization algorithm named CPSO was adopted. The SVM was compared with variants of Neural Networks (NN) with 3-mixed training and testing datasets from standard driving cycles in the real world and it gives better prediction accuracy and lower computational complexity than NN. The SVM gets better generalization ability than the cascaded neural network with node decoupled extended kalman filtering (CNN-NDEKF), can be trained faster than NN. The block diagram describing the prediction model is shown in the figure 27.

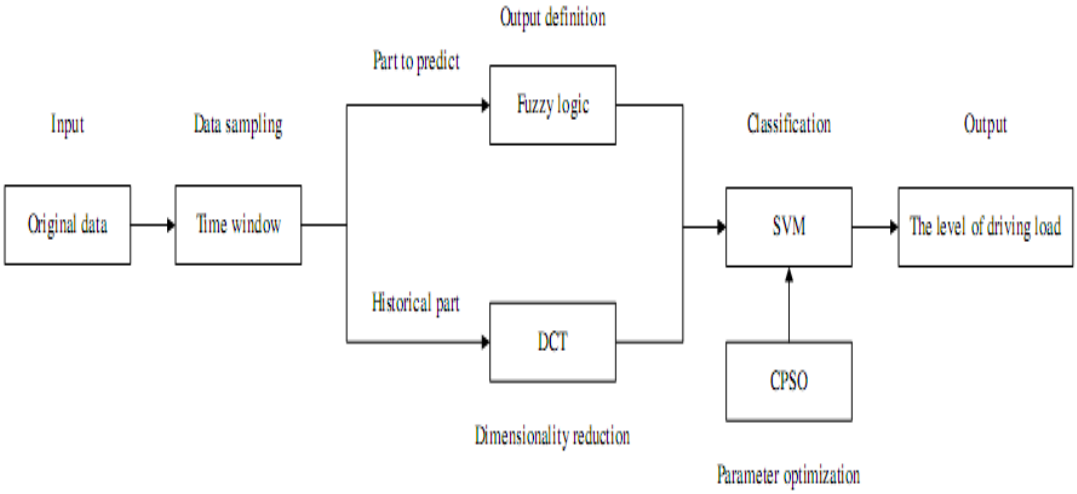

Fig. 27: Block diagram of driving load forecasting of HEV. Source Jian Yang et al [46]

In a related work, Xi Huang et al [47] and [78] attempted at correctly discriminating driving condition which was described as an important premise to an optimal control strategy for HEVs. The driving condition of hybrid vehicle is a complicated variable dependent on numerous external factors such as wetness of road, terrain, traffic congestion and weather and these factors may not have exact numerical quantities. Thus, classifying driving conditions based on vague data is a key research issue. Feature extraction of randomly truncated standard driving cycles was carried out and statistically significant features such as average speed, average acceleration, and maximum speed were chosen. Feature selection was carried out using principal component analysis. Analysis of variance (ANOVA) was used to test the significance of the features selected. A classification was carried out to compare the performance of the multilayer neural network, linear classifier, k-nearest neighbour and the SVM. The results show that the SVM is fit for classification of linear non-separable samples giving the best accuracy of 97%.

Similarly, the SVM via the support vector regression (SVR) was used to estimate the SOC of a high capacity lithium ion manganese phosphate battery pack as a function of cell voltage, cell current and cell temperature [67]. Calculating and controlling the SOC for EV and HEV applications is critical in order to give users an indication of available runtime left or range, prevent detrimental over charging and over discharging which usually leads to reduction in battery life. Due to the unpredictability of both battery and user behaviour (driving style or pattern), accurate estimation of soc is not straightforward. Several techniques used include current integration (ampere/coulomb counting), artificial neural networks, fuzzy logic, kalman filter based calculators etc. are employed. Accuracy varies in each of these methods but the cost of higher accuracy comes with higher implementation cost due to high computational complexity. For example, in [74], [75] and [76], the extended kalman filter (EKF) soc estimator designed was able to achieve a ±5% accuracy compared to the ±15% of coulomb counting method. The dual filter tweaks the system so that the effects of battery aging and degradation are accounted for and incorporated into the battery model in real time. However, a full implementation of this scheme requires a 40 MHz, 32-bit floating point processor.

The SVM's kernel approach provides a modular framework which can be applied to various domains such as biomedicine, bioinformatics, image analysis, machine vision and non-linear function estimation ([68], [69], [70], and [71]) to solve classification and regression problems. A kernel is the bridge between software applications and the real data processing done at hardware level. Apart from [67], [72] and [73] also used the SVM to model the EV battery behaviour. [72] Proposed an SOC estimator for a lithium ion polymer battery which extracts support vectors

from a battery operation history then uses only these support vectors to estimate the SOC, resulting in minimal computation load and suitable for real-time embedded system applications. Basically thousands of training data from real battery packs are taken in by the SVM and condensed into a smaller set of support vectors which can then be manipulated by an inexpensive 8-bit microprocessor to estimate the SOC. The experimental procedure carried out by [72] is summarised below:

Training

- Training data should be different from test data.
- Training data should cover the spread of operation of the battery under normal working conditions e.g. from 20% SOC to 85% SOC.
- Data should be realistic and represent a continuous flow of measured data.
- Data scaling/pre-processing is key to convergence; all vector elements in the range of 0.0~1.0

Optimizing SVM Parameters

- Cost parameter (C) controls the trade-off between allowing training errors and forcing rigid margins of classification.
- K; type of kernel function used (linear, polynomial, radial basis and sigmoid). Polynomial kernel was used for this research.
- Ɛ ; error constant

- SVM parameters used were: C= 13.86, Ɛ= 0.0001, s= 7.3 and r = 19.7. The last two are constants from the second degree polynomial kernel K(a,b)= s x $(a.b)^2$+r .

Testing Data and Results

- Data from simple SOC tests and dynamic SOC tests are done to obtain robust results.
- Optimal SVM tested with simple step input drive cycle; root-mean squared error is 5%, max. +ve error is 16% and max. –ve error is -9%.
- Optimal SVM tested with US06 driving cycle; root-mean squared error is 5.76%, max. +ve error is +12% and max. –ve error is -2%.
- A root-mean squared error closer to zero means that the model is a better predicitor.

The optimized SVM was implemented on an inexpensive 8-bit PIC18F8720 microcontroller running at 20Mhz and the SOC was computed in about 54ms. In a related work, Wang Junping et al [73] produced a research which models an 80Ah NiMH battery pack in order to estimate its SOC. The least square (LS) SVM algorithm was used for non-linear dynamic estimation of battery SOC. The model has 3 inputs (charge/discharge current, temperature and SOC) and one output (load voltage). In battery testing, the FUDS test cycle was used to charge and discharge the NiMH battery pack with the capacity of 80 Ah. Using a training set of 3000 data pairs, the SVM model with the RBF kernel was obtained. Testing was carried out with 6500 data pairs and the maximum relative error recorded was 3.61%. This shows that the

SVM model can simulate battery dynamics reasonably well even with small amounts of experimental data.

Variation in vehicle speed and acceleration represents driving behaviour which in turn determines the energy required to propel a vehicle [57]. In real life, driving behaviour is always constrained by traffic and road conditions, hence methods capable of modelling various generic driving behaviours are critical to trip oriented energy management systems.

An optimal power management system (PMS) was proposed for HEV's by utilizing the knowledge of future terrain and traffic conditions which will make more judicious use of the available electric energy [58]. While HEV experts acknowledge that such information can increase fuel or energy efficiency in vehicles, it has not been implemented yet. The figure below provides an overview of a predictive energy management system based on 3D terrain maps.

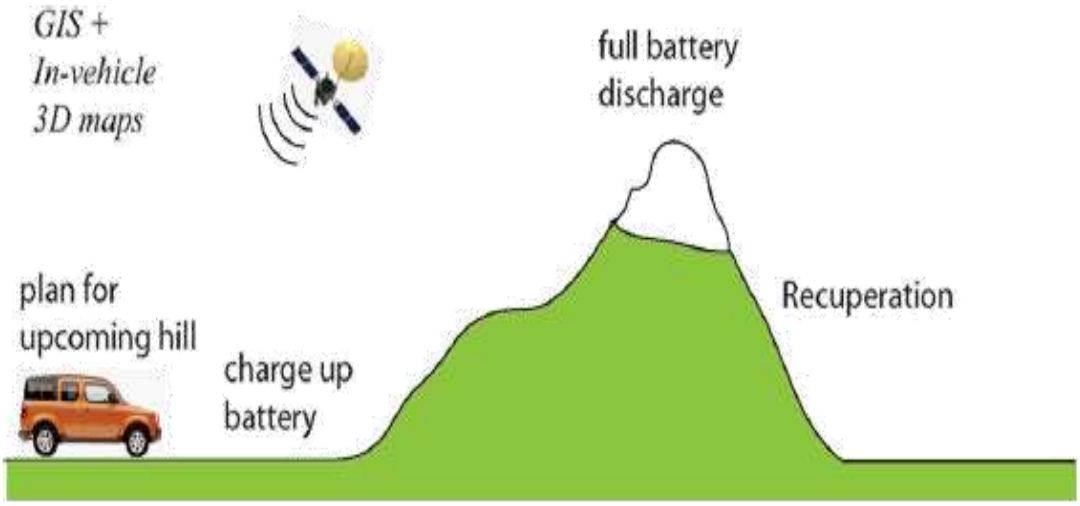

Fig. 28: Forecasting energy usage in HEV based on 3D terrain maps (Source Chen Zhang et al [58])

Rui Wang et al [59] identified three main techniques that were used to classify and predict future driving conditions. These are by using GPS or intelligent transport systems (ITS), statistical clustering analysis method and Markov chain based on stochastic process prediction technique. If the origin and destination of a trip is known a priori, GPS could be a useful tool for providing terrain information as described in [58]. In a series HEV, GPS data was used to predict the approximate driving distance, upcoming terrain data along with an estimated velocity [60]. Using a rule based strategy, 13% reduction in fuel consumption as well as 8% cost reduction was achieved. Statistic and clustering based classification involves collecting certain historical and current driving cycle parameters in order to predict the future pattern, typically 1-2 minutes ahead. Several literatures have identified various driving parameters or statistic features which affect the rate of fuel consumption and emissions. [61] Identified 10 parameters while [62] pointed out up to 62 parameters in total and classified them into 16 groups. On the other hand, [63] proposed only 2 parameters (average trip speed and distance per stop) which were used to cluster driving cycles into highway, suburban and urban respectively. The issue here is not the number of parameters identified, it is rather at what cost it comes at. Too many cause higher hardware cost and longer computational time which makes it not feasible to implement on board vehicles or in real time; on the other hand, too few parameters may misrepresent or misclassify driving conditions. Recent literature on this subject matter indicates that a reduction in the number of parameters is desired for real-time implementation and also maintaining good prediction accuracy. Rui Wang et al [59] concluded from extensive study that, ultimately, some parameters seem to be more prominent than others. They are

average speed, average acceleration/deceleration, maximum acceleration, maximum velocity, minimum deceleration and standard deviation of acceleration.

In a work related to this report's particular research interests, [48] relates battery/powertrain performance of an electric vehicle to its driving and usage patterns. A duty cycle in this work refers to a history of power usage of a vehicle i.e. power versus time curve while a drive pattern was used to describe a driving condition taking into account both road condition and driving behaviour. Time stamped trip data and charging data was collected by an automated on-board data acquisition device in a flash memory card during operation of the Hyundai Santa-Fe battery powered electric vehicle.

Drive cycle is broken down into a series of sequential isolated *drive pulses (DP)*. This paper defines the DP as an active driving period between two continuous stops in a trip. Distribution plot of Average speed Vs Distance is used as a basis to develop fuzzy logic membership functions and fuzzy rules to classify driving events using the variables of average speed and distance. By classifying a driving event for each DP, a drive cycle profile can be constructed. Driving events: STOP N GO (SnG), URBAN (U), SUBURBAN (SU), RURAL(R), HIGHWAY (H). The fuzzy rules for classifying driving events were manually tweaked until a proper interpretation of driving cycles among all trips in the database was achieved. The figure below is an example of how the fuzzy logic pattern recognition was used to categorize a drive cycle into the 5 driving events.

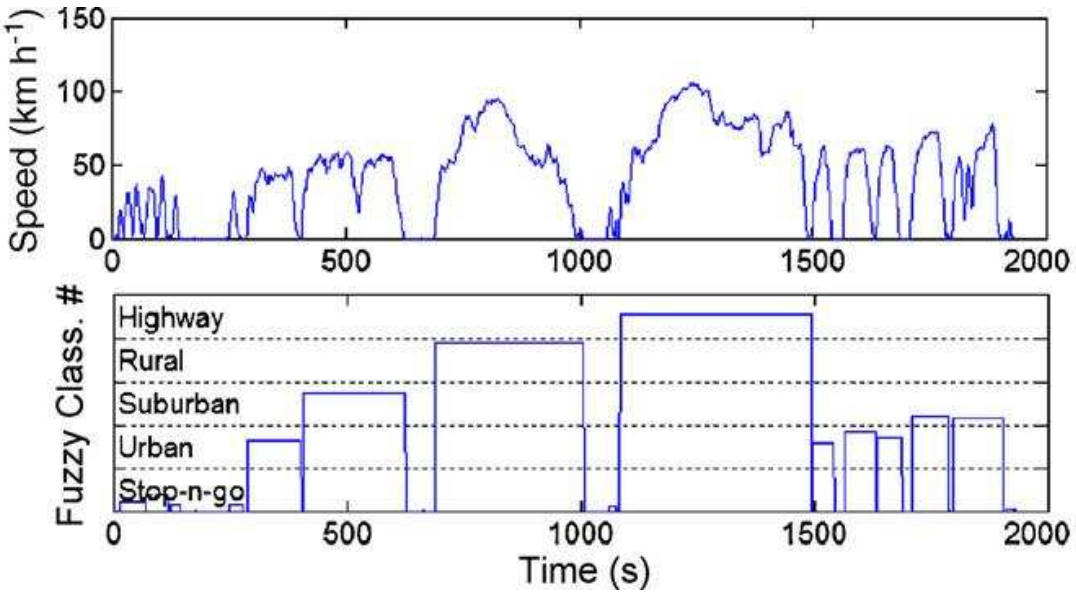

Fig. 29: Drive cycle analysis; fuzzy classification of drive pulses (DP).Source B.Y. Liaw et al [48].

The concept of microtrips was introduced by Shuming Shi et al [49], defined as the speed time profile between successive stops in a drive cycle. Principal component analysis (PCA) and fuzzy clustering was used separate real world drive data into microtrips. Interestingly raw velocity-time data was collected using Global Positioning Satellite (GPS) system as opposed to the traditional sensor system. Fifteen statsistical metrics/features based on previous research were chosen for cluster analysis. The core idea of PCA being dimension reduction as there is a certain correlation between these statistical features such that a linear combination could represent the majority of the whole original feature set. Principal components of microtrips corresponding to eigenvalues with a high sum of contribution rates were selected to represent information of all the original 15 metrics with a reduction in dimension. Results of the fuzzy clustering produced an optimal cluster

number of 11. Similarity was found between driving characteristics of the same cluster, but great difference exists among driving characteristics of different cluster.

PCA was applied to get the most valuable coefficients from the data of drive cycles which can be used as control input variables for intelligent control strategies for HEVs by JianFu et al [50]. Statistical software was used to lower the dimension of the weight factors which correlate with fuel economy in HEVS. Here, 14 metrics were used to describe driving data. Time, distance, max speed, average speed, maximum acceleration, maximum deceleration, average acceleration, average deceleration, idle time, number of stops, maximum up gradeability, average gradeability, maximum down gradeability, average down gradeability. Drive cycle data can be quite redundant and finding a correlation between metrics of the data can be complicated. The feasibility of PCA was verified using Kaiser Meyer Olkin KMO and Bartlett's test. Three principal components instead of multi-dimensional variables were derived and would be used for an intelligent control strategy to reduce fuel consumption in HEVs.

Chan Chiao et al [51] tackled power management in hybrid electric vehicles from a stochastic viewpoint. A design method for the power management control algorithm for hybrid electric vehicles was developed by using Markov chain modeling and stochastic dynamic programming techniques. The driver power demand was modeled as a Markov process to represent the future uncertainty of the driver power request under diverse driving conditions. As opposed to deterministic optimization over a given driving cycle, the stochastic approach optimizes the control policy over a family of diverse driving patterns. The infinite-

horizon SDP solution generates a time-invariant state-dependent power split strategy, which governs the engine and battery operations. The algorithm can be directly implemented in simulations and vehicle testing. Simulation results indicate that the SDP control strategy achieves improved performance in almost all driving scenarios over the sub-optimal rule-based control strategy which is trained based on deterministic DP-results. Furthermore, the proposed approach provides a directly implementable control design path, which is highly desirable because of its potential for a fully integrated optimal design and control process.

Genetic Algorithm (GA) was used to tune the parameters of a fuzzy logic controller based on similar driving pattern recognition and prediction for the energy management of a HEV [52]. The concept of micro-trips described in previous work was used. Driving pattern was classified based on the distribution of average speed for all collected microtrips; Congested condition (Average speed <7kph), urban (Average speed 7-15.5kph), Extra urban (15.5 – 23.5kph) and highway (> 23kph). A driving prediction model which contains traffic conditions of driving data history either offline or real time was proposed in this work using hidden markov model (HMM). In the case of an online (real time) operation, new driving experiences are used to update the model constantly. HMM is a popular stochastic tool for studying time series data. The control strategy was based on changing the membership function of the fuzzy logic control in response to changes in driving condition. The objective function to be minimized in this case was the integral of fuel consumption and engine emissions over a drive cycle. An appropriate fitness function was chosen to evaluate the status/fitness of each possible solution to the optimization problem. More information about the GA parameters used can be obtained from [52]. Finally,

simulation results show the effectiveness of the approach where reduction in the fuel consumption is achieved.

The concept of self learning of driving cycle was described in this work [53]. Real time speed profile was collected by an in vehicle device and a statistical analysis was done to calculate 28 characteristic parameters of the drive cycle. These were used as inputs to a self organizing map (SOM) to classify into clusters of one of three drive cycle representatives. The result of the classification was used to manipulate the driving control strategy accordingly for optimum performance. Self learning here means the use of a general packet radio service (GPRS) to transmit drive cycle data and also receives control parameter updates in real time.

On a rather theoretical level, several researchers have developed energy management and power management techniques that apply priory information regarding the vehicle propulsion power demands. These methods do provide a means to identify the maximum obtainable improvements in terms of energy efficiency and performance benefits. The findings also clearly support the grounds for further research in this area. However, in spite of significant contributions, there have not been many attempts to address the complete implementation process of a working system. The figure 30 sums up the literature survey.

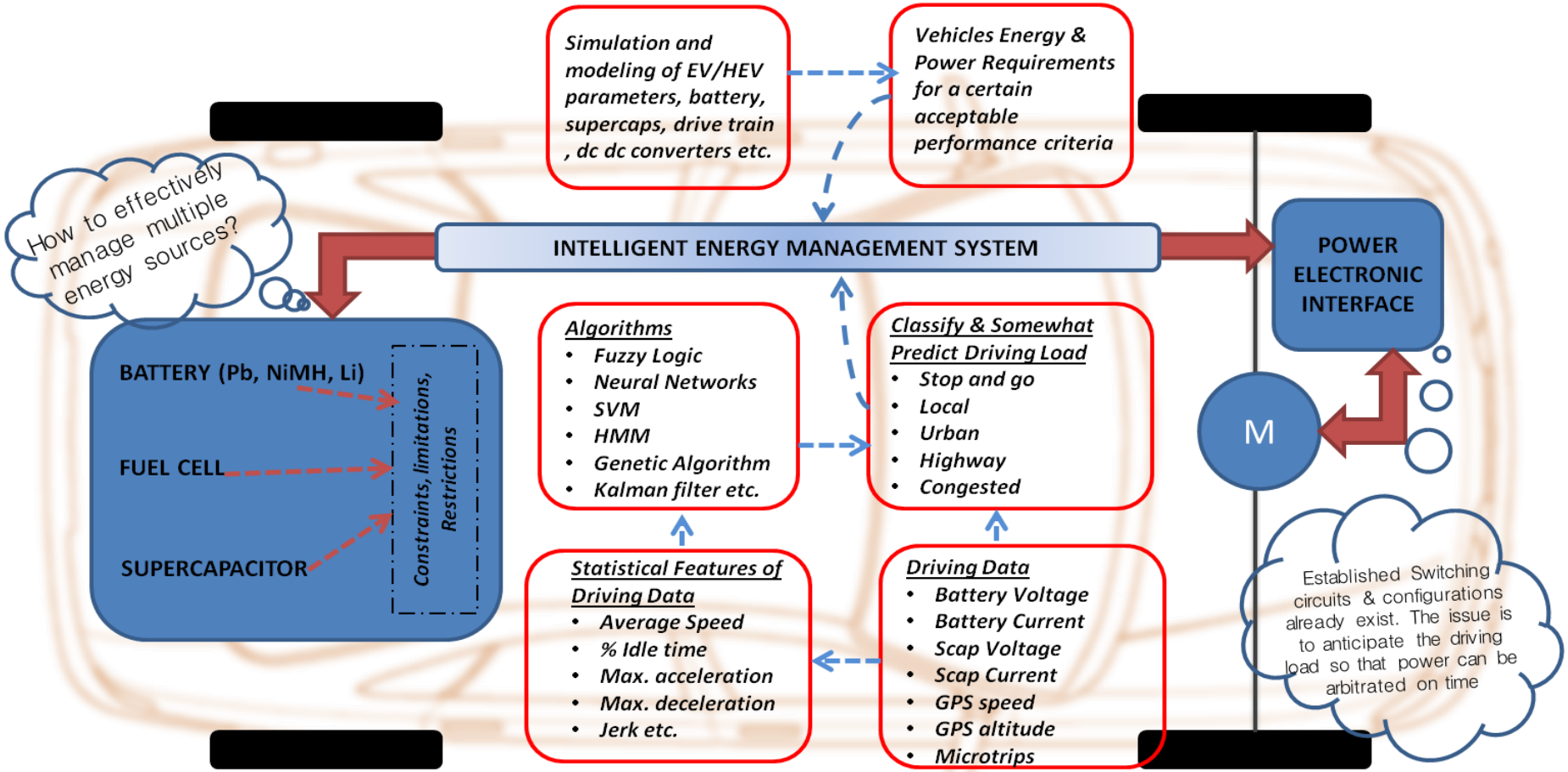

Fig. 30: A mind map of the literature review conducted during the course of this research

CHAPTER 3: METHODOLOGY

This chapter begins by describing the equations governing the movement of an electric vehicle on a level or inclined road surface. The propulsion system has to overcome certain forces (which consists of various components) in order to accelerate or retard the vehicle.

Using these equations, various software models were developed in MATLAB Simulink © environment in order to simulate the performance of the proposed experimental test electric vehicle conversion.

The third section of this chapter describes the step by step design and construction of the experimental test vehicle. Mechanical effort such as engine removal, motor coupling, battery and supercapacitor mounting are described. Also, the traction and control wiring, sensor setup, data acquisition system, on-board real time display of circuit parameters were laid out in detail.

The section that follows is the on-the-road test of the electric vehicle along a fixed route in the university premises and important drive cycle data is collected and stored for analysis. Statistical feature extraction of drive cycle data by dividing driving data into suitable “microtrips” was done and also the description of driving conditions based on statistical features of microtrips (i.e. urban, highway, stop and go, idle).

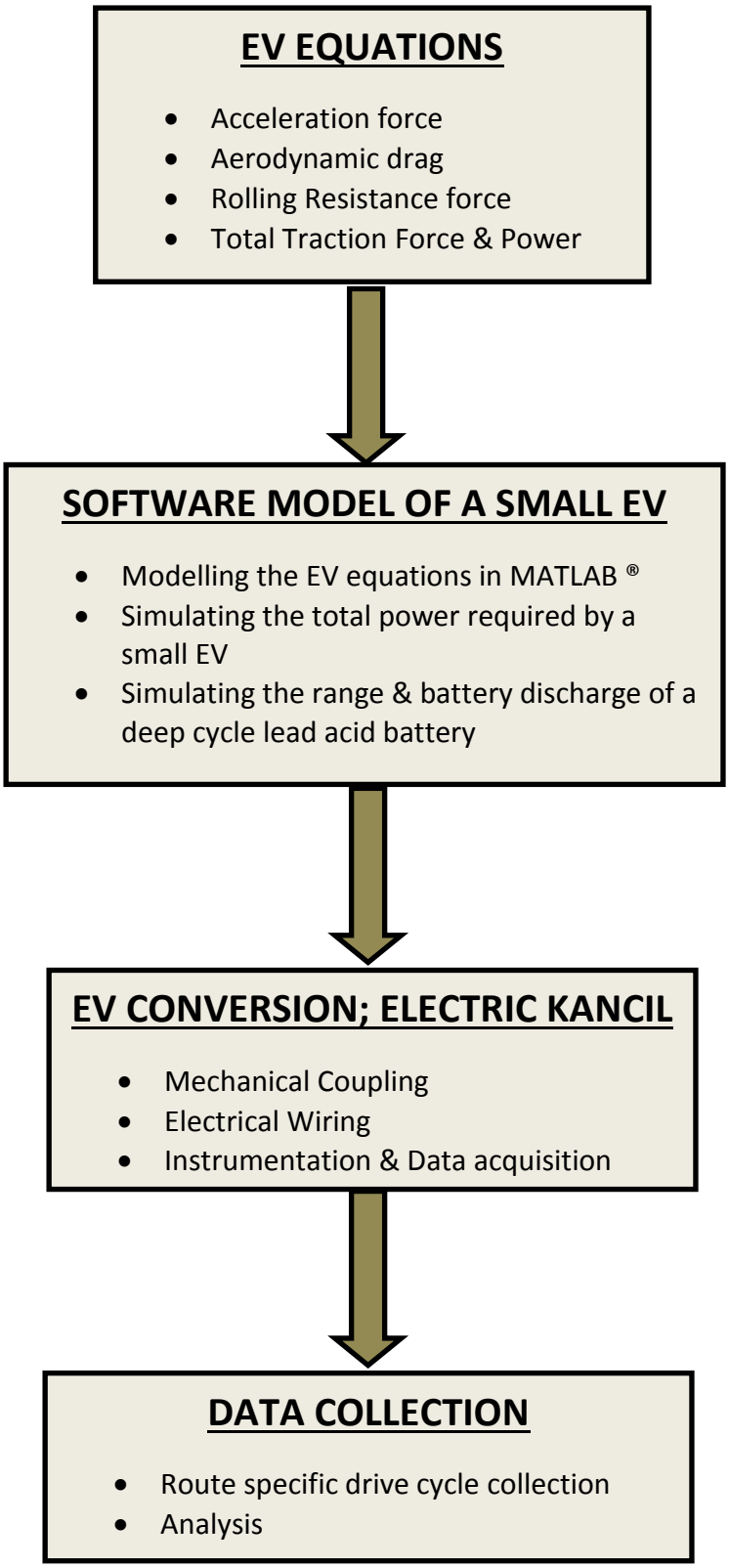

Fig 33: An Overview of Chapter 3

3.1 EV DESIGN CRITERIA

The design of an electric vehicle should be based on the most important task it is required to accomplish; a high speed (performance) car, a long range vehicle or a utility commuter vehicle midway between the two i.e. with reasonable performance and acceptable range.

An electric vehicle should be as light in weight as possible, streamlined with its body optimized for minimum drag, minimum rolling resistance from its tires, brakes and steering, and optimized for minimum drive-train losses [3].

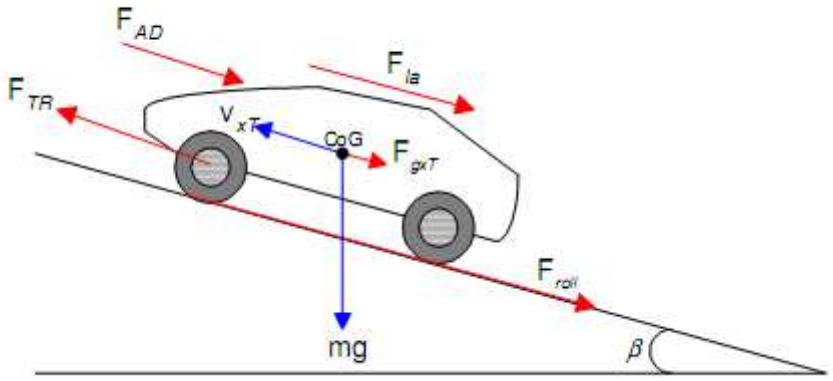

Fig 33: The forces acting on a car (Adapted from L.C Rosario [54])

Figure 33 above describes the forces that a vehicle is subjected to as it tries to accelerate or decelerates. These forces consist of several components and are described below:

Acceleration force (F_{La})

This force is derived from Newton's second law of motion.

$$F_{La} = m\frac{d}{dt}V_{xt}(dt) = ma$$

Where *a* is the linear acceleration of the point mass *m* travelling at a varying tangential velocityV_{xt}.

Weight (mg)

Weight affects acceleration, climbing, range and speed of the vehicle. F_{gxT} is the gravitational force acting on the vehicle on non-horizontal roads. When the vehicle is on a level road, this force is very close to zero.

$$\mathrm{F_{gxT}} = \mathrm{mg\sin\beta}$$

An uphill acceleration of the vehicle results in a positive force while a downhill motion results in a negative force.β is the angle of inclination

Aerodynamic drag of a vehicle F_{AD}

This part of the force is due to the friction of the vehicle body moving through the air. It is a function of the frontal area, shape, protrusions such as side mirrors, ducts and air passages, spoilers, and many other factors. Vehicles with internal combustion engines didn't need to be aerodynamically perfect as they packed enough horsepower at their disposal. However, batteries only provide about one

percent as much power per weight as gasoline and as such EVs need to be more aerodynamically aligned. The aerodynamic drag force can be expressed as:

$$F_{AD} = \frac{1}{2}.\rho.C_{d.}A.Vxt^2$$

A is the vehicle equivalent frontal area in m^2; the effective area a vehicle presents to the onrushing air stream. $C_{d.}$ is the coefficient of drag and it has to do with streamlining and air turbulence flows around the vehicle. The coefficient of drag is a measure of how easily a vehicle slides through the air. These characteristics are inherent in the shape and design of a vehicle. Typical values for C_d include: Cars 0.30 – 0.35, Vans: 0.33-0.35, Trucks: 0.42-0.46. It should be noted that modern vehicles may have lower or even higher coefficients, for example the Toyota Prius has a C_d of 0.26. Lowering the coefficient of drag is very desirable even in internal combustion engines as it helps to save fuel. An optimized electric vehicle with a very low C_d should have a finely sculptured rear, covered wheels, thin tires, enclosed underbody, and low nose with sloping windshields. Vxt is the vehicles speed ; since drag depends on velocity squared, increasing speed can have a dramatic negative effect. ρ is the air density in kg/m^3, a typical value would be 1.25 kg/m^3.

Rolling Resistance (F_{roll})

The rolling resistance is primarily related to the tires of the vehicle and secondarily related to the bearings and gears. It is a constant usually approximated and is independent of the vehicle speed. The rolling resistance force (F_{roll}) is given as:

$$F_{roll} = \mu_{rr}.mg$$

Where μ_{rr} is the coefficient of rolling resistance. The main factors controlling μ_{rr} are the type of tyre and the tyre pressure. μ_{rr} is estimated at 0.015 on a hard surface (concrete), 0.08 on a medium hard surface and 0.30 on a soft surface (sand) [Bob Brant]. Tires support the electric vehicle and battery weight while cushioning against shocks; develops front-to-rear forces for acceleration and braking and develop side-to-side forces for cornering. Ideally EV tires should be thin giving little contact area with the road, hard, and large diameter (higher mileage).

Total Tractive force F_{TR}

This is the minimum force required to move a vehicle from standstill and it is given as:

$$F_{TR} = F_{la} + F_{gxT} + F_{roll} + F_{AD}$$

The instantaneous traction power P_{TR} can be expressed as:

$$P_{TR}(t) = F_{TR}(t).V_{xt}(t)$$

If $P_{TR} > 0$ then the vehicle is in traction mode with positive traction

If $P_{TR} < 0$ then the vehicle is in braking mode with negative traction

If $P_{TR} = 0$ then either vehicle is coast mode (resistive forces equal to change in kinetic energy) or the vehicle is at rest.

3.2 SOFTWARE MODELLING OF A SMALL ELECTRIC VEHICLE

Based on the equations described in the previous section, a custom routine was written in MATLAB® m-file to estimate the instantaneous traction power of a small electric vehicle (see appendix for detailed matlab code). The input to this model is the New York drive cycle (NYCC) which features a mainly low speed, idle and stop-go condition. This drive cycle is ideal for this research work because the electric vehicle to be developed in the next section will be tested on a similar route. The outcome of this model is important because it serves as a yardstick for sizing the electric motor and batteries which will be used in order to meet the traction power demands of the vehicle.

The parameters for a typical small EV are assumed as follows:

Cd (coefficient of drag) = 0.19 A (frontal area) = $1.8m^2$

Urr (rolling resis. Coeff) = 0.015 Mass of Vehicle + 2 Passengers = 820kg

Tire radius = 0.261m 155/70R12 n_g (estimated gear efficiency) = 0.91

Density of Air = 1.25 kgm^{-3} Road gradient = 0^0

In order to account for losses in transmission, gears, electric motor, accessory devices, etc, a total system efficiency of 91% was used to simulate the model. From the figure below, a peak power of 17.08KW was recorded and an average non idling power of 7.23KW. This means that a motor with an average power rating of between 8KW and 10KW with a peak of up to 20KW would be suitable to propel this vehicle in question.

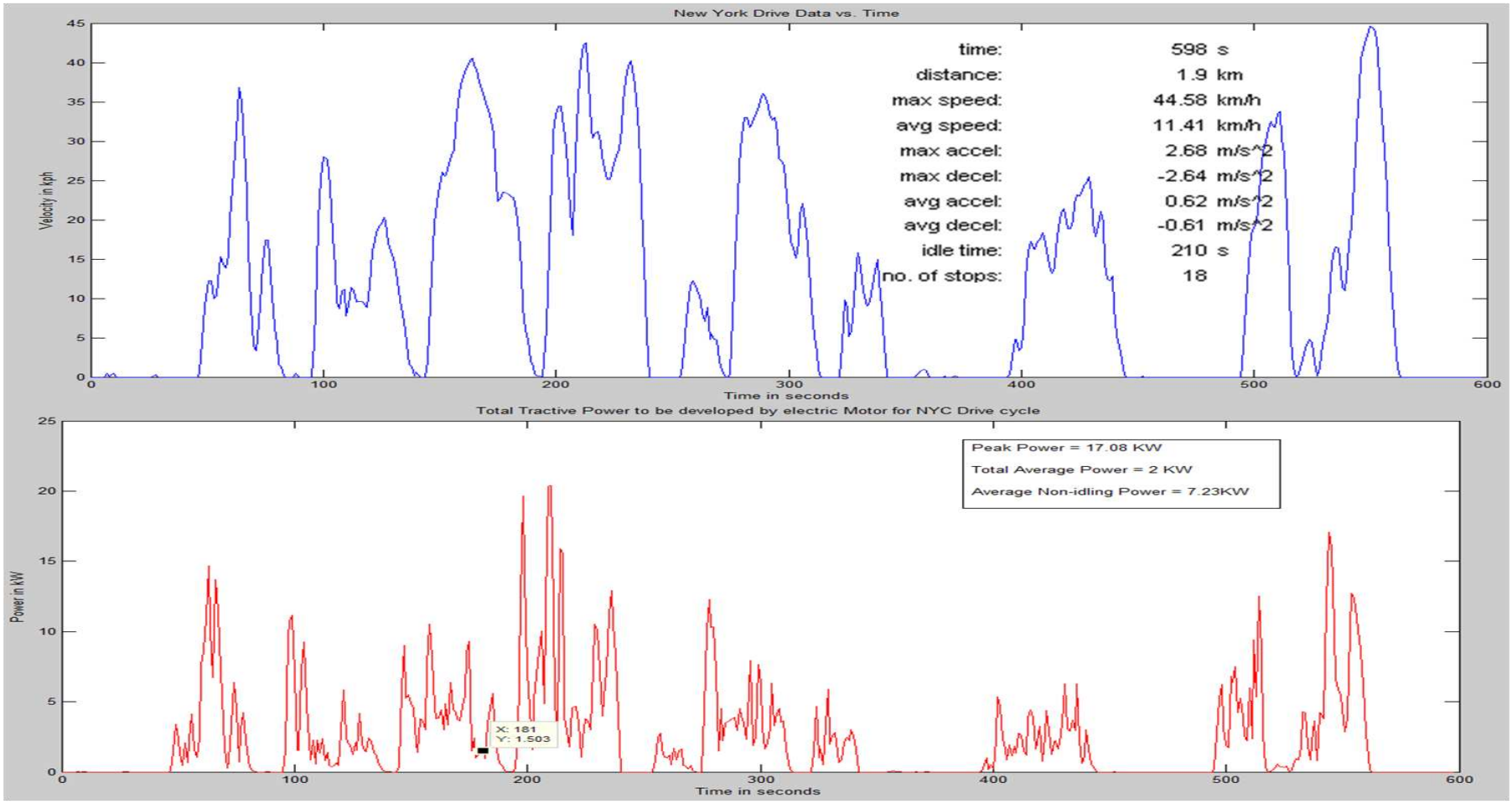

Fig 34: Simulating the Power (KW) needed by a Small Vehicle for low Speed Drive Cycle

The power required to make the vehicle move at a certain speed as described by a drive cycle in the figure above, directly relates to electrical power required by the electric motor from the battery pack. A deep cycle lead acid battery pack is simulated by coding the equations to calculate its open circuit voltage, state of charge and depth of discharge in matlab which have been described in chapter 2 of this work. Also the current which is drawn from the battery when it is operating at a certain power was simulated (see appendix for code).

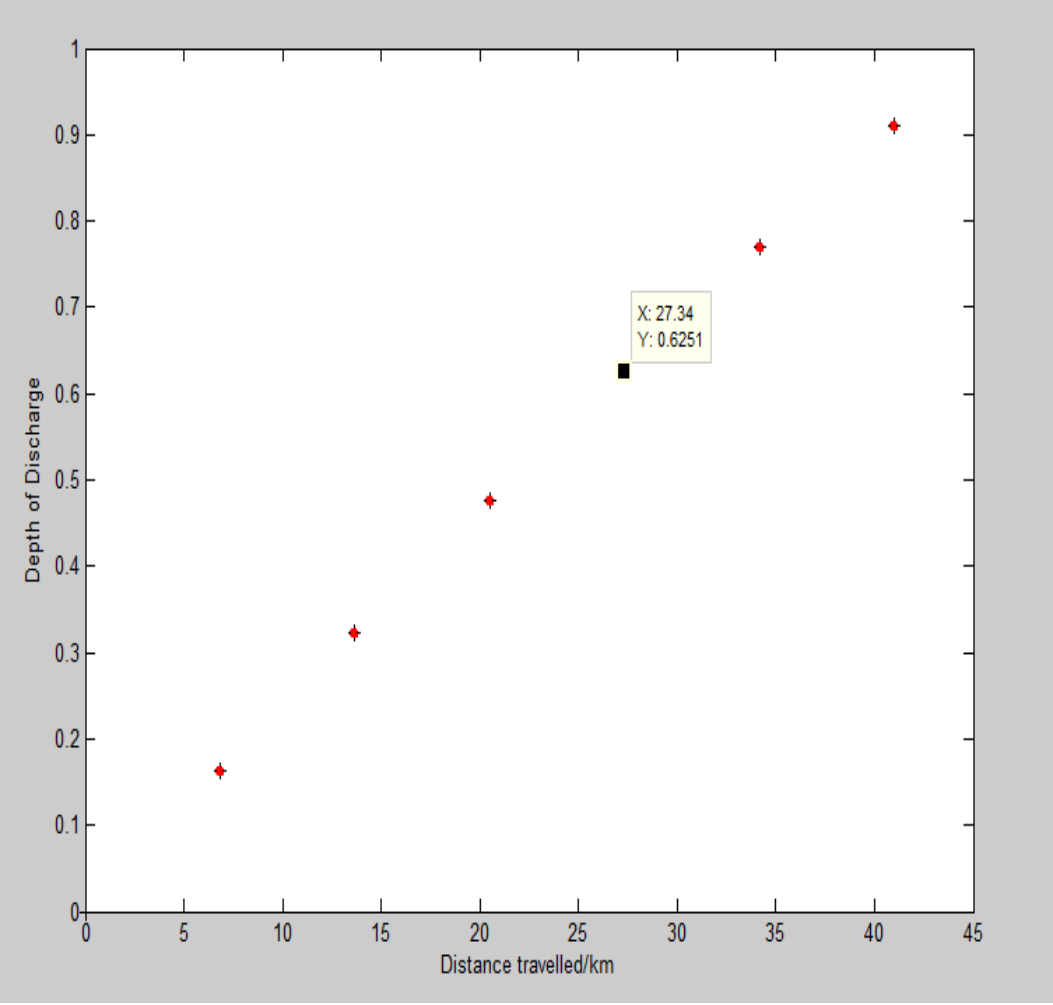

Fig 35: Simulating the Depth of Discharge of a Lead acid Battery pack versus distance travelled (range)

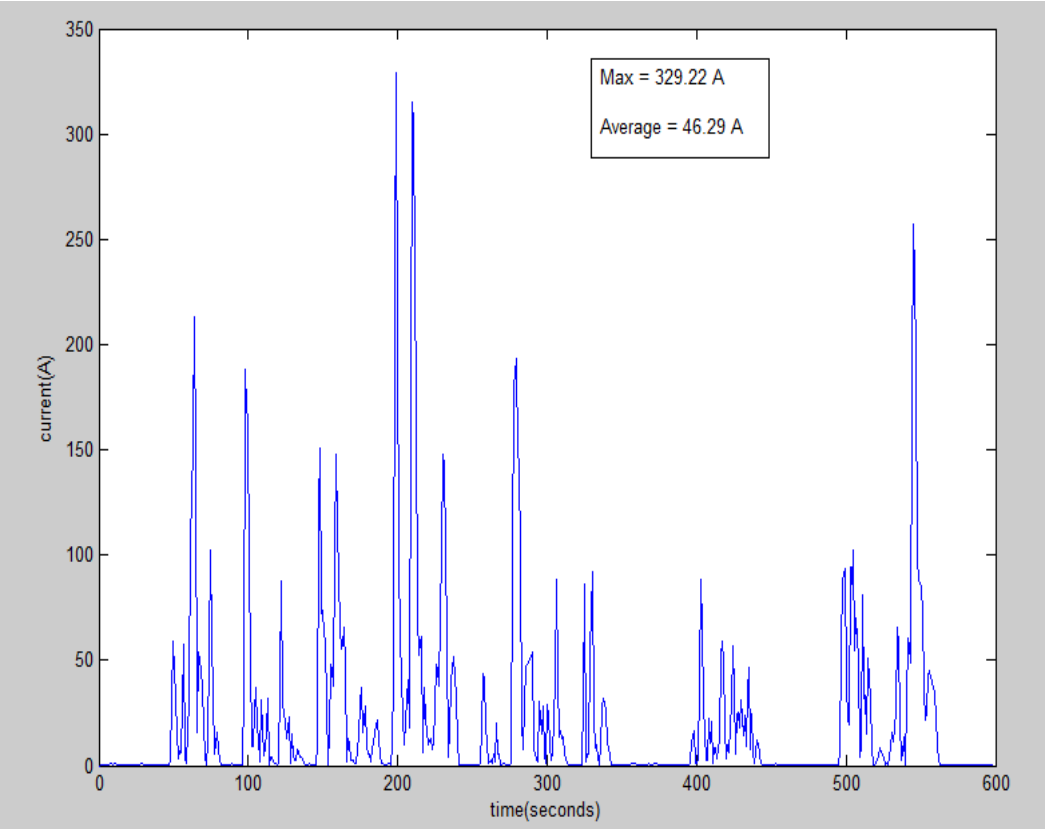

Fig 36: Simulating the Current drawn from the battery pack @ 48V 207Ah

Usually deep cycle batteries are designed to be discharged from 50% to 80% of its rated capacity [113]. They can be discharged down to 20% but this is detrimental to the health of the battery. A healthy 50- 60% is usually desirable. From the figure 35 above, the simulated EV can do a 27km route with the depth of discharge at about 62% i.e. remaining charge is 38%; again following the New York drive schedule. The current drawn from the battery pack reached peaks of 329.2 amperes. Assuming instantaneous battery voltage of 48V, this roughly estimates the peak power demand as 15.8KW and average power of 2.2KW.

The Modeling of the basic parameters or performance criteria of a small electric vehicle using matlab® has put things into perpective regarding the conversion of a small city electric vehicle.

3.3 INTEGRATION OF SUPERCAPACITORS INTO EV

This part of the project aims at proving beyond any reasonable doubt that the integration of supercapacitor banks into electric vehicles is justified by the following performance criteria.

(1) A significant improvement in battery life.

(2) Increase in range per charge

(3) Improved acceleration

In order to achieve the objectives above, we have to create a platform or basis on which testing, research and development can be carried out. The testing of the various system configurations may be done exclusively through software. The cost is relatively low as the resources needed are computers and specific software to carry out the simulation such as ADVISOR, PSAT, PSIM and VTB. Several researchers have already carried out similar simulation studies [105], [106], [107], [108]. In general, this procedure is simpler than the rest of approaches, but is also less accurate due to the impossibility to compare it to real world measurements. Most research simulations on EV configurations just end there without any real hardware implementation or breakthrough.

A test bench may be setup to emulate an electric vehicle drive performance. The test setup can be roughly divided into four main components: a dynamometer (programmable load motor), a real time data acquisition & processing system, power source (batteries + supercapacitor), and the electric propulsion system; motor under test (electric motor). This could be termed as a Hardware-In-the-Loop

(HIL) simulation where part of the system is real hardware (batteries, supercapacitor, dc dc converters) and part is software or artificially simulated (electronic load to emulate real world driving conditions). The figure below shows a sample EV test bench which may be used for this project. On-road tests sometime are not always possible to thoroughly test each sub system. These tests are likely done during very later phase. It is not easy to change too much configuration of the propulsion system on a test vehicle.

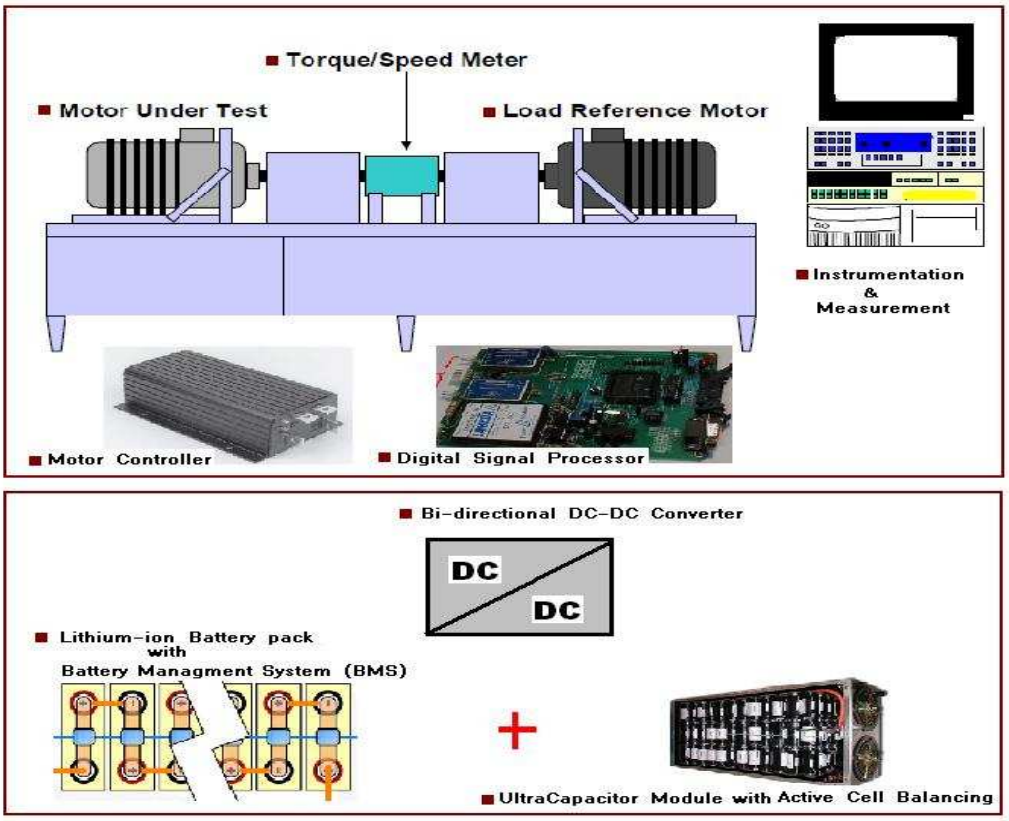

Fig 37: Setup for a Sample Electric Vehicle laboratory Test Bench

For the purpose of this research work, real EV capable batteries, motor and supercapacitor module would be purchased. However, it was discovered that a single piece of equipment which is able to emulate the driving load of a real world EV (programmable load) was beyond the research group's budget at the time. An experimental test vehicle would be constructed; basically a conversion from a

conventional ICE to electric. It would be fitted with state of the art data acquisition system which monitors the interaction between the energy and power sources as it tries to fulfil the load requirements of the vehicle. In this case, the load on the propulsion system comes from 100% real world driving. The only downside envisaged from this setup is the inability to replicate the exact same driving pattern over a fixed route.

As a preliminary work, an electric bicycle to be powered by a battery - supercapacitor hybrid combination was implemented. This is a scaled-down version of the actual electric vehicle to be implemented. Details of this work can be found in appendix c of this report.

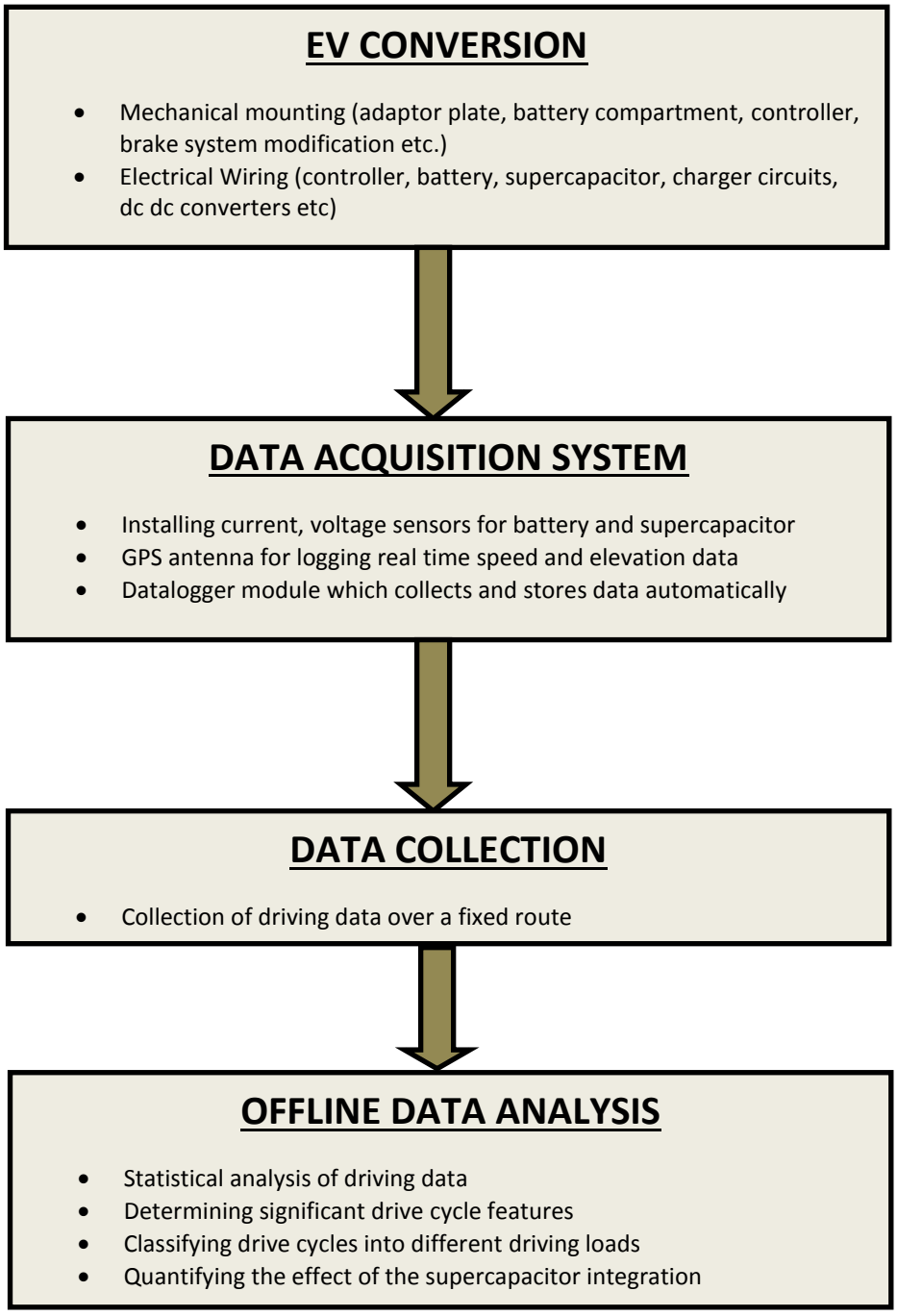

Fig 38: Work flow for EV conversion

3.3.1 Experimental Test Vehicle

Being a pioneer researcher on electric vehicles at the University of Nottingham Malaysia campus, generating interest or general awareness about electric cars among undergraduate students as well as faculty members becomes important in order to build a good research team for the future. Hence the decision to build an actual electric vehicle by converting a regular compact ICE city car was reached.

A considerable effort of this research work has been dedicated towards the development of an experimental vehicle to serve as a setup for investigating the effects of supercapacitor integration into electric vehicles. This section describes the experimental vehicle and the corresponding energy storage systems; deep cycle lead acid batteries and supercapacitor bank. Starting form a pure battery driven vehicle, the energy system was then augmented with the addition of a supercapacitor bank. Apart from manufacturer's information, there is very limited experimental data on supercapacitor field testing. As such, the vehicle provided a means to obtain unbiased empirical data to substantiate research claims and also to serve as a test platform for further work. Most of all, it provided a hands on experience.

A famous city car in Malaysia, the *Perodua Kancil, was* chosen for conversion into a fully electric vehicle due to its light weight, readily available spare parts and also suitability for a lower voltage conversion. It has a 660 cc (1997 model), three cylinder carbureted engine rated at 31 Hp (22.1KW), other specifications can be found below:

length	**3365mm**		**Engine**	**659cc, water cooled , 4 stroke, in-line 3 cylinder**
Height	1405mm		**Max Output power**	22.8 KW (31hp) / 6400rpm
Wheel base	2280mm		**Max Torque**	49Nm /3200 rpm
Kerb weight	681 kg		**Fuel system**	Carburetor; 32 liter fuel tank
Seating	5		**Power train**	Clutch, 5-speed Manual
Coeff. Of Drag	0.37		**Tires**	155/70R12
Frontal Area	$1.69m^2$		**Gear ratio**	1^{st}: 3.500 , 2^{nd} : 2.111 , 3^{rd}: 1.392, 4^{th} : 0.971, 5^{th}: 0.794, Final: 4.722

Table 4: Technical Specifications of the Perodua Kancil [100]

The first stage in any EV conversion is usually very mechanical. This involves removing the engine block totally from the vehicle which will make way for the electric motor. Also, the fuel tank was taken out and there was a weight reduction of about 150kg. Battery racks made of solid cast iron were fabricated and fitted to the rear compartment of the vehicle as shown in the figure below. Eight (6V, 225Ah) Trojan T105 deep cycle flooded type lead acid batteries were connected in series to produce a 48V, 225Ah battery pack. The overall weight of the battery pack was 240Kg; concentrated in the rear compartment due to convenience of installation and lack of space in the front compartment. However tougher coil springs were used instead of the normal springs installed in the vehicle in order to reinforce the rear suspension. The performance curves for the Trojan battery are simulated in the curves below.

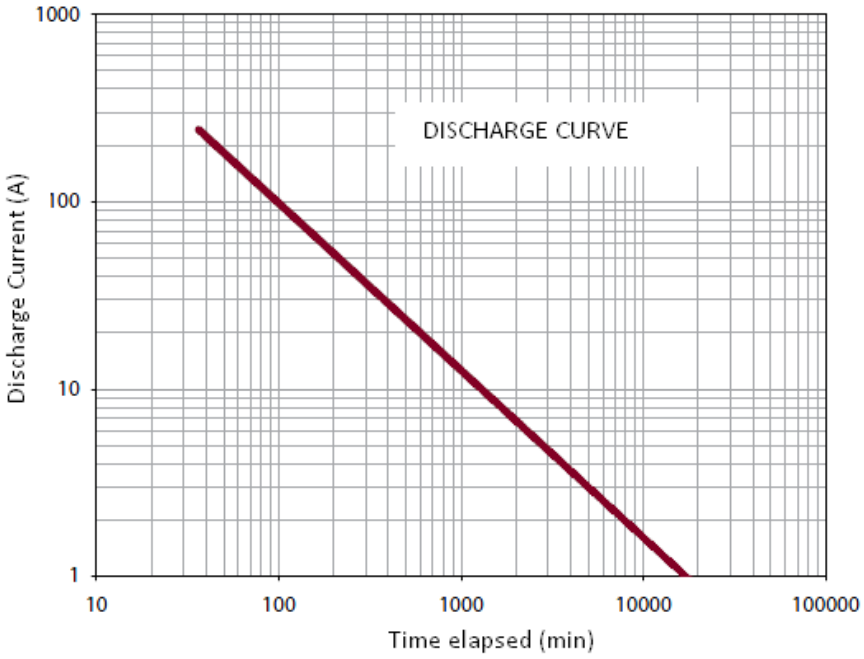

Fig. 39: Estimated Discharge Curve for Trojan T105 deep cycle battery

From the curve it can be deduced that for a constant discharge rate of 100A, the battery is able to sustain the load for approximately 100 minutes. Also if it is discharged between 40%-70% of its capacity, estimated cycle life is 800 – 1500 cycles.

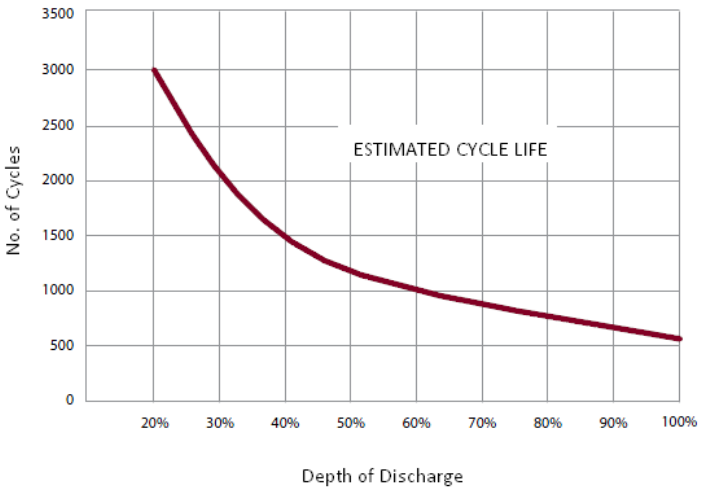

Fig. 40: Estimated life cycle Curve for T105 battery

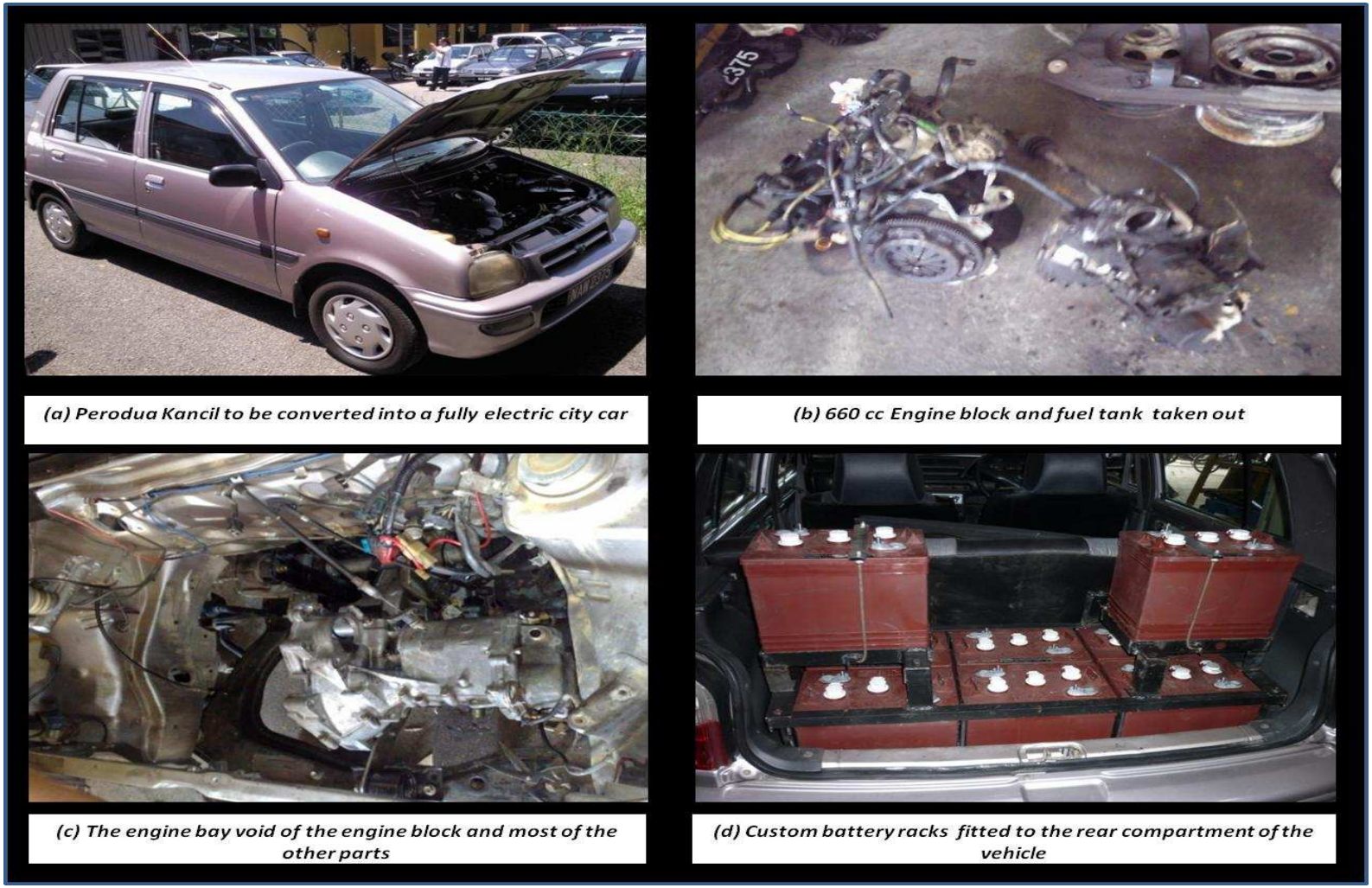

Fig 41: Mechanical Part of EV Conversion

3.3.2 Electric Motor Mounting & Coupling

In an internal combustion engine (ICE), the clutch is used to disengage the transmission from the engine (idle) and also to bring the vehicle up to speed in gears. An electric motor's RPM can be easily varied from zero to maximum at full torque eliminating the need for a clutch and also the flywheel which is used for building up inertia between the power strokes of the ICE. Hence drivability is only about shifting from second to third gears without a clutch which many cars can do rather smoothly.

The clutch, flywheel and pressure-plate assembly was removed and the electric motor was attached directly to the transmission input shaft by using a custom made adapter plate. The plate itself bolts to the transmission, a spacer if required, and a coupler or hub to connect the shaft of the motor to the transmission shaft. One side of the coupler was attached to the electric motor by a keyed shaft while the other end was fitted with a splined shaft to match the spline on the drive shaft coming from the gearbox. This provided a simple yet sturdy coupling of the electric motor to the clutch- less transmission which is capable of transmitting a large torque .Custom-made adaptor plate was fabricated with 5/8 inch hardened steel that mates the electric motor to the original transmission by matching the bolt pattern of the transmission on one side, and that of the motor on the other side. It must hold the motor shaft in exact alignment with the transmission shaft. The original mounting points to the chassis of the car were used where possible, similar mounting points were created using standard engine mounting rubber. The motor

was finally placed in with the help of a jack and then locking the mounting points in place.

Fig 42: Electric Motor with coupler (center), custom made adaptor plate (top right) and a spacer (bottom left).

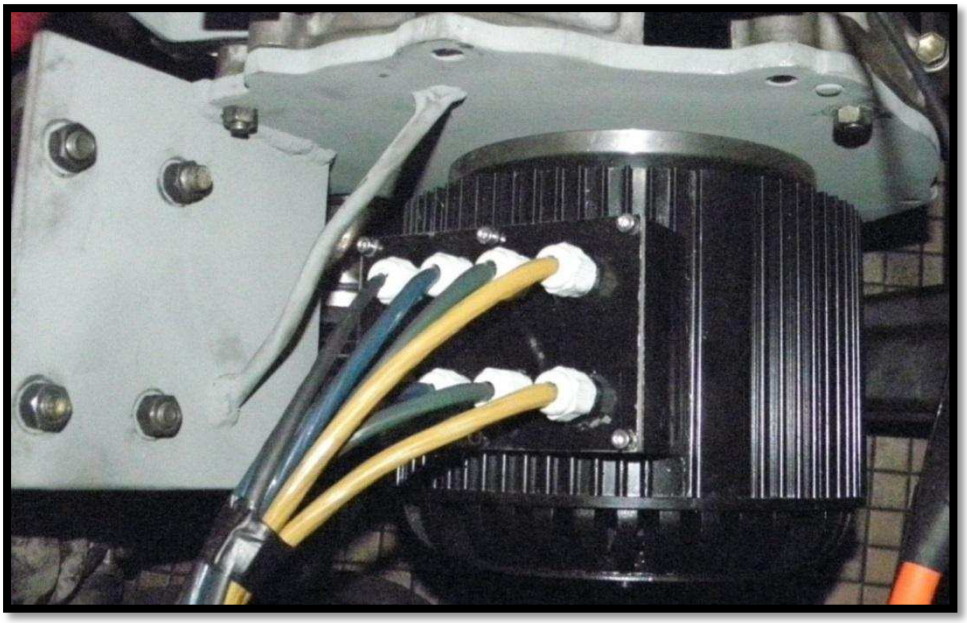

Fig. 43: Brushless DC Motor successfully mounted, adaptor plate matches the bolt pattern of the original transmission block. Reinforcement bracket is added to make the mount more stable.

The controller was mounted very close to the front grill of the vehicle as shown in the figure below on an aluminium heat sink plate. The vehicle will not be driven during wet or rainy conditions hence there was no need to make the controller waterproof.

Fig 44: 500A Motor Controller successfully mounted in the same position as the radiator of a conventional vehicle

3.3.3 Electrical Wiring

After all the main mechanical conversion part was done, the next stage was to wire it all up. The table below lists out all the parts which were used for this conversion and their specifications.

	Equipment /Part	Specification
1	Golden Motors HPM-1OkW Brushless DC Motor	• Model: HPM-10KW -- High Power BLDC Motor • Voltage:48V/72V/96V/120V • Rated Power:8KW-20KW • Peak up to 20KW • Efficiency: 91% • Phase Resistance (Milliohm): 3.1/48V; 6.0/72V; 18.0/120V • Phase Induction(100KHZ): 34uH/48V; 77uH/72V; 252uH/120v • Speed: 2000-6000rpm (customizable) • Weight:17Kgs Casing: Aluminium • Length (height): 170mm Diameter: 206mm
2	HPC Series Brushless DC Motor Controller	• Voltage Ranges:48V(~60V)/72V(~90V)/96V(~140 V)

		• Rated Current (Max):500A • Weight:2.9Kgs Dimensions: 192x208x77mm • Features: Programmable via USB port, • Regenerative Braking • Temperature Protection circuit
3	TROJAN T105 Deep cycle Flooded/wet lead-acid battery	• 6V ,225Ah (20hr rate) • 185Ah (5hr rate) • 28kg
4	MAXWELL ultracapacitor module BMOD0165P048	• 165F, 48.6V • ESR 7.1 milliOhms • 13kg • Individually balanced cells • Compact, rugged ,fully enclosed • Max. continuous current 150A
5	12V Albright contactor SW200B-84 12V	• 12VDC continuous duty coil with blowouts • Weld resistant silver alloy contact tips • 70% duty 300A
6	Foot Throttle	• 0-5V voltage output • micro switch • Casted aluminum • Water resistant

7	Emergency disconnect/kill switch	• Heavy duty 500A • Key operated
8	CR Magnetics Hall Effect Current and Voltage Transducer	• 0.001 precision • Input current:0-600A,output: 0- 5VDC • Input Voltage:0-60V , Output: 0-5V • Sensor Power Supply: 24V dc.
9	Panel meters: Voltage ,current (analog and digital meters)	• Voltage (0-80V) • Current (0-300A) with 50mv shunt
10	Auxiliary DC- DC converter	• Input: 40 → 64 VDC • Output: 13.2Vdc , 12A, 158W • Efficiency: 82%
11	Automotive Lead acid battery charger	• Input: 240Vac, 50Hz • No of batteries: 4 x 12Vdc or 8 x 6Vdc • Charging current: adjustable (20A Max)
12	Data Acquisition Card; DataTaker DT82E	• Low power design for remote applications • 12-24V dc input • 18 bit resolution • FTP for automatic data transfer • 12V regulated output to power sensors • Up to 6 Analog (+- 30V) sensor inputs

		• USB memory for easy data and program transfer • Interface with smart sensors such as GPS antenna.
13	GPS antenna; EM-406A	• Sirf star III chipset • Output NMEA 0183 and SirF binary protocol • 20 channel receiver • Hot start 1s; warm start 38s; cold start 42s • 10m Positional accuracy • 30mm x 30mm x 10.5mm, 16g • LED status indicator and battery backed RAM

Table 5: EV conversion parts and specifications

The parts listed in the table above were connected according to a certain wiring diagram (see figure 41). The thick lines represent 2/0 gauge welding cables which were used for the main traction wiring. It should be noted that wherever possible, fuses (10A, 5A) were used to protect the auxiliary circuit. The 12V chassis ground must be isolated from the 48V system. This is to ensure that through error, or accident, the chassis ground cannot complete a 48V potential loop. The 48V system has no common grounded chassis like the 12V system.

In conventional vehicles, the 12V auxiliary battery used for startup and accessories is usually charged by the alternator when the engine is running. In this EV conversion, a step down dc-dc converter was used to replace the alternator for charging the 12V battery. This converter taps 48V from the main battery pack and steps it down to 13.2V dc. Its operation is controlled by a relay which is activated by the ignition key switch of the car.

For safety reasons, the micro switch on the throttle was used to turn the main contactor on and off, in other words if your foot is off the throttle, the main contactor goes off. If something goes wrong such as a runaway motor, then by releasing the throttle (usually happens on instinct), the main contactor is turned off and the circuit is broken.

Also an emergency kill switch was installed in an accessible area (just beside the gear stick). This serves as emergency disconnect from battery pack in case of motor/controller failure.

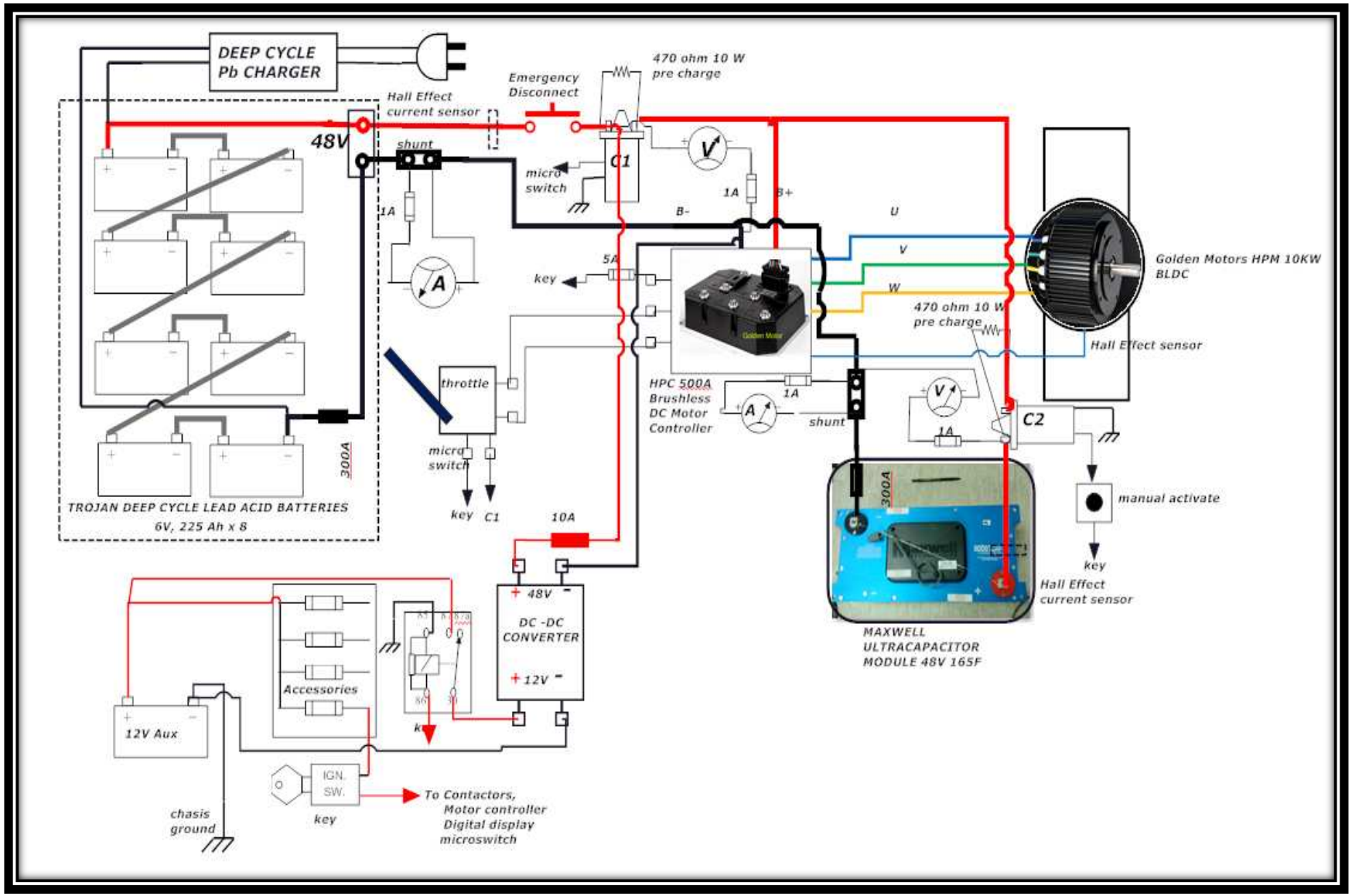

Fig 45: Complete Wiring Diagram for Electric Vehicle Conversion

3.3.4 Installation and testing of Supercapacitor Module

Custom made rack was fabricated to house the supercapacitor module in the front compartment, right above the electric motor mounting assembly. A 300A fuse was connected as well as digital voltmeters and ammeters in order to monitor the charging and discharging capabilities of the supercapacitor module. Figures below show the module before and after installation in the electric vehicle.

Fig. 46: BMOD0165P048; 165F, 48.6V supercapacitor which weighs 15kg

Fig 47: BMOD0165P048 installed just above the electric motor. Top right is the high current contactor which is activated by a 12V coil and a manual switch on the dashboard of the vehicle.

Using an online tool provided by the manufacturer [112], a constant current discharge profile was simulated for the supercapacitor module. This is shown in the figure below:

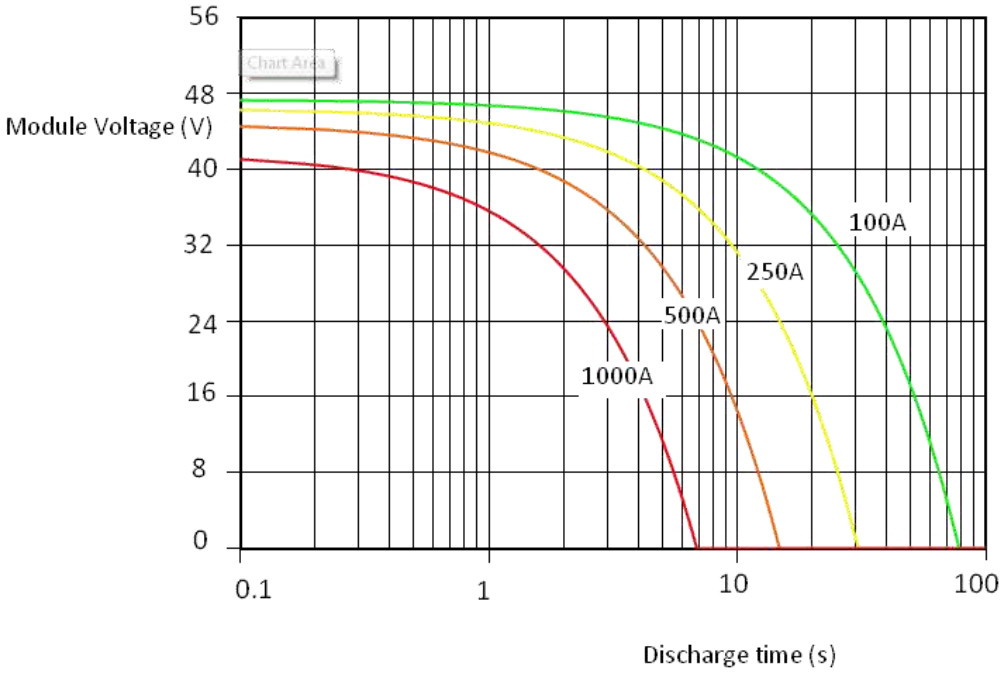

Fig. 48 Constant Current Discharge Profile for BMOD0165P048 Supercapacitor Module

3.3.5 Brake system modification

Almost all cars these days have vacuum assisted braking system. The perodua kancil does. Since the vacuum source; the engine, was removed, an alternative source of vacuum is needed to restore the functionality of the power brakes. A 12V vacuum pump which is controlled by a pressure switch was installed to act as vacuum booster for the power brakes. The figure below shows the wiring diagram.

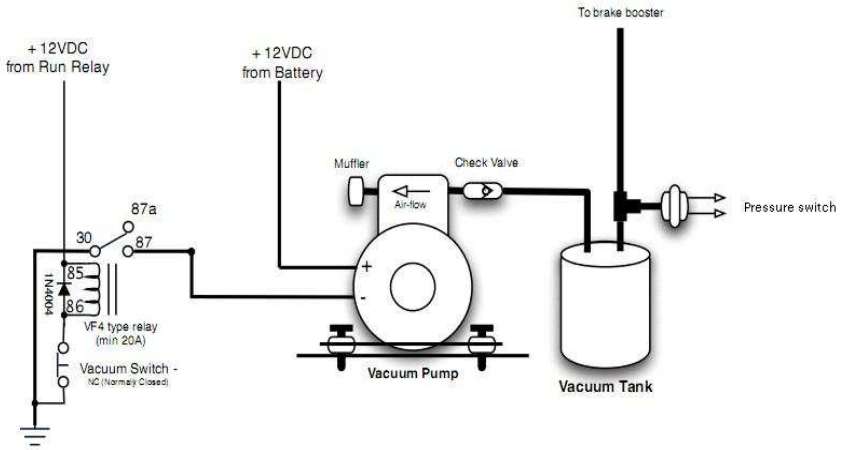

Fig. 49 Vacuum pump wiring diagram for brake system modification [111]

Fig 50: Electric Vacuum Pump (left) connected to the vacuum reservoir on one side and the brake booster on the other. A pressure sensor turns the pump on and off depending on the set level.

The pressure switch monitors the pressure in the vacuum tank. Once the suction pressure drops to 400millibar, the switch turns on the pump via the relay. As soon as 600millibar is attained, the vacuum is switched off. This way, vacuum is automatically maintained between these two limits. The vacuum pump was mounted on brackets firmly welded on to the chassis. Rubber mounts were used to mount the pump in order to minimize the vibration which would otherwise be transmitted onto the body of the vehicle.

Testing of the electric vacuum assist brakes was done and found to be satisfactory and on par with conventional vacuum assist from the engine. The vacuum pump turns on only after the brakes are depressed at least twice, draws a current of 3A at 12Vdc (36W) during operation and turns off when sufficient vacuum pressure is achieved.

Fig 51: front view of the EV with all the necessary connections in place.

3.4 DATA ACQUISITION SYSTEM AND TESTING

For initial testing purposes, a fixed driving route within the university's campus was chosen. A data logging device with external USB storage was setup in the car to collect data from current and voltage sensors which were used to monitor the power flow from the battery pack and the supercapacitor module respectively.

Fig 52: DataTaker DT82E Data logger with flash USB storage logs battery pack current and voltage, supercapacitor current and voltage, GPS timestamps as well as GPS speed.

The features of the data acquisition system include

- DataTaker DT82E logger: The DT82E is a smart data logger designed especially for outdoor monitoring. It is a robust, low power data logger featuring USB memory stick support, 18-bit resolution, extensive communications capabilities and built-in display [101]. It has 6 analog input channels, 4 bi directional digital input output channels, a smart serial sensor

port which was connected to a GPS antenna in this project and a 12V regulated power output.

- Hall Effect current transducers and voltage transducers: CR magnetic CR5210-600 provides a DC signal (between 0-5V) which is proportional to a DC sensed current. Two of these units were used to monitor the current drawn out of the battery pack and also supercapacitor module. This is shown in the figure below; the maximum dc current that can be sensed is 600A [102]. CR5310-100 dc voltage transducers provide an output DC signal (also 0-5V) that is proportional to the input DC voltage of the battery pack and supercapacitor module respectively; the maximum dc input voltage allowed is 100V [103]. The wiring diagram for these 2 sensors are described in the circuit below; the sensors require a 24V power supply which is provided by 2 12V sealed lead acid rechargeable batteries housed in the glove compartment of the vehicle. The outputs for these sensors are fed into the analog input channels of the DT82E data logger module.

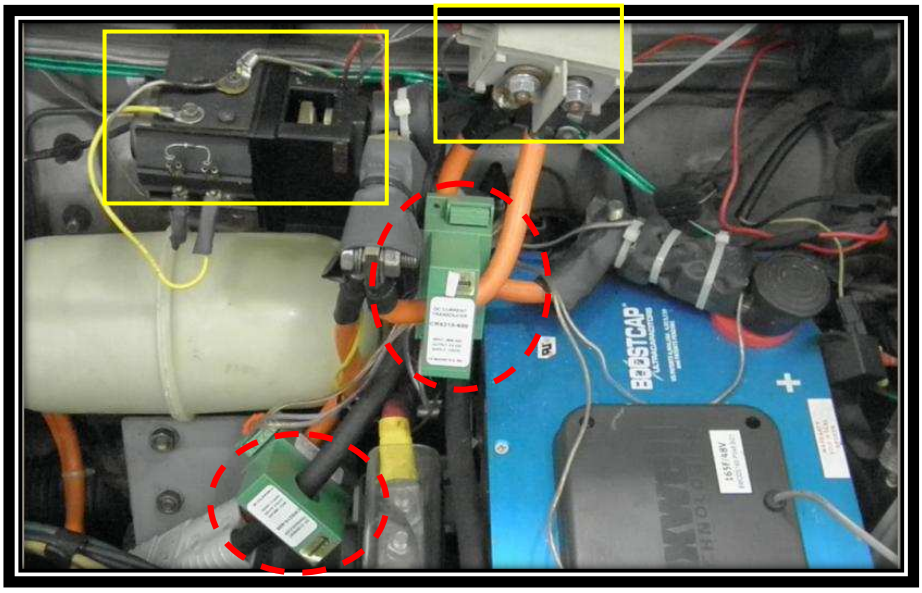

Fig 53: Hall-effect current transducers used to monitor battery and supercapacitor currents.

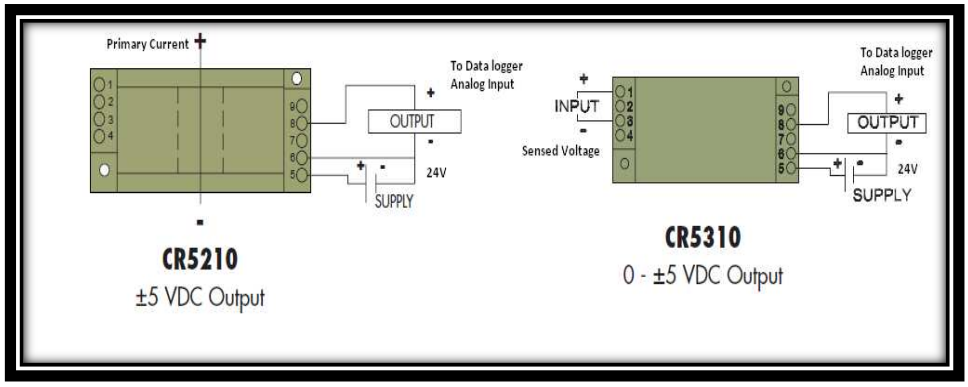

Fig 54: Differential Wiring diagram for Current and Voltage Transducer to data logging device [102], [103]

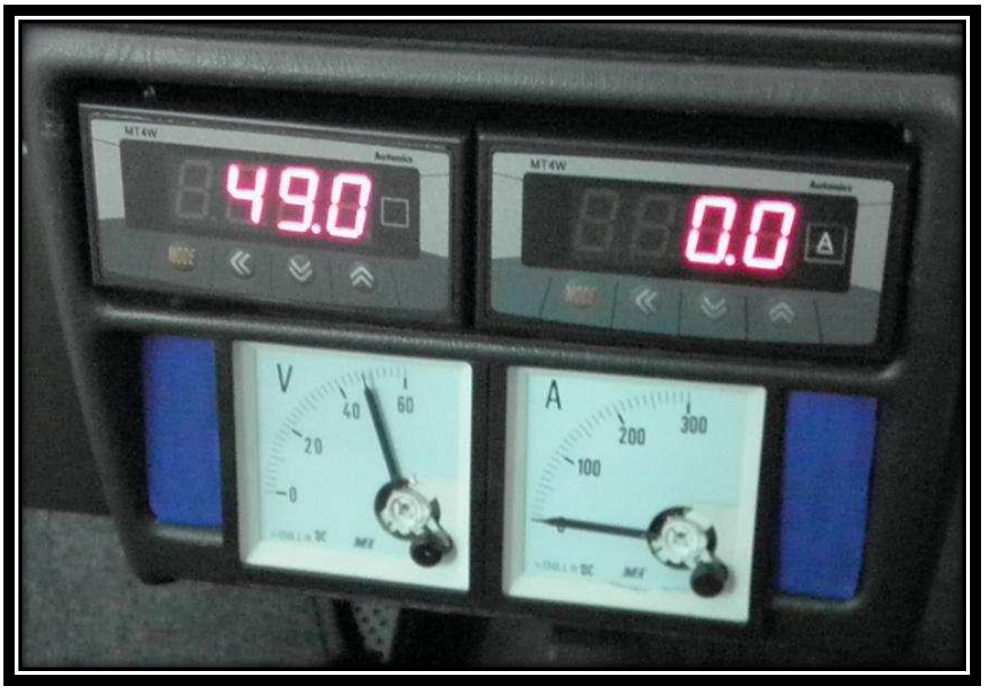

Fig 55: Dashboard Mounted Display; Top left: Supercap Voltage, Top Right: Supercap Current, Bottom Left: Battery Voltage, Bottom Left: Battery Current

- GPS receiver module: The EM-406a is a 20 channel compact, high performance, low power consumption GPS engine board (see figure 52 above). It uses the SiRF Star III low power Single GPS chipset which can track up to 20 satellites at a time, and can perform extremely fast time to first fix in weak signal environments. It is suitable for automotive navigation, personal positioning, mobile phone navigation, marine navigation among others [104].
- Analog and digital panel meters which were mounted on the dashboard (as shown in figure 55 above). The analog panels display the battery pack voltage and current while the digital panel meter displays the supercapacitor voltage and current.

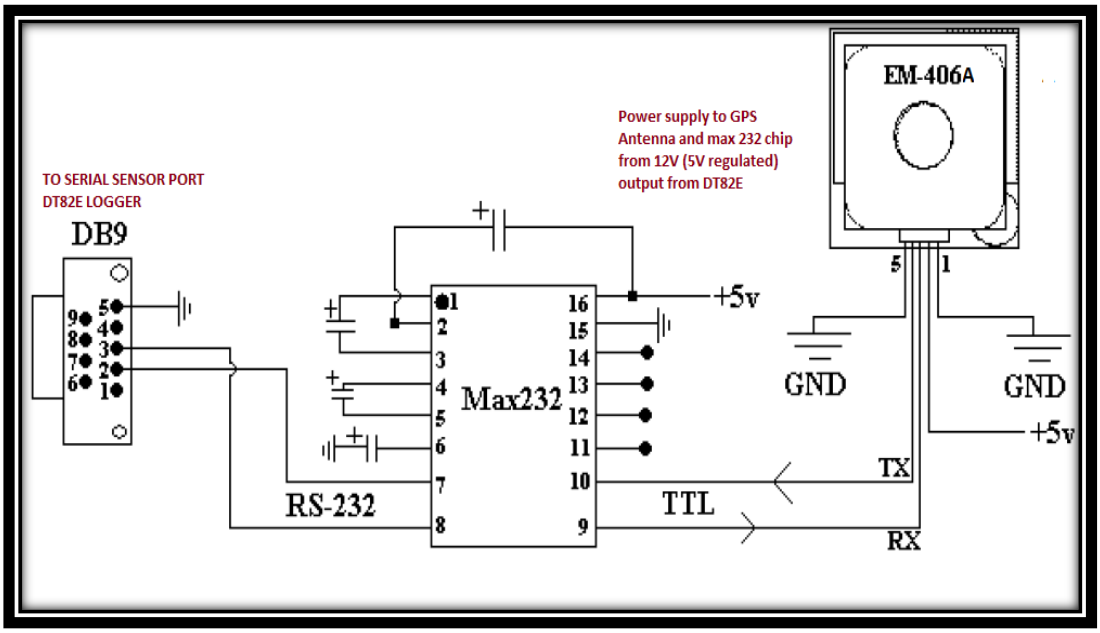

Fig 56: Wiring diagram for GPS antenna and MAX232 level converter pin-out to DB9 connector

Figure 56 above describes the connection between the GPS module and the serial port of the data logger module. A MAX 232 chip was used to convert the TTL output from the GPS module to RS-232 serial signal via a DB9 connector which plugs into the data logger serial port. A custom DataTaker code which is able to activate the GPS module, read the input strings and log important parameters such as GPS speed, altitude and total distance travelled was written. At the same time, readings from the current and voltage sensors are also logged following the same time stamp as with the GPS data. A copy of the program can be found in the index of this report. A real time display of the logged parameters was also displayed on the lcd screen of the data logger device. This can be seen in figure 52 where a battery pack voltage of 50.4V is displayed.

3.4.1 Driving Data Collection

Two fundamental methods have been used in the past to collect driving data; the chase car method and the on-board vehicle instrumentation method [109]. As the name suggests, the chase car protocol involves the installation of a range-finder laser system on a chase vehicle which collects second-by-second speed-time profiles from target vehicles. The on-board vehicle instrumentation involves installing the test vehicle with all the necessary sensors and transducers to measure the vehicle's real time speed-time profile. With the advent of GPS technology, non-contact method of logging speed (as opposed to rpm sensors) can be implemented for collecting on-road data. This research work adopts the on-board instrumentation method coupled with GPS technology. A data acquisition device is integrated into the system to store on-road data continuously. In general, drive cycle construction methods typically include the following steps:

- Collecting real world driving data
- Segmenting the driving data
- Constructing cycles
- Evaluating and selecting the final cycle.

Depending on the type of driving activity that is being using to construct the cycle, existing cycle construction methodologies for light-duty vehicles can be generalized into four types: micro-trip cycle construction; trip segment-based cycle construction, cycle construction based on pattern classification, and modal cycle construction [110]. Traditionally, drive cycles have been used to test conventional vehicle polluting emissions and fuel consumption.

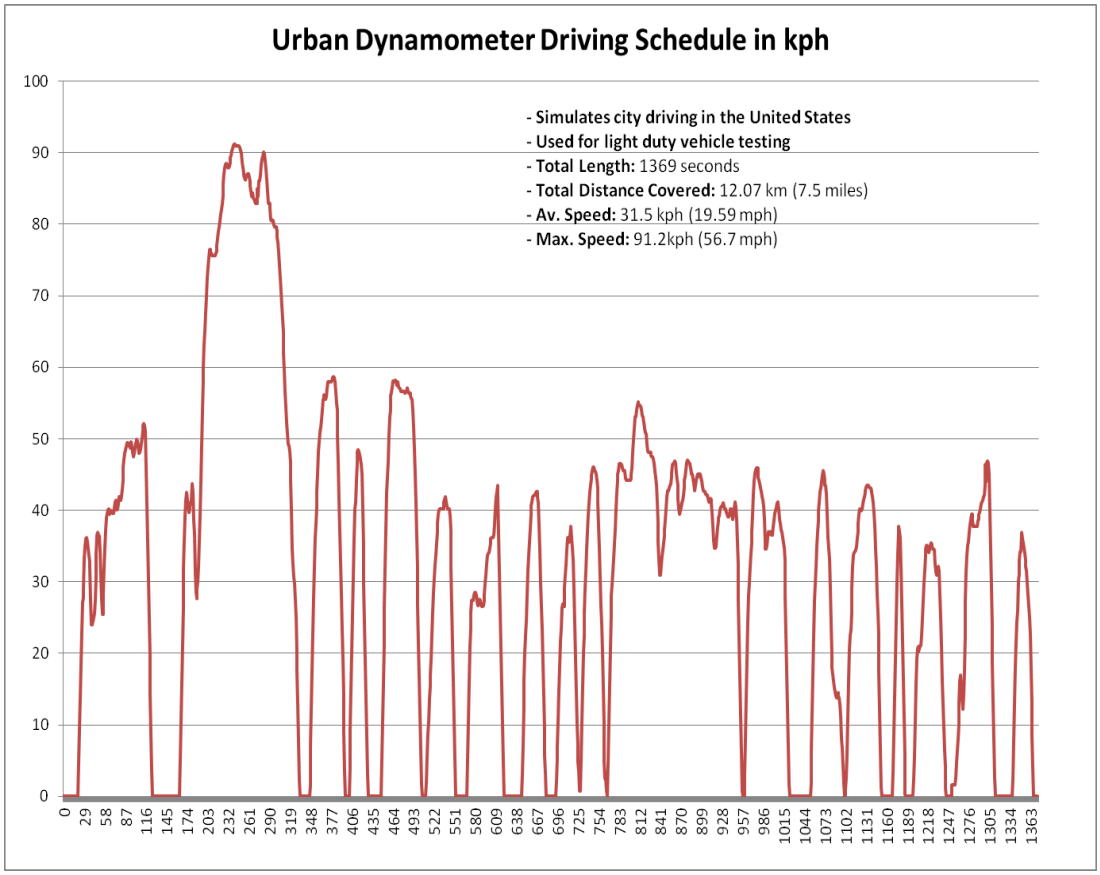

Fig 57: The UDDS drive cycle and some of its features

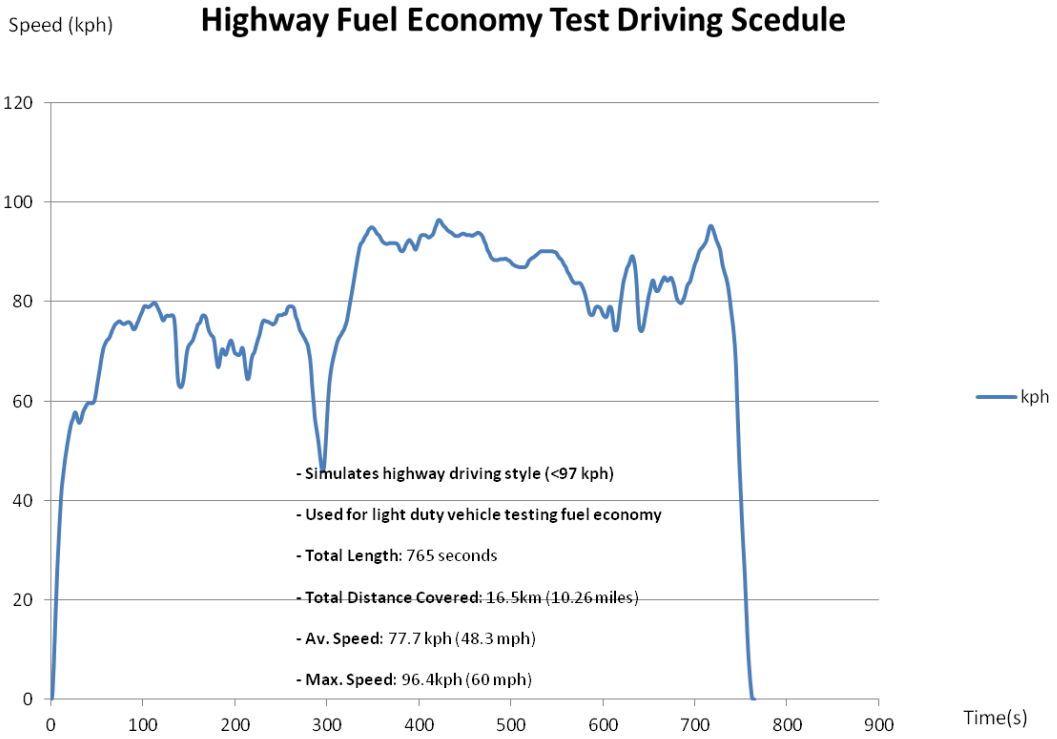

Fig 58: The HWFET drive cycle and some of its features

Figures 57 and 58 above represent existing standard driving schedules for city and highway driving in the United States. In comparison with ICE vehicles, the testing of electric and hybrid vehicles pose some unique problems that are specific to the technology used. For example, EV's can be designed for route-specific applications i.e. low speed city driving or specific neighborhoods only, therefore they will perform badly when subjected to other types of drive cycle. Standard driving cycles for ICE-vehicles are not necessarily adequate for vehicles with electric drive trains and provide insufficient basis for the comparison of different driveline technologies.

For power sources such as batteries in electric and hybrid vehicles, assessments on their performance are, most of the time, conducted in laboratories on test bench setups. Similar to standard driving schedule tests and analyses, these laboratory tests and duty cycle analyses have constraints in their validity to real-life operation. A main issue exists in both cases due to the problem with real-life operation where, even under specific driving cycles or duty cycles, energy consumption strongly depends on ambient operating conditions that are typically uncontrolled [48].

It is with this mindset that we decided to create our own driving schedule called the UNMC cycle. Due to existing local traffic regulations, an electric converted vehicle is not road legal, so testing was done within the university's campus. The route chosen is 1.04 km from the university's engineering faculty (point A in fig 19) through point C (cafeteria), around the accommodation complex and back to the original starting point. This route is very similar to city driving conditions or speed restricted driving conditions such as in residential areas with a lot of speed bumps. We shall refer to this drive route (cycle) as UNMC cycle.

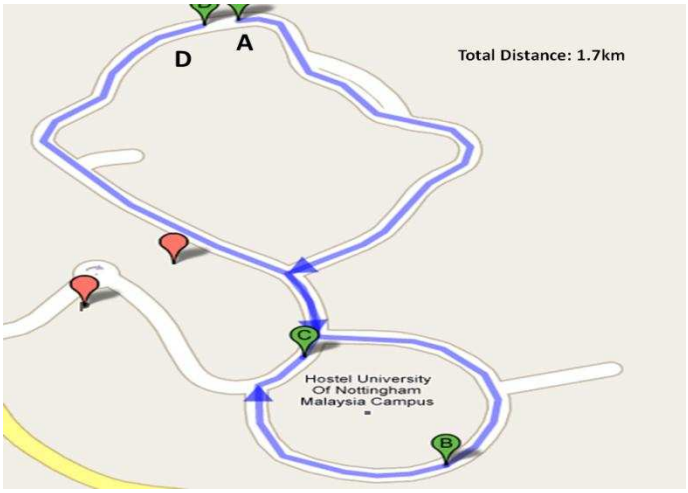

Fig 59: Fixed Driving route for EV testing at the University of Nottingham Malaysia.

In order to verify the effects of integrating supercapacitor into the system, the vehicle was tested with and without the ultracap module as shown in the figure below. It should be noted that the schematic below is simplified for better understanding. In reality the switch is a high current contactor which is controlled by a 12V relay coil, also protection diodes, fuses have been left out of the schematic.

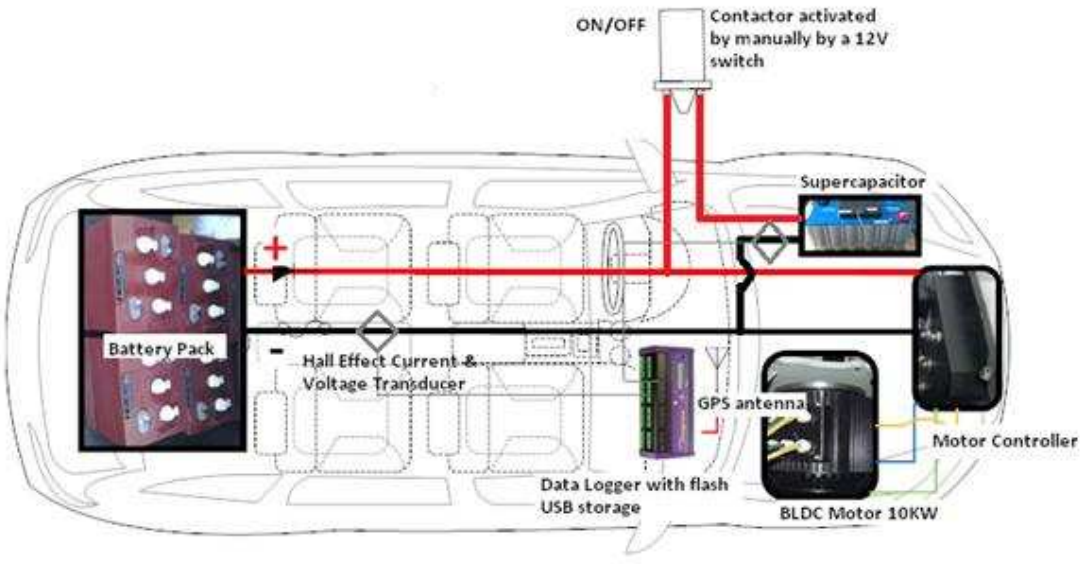

Fig 60: Testing and Data Collection With and Without Supercapacitor

The prototype electric kancil was driven through a specific route (figure 59) with the switch in the OFF position i.e. battery alone, to acquire reference data for comparison. This was repeated, but with the switch ON. Although the test driver simulated the same driving pattern with or without the supercapacitor, the status of traffic congestion and receiving stop light signals slightly varied through the test time.

Timestamp	Alt (m)	GPS State	Spd (kph)	kph (mps)	Trip (km)	V_scap (V)	V_bat (V)	Iscap (A)	Ibat (A)
17:18.0	38.4	1	0	0	0.0032	49	50.6	0	2.6
17:21.0	39.9	1	0	0	0.0032	48.9	50.5	0	6.9
17:24.0	44.9	1	0	0	0.0032	49	49	0	32.5
17:27.0	46.7	1	2.3	0.6	0.0041	48.9	46.5	0	84.1
17:30.0	45.4	1	8.9	2.5	0.0088	48.9	49.7	0	10.1
17:33.0	46.5	1	16.2	4.5	0.0192	49	49	0	26
17:36.0	45	1	17.4	4.8	0.0331	48.9	50.5	0	2.5
17:39.0	43.3	1	17.4	4.8	0.0477	48.9	50.6	0	1.6
17:42.0	45.3	1	12.4	3.5	0.0601	48.9	50.5	0	1.6
17:45.0	43.8	1	11.5	3.2	0.0701	48.9	50.6	0	2.4
17:48.0	43.6	1	11.9	3.3	0.0798	48.9	48.2	0	54
17:51.0	45.5	1	7.4	2	0.0878	48.9	49	0	15
17:54.0	46.9	1	14.4	4	0.099	48.9	48.7	0	34.7
17:57.0	48.1	1	18.6	5.2	0.1096	48.9	47.7	0	45.1
18:00.0	49	1	20.8	5.8	0.1261	48.9	50.4	0	2.5
18:03.0	48.2	1	23.3	6.5	0.1445	48.9	45.7	0	88.2
18:06.0	48.6	1	19.6	5.5	0.1624	48.9	48.8	0	33.1
18:09.0	50.2	1	23	6.4	0.1801	48.9	50.2	0	2.2
18:12.0	53.1	1	23.9	6.6	0.1995	48.9	48.7	0	33.6
18:15.0	53.8	1	25	6.9	0.22	48.9	48.3	0	45
18:18.0	53.6	1	24.3	6.7	0.2405	48.8	47.8	0	51.8
18:21.0	52.5	1	22	6.1	0.2598	48.8	47.4	0	58.4

Fig 61: Snapshot of the data obtained from the logging system at 0.33Hz

Figure 61 above represents the time stamped raw drive data which is obtained from the data logging device via the USB storage. The accumulated trip in km was calculated by integrating the GPS speed over the time step between each sample. This was achieved by some custom programming code. A MATLAB ® program was written to calculate certain parameters from the above real world drive cycle in order to characterize it and compare it with existing standard drive cycles.

CHAPTER 4: RESULTS & DISCUSSION

This chapter begins by presenting and describing the preliminary results of the electric vehicle conversion powered by a deep cycle lead acid battery and a supercapacitor module.

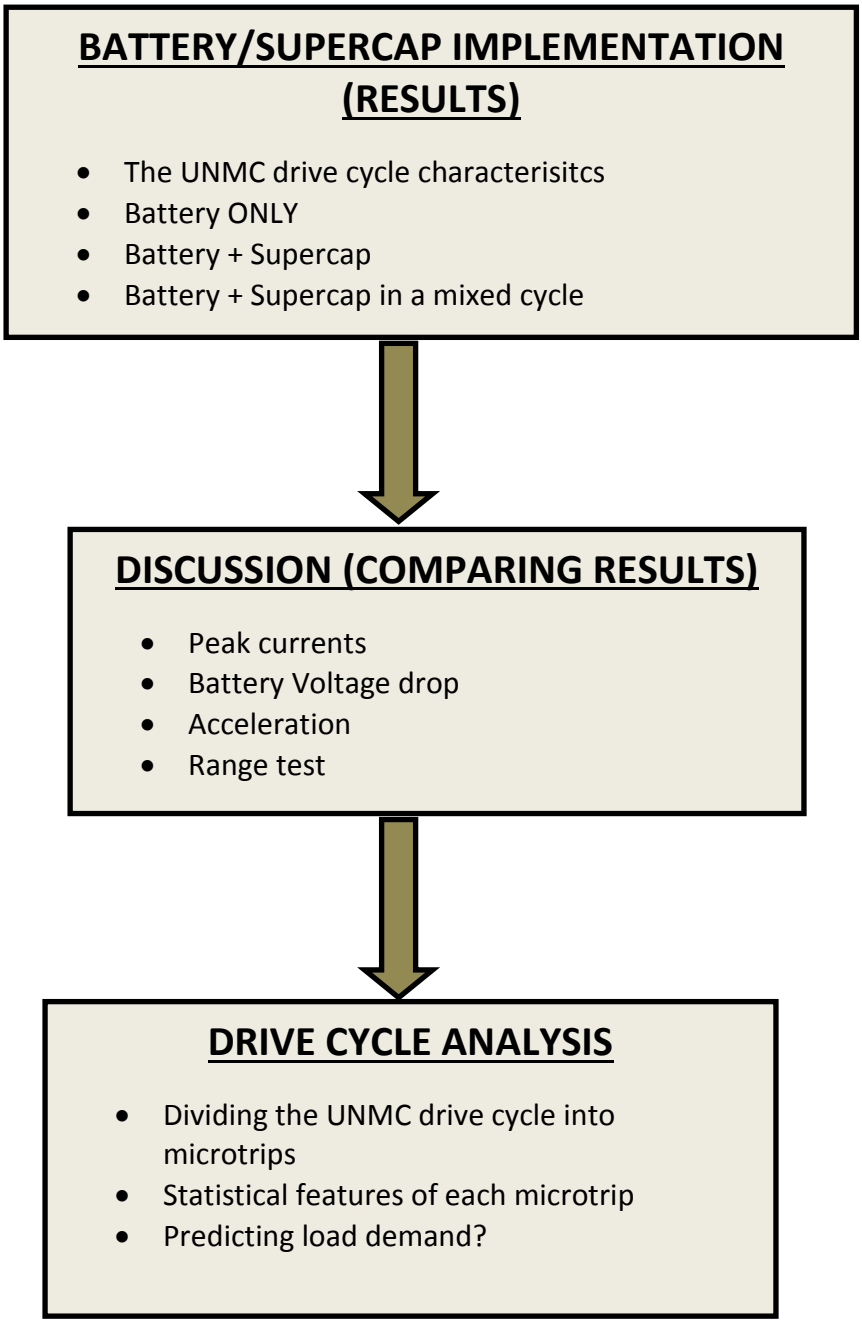

4.1 BATTERY-SUPERCAPACITOR IMPLEMENTATION

This section presents the results of the integration of supercapacitor module into a converted city electric vehicle. Raw data from the on-board data acquisition system was collected as shown in the previous chapter. By running custom routines on MATLAB software, basic parameters such as altitude, drive cycle data, current, voltages etc. are plotted as well as some derived quantities such as power in kilowatts, acceleration and jerk which are visualised.

A fixed driving route was adopted in the university's premises which will be referred to as the UNMC cycle. A total of 5 trips shown in figures 62 to 66 below, were made. Each trip consists of approximately 10 cycles of the UNMC route which amounts to a total distance of 10.4 km per trip. GPS altitude data collected showed a variation from 53m to 96m with an average of 76m above sea level. It is important to note that altitude data from GPS is subject to error (10 – 20 m accuracy) [104], hence it is only used to prove that the test route was consistent with all test trips made.

Due to existing local traffic regulations, an electric converted vehicle is not road legal, so testing was done within the university's campus. This route is very similar to speed restricted driving conditions such as in residential areas with a lot of speed bumps. Trips were done at different times of the day and also different days of the week to see the effect on driving pattern. However, the same driver was maintained in all cases.

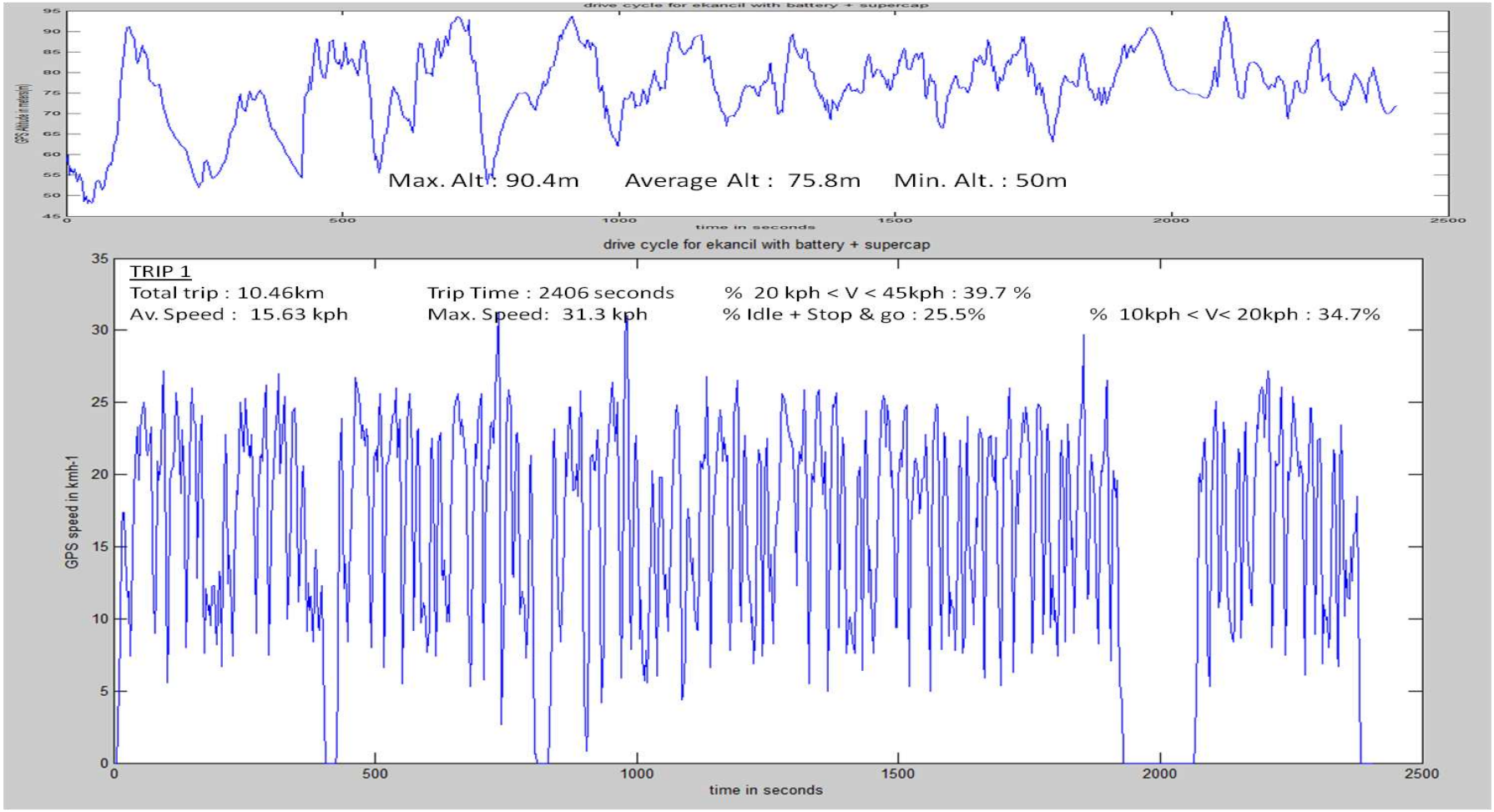

Fig 62 : UNMC Drive Cycle Trip 1

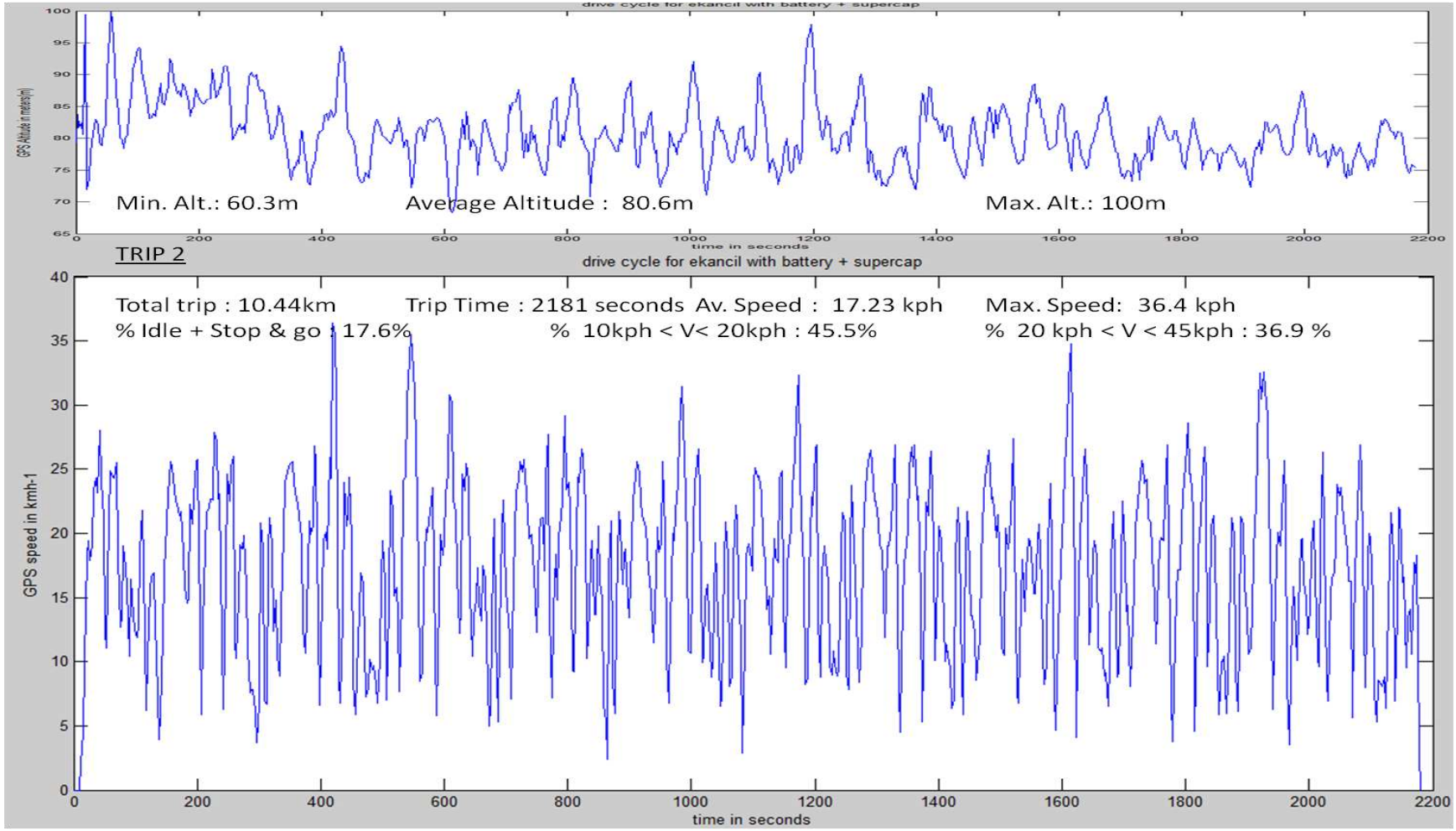

Fig 63 : UNMC Drive Cycle Trip 2

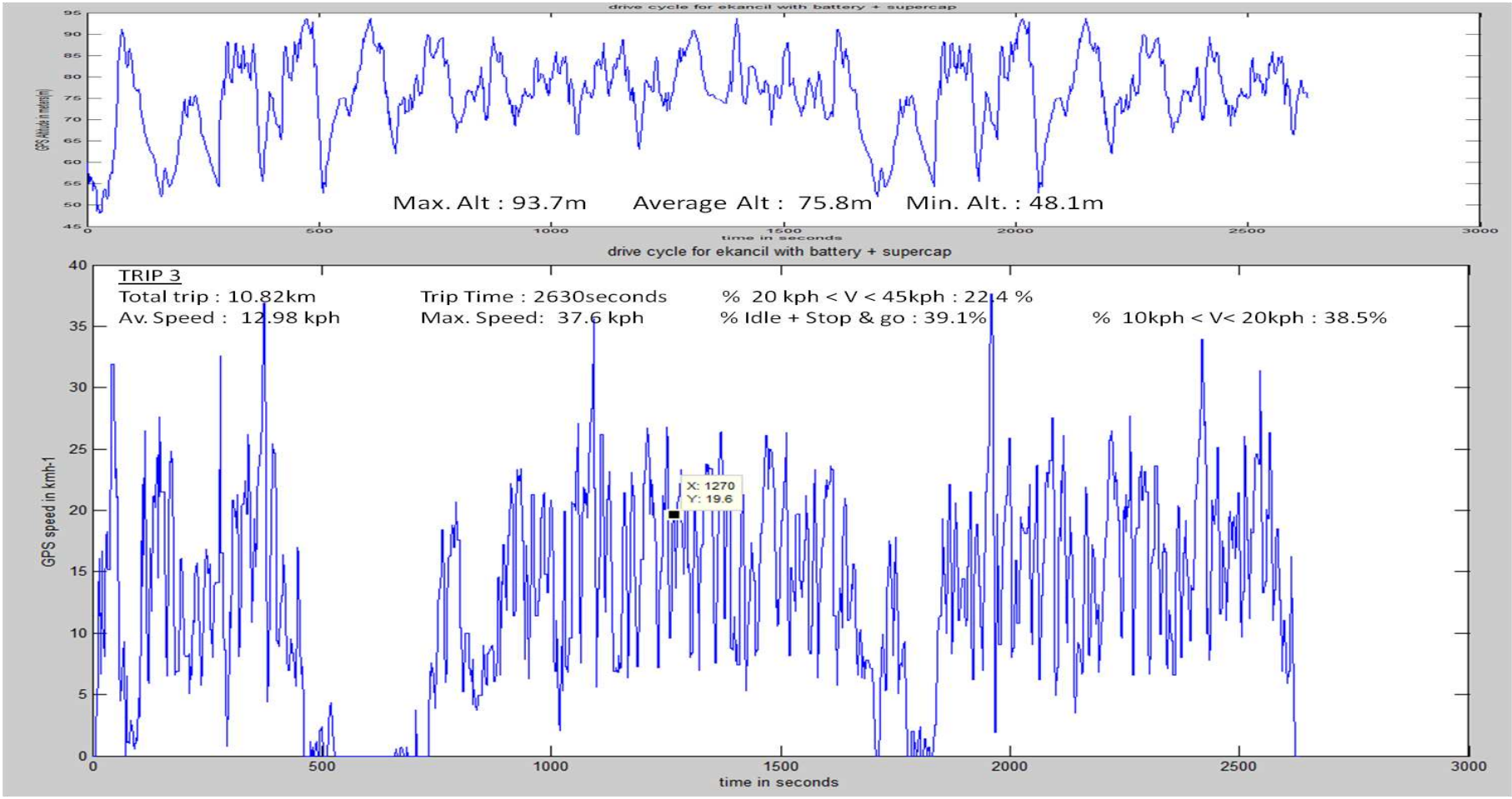

Fig 64 : UNMC Drive Cycle Trip 3

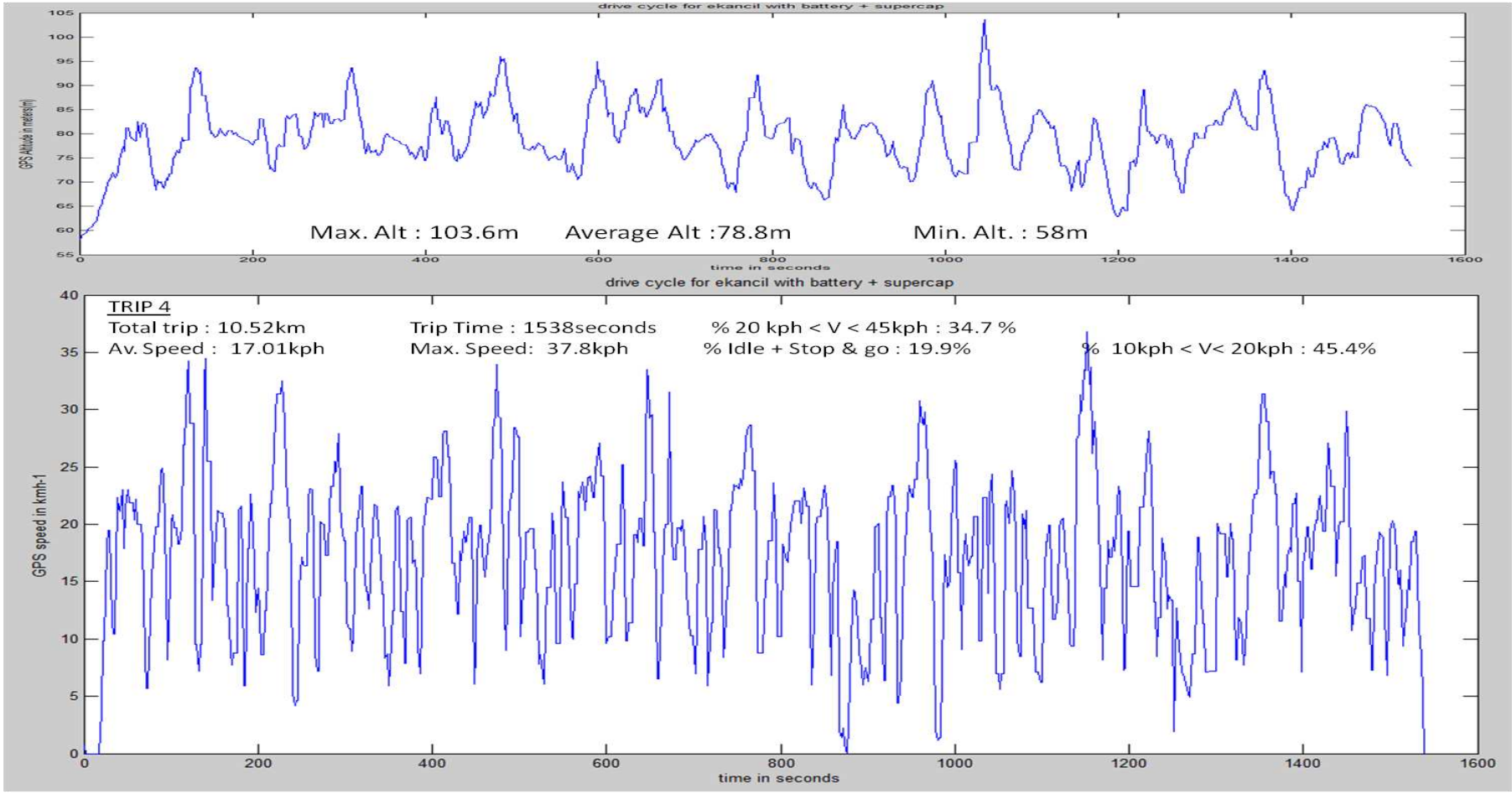

Fig 65 : UNMC Drive Cycle Trip 4

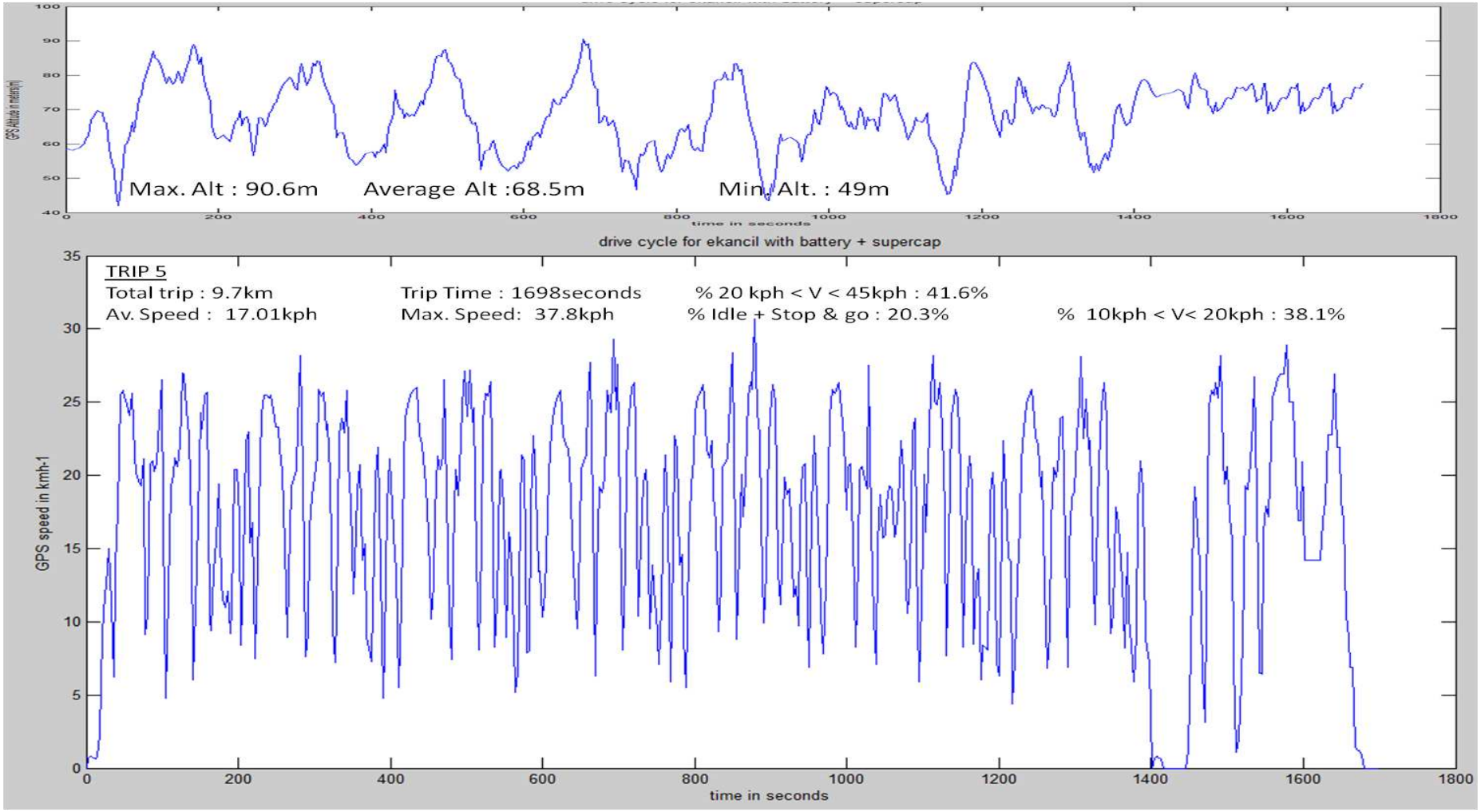

Fig 66 : UNMC Drive Cycle Trip 5

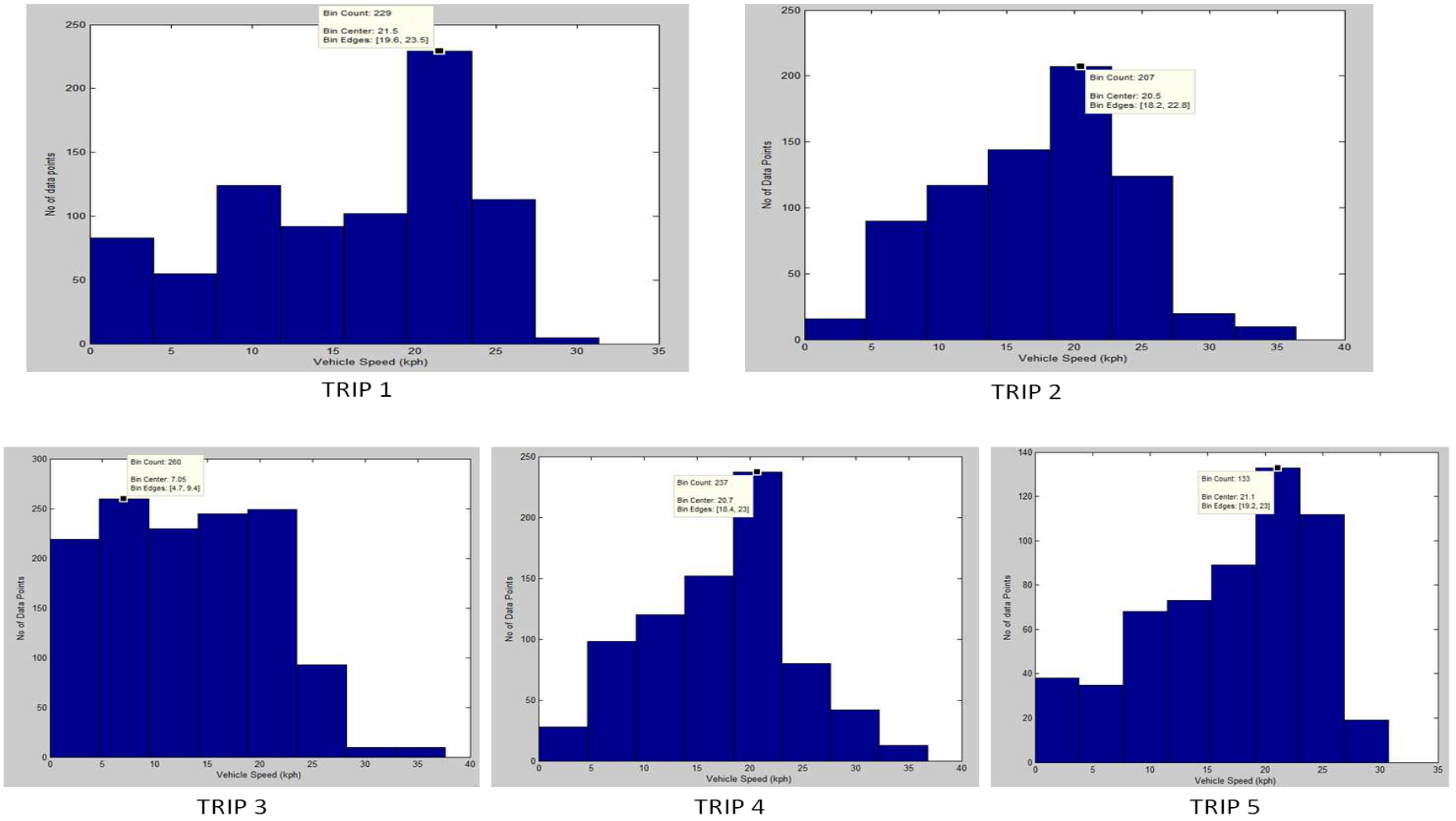

Fig 67 : Frequency distribution (histogram) of UNMC drive cycle TRIPS 1-5.

		TRIP 1	TRIP 2	TRIP 3	TRIP 4	TRIP 5
1	**Total time (seconds)**	2406	2181	2603	1538	1698
2	**Total Distance (km)**	10.46	10.44	10.82	10.52	10.20
3	**Altitude (m)**					
	Min|Mean|Max	50|75.8|90.4	60.3|80.6|100	48.1|75.8|93.7	58|78.8|103.6	49|68.5|90.6
4	**Average Speed (kph)**	15.63	17.23	12.98	17.01	17.01
5	**Max. Speed (kph)**	31.3	36.4	37.6	37.8	37.8
6	**Stop + idle (%)**	9.6	0.7	12.54	1.68	5.29
7	**1< Speed < 10kph (%)**	15.9	16.9	26.6	18.2	15
8	**10 < Speed < 20kph (%)**	34.7	45.5	38.5	45.4	38.1
9	**20 < Speed < 45kph (%)**	39.7	36.9	22.4	34.7	41.6
10	**Speed > 45kph (%)**	0	0	0	0	0

Table 6: Summary of the main characteristics of the UNMC drive cycle for 5 different trips

Table 6 above summarizes the main characteristics of the UNMC drive cycle. For over 70% of the total drive cycle, speeds of between 10 kmh^{-1} and 45 kmh^{-1} were recorded and none above. Stop plus Idling time recorded was up to 12.5% which could vary depending on amount of traffic on campus at the time of testing. Taking a look at figure 67 above, trips 1 to 5 show very similar frequency distribution histograms except for the idling time i.e. between 0 and 5kph. This is particularly evident in trips 1 and 3 where the idling time is 9.6% and 12.5% respectively. Maximum speed recorded was about 38 km/h in all trips. In the real world, this could represent a driving trip in a residential community from say the house to the grocery shop encountering a lot of speed bumps on the way.

4.1.1 Results: Battery Only (Supercapacitor OFF)

The electric kancil was driven over a fixed route as described in the section above, solely powered by the 48V, 225Ah (20-hour rating) Trojan T105 deep-cycle lead acid battery pack. The results of the power flow from the battery pack to the motor and vice versa is summarised in the table below. It should be noted that the battery pack is charged to 100% state of charge before carrying out the test.

Initial Battery Voltage	**49.6 V**
Average Battery Voltage Drop	2.7 V
Max. Voltage Drop	9.9 V (47.4 → 37.6)
Average Current	43.8 A
Peak Current	228.1 A
Average Instantaneous Power	1934.7 W
Peak Instantaneous Power	8553.8 W
Average Acceleration	0.37 ms^{-2}
Max. Acceleration	1.37 ms^{-2}
Average deceleration	0.38 ms^{-2}
Max. deceleration	2.01 ms^{-2}

Table 7: Summary of results (battery only)

Figures 67 to 74 are graphical plots and frequency distribution charts of battery voltage, battery current (drawn by the load while driving), the instantaneous power and the acceleration of the vehicle. The supercapacitor module was disconnected via a high power contactor which operates on a 12V dc coil powered by the vehicles accessory circuit. A maximum voltage drop of 9.9V was recorded. At that point, it

resulted in a dip from 47.4V to a record low of 37.6V which drew a current of 228.1 A from the battery pack. According to the Trojan T105 manufacturer's datasheet, the lower voltage limit of each cell in the battery should not be below 1.75V at all times during constant discharge [114]. Per battery, this amounts to 5.25V and the entire pack's lower voltage limit is 42V. Therefore, any voltage below this limit is considered to be a severe deep discharge which is detrimental to the health of the battery in the long run. More so, these deep discharges are sudden and haphazard depending on the acceleration demand of the vehicle and last only for a couple (3-5) of seconds. This adds more strain on the battery.

An average current of 43.8 A was recorded for this particular trip which generally produced an average voltage drop of 2.7 V during the trip. An average acceleration of $0.37ms^{-2}$ up to a maximum of 1.37 ms^{-2} was recorded. The New York drive cycle (NYCC) which features a mainly low speed, idle and stop-go condition has an average acceleration of $0.62ms^{-2}$ and a maximum of 2.68 ms^{-2}. Due to the low voltage used in the experimental vehicle, the acceleration is limited. The aim of the first phase of this research work was to investigate the effect of integrating a supercapacitor system into an electric vehicle to act as a power buffer system. The average instantaneous power delivered by the battery was approximately 1.9KW while it peaked to a maximum of 8.6KW.

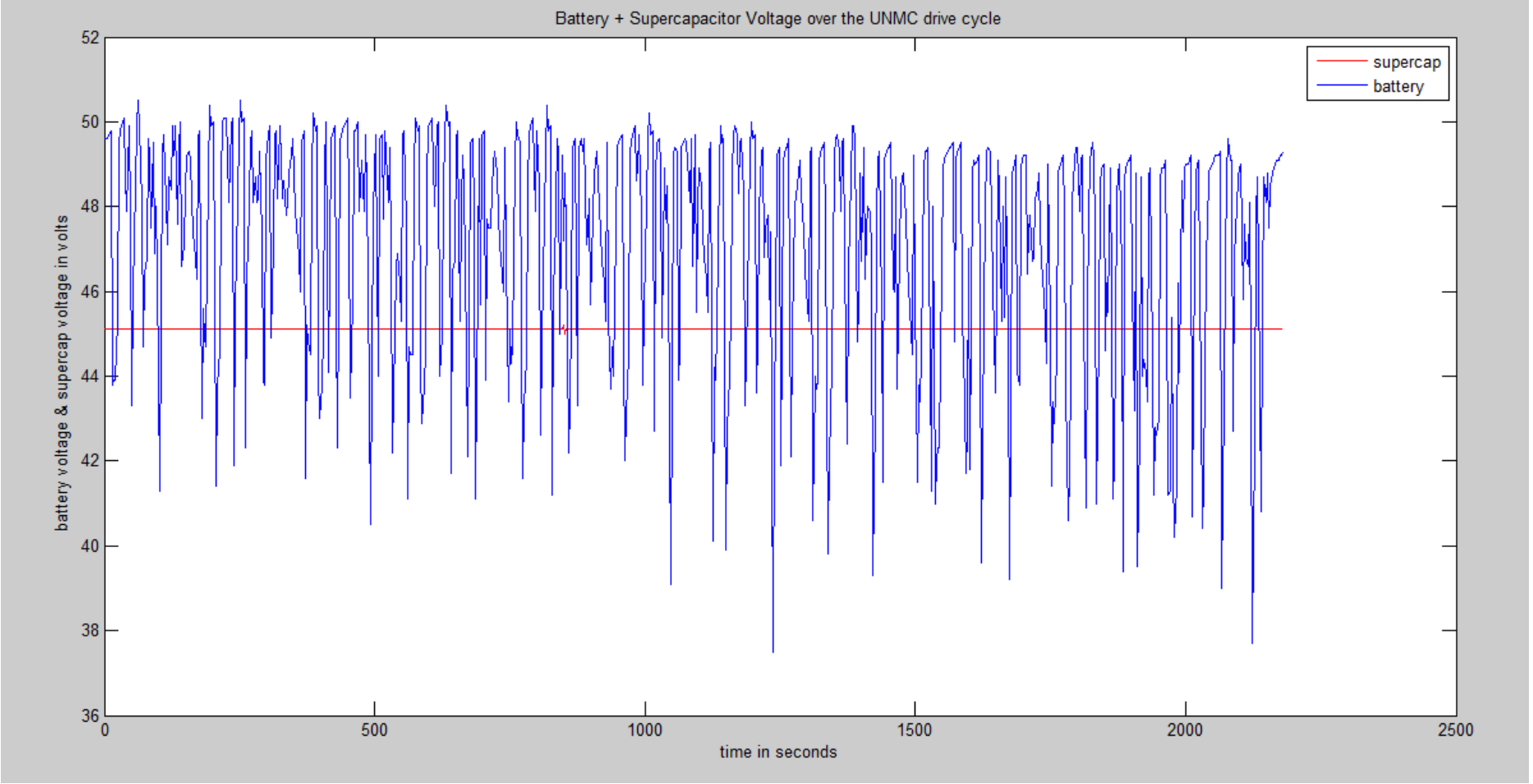

Fig 68 : Battery Voltage

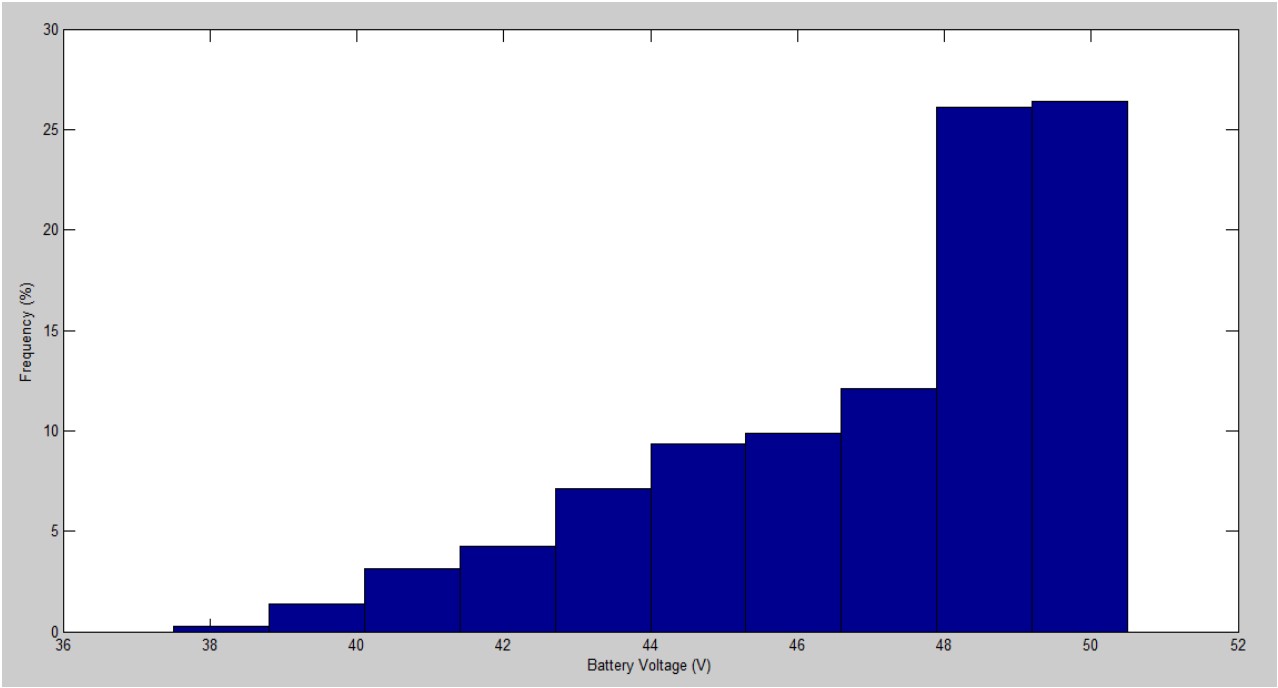

Fig 69: Frequency Distribution of Battery Voltage

Bin Average (V)	38.2	39.5	40.8	42.1	43.4	44.7	46.0	47.3	48.6	49.9
Freq (%)	0.3	1.4	3.2	4.3	7.1	9.3	9.9	12.1	26.1	26.4

Table 8: Frequency table of Battery Voltage

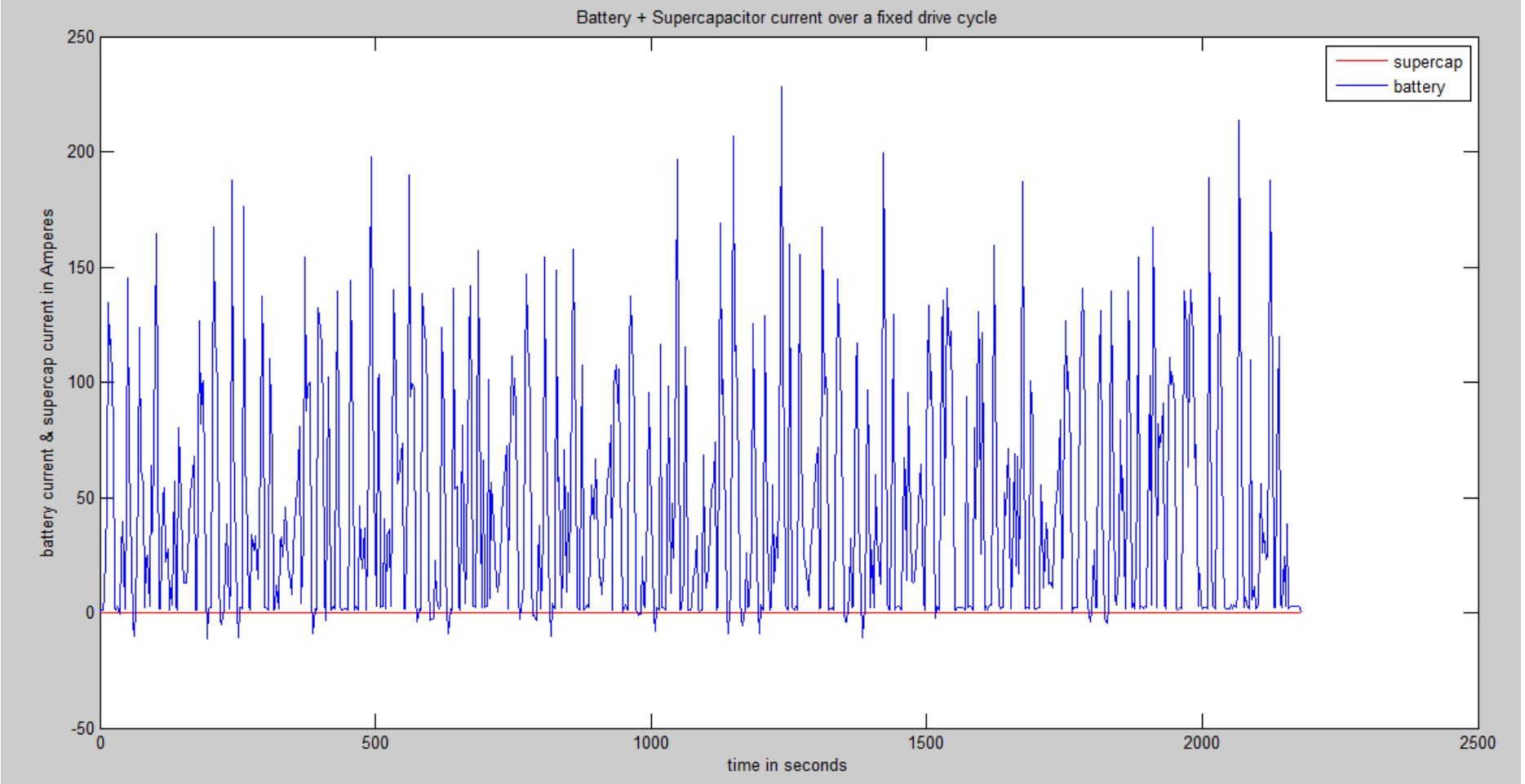

Fig 70 : Battery Current

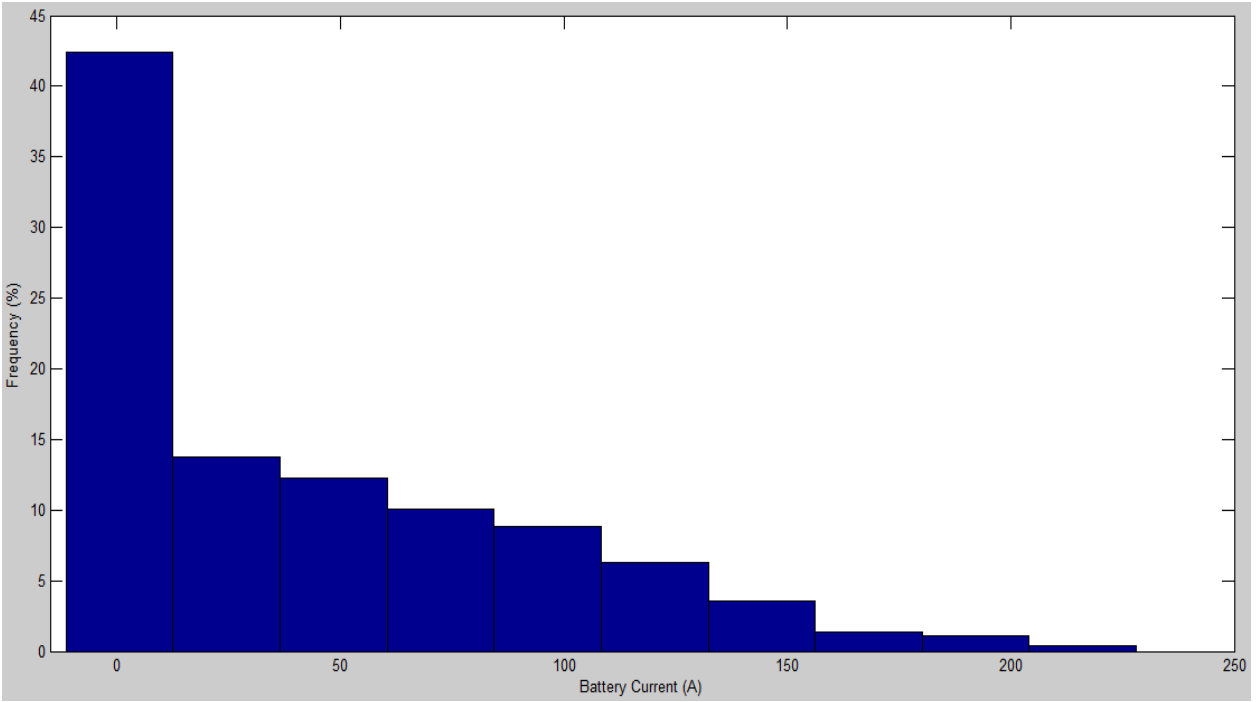

Fig 71: Frequency Distribution of Battery Current

Bin Average(A)	0.6	24.5	48.5	72.4	96.4	120.3	144.3	168.2	192.2	216.1
Freq (%)	42.4	13.7	12.2	10.0	8.8	6.3	3.6	1.4	1.1	0.4

Table 9: Frequency table of Battery Current

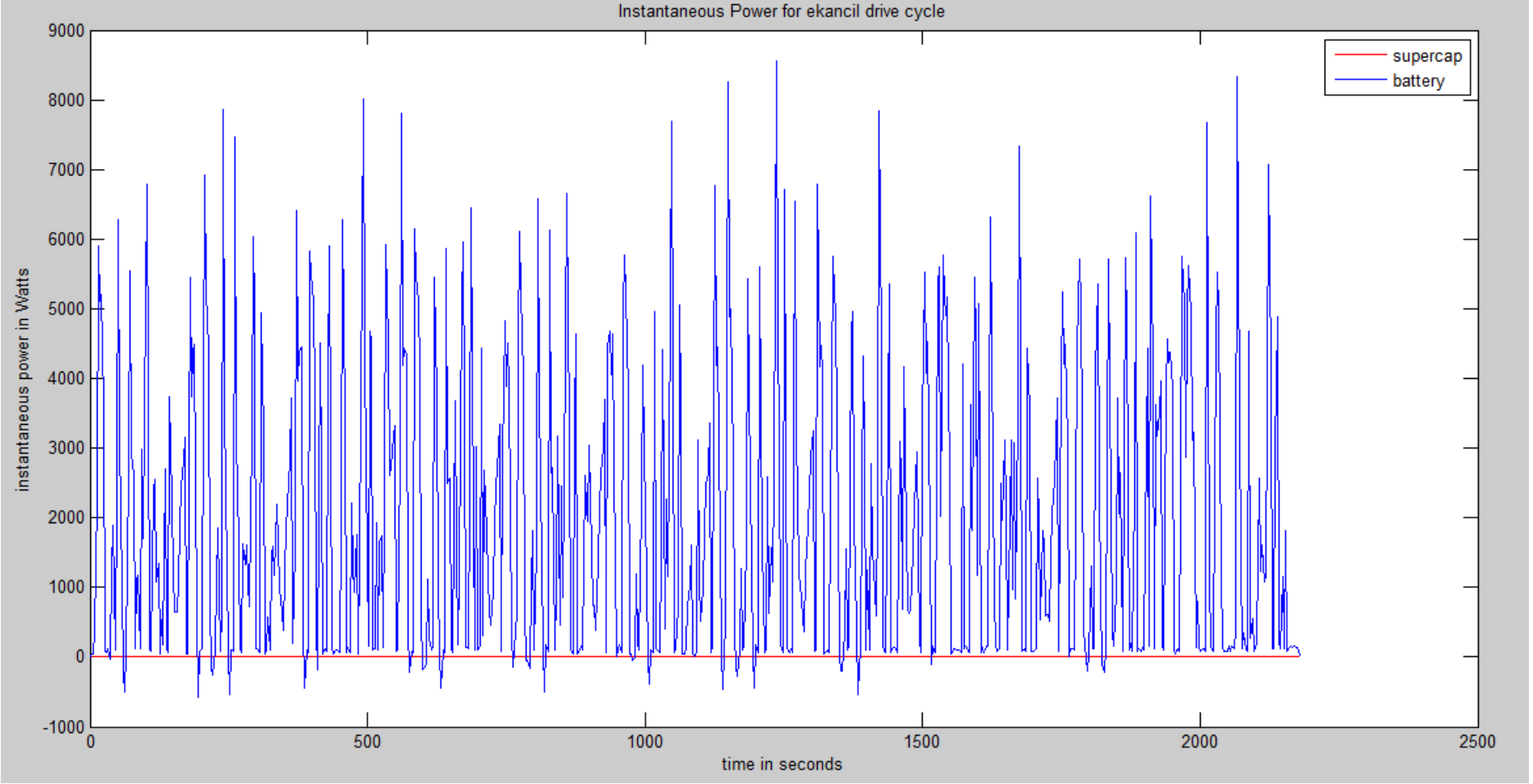

Fig 72 : Instantaneous Power

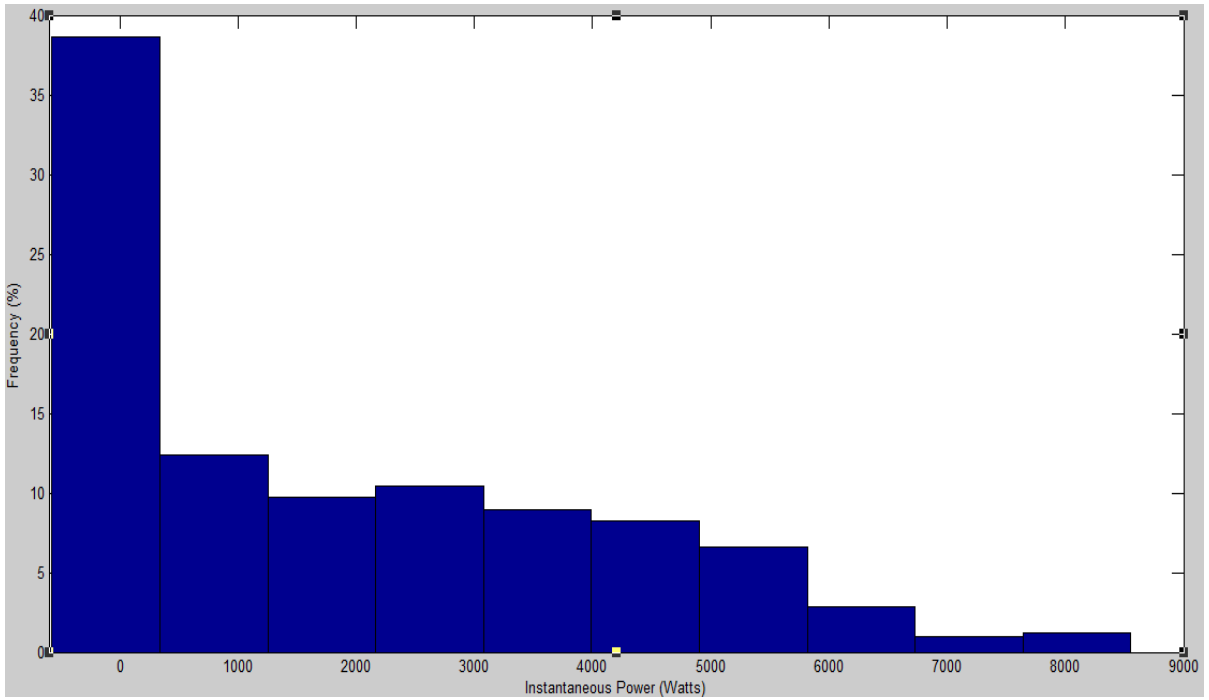

Fig 73: Frequency Distribution of Instantaneous Power

Bin Average (KW)	-0.1	0.8	1.7	2.6	3.5	4.4	5.4	6.3	7.2	8.1
Freq (%)	38.6	12.4	9.7	10.4	8.9	8.2	6.6	2.9	1.0	1.2

Table 10: Frequency table of Instantaneous Power delivered by Battery

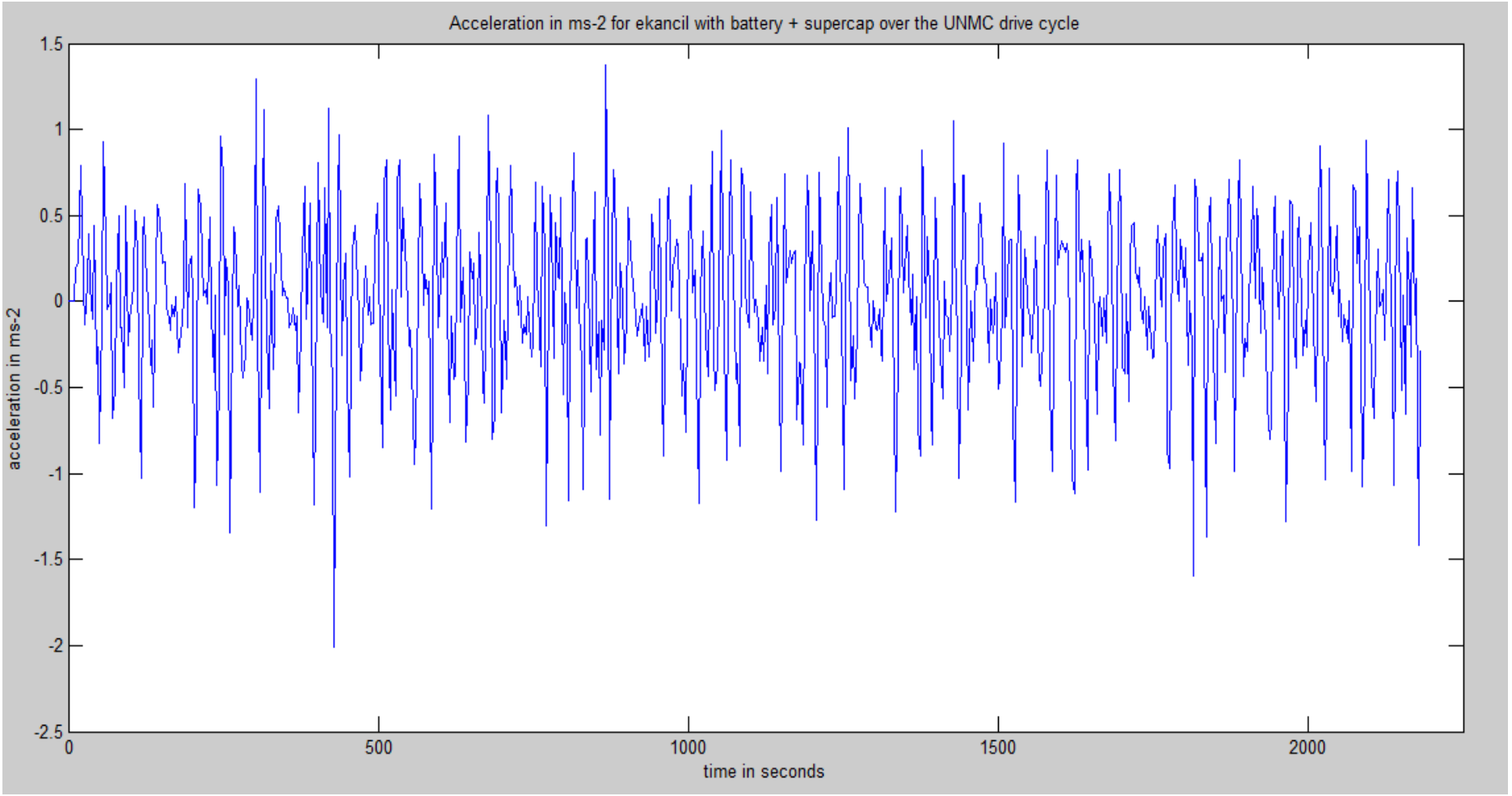

Fig 74 : Vehicle Acceleration

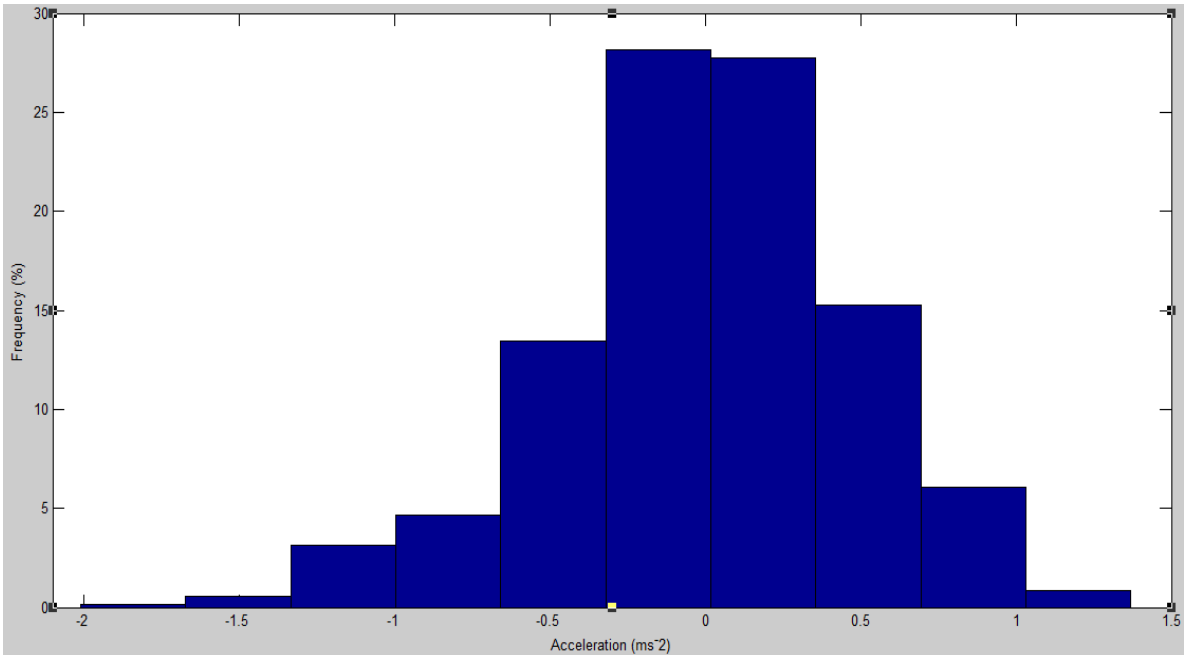

Fig 75: Frequency Distribution of Vehicle Acceleration

Bin Average (ms^{-2})	-1.8	-1.5	-1.2	-0.8	-0.5	-0.2	0.2	0.5	0.9	1.2
Freq (%)	0.1	0.5	3.2	4.7	13.5	28.2	27.7	15.2	6.0	0.8

Table 11: Frequency table of Vehicle Acceleration

4.1.2 Results: Battery + Supercapacitor in Parallel

(48.3 → 45.8)

	Battery	Supercap
Initial Voltage (V)	49.7	49.7
Average Voltage Drop (V)	0.51	0.48
Max. Voltage Drop during Drive Cycle (V)	2.5	2.2
Average Current delivered by : (A)	33.10	0.44
Peak Current delivered by : (A)	111.2	131.2
Average Instantaneous Power delivered by: (W)	1530.8	16.8
Average Instantaneous Power delivered by Bat + Supercap (W)	1547.6	
Peak Instantaneous Power delivered by: (W)	4714.9	5956.9
Peak Instantaneous Power delivered by Bat + Supercap : (W)	9356.3	
Average Acceleration (ms^{-2})	0.44	-
Max. Acceleration (ms^{-2})	2.57	-
Average deceleration (ms^{-2})	0.49	-
Max. deceleration (ms^{-2})	2.78	-

Table 12: Summary of results (battery + supercapacitor)

Figures 71 to 75 are graphical plots of battery voltage, battery current (drawn by the load while driving), the instantaneous power and the acceleration of the vehicle. The supercapacitor module was connected in parallel to the battery pack via a high power contactor which operates on a 12V dc coil powered by the

vehicle's accessory circuit. A switch attached to the dashboard of the vehicle triggers this contactor. As suggested by Pay et al [31], the supercapacitor was pre charged to the battery's terminal voltage (48V) before use. This is to ensure the former's voltage is tied to the latter's voltage at all times. A maximum battery voltage drop of 2.5V was recorded. At that point, it resulted in a dip from 48.3V to 45.8V which drew a current of 111.2 A from the battery pack. This is a 49% reduction in peak current drawn as compared to battery alone. An average current of 33.1 A was recorded for this particular trip which generally produced an average voltage drop of only 0.51 V during the trip. An Increase in acceleration was recorded with an average acceleration of $0.44ms^{-2}$ (18.9% increase) up to a maximum of 2.78 ms^{-2} (102.9% increase).

Shifting our attention to the supercapacitor module, we compare the figures 68 and 72 showing the current plots. In figure 68, large/sudden spikes or surges are observed to be drawn from the battery pack, 40% of the current drawn from the battery was above the 50A average while 17% of that current was above 100A. In figure 72 (blue plot indicates battery current), only 21% of the battery current logged was above 50A mark while a remarkable 0.38% of the 21% was above the 100A mark. This means that for 79% of the trip the battery provided less than 50A which is not detrimental to its health. In the long run, this will result in prolonged battery life. On the other hand, looking at the red plot (supercapacitor current), the entire peak current demands (spikes) come from the buffer supercapacitor module; up to a peak of 131.2 A. However there is a significant amount of negative current, which indicates that its interaction (charging) with the battery pack is key to the

entire hybrid system's ability to meet the load requirements of the vehicle. The average positive current drawn from the supercapacitor was found to be less than 1A throughout the whole trip.

Figure 74 plots the instantaneous total power of the hybrid power source i.e. battery + supercapacitor in a direct parallel combination. The total power delivered is equal to the sum of the powers delivered by the individual sources. The combined average power was equal to 1.5KW while the peak power was 9.4KW. This is equivalent to, or even surpasses the average power delivered by the battery alone with the extra advantage of diverting those high current surges from the battery pack.

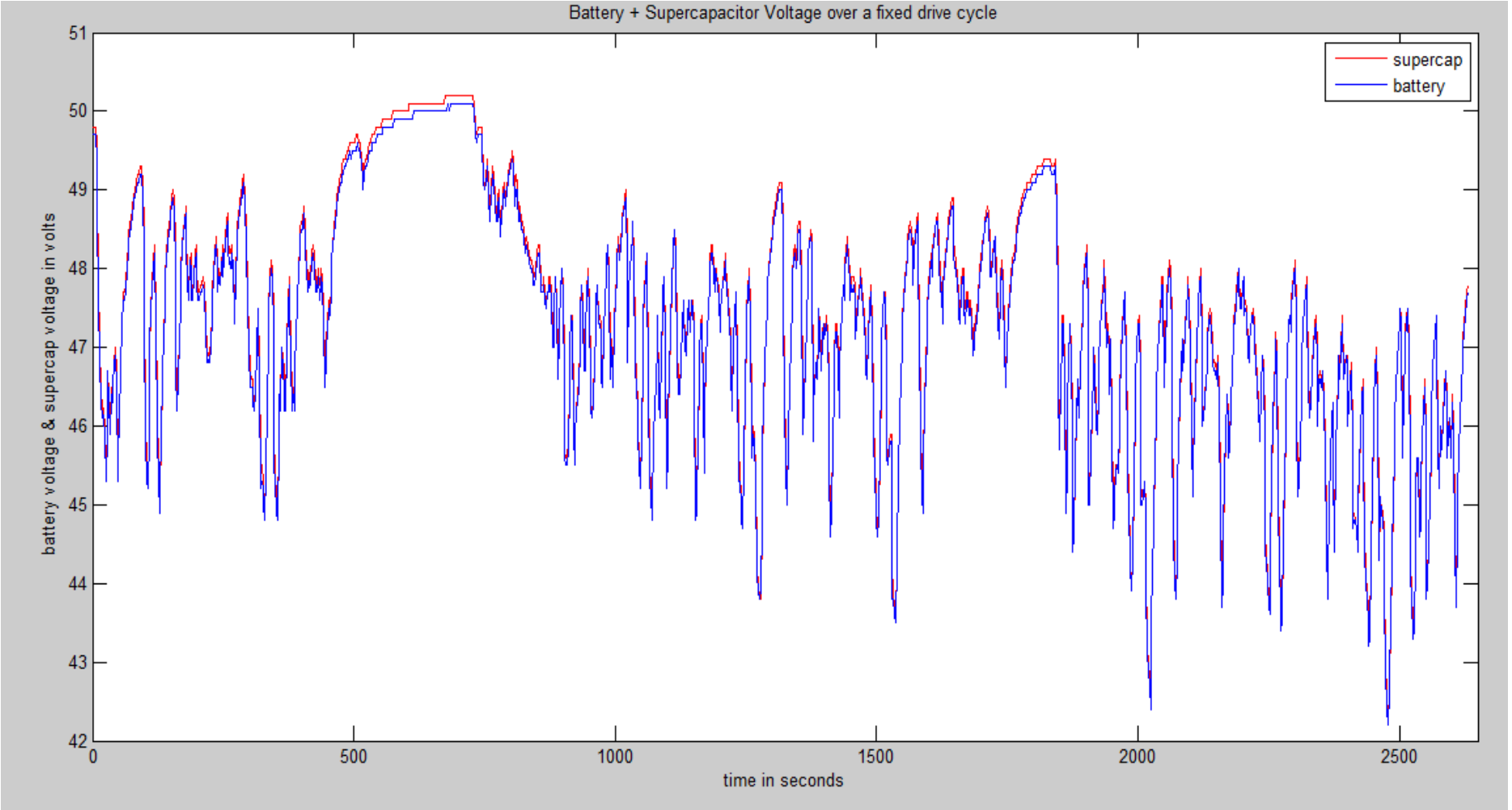

Fig 76: Battery + Supercapacitor Voltage

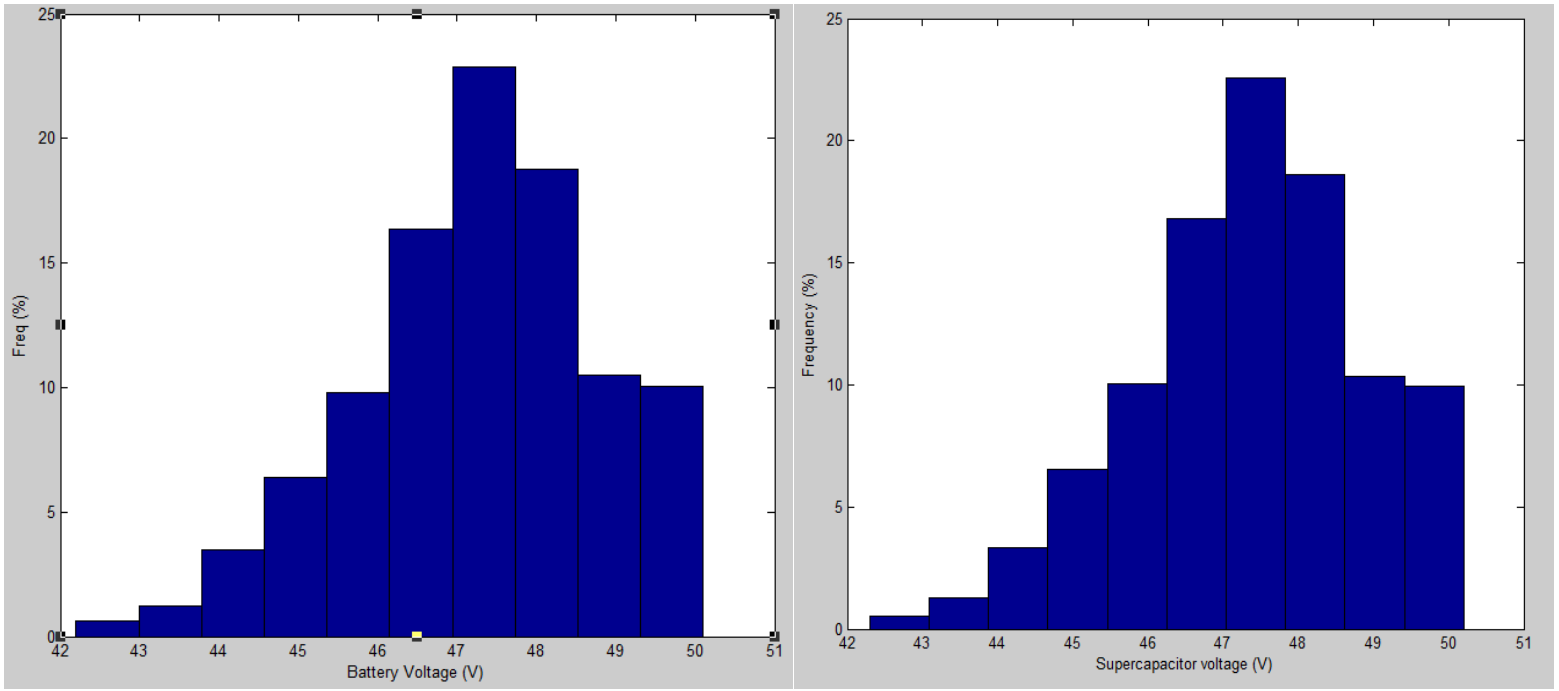

Fig 77: Frequency Distribution of Battery + Supercapacitor Voltage

Bin Average; Battery (V)	42.6	43.4	44.2	45.0	45.8	46.5	47.3	48.1	48.9	49.7
Freq (%)	0.6	1.2	3.5	6.4	9.8	16.3	22.9	18.8	10.5	10.0

Table 13: Frequency table of Battery Voltage

Bin Average ; Supercap(V)	42.7	43.5	44.3	45.0	45.9	46.6	47.4	48.2	49.0	49.8
Freq (%)	0.5	1.3	3.3	6.5	10.0	16.8	22.6	18.6	10.3	10.0

Table 14: Frequency table of Supercapacitor Voltage

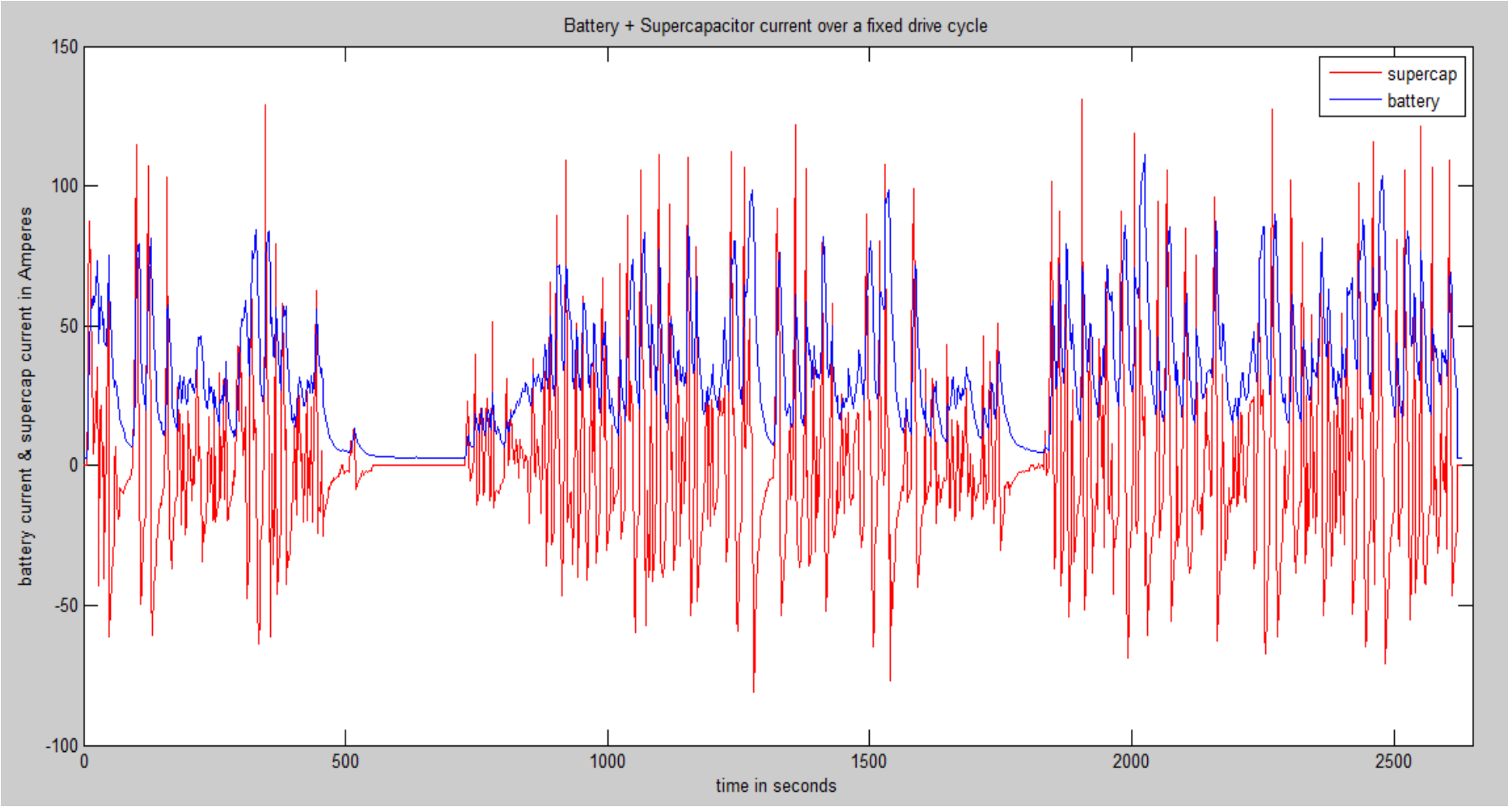

Fig 78:Battery + Supercapacitor Current

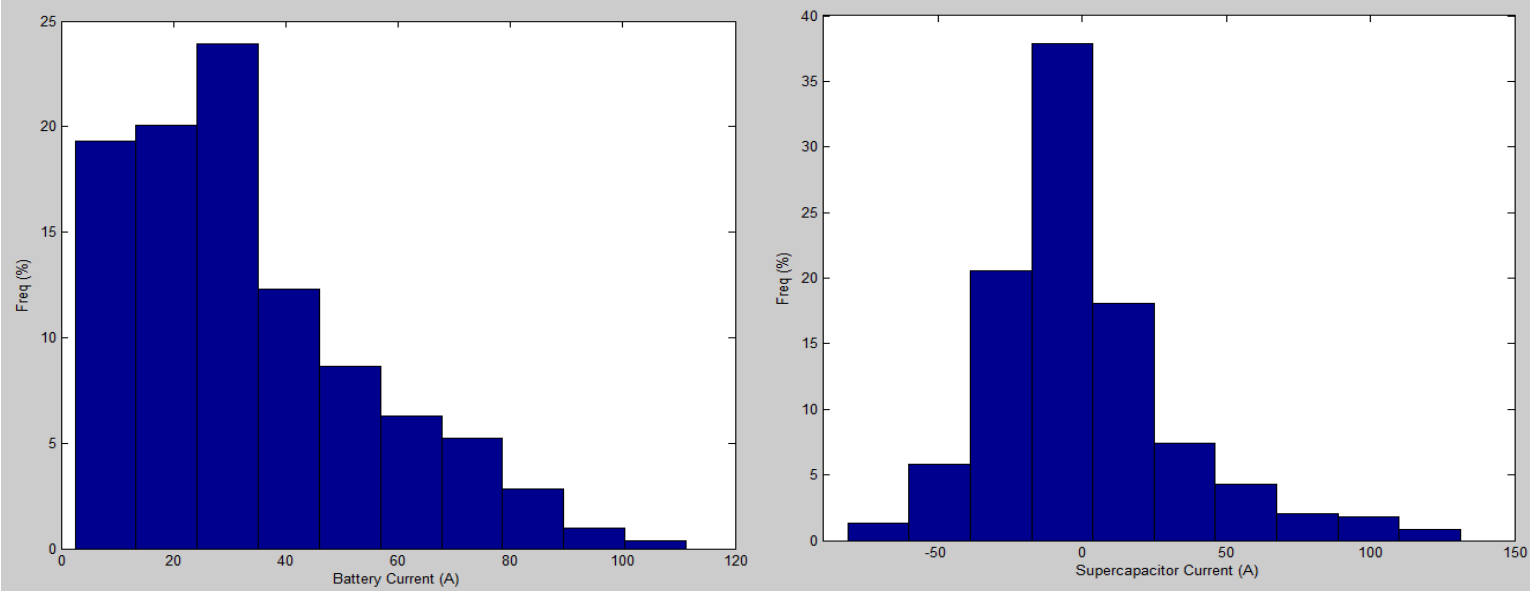

Fig. 79: Frequency Distribution of Battery + Supercapacitor Current

Bin Average; Battery(A)	7.9	18.8	29.8	40.5	51.4	62.3	73.2	84.0	94.9	105.8
Freq (%)	19.3	20.1	23.9	12.3	8.7	6.3	5.22	2.8	1.0	0.4

Table 15: Frequency table of Battery Current

Bin Average; Supercap(A)	-70.6	-49.3	-28.1	-6.9	14.4	35.6	56.89	78.1	99.3	120.6
Freq (%)	1.3	5.8	20.6	37.8	18.1	7.4	4.3	2.1	1.8	0.8

Table 16: Frequency table of Supercapacitor Current

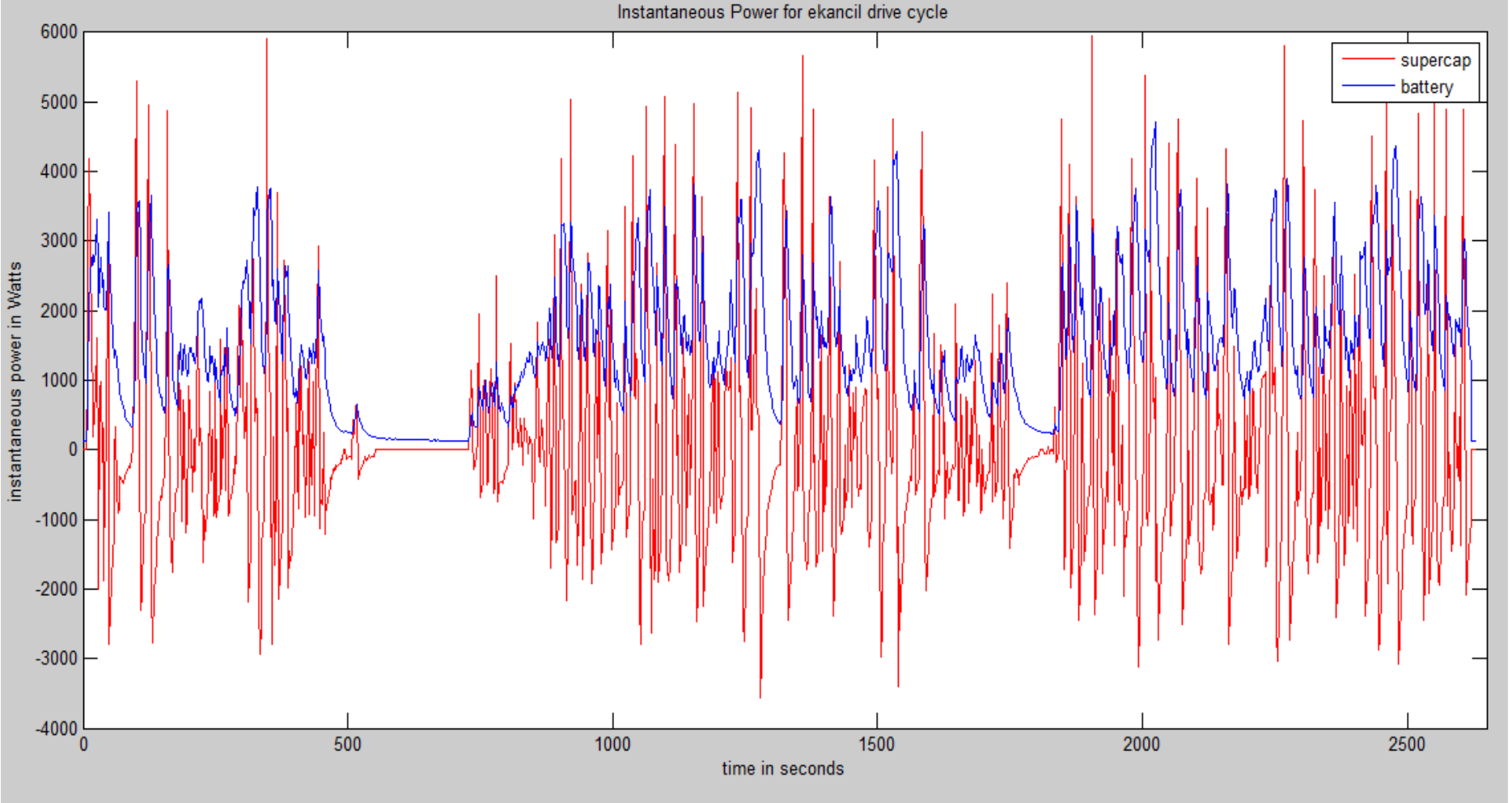

Fig 80: Instantaneous Power delivered by Battery + Supercapacitor Hybrid

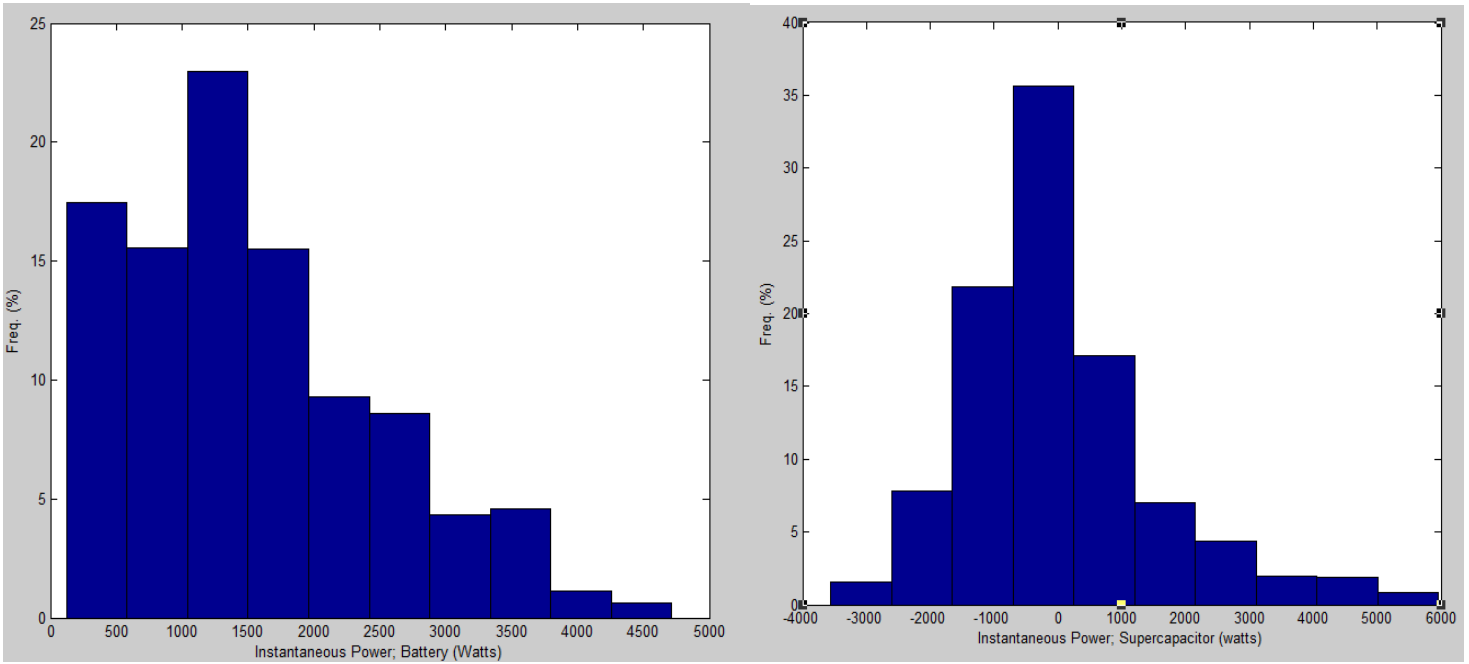

Fig 81: Frequency Distribution of Battery + Supercapacitor Instantaneous Power

Bin Average; Battery (KW)	0.4	0.8	1.3	1.7	2.2	2.6	3.1	3.6	4.0	4.5
Freq (%)	17.5	15.6	22.9	15.5	9.3	8.6	4.3	4.6	1.13	0.6

Table 17: Frequency table of Power delivered by Battery

Bin Average; Supercapacitor (KW)	-3.1	-2.1	-1.1	-0.2	0.7	1.7	2.6	3.6	4.5	5.5
Freq (%)	1.6	7.8	21.8	35.6	17.1	7.0	4.3	2.0	1.9	0.8

Table 18: Frequency table of Power delivered by Supercapacitor

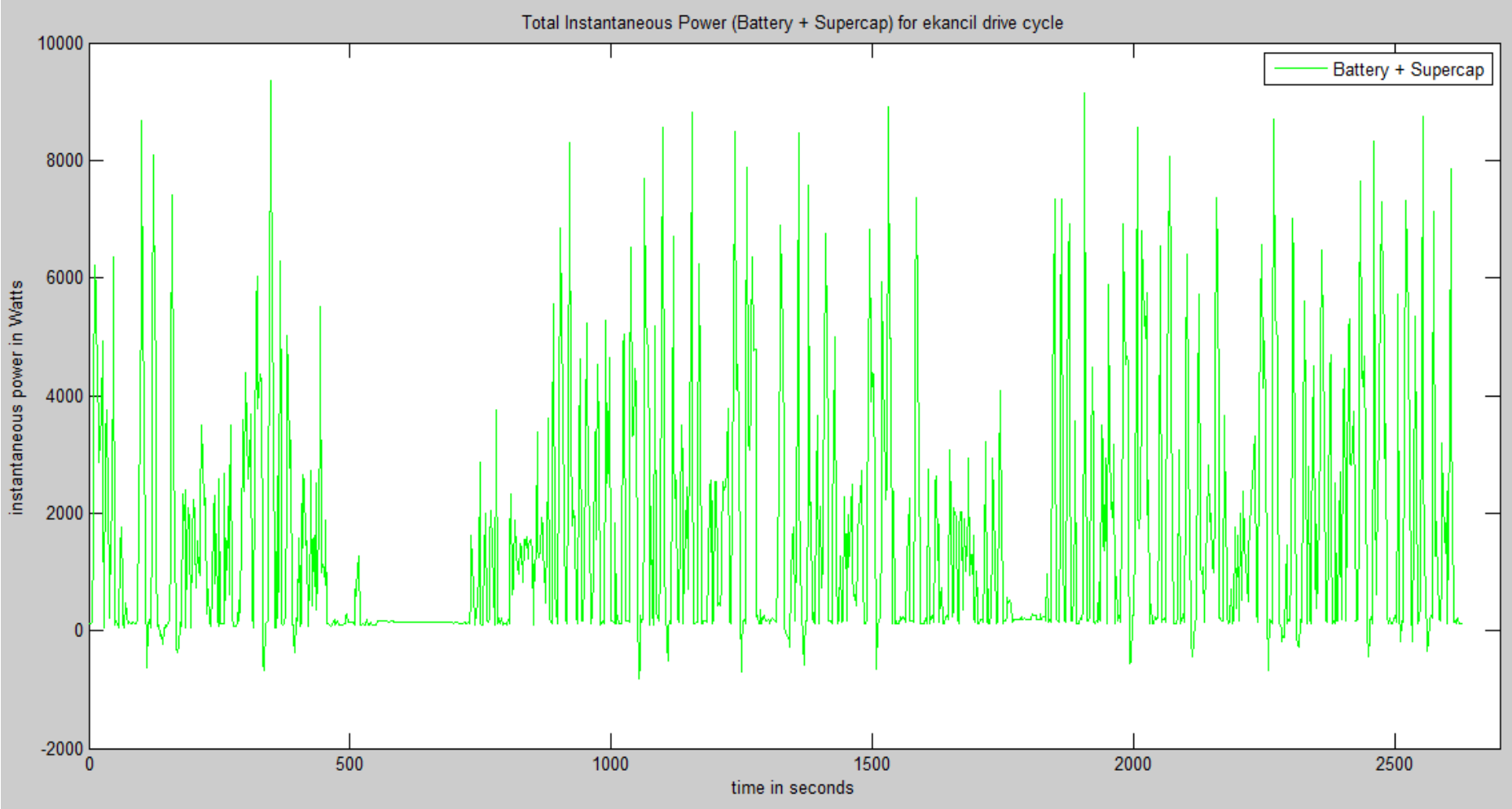

Fig 82: Effective Instantaneous Power delivered by Battery + Supercapacitor Hybrid

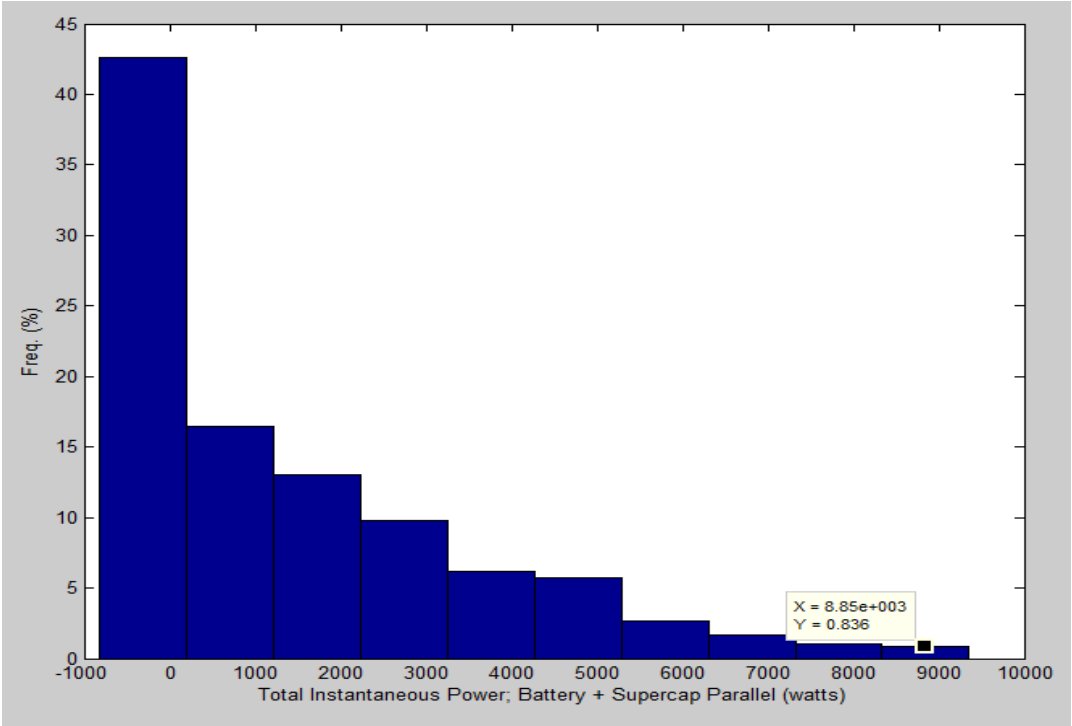

Fig 83: Frequency Distribution of Effective Instantaneous Power

Bin Average (KW)	-0.3	0.7	1.7	2.7	3.8	4.8	5.8	6.8	7.8	8.8
Freq (%)	42.6	16.4	13.1	9.8	6.2	5.7	2.7	1.7	1.1	0.8

Table 19: Frequency table of Effective Power delivered by Hybrid Source

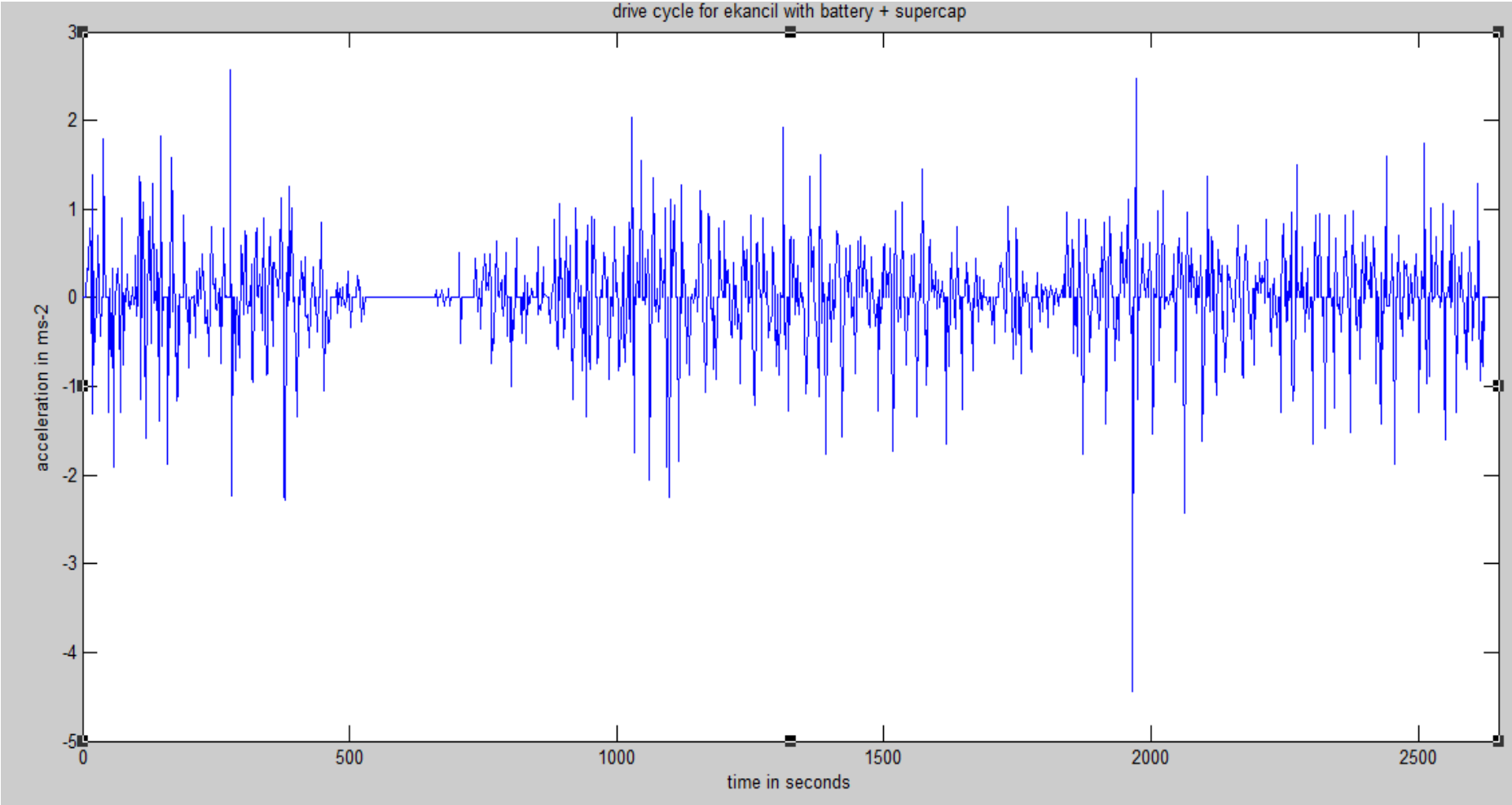

Fig 84: Vehicle Acceleration

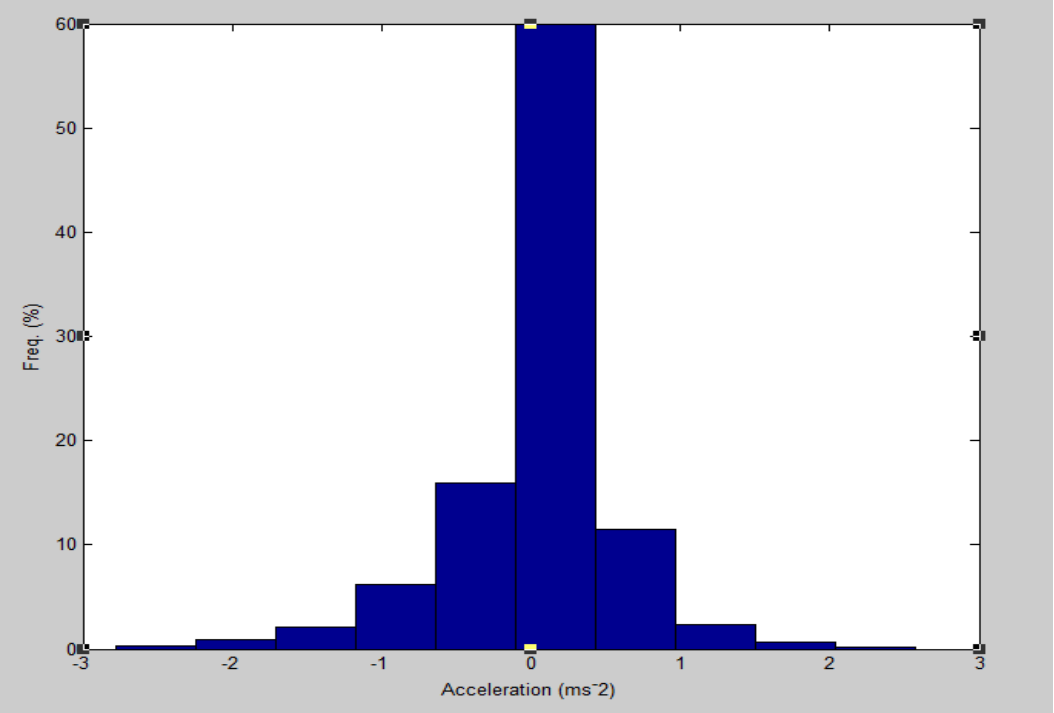

Fig 85: Frequency Distribution of Vehicle Acceleration

Bin Average (ms^{-2})	-2.5	-2.0	-1.4	-0.9	-0.4	0.2	0.7	1.2	1.8	2.3
Freq (%)	0.3	0.9	2.1	6.2	16.0	60	11.5	2.4	0.7	0.2

Table 20: Frequency table of Vehicle Acceleration

4.1.3 Results: Battery + Supercapacitor in Parallel (Mixed cycle)

The third part of the on-road vehicle testing experiment involves a mixed cycle i.e. switching on the supercapacitor module during the trip. As with previous tests, both sources are pre-charged to the same level before testing. Table 21 below summarizes the first 400 seconds of the trip which only utilizes the battery pack to power the electric vehicle. An average voltage drop of 1.98V was recorded while a whopping maximum of 8V drop was recorded which lead to a dip from 47.5V to 39.5V. This is far below the battery's safety net of 42V i.e. 1.75V per cell. An average current of 39.5A up to a maximum peak of 207.2A was drawn from the battery pack.

0 → 400 Seconds: Battery ON, Supercap OFF

	Battery
Initial Voltage (V)	49.0
Average Voltage Drop (V)	1.98
Max. Voltage Drop during Drive Cycle (V)	8.0
Average Current delivered by : (A)	39.50
Peak Current delivered by : (A)	207.2
Average Instantaneous Power delivered by: (W)	1816.2
Peak Instantaneous Power delivered by: (W)	8495.2
Average Acceleration (ms^{-2})	0.29
Max. Acceleration (ms^{-2})	0.92
Average deceleration (ms^{-2})	0.49

Max. deceleration (ms^{-2})	1.42

Table 21: Summary of results (Mixed cycle I)

While driving the electric vehicle, the supercapacitor module was switched on at 401 seconds till the end of the trip (see figure 86 below). Table 22 summarises the results which have been plotted in figures 86 to 90 below. An average voltage drop of 0.87V for the battery and 0.78V for the supercapacitor was recorded while a maximum of approximately 3V drop was recorded for both. This keeps the battery within the safety zone (> 42V) unlike during the first 400 seconds of the drive cycle. Figure 86 shows the voltage plots for both sources. The dashed green line divides the plot into two parts; battery ON, Supercap OFF and Battery ON Supercap ON. The difference between these two situations is very evident as the battery voltage is haphazard for the first 400 seconds and later is held to a more stable discharge rate by the supercapacitor module. The average current drawn from the battery pack remains the same as expected (39.3 A) while the peak demand drastically drops (207.2A to 89.9 A). On the other hand, the supercapacitor takes full responsibility for fulfilling peak power demands. 195A peak was recorded while only an average current of 0.55A was drawn from the supercapacitor. By comparing tables 21 and 22 respectively in terms of power delivered to the load, single source (battery only) was able to provide an average power of 1.8KW and a peak of 8.5KW while the hybrid source (battery + supercap) was able to deliver average power on par (1.8KW) and even surpass the peak power demand (12.5KW). An Increase in acceleration was recorded with an average acceleration of $0.29ms^{-2}$ to $0.87ms^{-2}$ and a maximum of 0.92 ms^{-2} to 1.25 ms^{-2} (see figure 90).

401 → 2406 Seconds: Battery ON, Supercap ON

	Battery	Supercap
Initial Voltage (V)	48.7	48.9
Average Voltage Drop (V)	0.87	0.78
Max. Voltage Drop during Drive Cycle (V)	3.2	2.9
Average Current delivered by : (A)	39.30	0.55
Peak Current delivered by : (A)	89.9	195.8
Average Instantaneous Power delivered by: (W)	1829.0	33.8
Peak Instantaneous Power delivered by: (W)	4049.9	9300.5
Average Instantaneous Power delivered by Bat + Supercap: (W)	1795.2	
Peak Instantaneous Power delivered by Bat + Supercap : (W)	12520	
Average Acceleration (ms^{-2})	0.87	-
Max. Acceleration (ms^{-2})	1.25	-
Average deceleration (ms^{-2})	0.49	-
Max. deceleration (ms^{-2})	1.48	-

Table 22: Summary of results (Mixed Cycle II)

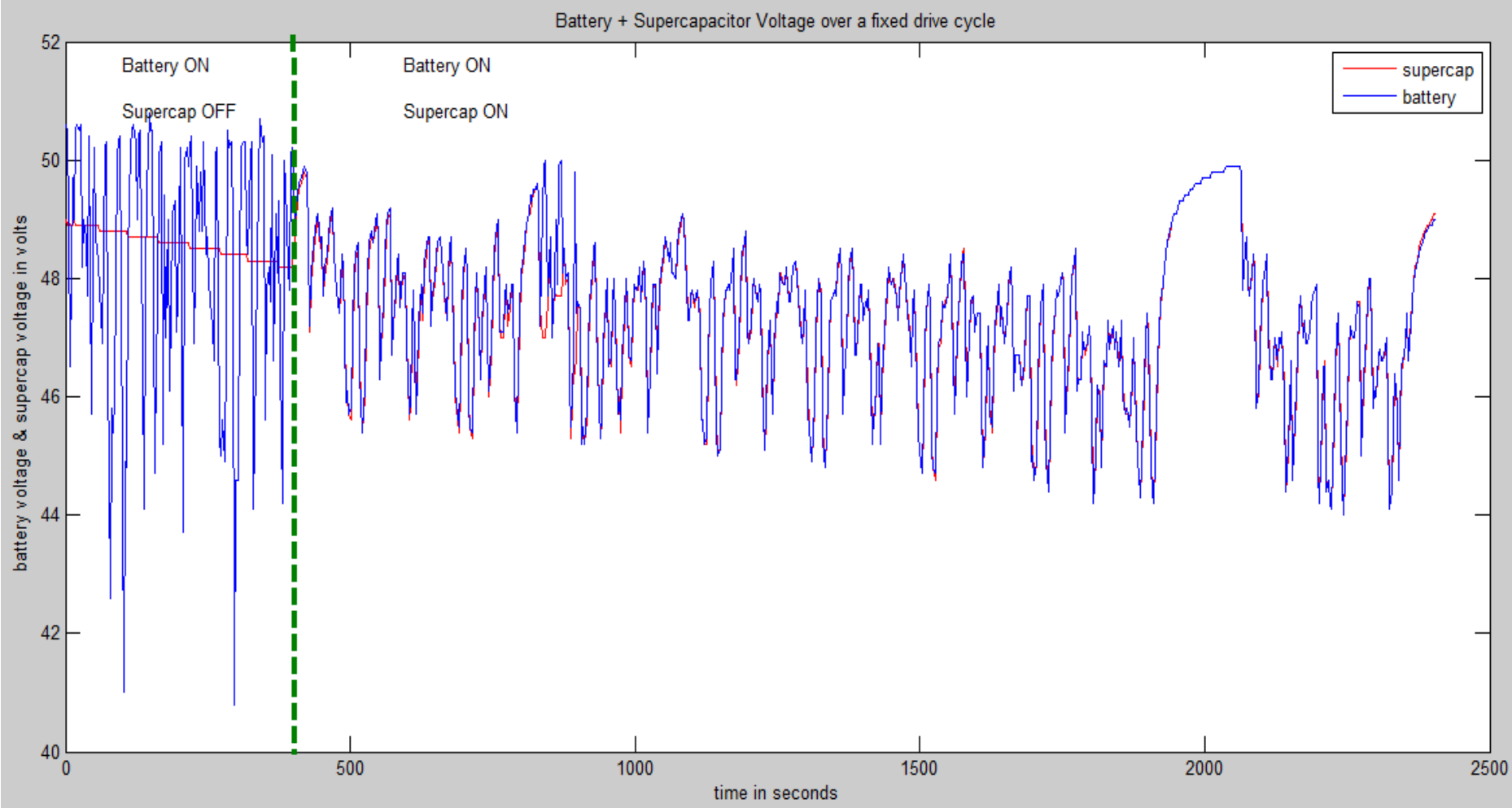

Fig 86: Battery + Supercapacitor Voltage (Mixed Cycle)

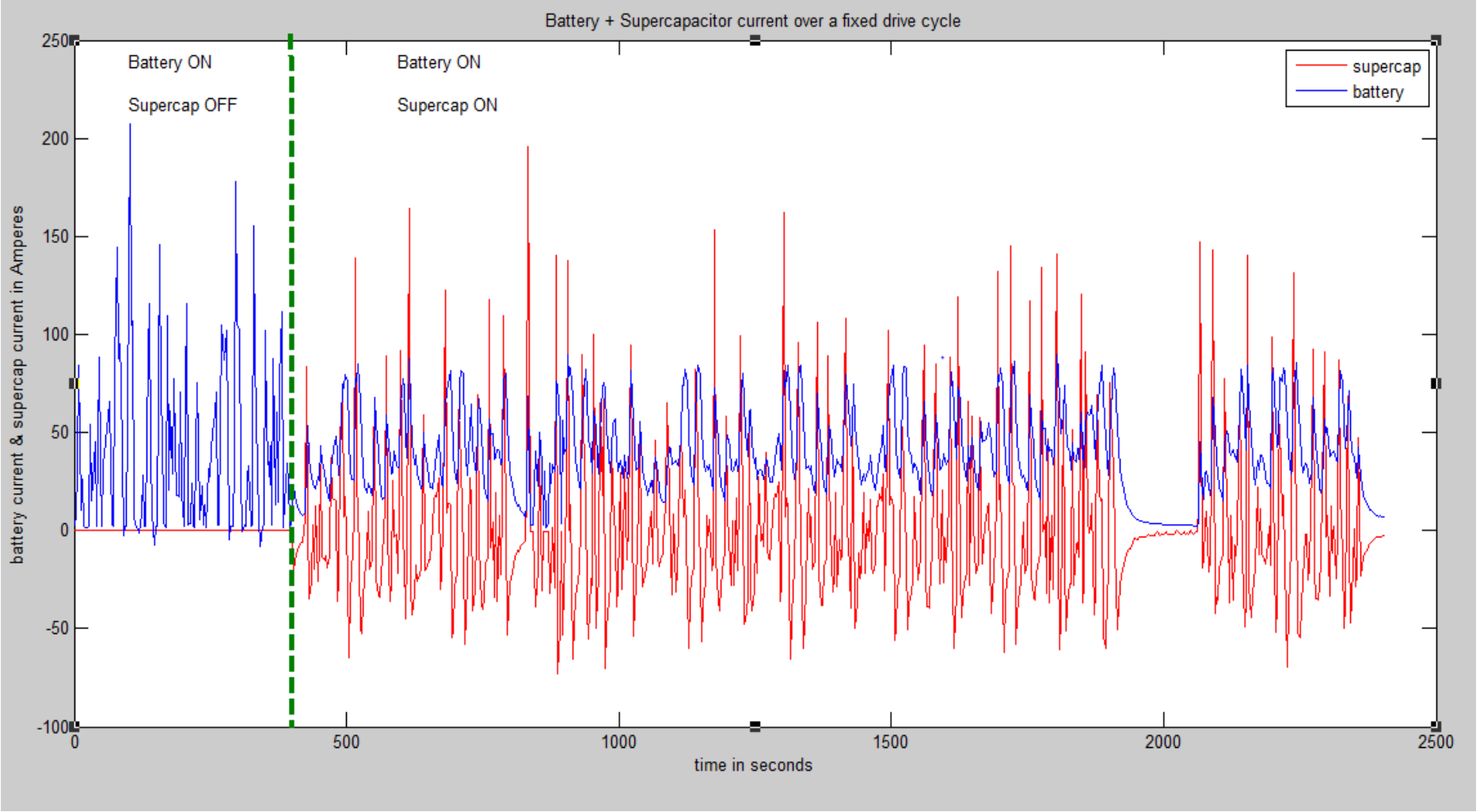

Fig. 87: Battery + Supercapacitor Current (Mixed Cycle)

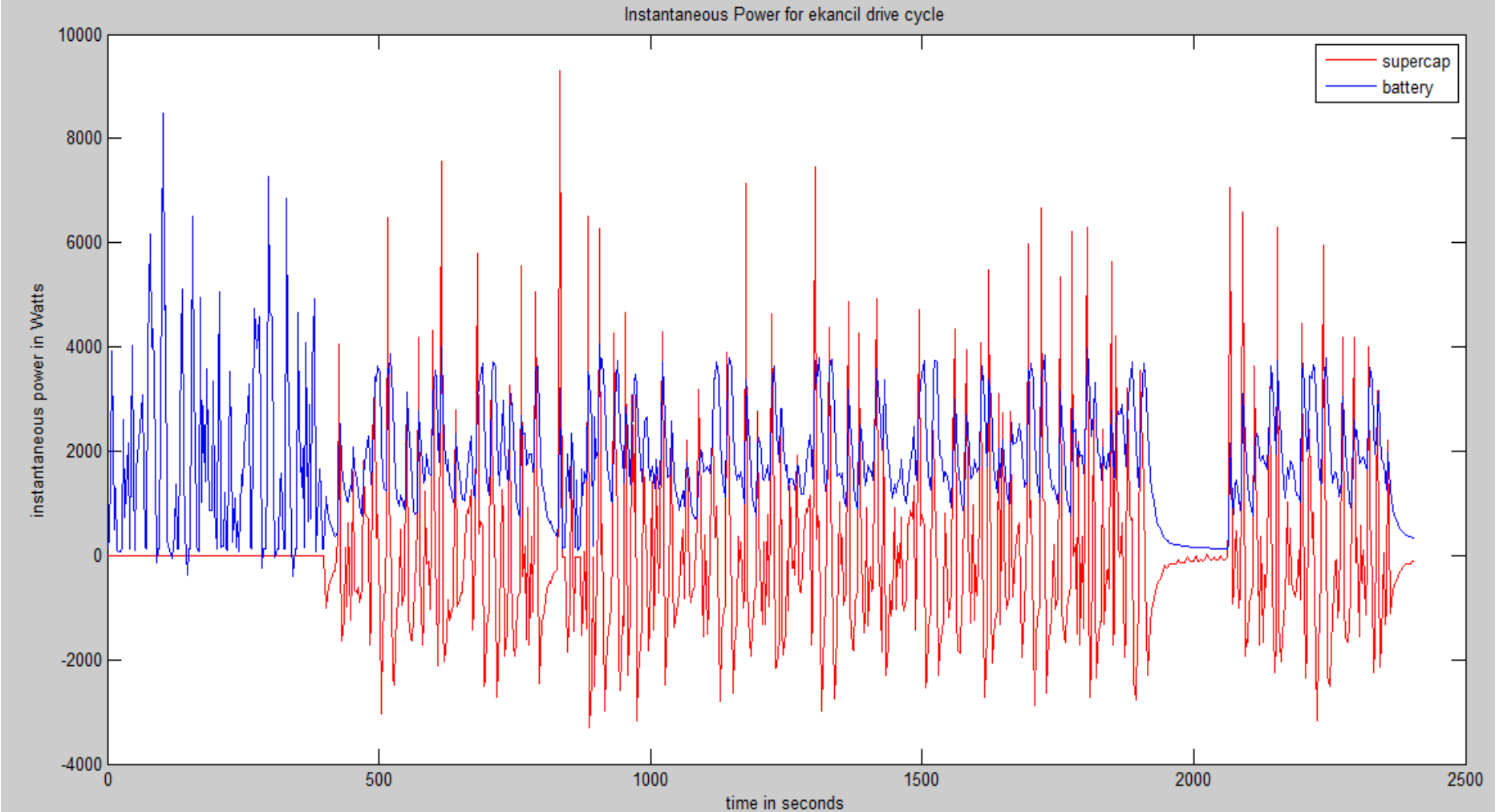

Fig 88: Battery + Supercapacitor Instantaneous Power (Mixed Cycle)

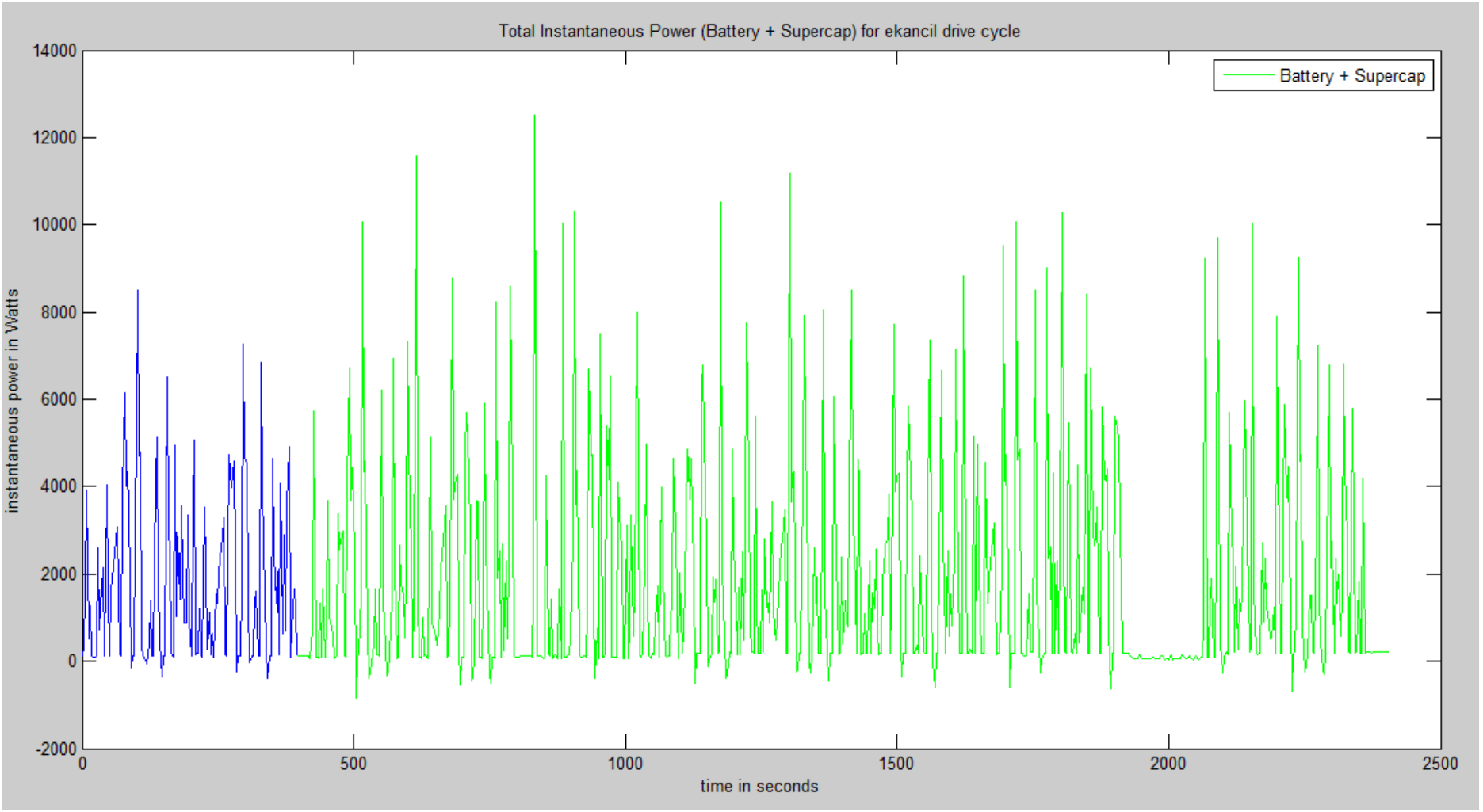

Fig 89: Effective Instantaneous Power of Hybrid Source (Mixed Cycle).

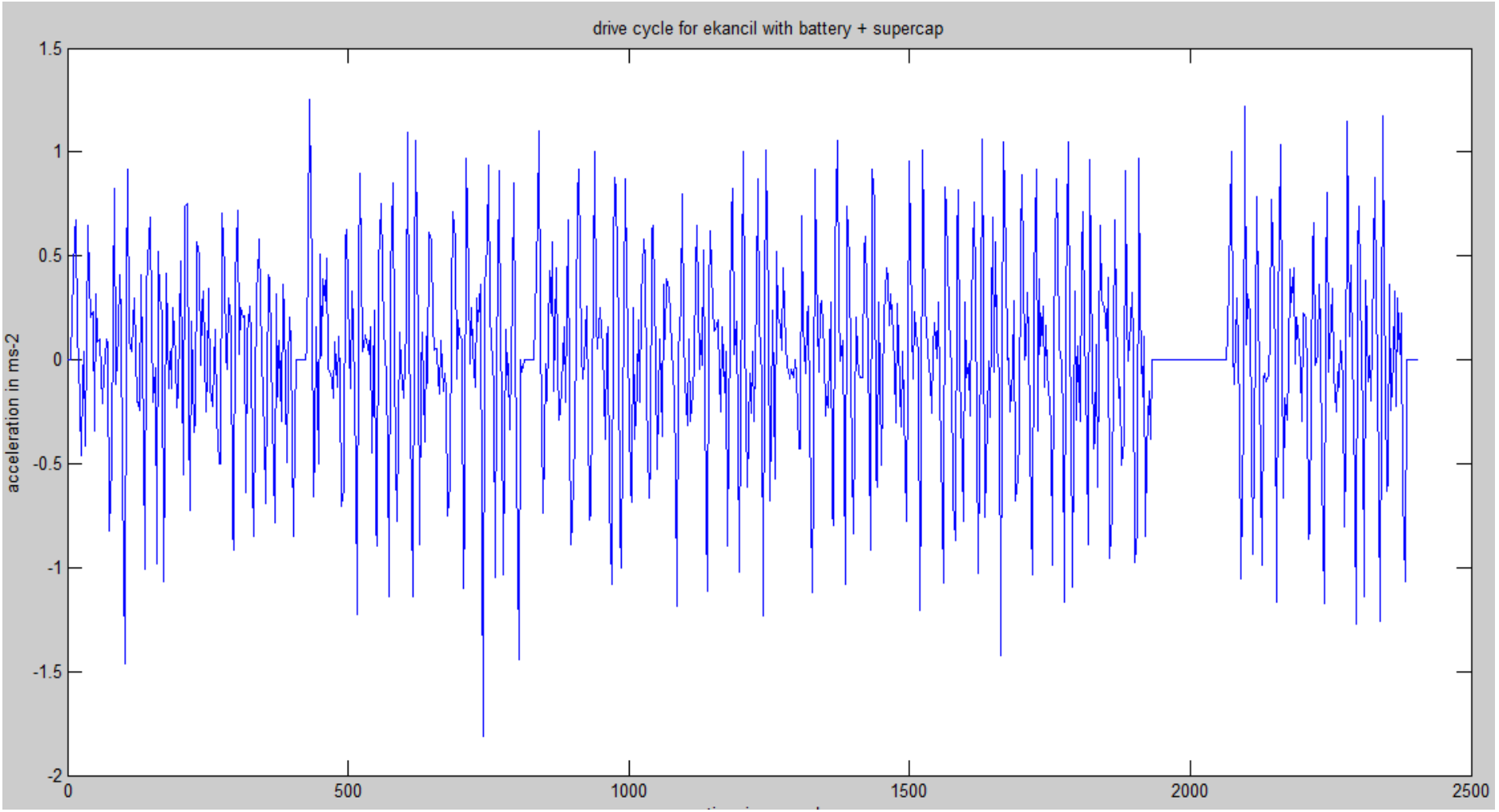

Fig 90: Vehicle Acceleration (Mixed cycle)

4.1.4 Results: Range test

Range anxiety is a major stumbling block to the popularity of EVs. There is a constant concern of running out of energy and being stranded on the way. This is caused by the limited amount of cruising range of the energy source. For the purpose of this research work, we are constrained by the type of battery pack used i.e. Trojan T105 deep cycle lead acid batteries. A range test was carried out to determine the effect of the supercapacitor module on the vehicle's range per charge. The same route was chosen i.e. the UNMC drive cycle and the same driver except for varying traffic conditions which generally could not be helped at the time of this experiment. In all cases the battery is charged to 100% SOC and the total range is estimated after the battery SOC swings to 50%. Table 23 below summarizes the results obtained from the range test.

	TOTAL RANGE PER CHARGE (KM)		
TEST NO	BATTERY ONLY	BATTERY+ SUPERCAPACITOR	% IMPROVEMENT
1	35.7	44.1	25.5
2	33.1	40.3	21.8
3	32.4	39.9	23.1
4	33.2	40.9	23.2
5	29.5	38.2	29.5
6	30.2	39.4	30.5
7	29.0	38.1	31.3
8	33.4	39.6	18.6
9	29.3	38.9	32.8
10	29.8	38.3	28.5

Table 23: Summary of the Range Test for electric kancil

From the results above, the battery can power the electric vehicle solely from between 29km to 35.7km with an average range per charge of 28.2km. However, with the supercapacitor module directly in parallel with the battery pack, there is a significant increase in range per charge (between 21.8% and 32.8%), which resulted

in an average increase in range per charge to 39.8km. It should be noted that both battery and supercapacitor are charged to 100% SOC before testing.

4.2 UNMC DRIVE CYCLE ANALYSES

This section is concerned with the analysis of the UNMC drive cycle for the electric vehicle conversion. A drive cycle as we know it, is merely a representation of how any vehicle is driven (i.e. speed versus time). Actual On-the-road drive cycles are important for battery energy consumption and sizing studies in electric vehicles and they represent driving patterns much better than synthesized drive cycles [114]. Even though they are difficult to implement on standard dynamometer chassis and are plagued by poor repeatability issues, they are able to provide the most accurate situation in terms of power flow between battery pack, supercapacitor and the vehicles load demand for this research work. With the on-board data acquisition system setup for the electric vehicle, we are able to see firsthand, the interaction between the battery and the supercapacitor module during a drive cycle.

We will divide the UNMC drive cycle as shown in the previous section into microtrips and analyse each trip based on some statistical features which have been determined by researchers as described in the literature review of this thesis. [116] describes a subsection of a drive cycle consisting of all data points between two idle periods as a driving pulse which we refer to as microtrip. They further go on to describe it as consisting of an acceleration phase, cruising phase and a subsequent phase deceleration phase. However, the time window size for each microtrip will vary based on the driving scenario. For example, idle + stop and go scenarios will have a small time window while highway scenarios will have a larger window size. A fixed time window may result in misrepresentation of actual driving scenario. A small window size may not be able to capture the entire acceleration and

deceleration event, while a large window size may record multiple events. The figure below shows UNMC drive cycle divided into 52 microtrips; 11 of which are shown.

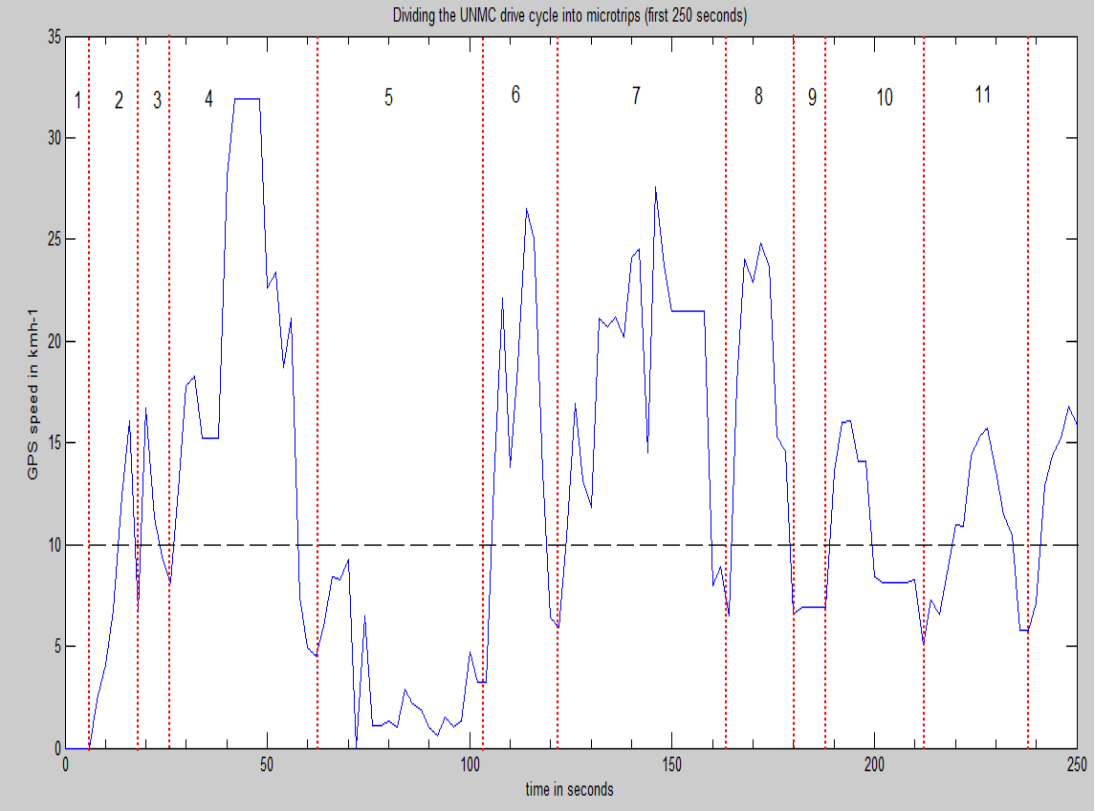

Fig 91: Dividing the UNMC Drive Cycle into Microtrips

For each microtrip, 14 statistical features were calculated by a custom MATLAB program (see appendix). The results are shown in tables 24 to 28 below. Apart from the features described in [61]-[66] of the literature review, two additional features, the maximum positive jerk and the average positive jerk are calculated. This is to observe the driver aggressiveness which has an effect on amount of current drawn [64]. Columns highlighted in red represent a stop condition while columns in yellow represent stop and go i.e. < 10kph.

	Microtrip 1	Microtrip 2	Microtrip 3	Microtrip 4	Microtrip 5	Microtrip 6	Microtrip 7	Microtrip 8	Microtrip 9	Microtrip 10
Trip Time (s)	14	10	38	44	20	44	18	10	26	28
Max. Speed (kph)	16.1	16.7	31.9	9.3	26.5	27.6	24.8	6.9	16.1	15.7
Max. Acceleration (m/s2)	0.78	1.39	1.79	0.90	1.36	1.82	1.58	0.04	0.93	0.49
Max. Decceleration (m/s2)	-1.31	-1.31	-1.90	-1.29	-1.58	-1.88	-1.17	-1.11	-0.79	-0.65
Max. +ve Jerk (m/s3)	0.20	1.35	0.90	1.10	0.92	1.60	0.96	0.58	0.47	0.38
Mean Speed (kph)	6.93	10.44	18.99	3.23	14.83	17.57	17.37	6.84	10.38	10.15
Mean Acceleration (m/s2)	0.45	1.39	0.60	0.28	1.10	0.68	0.90	0.04	0.33	0.26
Std. Dev. Acceleration	0.21	0.00	0.58	0.27	0.29	0.64	0.66	0.00	0.43	0.15
Mean Decceleration (m/s2)	-1.31	-0.63	-0.69	-0.25	-0.80	-0.54	-0.50	-1.11	-0.39	-0.28
Mean +ve Jerk (m/s3)	0.50	0.31	0.33	0.17	0.34	0.44	0.58	0.04	0.18	0.21
% idle (stops)	14.29	0.00	0.00	4.55	0.00	0.00	0.00	0.00	0.00	0.00
% < 10kph	57.14	60.00	21.05	95.45	30.00	18.18	22.22	100.00	61.54	42.86
% 10 < V< 20kph	28.57	40.00	36.84	0.00	40.00	22.73	33.33	0.00	38.46	57.14
% 20< V< 45kph	0.00	0.00	42.11	0.00	30.00	59.09	44.44	0.00	0.00	0.00

Table 24: Statistical features of UNMC drive cycle: Microtrips 1:10

	Microtrip 11	Microtrip 12	Microtrip 13	Microtrip 14	Microtrip 15	Microtrip 16	Microtrip 17	Microtrip 18	Microtrip 19	Microtrip 20
Trip Time (s)	26	34	28	62	30	22	18	20	286	28
Max. Speed (kph)	16.80	32.60	21.30	36.90	25.40	16.40	9.50	17.00	7.60	18.40
Max. Acceleration (m/s2)	0.81	2.57	0.75	1.13	1.25	0.46	0.35	0.85	0.51	0.50
Max. Decceleration (m/s2)	-0.74	-2.24	-0.94	-2.28	-2.28	-0.57	-0.39	-1.06	-0.51	-0.74
Max. +ve Jerk (m/s3)	0.37	1.28	0.63	0.57	1.28	0.24	0.20	0.42	0.26	0.35
Mean Speed (kph)	12.47	13.08	13.95	20.54	14.65	11.41	7.36	8.48	0.54	10.93
Mean Acceleration (m/s2)	0.27	1.14	0.56	0.41	0.76	0.35	0.18	0.55	0.17	0.24
Std. Dev. Acceleration	0.27	1.29	0.15	0.32	0.45	0.16	0.24	0.41	0.15	0.16
Mean Decceleration (m/s2)	-0.33	-0.79	-0.43	-0.94	-0.67	-0.22	-0.14	-0.41	-0.19	-0.52
Mean +ve Jerk (m/s3)	0.19	0.52	0.43	0.38	0.43	0.09	0.04	0.03	0.09	0.18
% idle (stops)	0.00	0.00	0.00	0.00	0.00	0.00	0.00	10.00	80.42	0.00
% < 10kph	23.08	29.41	28.57	9.68	46.67	36.36	100.00	60.00	19.58	42.86
% 10 < V< 20kph	76.92	64.71	50.00	35.48	26.67	63.64	0.00	30.00	0.00	57.14
% 20< V< 45kph	0.00	5.88	21.43	54.84	26.67	0.00	0.00	0.00	0.00	0.00

Table 25: Statistical features of UNMC drive cycle: Microtrips 11:20

	Microtrip 21	Microtrip 22	Microtrip 23	Microtrip 24	Microtrip 25	Microtrip 26	Microtrip 27	Microtrip 28	Microtrip 29	Microtrip 30
Trip Time (s)	110	12	132	26	24	36	56	16	24	120
Max. Speed (kph)	20.70	14.60	23.40	19.90	27.10	35.60	26.20	21.40	23.10	26.80
Max. Acceleration (m/s2)	0.67	0.88	1.06	2.03	1.54	1.35	1.28	1.21	0.94	0.93
Max. Decceleration (m/s2)	-1.00	-0.58	-1.33	-1.75	-2.06	-2.25	-1.85	-1.07	-0.92	-1.21
Max. +ve Jerk (m/s3)	0.50	0.34	0.90	1.26	0.77	1.13	1.13	0.60	0.47	0.86
Mean Speed (kph)	9.60	10.25	14.93	9.65	18.33	20.70	14.22	14.95	14.38	17.74
Mean Acceleration (m/s2)	0.24	0.30	0.47	0.84	0.65	0.54	0.59	0.99	0.77	0.43
Std. Dev. Acceleration	0.23	0.39	0.33	0.85	0.63	0.44	0.51	0.31	0.26	0.27
Mean Decceleration (m/s2)	-0.27	-0.56	-0.51	-0.77	-0.70	-0.93	-0.64	-0.52	-0.44	-0.45
Mean +ve Jerk (m/s3)	0.17	0.39	0.24	0.67	0.32	0.38	0.36	0.37	0.13	0.31
% idle (stops)	0.00	0.00	0.00	0.00	0.00	0.00	0.00	0.00	0.00	0.00
% < 10kph	70.91	50.00	16.67	84.62	25.00	16.67	39.29	37.50	41.67	13.33
% 10 < V< 20kph	27.27	50.00	63.64	15.38	16.67	16.67	32.14	25.00	25.00	46.67
% 20< V< 45kph	1.82	0.00	19.70	0.00	58.33	66.67	28.57	37.50	33.33	40.00

Table 26: Statistical features of UNMC drive cycle: Microtrips 21:30

	Microtrip 31	Microtrip 32	Microtrip 33	Microtrip 34	Microtrip 35	Microtrip 36	Microtrip 37	Microtrip 38	Microtrip 39	Microtrip 40
Trip Time (s)	54	52	18	22	76	48	60	48	62	28
Max. Speed (kph)	23.80	26.40	21.40	17.40	26.30	21.20	23.60	21.00	10.30	17.80
Max. Acceleration (m/s2)	1.92	1.61	0.75	0.60	0.68	1.08	1.46	0.81	0.44	1.03
Max. Decceleration (m/s2)	-1.28	-1.76	-1.57	-0.85	-1.74	-1.33	-1.65	-1.26	-0.51	-0.85
Max. +ve Jerk (m/s3)	0.96	0.88	0.50	0.31	0.68	0.65	0.83	0.63	0.63	0.65
Mean Speed (kph)	17.18	15.57	13.67	12.61	18.42	14.93	16.34	13.23	6.04	13.29
Mean Acceleration (m/s2)	0.57	0.55	0.65	0.42	0.35	0.54	0.32	0.33	0.26	0.43
Std. Dev. Acceleration	0.60	0.56	0.15	0.21	0.25	0.43	0.36	0.23	0.15	0.37
Mean Decceleration (m/s2)	-0.52	-0.50	-0.56	-0.34	-0.61	-0.46	-0.56	-0.32	-0.20	-0.51
Mean +ve Jerk (m/s3)	0.33	0.43	0.03	0.22	0.24	0.29	0.21	0.24	0.02	0.34
% idle (stops)	0.00	0.00	0.00	0.00	0.00	0.00	0.00	0.00	12.90	0.00
% < 10kph	22.22	34.62	44.44	27.27	13.16	16.67	13.33	16.67	83.87	21.43
% 10 < V< 20kph	29.63	26.92	22.22	72.73	39.47	79.17	46.67	70.83	3.23	78.57
% 20< V< 45kph	48.15	38.46	33.33	0.00	47.37	4.17	40.00	12.50	0.00	0.00

Table 27: Statistical features of UNMC drive cycle: Microtrips 31:40

	Microtrip 41	Microtrip 42	Microtrip 43	Microtrip 44	Microtrip 45	Microtrip 46	Microtrip 47	Microtrip 48	Microtrip 49	Microtrip 50	Microtrip 51	Microtrip 52
Trip Time (s)	86.00	132.00	42.00	56.00	38.00	44.00	16.00	114.00	38.00	58.00	214.00	60.00
Max. Speed (kph)	9.30	37.60	25.90	23.70	27.50	26.10	9.20	27.70	23.60	23.60	33.90	18.50
Max. Acceleration (m/s2)	0.31	1.11	2.47	1.21	0.96	1.38	0.36	0.96	1.50	0.94	1.75	1.29
Max. Decceleration (m/s2)	-0.85	-2.78	-2.78	-2.43	-1.61	-1.10	-0.36	-1.29	-1.65	-1.47	-1.88	-1.29
Max. +ve Jerk (m/s3)	0.41	0.41	2.63	1.22	1.22	0.69	0.36	0.63	0.75	0.74	0.95	0.65
Mean Speed (kph)	2.38	16.16	14.75	15.95	17.68	14.90	7.45	16.63	17.98	13.56	18.05	9.35
Mean Acceleration (m/s2)	0.13	0.51	0.55	0.48	0.45	0.47	0.26	0.34	0.54	0.58	0.48	0.51
Std. Dev. Acceleration	0.09	0.31	0.75	0.39	0.26	0.38	0.09	0.28	0.56	0.38	0.39	0.42
Mean Decceleration (m/s2)	-0.34	-0.77	-1.35	-0.73	-0.83	-0.49	-0.14	-0.43	-0.73	-0.45	-0.55	-0.65
Mean +ve Jerk (m/s3)	0.08	0.04	0.31	0.34	0.14	0.17	0.08	0.30	0.13	0.23	0.36	0.17
% idle (stops)	34.88	0.00	0.00	0.00	0.00	0.00	0.00	0.00	0.00	0.00	0.00	16.67
% < 10kph	65.12	13.64	38.10	14.29	21.05	31.82	100.00	21.05	21.05	41.38	10.28	33.33
% 10 < V< 20kph	0.00	59.09	38.10	75.00	31.58	45.45	0.00	45.61	26.32	41.38	54.21	50.00
% 20< V< 45kph	0.00	27.27	23.81	10.71	47.37	22.73	0.00	33.33	52.63	17.24	35.51	0.00

Table 28: Statistical features of UNMC drive cycle: Microtrips 41:52

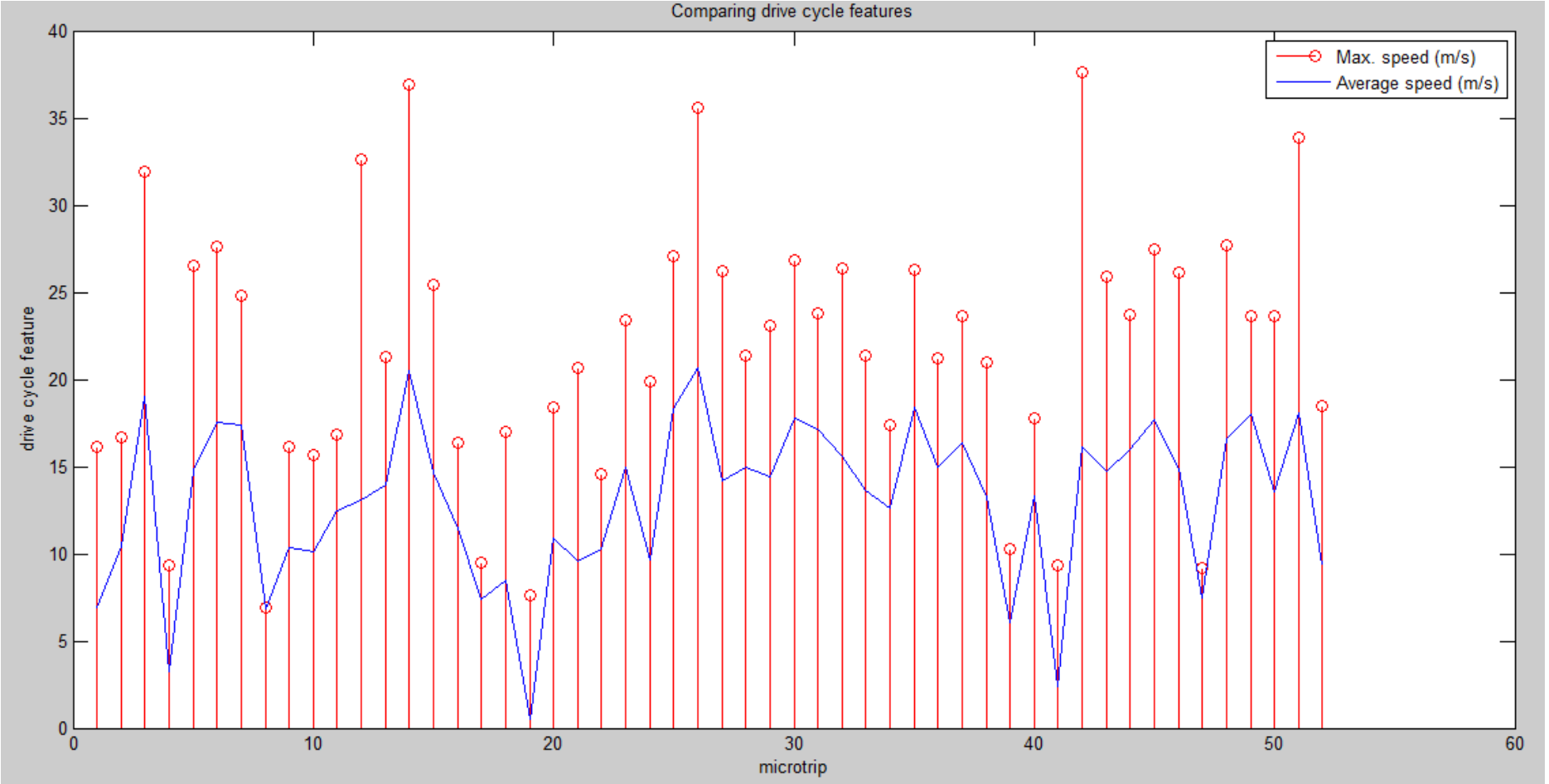

Fig 92: Stem Plot of Max. Speed & Average Speed versus 52 Microtrips(UNMC drive cycle)

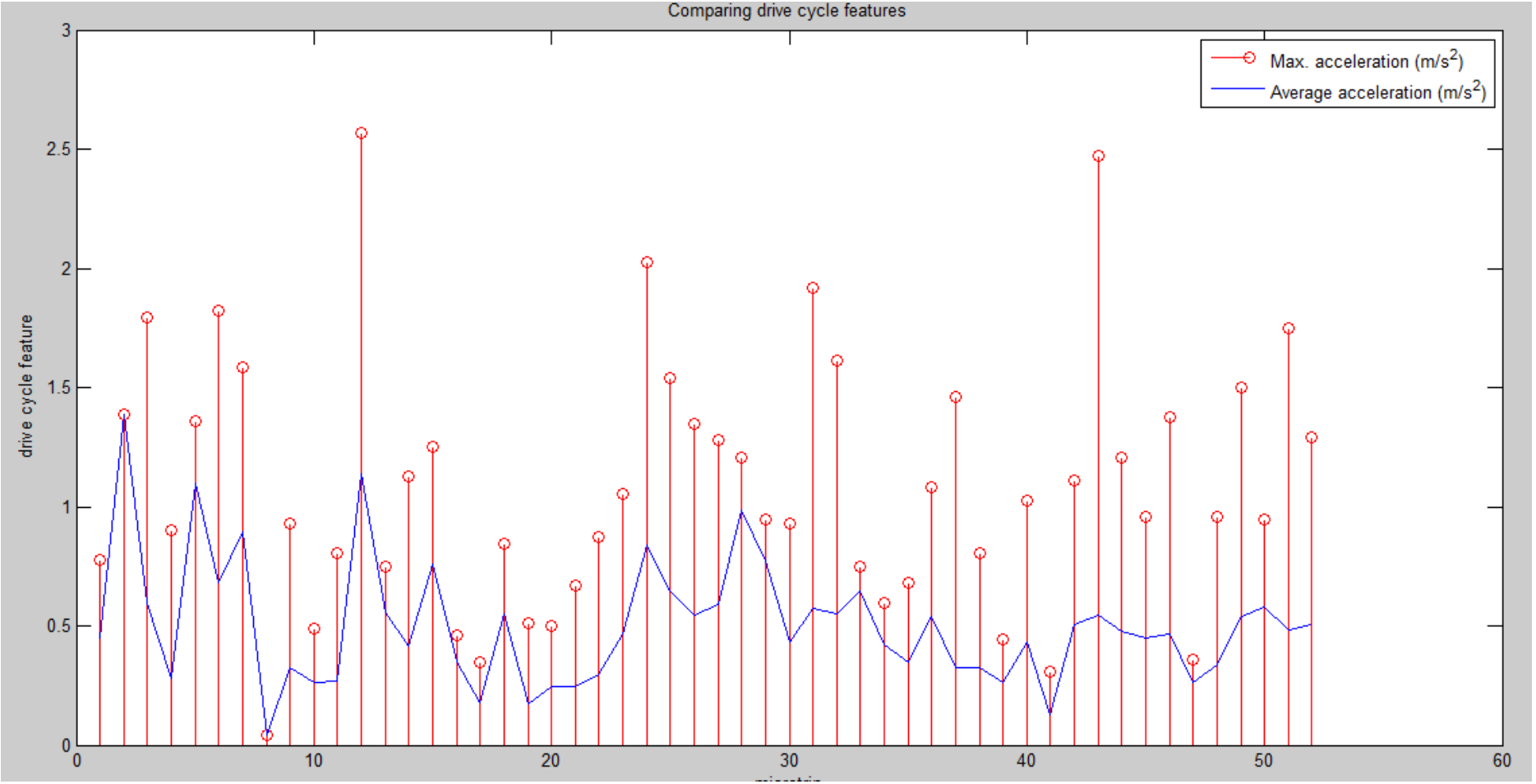

Fig 93: Stem Plot of Max. & Average Acceleration versus 52 Microtrips (UNMC drive cycle)

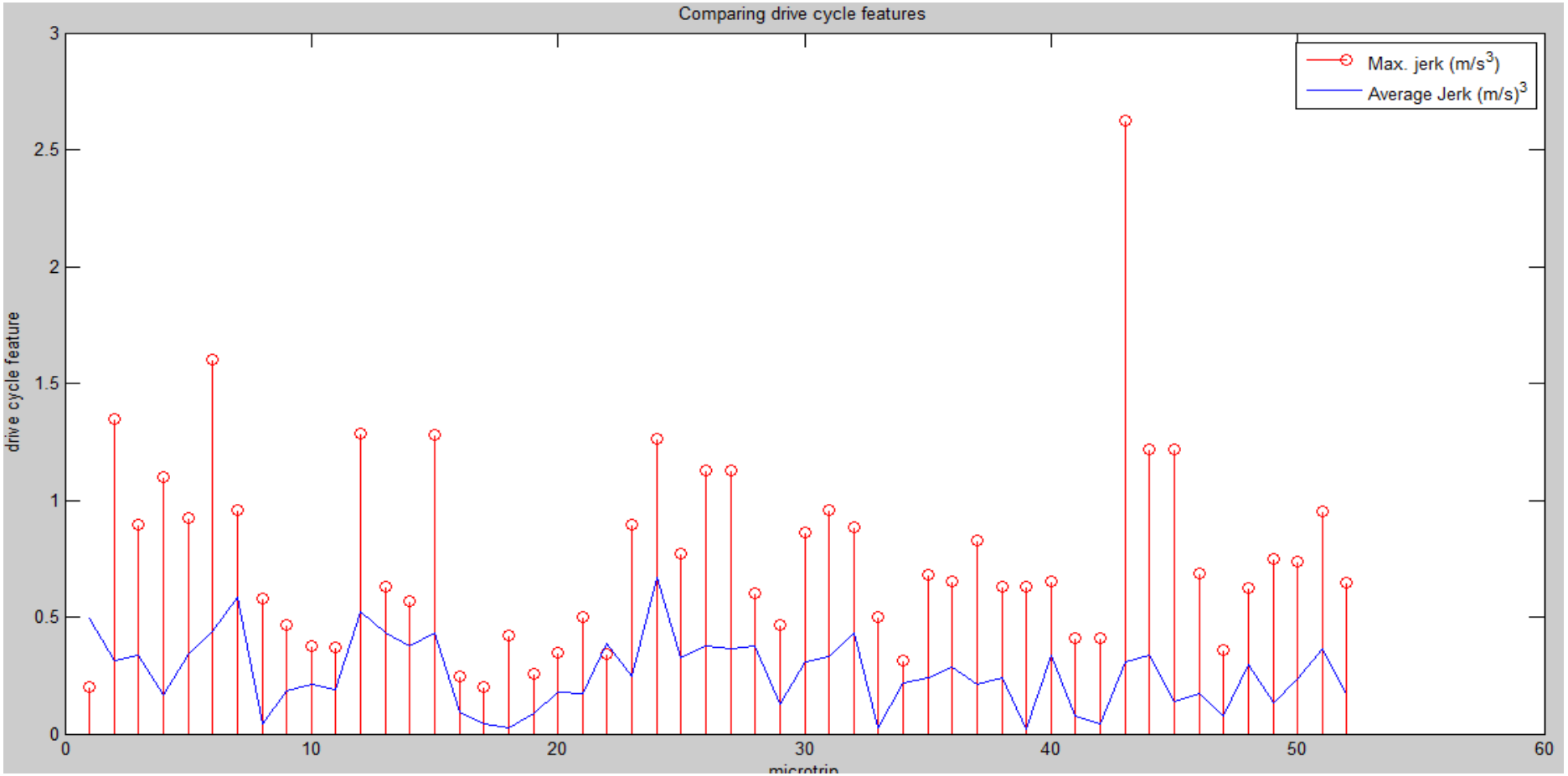

Fig 94: Stem Plot of Max. & Average Jerk versus 52 Microtrips (UNMC drive cycle)

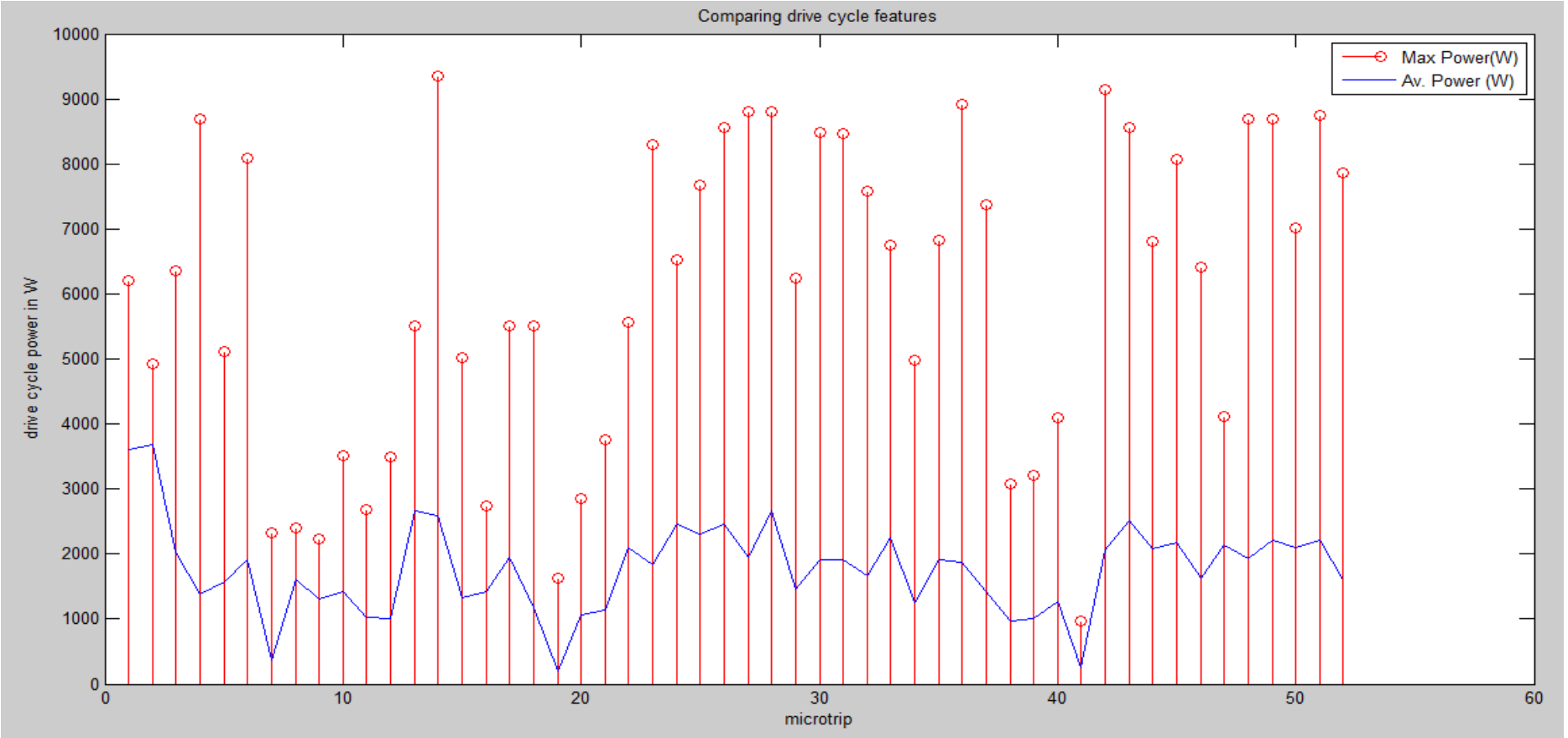

Fig 95: Stem Plot of Max. & Average Power versus 52 Microtrips (UNMC drive cycle)

Figures 92 – 95 above represent the stem plots of the drive cycle features against the microtrips of the UNMC drive cycle. According to J.S Won's driving trend identifier [44], the UNMC drive cycle falls under the category of low speed cruises whereby the average speed is under 40kph or 25mph. In order to identify the microtrips which contain aggressive driving i.e. rapid acceleration rates that draw peak currents from the energy source, a ratio called the acceleration feature is used [44]. This ratio is basically the standard deviation of positive acceleration divided by the mean positive acceleration per microtrip. This has enabled us to identify microtrips with high acceleration rates which correspond to peak power as shown in the step plot in figure 95 above. In order to analyse the energy contributed by the supercapacitor module during a peak load demand, exploded view of the power vs time graph (microtrips 2-6) is shown in the figures below. To calculate the energy contributed by the supercapacitor during peak load demands, the area under the power vs time plot (red shading) is found by numerical integration methods. According to [122], the usable energy of a supercapacitor cell or module is about 75% of its total energy E. This is in line with the assumption that the voltage is allowed to vary to half of its rated value via a suitable dc to dc converter. However, in this project a pure parallel connection means that the terminal voltage of the supercapacitor is always dictated by the battery pack's terminal voltage. Every discharge phase of the supercapacitor is always followed by a subsequent charge phase from the traction battery (negative red shaded area). Hence the supercapacitor is utilized on the average by about 23.6% of its total capability.

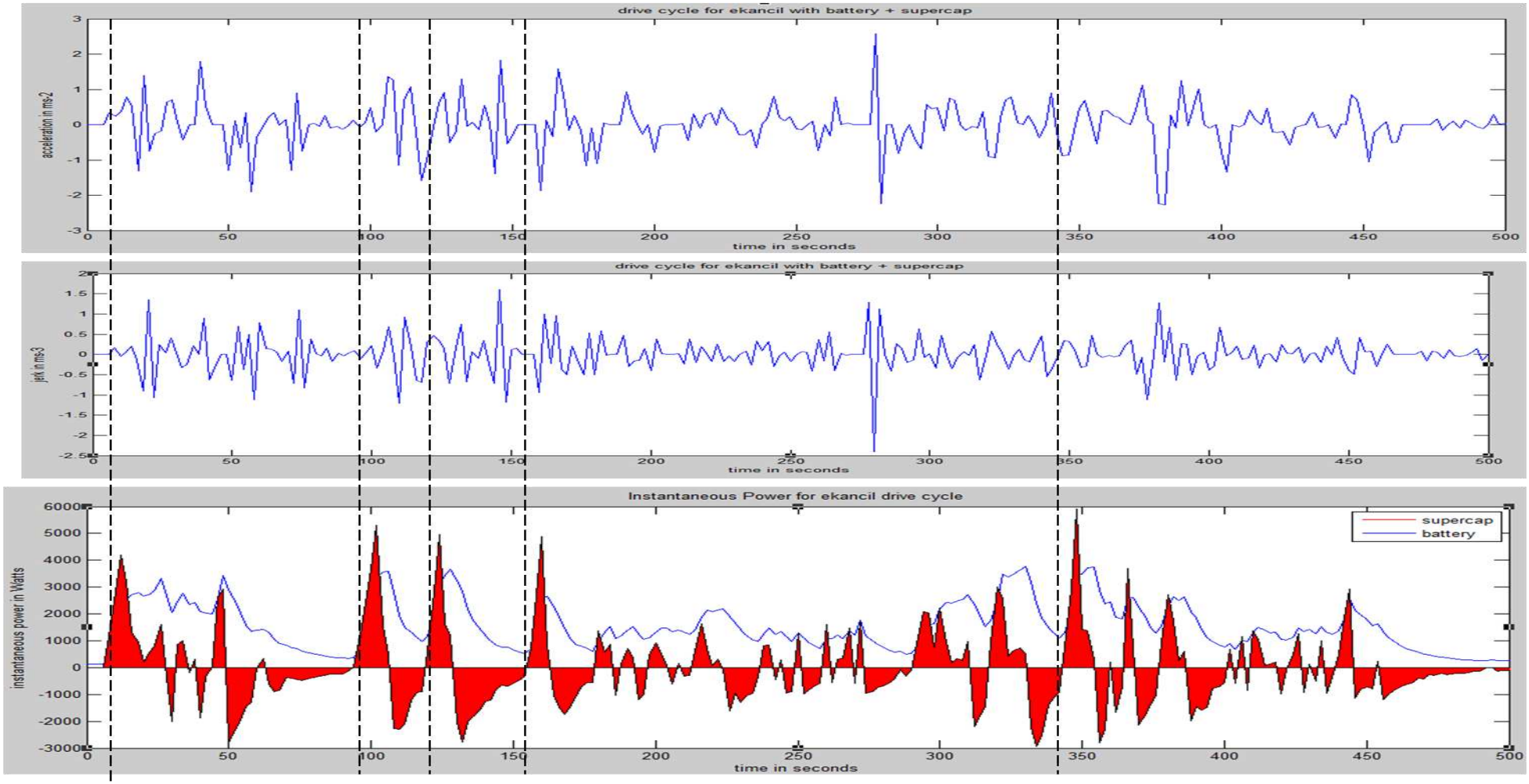

Figure 96: Comparing the Acceleration and Jerk Plots with the Instantaneous Power by Supercap & Battery.

CHAPTER 5: CONCLUSION AND FURTHER WORK

This chapter concludes this thesis; the achievements are reviewed in terms of how much of the original research objectives set out initially, was achieved. Apart from the set objectives, this research work has contributed to the knowledge bank by providing first hand insight into the inner workings of a parallel battery-supercapacitor powered electric vehicle. Rather than the normal simulation studies, a bold step was taken towards real world drive data analysis. On a positive note, several novel ideas will emerge from the joint efforts of many small but progressive research contributions such as this one.

The first objective was to create a solid platform for the university's electric vehicle team to carry out research and development for the present and future researchers. A 660 cc compact city car engine was replaced with a brushless DC motor rated at 8KW continuous and 20KW peak. The battery pack consists of eight T105 Trojan 6V-225 Ah deep cycle lead acid battery which builds up a voltage of 48V. In addition to this, a supercapacitor module (165F, 48V) is connected in parallel using high power contactors in order to investigate the increase in performance criteria such as acceleration, range, battery life etc which have been proven in various literatures via simulation studies.

The second and third objectives were to collect real world drive data from the electric vehicle test bench cum electric car which will provide real and novel data for an in-depth study and analysis of the interaction between a deep-cycle lead-acid

battery pack and a supercapacitor module in parallel powering an electric vehicle. The findings are summarized in tables 29 and the subsequent write-ups below.

UNMC Drive Cycle Parameter	Value
Total Trip Time	2085 seconds
Total Distance	10.50 km
Average Speed	16.00 kmh^{-1}
Maximum Speed	37.80 kmh^{-1}
% Stop/ Idling	0 – 12.5%
% 10< Speed < 20 kmh^{-1}	34.4 – 45.5%
% 20< Speed < 45 kmh^{-1}	22.4 – 39.7%
% Speed > 45 kmh^{-1}	Nil
Average Acceleration	0.37 ms^{-2}
Maximum Acceleration	1.37 ms^{-2}
Average Deceleration	0.38 ms^{-2}
Maximum Deceleration	2.01 ms^{-2}

Table 29: Characteristics of the UNMC drive cycle

The UNMC drive cycle formed the basis for testing the battery –supercapacitor powered test vehicle. All results obtained are limited to this test cycle.

Improvement in Battery Life

- Overall Peak currents delivered by the battery pack reduced from 228.1A to 111.2A; this is a 49% reduction.
- Voltage drops experienced by the battery pack reduced from 9.9V to 2.5V. With this, a relatively constant load profile is created for the battery pack which is good for its life and general health.
- In comparison with existing research work by Pay et al [31], results such as a 40% reduction in battery pack current and 30% improvement in dc bus voltage regulation were obtained. However, it was observed that the state of charge (SOC) of the supercapacitor dropped considerably after an acceleration.

Improvement in System Average and Peak Power Capabilities

- Average power demands are handled capably by the dense battery pack (1.8 KW up to 5KW) while peak power caused by acceleration of the vehicle is diverted to the power dense supercapacitor (9.5KW up to 12.5KW).

Improvement in Acceleration

- An Increase in acceleration was recorded with an average acceleration from 0.37 ms^{-2} to 0.44ms^{-2} (an 18.9% increase). The maximum acceleration increased from 1.37 ms^{-2} to 2.78 ms^{-2} (a 102.9% increase).
- Results from Shin, Donghwa, et al [33] show that an improvement in acceleration was achieved as a result of the supercapacitors; 16.1% higher for 0-40 km/h acceleration, 31.3% for 0-60km/h and 38.5% for 0-80km/h. In

terms of range, a 10.76% improvement was recorded on a fast track and a 16.67% improvement on a slow track. Fast track in this context refers to highway speeds with longer periods of acceleration with little or no stops (i.e. supercapacitor has little or no chance of recharging via regenerative braking). Slow track refers to city speeds; short bursts of acceleration as well as braking (i.e. the supercapacitor is constantly being topped off).

Improvement in Range per Charge

- With the limitations of driving style and traffic condition, the increase in average range per charge recorded was from 28.2km to 39.8km; this is a 41% increase.
- ATT R&D Co. and Ness Capacitor Co. Ltd [34] reported a 15.4% increase in range per charge.

Results of UNMC drive cycle analysis

- 52 microtrips were obtained from the unmc cycle and 14 parameters were calculated including the acceleration and jerk ratios which enabled us to identify microtrips with aggressive driving features. These microtrips were analysed to estimate the amount of energy contributed by the supercapacitor module towards the load demand. By numerical integration methods, an average of 23.6% utilization was arrived at.

As a final conclusion, this research work shows that electric vehicle load profiles are haphazard and meeting this load demand is very crucial to the vehicles performance as perceived by the driver. As seen from figure 96, being able to

respond to acceleration demands will affect the performance of the vehicle. Power electronics in terms of switching circuits are able to arbitrate power between battery and supercapacitor but the response time is very important. Complex control schemes, no matter how efficient or optimal they are, as long as they are unable to fulfil this requirement will be eventually inadequate for electric vehicles.

FURTHER WORK

This research work formed the genesis of an entire research group dedicated to the research and development of supercapacitors in electric vehicles. This thesis produced novel real world experimental data that clearly shows the interaction between a battery pack and supercapacitor module while powering a pure electric vehicle. This hands-on approach was taken to create a strong background and generate interest for future researchers

Given that this report contains a thorough literature survey on intelligent energy management techniques, future work would be to capitalize on the novel data produced in this work. Plans to develop an energy management system that exploits the predicted power by the drive cycle analysis are in order. For example, we can enhance the accuracy of the acceleration prediction by sensing the driver's motion on the acceleration pedal. Besides, we may employ more accurate power requirement models. Since these models are complex, it would be interesting to investigate how to adapt them for real-time prediction.

REFERENCES

[1] Pistoia, Gianfranco. "*Battery operated devices and systems: From portable electronics to industrial products*". Elsevier Science Limited, 2009.

[2] John Larminie John Lowry., "*Electric Vehicle Technology Explained*" John Wiley and Sons Ltd, 2003.

[3] Brant, Bob. Build your own electric vehicle. TAB books, 1994.

[4] Beaton, Stuart P., Gary A. Bishop, Yi Zhang, Lowell L. Ashbaugh, Douglas R. Lawson, and Donald H. Stedman. "On-road vehicle emissions: regulations, costs, and benefits." Science 268, no. 5213 (1995): 991-993.

[5] Rogelio A. Sullivan, "The Technical Background of Hybrid Electric Vehicles", US Department of Energy (DoE), Office of Transportation , July 1999. URL: HTTP://WWW.OTT.DOE.GOV/OAAT/HEV.HTML

[6] Chiasson, John, and Baskar Vairamohan. "Estimating the state of charge of a battery." Control Systems Technology, IEEE Transactions on 13.3 (2005): 465-470.

[7] Coleman, Martin, William Gerard Hurley, and Chin Kwan Lee. "An improved battery characterization method using a two-pulse load test." Energy Conversion, IEEE Transactions on 23.2 (2008): 708-713.

[8] Khaligh, Alireza, and Zhihao Li. "Battery, ultracapacitor, fuel cell, and hybrid energy storage systems for electric, hybrid electric, fuel cell, and plug-in hybrid electric vehicles: State of the art." Vehicular Technology, IEEE Transactions on 59.6 (2010): 2806-2814

[9] Spotnitz, R. "Simulation of capacity fade in lithium-ion batteries." Journal of Power Sources 113.1 (2003): 72-80.

[10] Buchmann, Isidor. "Will Lithium-Ion batteries power the new millennium?" Cadex Electronics Inc., Richmond, BC, Canada (2001).

[11] "Learn about batteries." Battery University, URL: http://batteryuniversity.com/learn/article/types of lithium ion

[12] M. S. Halper and J. C. Ellenbogen ,"Supercapacitor: A Brief Overview" , 2006 URL: http://www.mitre.org

[13] Eugenio Faggioli, Piergeorgio Rena, Veronique Danel, X Andrieu, Ronald Mallant, Hans Kahlen, Supercapacitors for the energy management of electric vehicles, Journal of Power Sources, Volume 84, Issue 2, December 1999, Pages 261-269, ISSN 0378-7753, 10.1016/S0378-7753(99)00326-2.

[14] Ngqongwa, Lundi Vincent. Electrochemical characterization of nanostructured SnO2 and TiO2 for potential application as dielectric materials in sulfonated-polyaniline-based supercapacitors. Diss. Department of Chemistry, University of the Western Cape, 2010.

[15] Miller, John M., and Richard Smith. "Ultra-capacitor assisted electric drives for transportation." In Electric Machines and Drives Conference, 2003. IEMDC'03. IEEE International, vol. 2, pp. 670-676. IEEE, 2003.

[16] Guidi, Giuseppe, Energy management systems on board of electric vehicles, based on power electronics. - , 2009. - (Doctoral Theses at NTNU ; 2009:38)

[17] Adrian Schneuwly, Bobby Maher, Juergen Auer. "*Ultracapacitors, the New Thinking in the Automotive World*". Maxwell Technologies Inc.

[18] Shah, V. A., Jivanadhar A. Joshi, Ranjan Maheshwari, and Ranjit Roy. "Review of ultracapacitor technology and its applications." In Fifteenth National Power Systems Conference (NPSC), IIT Bombay, p. 142. 2008.

[19] Kuperman, Alon, and Ilan Aharon. "Battery–ultracapacitor hybrids for pulsed current loads: A review." Renewable and Sustainable Energy Reviews 15, no. 2 (2011): 981-992.

[20] Conway, B. E. Electrochemical supercapacitors: scientific fundamentals and technological applications (POD). Kluwer Academic/plenum. New York, 1999.

[21] Young, Kwo, Caisheng Wang, and Kai Strunz. "Electric Vehicle Battery Technologies." In Electric Vehicle Integration into Modern Power Networks, pp. 15-56. Springer New York, 2013.

[23] Burke, Andrew, et al. "Battery Electric Vehicles: An Assessment of the Technology and Factors Influencing Market Readiness." Public Interest Energy Research (PIER) Program California Energy Commission (2007).

[24] Dhameja, Sandeep. Electric vehicle battery systems. Newnes, 2002.

[25] Cadar, Dorin V., Dorin M. Petreus, and Cristian A. Orian. "A method of determining a lithium-ion battery's state of charge." *Design and Technology of Electronics Packages,(SIITME) 2009 15th International Symposium for*. IEEE, 2009.

[26] Chalk, Steven G., and James F. Miller. "Key challenges and recent progress in batteries, fuel cells, and hydrogen storage for clean energy systems." Journal of Power Sources 159.1 (2006): 73-80.

[27] Fetcenko, M. A., et al. "Recent advances in NiMH battery technology." Journal of Power Sources 165.2 (2007): 544-551.

[28] Cao, Jian. Battery/ultra-capacitor hybrid energy storage system for electric, hybrid electric and plug-in hybrid electric vehicles. Illinois Institute of Technology, 2010.

[29] Dougal, Roger A., Shengyi Liu, and Ralph E. White. "Power and life extension of battery-ultracapacitor hybrids." *Components and Packaging Technologies, IEEE Transactions on* 25.1 (2002): 120-131.

[30] Colton, Shane. "A Simple Series Battery/Ultracapacitor Drive System for Light Vehicles and Educational Demonstration." *Proc. EVER'09* (2009).

[31] Pay S., and Y. Baghzouz. "Effectiveness of battery-supercapacitor combination in electric vehicles." *Power Tech Conference Proceedings, 2003 IEEE Bologna*. Vol. 3. IEEE, 2003.

[32] Shin, Donghwa, et al. "Constant-current regulator-based battery-supercapacitor hybrid architecture for high-rate pulsed load applications." *Journal of Power Sources* 205 (2012): 516-524.

[33] Dixon, Juan, et al. "Electric vehicle using a combination of ultracapacitors and ZEBRA battery." *Industrial Electronics, IEEE Transactions on* 57.3 (2010): 943-949.

[34] Kim, Mahn Shik, and Young Ho Kim. "ATT R&D's Invita, a Neighborhood Electric Vehicle with Ultracapacitors."

[35] Bentley, Paul, David A. Stone, and Nigel Schofield. "The parallel combination of a VRLA cell and supercapacitor for use as a hybrid vehicle peak power buffer."*Journal of power sources* 147.1 (2005): 288-294.

[36] Dixon, J.W.; Ortuzar, M.E.; "Ultracapacitors + DC-DC converters in regenerative braking system," *Aerospace and Electronic Systems Magazine, IEEE* , vol.17, no.8, pp. 16- 21, Aug 2002

[37] Jinrui N, Fengchun S, Qinglian *"A Study of Energy Management System of Electric Vehicles"* , Vehicle Power and Propulsion Conference, 2006. VPPC '06. IEEE.

[38] Ortuzar, M.; Moreno, J.; Dixon, J.; , "Ultracapacitor-Based Auxiliary Energy System for an Electric Vehicle: Implementation and Evaluation," *Industrial Electronics, IEEE Transactions on* , vol.54, no.4, pp.2147-2156, Aug. 2007

[39] Styler, Alexander, et al. "Active management of a heterogeneous energy store for electric vehicles." *Integrated and Sustainable Transportation System (FISTS), 2011 IEEE Forum on*. IEEE, 2011.

[40] Chan, C. C. "The state of the art of electric and hybrid vehicles." *Proceedings of the IEEE* 90.2 (2002): 247-275.

[41] Chen, Zhi Hang, M. Abul Masrur, and Yi L. Murphey. "Intelligent vehicle power management using machine learning and fuzzy logic." *Fuzzy Systems, 2008. FUZZ-IEEE 2008.(IEEE World Congress on Computational Intelligence). IEEE International Conference on*. IEEE, 2008.

[42] Murphey, Yi L., et al. "Neural learning of driving environment prediction for vehicle power management." *Neural Networks, 2008. IJCNN 2008.(IEEE World Congress on Computational Intelligence). IEEE International Joint Conference on*. IEEE, 2008.

[43] Langari, Reza, and Jong-Seob Won. "Integrated drive cycle analysis for fuzzy logic based energy management in hybrid vehicles." *Fuzzy Systems, 2003. FUZZ'03. The 12th IEEE International Conference on*. Vol. 1. IEEE, 2003.

[44] J. S. Won, "Intelligent Energy Mangament Agent for Parallel Hybrid Electric Vehicles," Texas A&M University, 2003, pp. 104.

[45] Ferreira, André Augusto, et al. "Energy management fuzzy logic supervisory for electric vehicle power supplies system." *Power Electronics, IEEE Transactions on* 23.1 (2008): 107-115.

[46] Yang, Jian, et al. "Forecast of driving load of hybrid electric vehicles by using discrete cosine transform and support vector machine." *Neural Networks, 2008. IJCNN 2008.(IEEE World Congress on Computational Intelligence). IEEE International Joint Conference on*. IEEE, 2008.

[47] Huang, Xi, Ying Tan, and Xingui He. "An Intelligent Multifeature Statistical Approach for the Discrimination of Driving Conditions of a Hybrid Electric Vehicle." *Intelligent Transportation Systems, IEEE Transactions on* 12.2 (2011): 453-465.

[48] Liaw, Bor Yann, and Matthieu Dubarry. "From driving cycle analysis to understanding battery performance in real-life electric hybrid vehicle operation."*Journal of power sources* 174.1 (2007): 76-88.

[49] Shi, Shuming, et al. "Study on the fuzzy clustering method of the microtrips for passenger car driving cycle in Changchun." *Vehicle Power and Propulsion Conference, 2009. VPPC'09. IEEE*. IEEE, 2009.

[50] Fu, Jianfu, Wenzhong Gao, and Liwei Song. "Principal component analysis based on drive cycles for hybrid electric vehicle." *Vehicle Power and Propulsion Conference, 2009. VPPC'09. IEEE*. IEEE, 2009.

[51] Lin, Chan-Chiao, Huei Peng, and J. W. Grizzle. "A stochastic control strategy for hybrid electric vehicles." *American Control Conference, 2004. Proceedings of the 2004*. Vol. 5. IEEE, 2004.

[52] Montazeri-Gh, M., A. Ahmadi, and M. Asadi. "Driving condition recognition for genetic-fuzzy HEV Control." *Genetic and Evolving Systems, 2008. GEFS 2008. 3rd International Workshop on*. IEEE, 2008.

[53] Ji-Hui, Zhuang, Xie Hui, and Yan Ying. "Remote self-learning of driving cycle for electric vehicle demonstrating area." *Vehicle Power and Propulsion Conference, 2008. VPPC'08. IEEE*. IEEE, 2008.

[54] Leon C. Rosario “Power and Energy Management of Multiple Energy Storage systems in Electric Vehicles” Cranfield University June 2007 p100.

[55] Gao, Lijun, Roger A. Dougal, and Shengyi Liu. "Power enhancement of an actively controlled battery/ultracapacitor hybrid." *Power Electronics, IEEE Transactions on* 20.1 (2005): 236-243.

[56] Carter, R., and A. Cruden. "Strategies for control of a battery-supercapacitor system in an electric vehicle." *Power Electronics, Electrical Drives, Automation and Motion, 2008. SPEEDAM 2008. International Symposium on*. IEEE, 2008.

[57] Yu, Hai, Finn Tseng, and Ryan McGee. "Driving pattern identification for EV range estimation." *Electric Vehicle Conference (IEVC), 2012 IEEE International*. IEEE, 2012.

[58] Zhang, Chen, et al. "Role of terrain preview in energy management of hybrid electric vehicles." *Vehicular Technology, IEEE Transactions on* 59.3 (2010): 1139-1147.

[59] Wang, Rui, and Srdjan M. Lukic. "Review of driving conditions prediction and driving style recognition based control algorithms for hybrid electric vehicles."*Vehicle Power and Propulsion Conference (VPPC), 2011 IEEE*. IEEE, 2011.

[60] Zhang, Chen, and A. Vahid. "Real-time optimal control of plug-in hybrid vehicles with trip preview." *American Control Conference (ACC), 2010*. IEEE, 2010.

[61] Kuhler, M. "Improved driving cycle for testing automotive exhaust emissions." (1978).

[62] Ericsson, Eva. "Independent driving pattern factors and their influence on fuel-use and exhaust emission factors." *Transportation Research Part D: Transport and Environment* 6.5 (2001): 325-345.

[63] Staackmann, Milton, Bor Yann Liaw, and David YY Yun. "Dynamic driving cycle analyses using electric vehicle time-series data." *Energy Conversion Engineering Conference, 1997. IECEC-97., Proceedings of the 32nd Intersociety*. Vol. 3. IEEE, 1997.

[64] Murphey, Yi Lu, Robert Milton, and Leonidas Kiliaris. "Driver's style classification using jerk analysis." *Computational Intelligence in Vehicles and Vehicular Systems, 2009. CIVVS'09. IEEE Workshop on*. IEEE, 2009.

[65] Carlson, T. R., and R. C. Austin. "Development of speed correction cycles."*Sierra Research, Inc., Sacramento, CA, Report SR97-04-01* (1997).

[66] Sierra Research," SCF Improvement - Cycle Development," Sierra Report No. SR2003-06-02, 2003.

[67] Alvarez Anton, J.C.; Garcia Nieto, P.J.; Blanco Viejo, C.; Vilan Vilan, J.A., "Support vector machines used to estimate the battery state-of-charge," Power Electronics, IEEE Transactions on (2013) , vol.PP, no.99, pp.1,1, 0

[68] Furey, Terrence S., et al. "Support vector machine classification and validation of cancer tissue samples using microarray expression data." *Bioinformatics*16.10 (2000): 906-914.

[69] Guo, Guodong, Stan Z. Li, and Kap Luk Chan. "Support vector machines for face recognition." *Image and Vision computing* 19.9 (2001): 631-638.

[70] Taboada, J., et al. "Creating a quality map of a slate deposit using support vector machines." *Journal of computational and applied mathematics* 204.1 (2007): 84-94.

[71] Li, Xiugang, et al. "Predicting motor vehicle crashes using support vector machine models." *Accident Analysis & Prevention* 40.4 (2008): 1611-1618.

[72] Hansen, Terry, and Chia-Jiu Wang. "Support vector based battery state of charge estimator." *Journal of Power Sources* 141.2 (2005): 351-358.

[73] Junping, Wang, Chen Quanshi, and Cao Binggang. "Support vector machine based battery model for electric vehicles." *Energy conversion and management*47.7 (2006): 858-864.

[74] Plett, Gregory L. "Extended Kalman filtering for battery management systems of LiPB-based HEV battery packs: Part 1. Background." *Journal of Power sources* 134.2 (2004): 252-261.

[75] Plett, Gregory L. "Extended Kalman filtering for battery management systems of LiPB-based HEV battery packs: Part 2. Modeling and identification." *Journal of power sources* 134.2 (2004): 262-276.

[76] Plett, Gregory L. "Extended Kalman filtering for battery management systems of LiPB-based HEV battery packs: Part 3. State and parameter estimation."*Journal of Power sources* 134.2 (2004): 277-292.

[77] Chang, Chih-Chung, and Chih-Jen Lin. "LIBSVM: a library for support vector machines." *ACM Transactions on Intelligent Systems and Technology (TIST)*2.3 (2011): 27.

[78] Huang, Xi, Ying Tan, and Xingui He. "An intelligent multifeature statistical approach for the discrimination of driving conditions of a hybrid electric vehicle."*Intelligent Transportation Systems, IEEE Transactions on* 12.2 (2011): 453-465.

[79] Marshall Brain, “How Electric Cars Work”, Howstuffworks, URL: http://auto.howstuffworks.com/electric-car2.htm

[80] Sustainability-ed, “Are Electric Cars Sustainable”, URL: http://www.sustainability-ed.org.uk/pages/example3-1.htm.

[81] Battery University, “Are Hybrid Cars Here to Stay?” URL: http://batteryuniversity.com/learn/article/are_hybrid_cars_here_to_stay.

[82] EAMEX Capacitors Japan, "Supercapacitor", URL: http://www.eamex.co.jp/capa2_e.html

[83] Don Tuite ,"Get the Lowdown on Ultracapacitors", Technology report electronic design online , November 2007. URL: http://electronicdesign.com/Articles/ArticleID/17465/17465.html

[84] Adrian Schneuwly, " Designing Powerful Electronic Solutions with Ultracapacitors", EEtimes design, March 2006. URL: http://eetimes.com/design/power-management-design/4012062/Designing-powerful-electronic-solutions-with-ultracapacitors

[85] M. Ortuzar "Design, Implementation and evaluation of an auxiliary energy system for electric vehicles, based on ultracapacitors and buck-boost converter", 2005

[99] Ghosh, A., et al. "Pattern classification of fabric defects using support vector machines." *International Journal of Clothing Science and Technology* 23.2/3 (2011): 142-151.

[100] Perodua Kancil Specifications URL: http://lordq8.tripod.com/kancil_specification.htm

[101] DataTaker DT82E Technical specifications. Available online at: http://www.datataker.com/DT82E.php

[102] CR Magnetics Split Core Hall Effect Current Transducers. Available online at: http://www.crmagnetics.com/Products/CR-541011S--P27.aspx

[103] CR Magnetics DC VoltageTransducer. Available online at: http://www.crmagnetics.com/Products/CR-53101120-P51.aspx

[104] 20 Channel EM-406A SiRF III Receiver with Antenna Technical Data Sheet. Available online at:

https://www.sparkfun.com/products/465

[105] Gauchia, Lucia, and Javier Sanz. "Dynamic Modelling and Simulation of Electrochemical Energy Systems for Electric Vehicles." *Urban Transport and Hybrid Vehicles* (2010): 127-150.

[106] Baisden, Andrew C., and Ali Emadi. "ADVISOR-based model of a battery and an ultra-capacitor energy source for hybrid electric vehicles." *Vehicular Technology, IEEE Transactions on* 53.1 (2004): 199-205.

[107] Jinrui, N., W. Zhifu, and R. Qinglian. "Simulation and Analysis of Performance of a Pure Electric Vehicle with a Super-capacitor." *Vehicle Power and Propulsion Conference, 2006. VPPC'06. IEEE*. IEEE, 2006.

[108] Gao, David Wenzhong, Chris Mi, and Ali Emadi. "Modeling and simulation of electric and hybrid vehicles." *Proceedings of the IEEE* 95.4 (2007): 729-745.

[109] Niemeier, Debbie A., Thirayoot Limanond, and Jennifer E. Morey. *Data collection for driving cycle development: evaluation of data collection protocols*. Institute of Transportation Studies, University of California at Davis, 1999.

[110] Dai, Zhen, Deb Niemeier, and Douglas Eisinger. "Driving Cycles: A New Cycle-Building Method that Better Represents Real-World Emissions." *Department of Civil and Environmental Engineering, University of California, Davis* (2008).

[111] Schematic Diagram for Electric Vacuum Brake Pump System. Available online at: http://www.zuglet.com/ev/saturn/vacuum.html

[112] Maxwell Technologies Ultracapacitor Discharge Profiles. Available online at: http://www.maxwell.com/products/ultracapacitors/downloads

[113] Linden, David, and Thomas B. Reddy. "Handbook of batteries." *New York*(2002).

[114] Trojan® T105 Deep cycle lead acid batteries, technical specifications. Available online at: http://www.trojanbatteryre.com/PDF/datasheets/T105_TrojanRE_Data_Sheets.pdf

[115] Kamble, Sanghpriya H.,Tom V. Mathew, and G.K. Sharma. " Development of real world driving cycle: Case Study of Pune, India." Transportation Research Part D: Transport and Environment 14.2 (2009): 132-140.

[116] Schwarzer, V., Ghorbani, R, "Drive Cycle Generation for Design Optimization of Electric Vehicles", *Vehicular Technology, IEEE Transactions on, vol. 62, no.1,pp.89,97*, Jan 2013.

[117] Maxwell's BMOD0165P048 ultracapacitor module, technical specifications. Available online at:

http://www.maxwell.com/products/ultracapacitors/docs/datasheet_48v_series_1009365.pdf

[118] Golden Motors International, HPM-1OkW Brushless DC Motor, Technical specicifations. Available online at: http://www.goldenmotor.com/eCar/HPM10KW%20(48V)%20Curve.pdf

[119] Golden Motors International, HPC500 Series -- Brushless Motor Controller, Technical Specifications available online at: http://www.goldenmotor.com/HPC%20Series%20Controller%20User%20Guide.pdf

[120]Holmén, Britt A., and Debbie A. Niemeier. "Characterizing the effects of driver variability on real-world vehicle emissions." Transportation Research Part D: Transport and Environment 3.2 (1998): 117-128.

[121]De Vlieger, I., D. De Keukeleere, and J. G. Kretzschmar. "Environmental effects of driving behaviour and congestion related to passenger cars." Atmospheric Environment 34.27 (2000): 4649-4655.

[122]Burke, Andrew. "Ultracapacitor technologies and application in hybrid and electric vehicles." International Journal of Energy Research 34.2 (2010): 133-151.

APPENDIX A

Software Modelling of a Small EV

```
%Initialize vehicle data
g=9.80665;
A=1.8;%m^2
Cd=0.31;
mass_v=821;%kg
tire_radius=.261;%m
f=0.015;%coefficient of rolling resistance
final_drive_ratio=4.722;
rear_transaxle_final_drive_ratio=10.10;
Eff_dt_rear=0.98;
mass_total=mass_v+80;%kg
weight_total=mass_total*g;%N
grade=0;
rho_air_20C=1.25;%kg/m^3
Eff_dt=0.91;
%1.) velocity is from 30 to 100 km/hr in 5th gear
gear_ratio=0.794;Eff_dt=0.98;gamma=0.03;
i=0;
%for V=30:100;
   % i=i+1;
   % V_(i)=V;%km/hr
   % V=V*1000/(60*60);%m/s
  %  P_aero(i)=(.5*rho_air_20C*Cd*A*V^3)/1000;%kW
  %  P_roll(i)=(f*weight_total*V)/1000;%kW
   % P_dw(i)=P_aero(i)+P_roll(i);%kW
  %  P_eng(i)=P_dw(i)/Eff_dt;%kW
  %  P_loss(i)=P_eng(i)-P_dw(i);%kW
%end
%figure(1);
%plot(V_,P_aero,'r',V_,P_roll,'b',V_,P_dw,'g',V_,P_eng,'k',V_,P_loss,'c');
%title('Power vs. Velocity');


figure(1);
plot(nyc(:,1),nyc(:,2),'b');
title('New York Drive Data vs. Time');
xlabel('Time in seconds');
ylabel('Velocity in kph');
timenyc=nyc(:,1);
kphnyc=nyc(:,2);
gamma=0.06;
```

```
for i=1:599;
    V_kph(i)=kphnyc(i);%kph
    V_mps(i)=V_kph(i)*1000/(60*60);%m/s
    P_aero(i)=(.5*rho_air_20C*Cd*A*V_mps(i)^3)/1000;%kW
    P_roll(i)=(f*weight_total*V_mps(i))/1000;%kW
    if i>1;
        a(i)=(V_mps(i)-V_mps(i-1))/1;%acceleration
        if a(i)<0;
            a(i)=a(i)*-1;
        else a(i)=a(i);
        end;
        P_accel(i)=(mass_total*(1+gamma)*V_mps(i)*a(i))/1000;%kW
        P_total(i)=P_aero(i)+P_roll(i)+P_accel(i);%kW
        P_motor(i)=P_total(i)/Eff_dt;%kW
        P_loss(i)=P_motor(i)-P_total(i);%kW
    end
end
figure(2);
plot(timenyc,P_motor,'r');
title('Total Tractive Power to be developed by electric Motor for NYC Drive cycle');
ylabel('Power in kW');
xlabel('Time in seconds');
powertotal=transpose(P_motor);
av_powertotal = mean(powertotal);
max_powertotal = max(powertotal);
```

APPENDIX B

Drive Cycle Data Collection & Processing – Routine

DataTaker logging Routine

```
PROFILE HOST_PORT FUNCTION=SERIAL
PROFILE HOST_PORT BPS=4800
PROFILE HOST_PORT PARITY=NONE
PROFILE HOST_PORT FLOW=NONE
FUNCTION1="ZERO TRIP"{24CV=0}
FUNCTION2="Delete Data"{DELDATA*}
FUNCTION3="ON"{1SSPWR(W)=1}
FUNCTION4="OFF"{1SSPWR(W)=0}
FUNCTION5="Start Logging"{69CV(W)=1}
FUNCTION6="Stop Logging"{69CV(W)=0}
42CV("Spd Lmt",W)=0.3
SATTN;

' Turn off the unnecessary GPS messages
2SERIAL("{$PSRF103,04,00,01,01}",W)
2SERIAL("{$PSRF103,00,00,01,01}",W)
2SERIAL("{$PSRF103,02,00,00,01}",W)
2SERIAL("{$PSRF103,03,00,00,01}",W)
2SERIAL("{$PSRF103,01,00,00,01}",W)
2SERIAL("{$PSRF103,05,00,00,01}",W)

DELAY(W)=1000

 2SERIAL(RS232,"$GPGGA,%*f,%*f,%*1s,%*f,%*1s,%f[30CV]",=99CV,.1,W)
 IF(43CV><1,2){11CV(W)=-11CV}
 IF(44CV><1,2){13CV(W)=-13CV}
 ' Check 30CV value if you have a Valid GPS signal read the rest of the string
 IF(30CV>1){2SERIAL(RS232,",%*f,%f[16CV],%f[15CV],%43s[1$]$GPRMC,%*f,%*1s,%*f,%*1s,
        %*f,%*1s,%f[18CV],%f[19CV]",=99CV,.1,W)}
 ' If we have a valid GPS signal clear the ATTN led
 ALARM(30CV>1){CATTN}
 ' If the GPS signal is not valid set the ATTN led ON and set the CV's to zero..
 ALARM(30CV><0,1){SATTN 16CV(W)=-1 15CV(W)=0 19CV(W)=0 18CV(W)=0}
 '10CV("GPSTime")
 '11CV("LatD~Deg",FF0) 12CV("LatM~Min",FF7)
 '13CV("LonD~Deg",FF0) 14CV("LonM~Min",FF7)
 15CV("Alt~m")
 '16CV("HErr~m",FF2)
 30CV("GPS State",FF0)
 '27CV("Head~deg")=(18CV>42CV)*17CV+(18CV<=42CV)*27CV
 18CV("spd~knots",W)
 20CV("Spd~kph",=21CV)=(18CV>42CV)*18CV*1.85199 ' Calc kph from knots
 22CV("kph~mps",=23CV)=(18CV>42CV)*21CV*1000/3600
 23CV("m",IB,+=24CV,W) ' Integrate mps and accumulate reading to 24CV
 24CV("Trip~km",.001,FF4)  ' Report 24CV in m as km
 2SERIAL(RS232,"\e",=99CV,.1,W)
```

Data Processing Routine MATLAB

```
load unmcdrivecycle3
figure(1);
plot(unmcdrivecycle3(:,1),unmcdrivecycle3(:,7),'r');
title ('Battery + Supercapacitor current over a fixed drive cycle');
hold on
plot(unmcdrivecycle3(:,1),unmcdrivecycle3(:,8),'b');
xlabel('time in seconds');
ylabel('battery current & supercap current in Amperes');
legend('supercap','battery');

hold off

figure(2);
plot(unmcdrivecycle3(:,1),unmcdrivecycle3(:,5),'r');
title ('Battery + Supercapacitor Voltage over a fixed drive cycle');
hold on
plot(unmcdrivecycle3(:,1),unmcdrivecycle3(:,6),'b');
xlabel('time in seconds');
ylabel('battery voltage & supercap voltage in volts');
legend('supercap','battery');
hold off

figure(3);

plot(unmcdrivecycle3(:,1),unmcdrivecycle3(:,3),'b');
title ('drive cycle for ekancil with battery + supercap');
xlabel('time in seconds');
ylabel('GPS speed in kmh-1');

figure(4);

plot(unmcdrivecycle3(:,1),unmcdrivecycle3(:,2),'b');
title ('drive cycle for ekancil with battery + supercap');
xlabel('time in seconds');
ylabel('GPS Altitude in meters(m)');



figure(5);

[powerdata1]=(unmcdrivecycle3(:,5)).*unmcdrivecycle3(:,7);
plot(unmcdrivecycle3(:,1),powerdata1,'r');
hold on
[powerdata2]=(unmcdrivecycle3(:,6)).*unmcdrivecycle3(:,8);
plot(unmcdrivecycle3(:,1),powerdata2,'b');
title ('Instantaneous Power for ekancil drive cycle');
xlabel('time in seconds');
ylabel('instantaneous power in Watts');
legend('supercap','battery');
hold off
 peakcurrent = max(unmcdrivecycle3(:,8));
peakpower = max(powerdata2);
minVdrop= min (unmcdrivecycle3(:,6));
peakcurrentscap = max(unmcdrivecycle3(:,7));
peakpowerscap = max(powerdata1);
averagepowerbat= mean(powerdata2);
```

```
averagepowerscap = mean(powerdata1);
minVdropscap= min (unmcdrivecycle3(:,5));
maxspeed = max(unmcdrivecycle3(:,3));
[totalpower]=[powerdata2]+[powerdata1];

figure(6);

plot(unmcdrivecycle3(:,1),totalpower,'g');
title ('Total Instantaneous Power (Battery + Supercap) for ekancil
drive cycle');
xlabel('time in seconds');
ylabel('instantaneous power in Watts');
legend('Battery + Supercap');

%time_=num_(:,1);
kph=unmcdrivecycle3(:,3);
ms1=(kph*10)/36; % kph to ms1
a(1)=0;
for i=1:length(ms1);
    %for j=1:361;
    V_ms(i)=ms1(i);
    %t(j)=time_FUDS(j);
    if i>1 %&& j>1;
        a(i)=((V_ms(i)-V_ms(i-1))/2);
    %end
    end
end
ms2=transpose(a);

a2(1)=0;
for i=1:length(ms2);
    %for j=1:361;
    V_ms2(i)=ms2(i);
    %t(j)=time_FUDS(j);
    if i>1 %&& j>1;
        a2(i)=((V_ms2(i)-V_ms2(i-1))/2);
    %end
    end
end
ms3=transpose(a2);

V_bat= unmcdrivecycle3(:,6);
for i=1:1315;

    if i>0; %&& j>1;
       V_drop(i)=V_bat(i)-V_bat(i+1);
    %end
    end
end
V_dropbat=transpose(V_drop);

positiveV_dropindex= find (V_dropbat>0);
%positiveV_drop= mean(V_dropbat(positiveV_dropindex));
positiveV_drop= (V_dropbat(positiveV_dropindex));
%positiveV_drop= mean(V_dropbat(positiveV_dropindex));

V_scap= unmcdrivecycle3(:,5);
for i=1:1315;
```

```
  V_dropcap(i)=V_scap(i)-V_scap(i+1);


end
V_dropscap=transpose(V_dropcap);

positiveV_dropscapindex= find (V_dropscap>0);
positiveV_dropscap= mean(V_dropscap(positiveV_dropscapindex));
%positiveV_dropscap= (V_dropscap(positiveV_dropscapindex));
%positiveV_drop= mean(V_dropbat(positiveV_dropindex));

figure(7);

plot(unmcdrivecycle3(:,1),ms2,'b');
title ('drive cycle for ekancil with battery + supercap');
xlabel('time in seconds');
ylabel('acceleration in ms-2');

figure(8);

plot(unmcdrivecycle3(:,1),ms3,'b');
title ('drive cycle for ekancil with battery + supercap');
xlabel('time in seconds');
ylabel('jerk in ms-3');

av_speed = mean(V_ms);
max_speed = max(V_ms);
std_speed = std(V_ms);
max_a = max(ms2);
max_decc=min(ms2);

sum_acc=0;
sum_decc=0;
acc_count=0;
decc_count=0;
for i=1:length(unmcdrivecycle3)
    if ms2(i)>0.0;
   sum_acc=sum_acc+ms2(i);
   acc_count = acc_count + 1;
    end

   if ms2(i)<0.0
   sum_decc=sum_decc+ms2(i);
   decc_count = decc_count + 1;
    end
end

mean_av_acc=sum_acc/acc_count;
mean_av_decc=sum_decc/decc_count;

idle_count=0;
for i= 1: length(unmcdrivecycle3);
    if V_ms(i)>=0 && V_ms(i)<= 0.3;
        idle_count=idle_count+1;
    end;
end;
percentidle = (idle_count/length(V_ms))*100;
```

```
% to find the percentage of time in speed interval PLS USE "FIND"
% instruction
count1=0;
count2=0;
count3=0;
count4=0;
for i= 1: length(V_ms);
    if V_ms(i)>0.3 && V_ms(i)<= 2.7778 ; % 0 - 10km/h
        count1=count1+1;
    end;
end;
 percent010=(count1/length(V_ms))*100;

 for i= 1: length(V_ms);
    if V_ms(i)>2.7778 && V_ms(i)<= 5.5556 ; % 10km/h - 20km/h
        count2=count2+1;
    end;
 end;
 percent1020=(count2/length(V_ms))*100;

  for i= 1: length(V_ms);
    if V_ms(i)>5.5556 && V_ms(i)<= 12.5 ; % 20km/h - 45 km/h
        count3=count3+1;
    end;
 end;
  percent2045=(count3/length(V_ms))*100;

for i= 1: length(V_ms);
    if V_ms(i)>12.5 ; % above 45km/h
        count4=count4+1;
    end;
 end;
  percent45=(count4/length(V_ms))*100;
```

Drive Cycle Analysis MATLAB

```
clear all
load trip3analysis

%% microtrips for the UNMC drive cycle trip 3
% microtrip 1
utrip1=trip3analysis(4:10,2);
utrip1_acc=trip3analysis(4:10,3);
utrip1_jerk=trip3analysis(4:10,4);
utrip1_triptime = length(utrip1)* 2;
av_speed_utrip1=mean(utrip1);
max_speed_utrip1=max(utrip1);
max_acc_utrip1 = max(utrip1_acc);
max_decc_utrip1=min(utrip1_acc);

utrip1_power=trip3analysis(4:10,5);
mean_power_utrip1=mean(utrip1_power);
max_power_utrip1=max(utrip1_power);

utrip1_acc_index = find(utrip1_acc > 0);
```

```
utrip1_acc_values = utrip1_acc(utrip1_acc_index); % list all the
acceleration values

utrip1_decc_index = find(utrip1_acc < 0);
utrip1_decc_values = utrip1_acc(utrip1_decc_index); % list all the
decceleration values
std_acc_utrip1 = std(utrip1_acc_values);
mean_acc_utrip1= sum(utrip1_acc_values)/length(utrip1_acc_values);
mean_decc_utrip1=sum(utrip1_decc_values)/length(utrip1_decc_values);

max_jerk_utrip1=max (utrip1_jerk);
utrip1_jerk_index = find(utrip1_jerk > 0);
utrip1_jerk_values = utrip1_acc(utrip1_jerk_index); % list all the
postive jerk values
mean_jerk_utrip1=sum(utrip1_jerk_values)/length(utrip1_jerk_values);

% to find the percentage of time in speed interval PLS USE "FIND"
% instruction
percent010_utrip1_index = find(utrip1>0 & utrip1<=10); % 0-10 km/h
percent010_utrip1_values=utrip1(percent010_utrip1_index);
percent010_utrip1 =
(length(percent010_utrip1_values)/length(utrip1))*100;

percent1020_utrip1_index = find(utrip1>10 & utrip1<=20); % 10-20
km/h
percent1020_utrip1_values=utrip1(percent1020_utrip1_index);
percent1020_utrip1 =
(length(percent1020_utrip1_values)/length(utrip1))*100;

percent2045_utrip1_index = find(utrip1>20 & utrip1<=45); % 20-45
km/h
percent2045_utrip1_values=utrip1(percent2045_utrip1_index);
percent2045_utrip1 =
(length(percent2045_utrip1_values)/length(utrip1))*100;


percentidle_utrip1_index = find(utrip1==0);
percentidle_utrip1_values = utrip1(percentidle_utrip1_index);
percentidle_utrip1=(length(percentidle_utrip1_values)/(length(utrip1
)))*100;


feature_utrip1 =
[utrip1_triptime;max_speed_utrip1;max_acc_utrip1;max_decc_utrip1;max
_jerk_utrip1;av_speed_utrip1;

mean_acc_utrip1;std_acc_utrip1;mean_decc_utrip1;mean_jerk_utrip1;per
centidle_utrip1;percent010_utrip1;percent1020_utrip1;
    percent2045_utrip1];


%% microtrip 2

utrip2=trip3analysis(10:14,2);
utrip2_acc=trip3analysis(10:14,3);
utrip2_jerk=trip3analysis(10:14,4);
utrip2_triptime = length(utrip2)* 2;
av_speed_utrip2=mean(utrip2);
max_speed_utrip2=max(utrip2);
```

```
max_acc_utrip2 = max(utrip2_acc);
max_decc_utrip2=min(utrip2_acc);

utrip2_power=trip3analysis(10:14,5);
mean_power_utrip2=mean(utrip2_power);
max_power_utrip2=max(utrip2_power);


utrip2_acc_index = find(utrip2_acc > 0);
utrip2_acc_values = utrip2_acc(utrip2_acc_index); % list all the
acceleration values

utrip2_decc_index = find(utrip2_acc < 0);
utrip2_decc_values = utrip2_acc(utrip2_decc_index); % list all the
decceleration values

std_acc_utrip2 = std(utrip2_acc_values);


mean_acc_utrip2= sum(utrip2_acc_values)/length(utrip2_acc_values);
mean_decc_utrip2=sum(utrip2_decc_values)/length(utrip2_decc_values);

max_jerk_utrip2=max (utrip2_jerk);
utrip2_jerk_index = find(utrip2_jerk > 0);
utrip2_jerk_values = utrip2_acc(utrip2_jerk_index); % list all the
postive jerk values
mean_jerk_utrip2=sum(utrip2_jerk_values)/length(utrip2_jerk_values);


% to find the percentage of time in speed interval PLS USE "FIND"
% instruction
percent010_utrip2_index = find(utrip2>0 & utrip2<=10); % 0-10 km/h
percent010_utrip2_values=utrip2(percent010_utrip2_index);
percent010_utrip2 =
(length(percent010_utrip2_values)/length(utrip2))*100;

percent1020_utrip2_index = find(utrip2>10 & utrip2<=20); % 10-20
km/h
percent1020_utrip2_values=utrip2(percent1020_utrip2_index);
percent1020_utrip2 =
(length(percent1020_utrip2_values)/length(utrip2))*100;

percent2045_utrip2_index = find(utrip2>20 & utrip2<=45); % 20-45
km/h
percent2045_utrip2_values=utrip2(percent2045_utrip2_index);
percent2045_utrip2 =
(length(percent2045_utrip2_values)/length(utrip2))*100;


percentidle_utrip2_index = find(utrip2==0);
percentidle_utrip2_values = utrip2(percentidle_utrip2_index);
percentidle_utrip2=(length(percentidle_utrip2_values)/(length(utrip2
)))*100;


feature_utrip2 =
[utrip2_triptime;max_speed_utrip2;max_acc_utrip2;max_decc_utrip2;max
_jerk_utrip2;av_speed_utrip2;
```

```
mean_acc_utrip2;std_acc_utrip2;mean_decc_utrip2;mean_jerk_utrip2;per
centidle_utrip2;percent010_utrip2;percent1020_utrip2;
    percent2045_utrip2];



.

.

.

%% microtrip52

utrip52=trip3analysis(1287:1316,2);
utrip52_acc=trip3analysis(1287:1316,3);
utrip52_jerk=trip3analysis(1287:1316,4);
utrip52_triptime = length(utrip52)* 2;
av_speed_utrip52=mean(utrip52);
max_speed_utrip52=max(utrip52);
max_acc_utrip52 = max(utrip52_acc);
max_decc_utrip52=min(utrip52_acc);

utrip52_power=trip3analysis(1287:1316,5);
mean_power_utrip52=mean(utrip52_power);
max_power_utrip52=max(utrip52_power);

utrip52_acc_index = find(utrip52_acc > 0);
utrip52_acc_values = utrip52_acc(utrip52_acc_index); % list all the
acceleration values

utrip52_decc_index = find(utrip52_acc < 0);
utrip52_decc_values = utrip52_acc(utrip52_decc_index); % list all
the decceleration values

std_acc_utrip52 = std(utrip52_acc_values);


mean_acc_utrip52=
sum(utrip52_acc_values)/length(utrip52_acc_values);
mean_decc_utrip52=sum(utrip52_decc_values)/length(utrip52_decc_value
s);

max_jerk_utrip52=max (utrip52_jerk);
utrip52_jerk_index = find(utrip52_jerk > 0);
utrip52_jerk_values = utrip52_acc(utrip52_jerk_index); % list all
the postive jerk values
mean_jerk_utrip52=sum(utrip52_jerk_values)/length(utrip52_jerk_value
s);

% to find the percentage of time in speed interval PLS USE "FIND"
% instruction
percent010_utrip52_index = find(utrip52>0 & utrip52<=10); % 0-10
km/h
percent010_utrip52_values=utrip52(percent010_utrip52_index);
percent010_utrip52 =
(length(percent010_utrip52_values)/length(utrip52))*100;
```

```
percent1020_utrip52_index = find(utrip52>10 & utrip52<=20); % 10-20
km/h
percent1020_utrip52_values=utrip52(percent1020_utrip52_index);
percent1020_utrip52 =
(length(percent1020_utrip52_values)/length(utrip52))*100;

percent2045_utrip52_index = find(utrip52>20 & utrip52<=45); % 20-45
km/h
percent2045_utrip52_values=utrip52(percent2045_utrip52_index);
percent2045_utrip52 =
(length(percent2045_utrip52_values)/length(utrip52))*100;


percentidle_utrip52_index = find(utrip52==0);
percentidle_utrip52_values = utrip52(percentidle_utrip52_index);
percentidle_utrip52=(length(percentidle_utrip52_values)/(length(utri
p52)))*100;


feature_utrip52 =
[utrip52_triptime;max_speed_utrip52;max_acc_utrip52;max_decc_utrip52
;max_jerk_utrip52;av_speed_utrip52;

mean_acc_utrip52;std_acc_utrip52;mean_decc_utrip52;mean_jerk_utrip52
;percentidle_utrip52;percent010_utrip52;percent1020_utrip52;
    percent2045_utrip52];
%%
UDDS_parameters = [feature_utrip1 feature_utrip2 feature_utrip3
feature_utrip4 feature_utrip5 feature_utrip6 feature_utrip7
feature_utrip8 feature_utrip9 feature_utrip10 feature_utrip11
feature_utrip12 feature_utrip13 feature_utrip14 feature_utrip15
feature_utrip16 feature_utrip17 feature_utrip18 feature_utrip19
feature_utrip20 feature_utrip21 feature_utrip22 feature_utrip23
feature_utrip24 feature_utrip25 feature_utrip26 feature_utrip27
feature_utrip28 feature_utrip29 feature_utrip30 feature_utrip31
feature_utrip32 feature_utrip33 feature_utrip34 feature_utrip35
feature_utrip36 feature_utrip37 feature_utrip38 feature_utrip39
feature_utrip40 feature_utrip41 feature_utrip42 feature_utrip43
feature_utrip44 feature_utrip45 feature_utrip46 feature_utrip47
feature_utrip48 feature_utrip49 feature_utrip50 feature_utrip51
feature_utrip52 ];
UDDS_parameters=transpose(UDDS_parameters);

avpower_drive_cycle =
[mean_power_utrip1;mean_power_utrip2;mean_power_utrip3;mean_power_ut
rip4;mean_power_utrip5;mean_power_utrip6;mean_power_utrip7;

mean_power_utrip8;mean_power_utrip9;mean_power_utrip10;mean_power_ut
rip11;mean_power_utrip12;mean_power_utrip13;mean_power_utrip14;mean_
power_utrip15;

mean_power_utrip16;mean_power_utrip17;mean_power_utrip18;mean_power_
utrip19;mean_power_utrip20;mean_power_utrip21;mean_power_utrip22;mea
n_power_utrip23;

mean_power_utrip24;mean_power_utrip25;mean_power_utrip26;mean_power_
utrip27;mean_power_utrip28;mean_power_utrip29;mean_power_utrip30;mea
n_power_utrip31;
```

```
mean_power_utrip32;mean_power_utrip33;mean_power_utrip34;mean_power_
utrip35;mean_power_utrip36;mean_power_utrip37;mean_power_utrip38;mea
n_power_utrip39;

mean_power_utrip40;mean_power_utrip41;mean_power_utrip42;mean_power_
utrip43;mean_power_utrip44;mean_power_utrip45;mean_power_utrip46;mea
n_power_utrip47;

mean_power_utrip48;mean_power_utrip49;mean_power_utrip50;mean_power_
utrip51;mean_power_utrip52];

maxpower_drive_cycle =
[max_power_utrip1;max_power_utrip2;max_power_utrip3;max_power_utrip4
;max_power_utrip5;max_power_utrip6;max_power_utrip7;

max_power_utrip8;max_power_utrip9;max_power_utrip10;max_power_utrip1
1;max_power_utrip12;max_power_utrip13;max_power_utrip14;max_power_ut
rip15;

max_power_utrip16;max_power_utrip17;max_power_utrip18;max_power_utri
p19;max_power_utrip20;max_power_utrip21;max_power_utrip22;max_power_
utrip23;

max_power_utrip24;max_power_utrip25;max_power_utrip26;max_power_utri
p27;max_power_utrip28;max_power_utrip29;max_power_utrip30;max_power_
utrip31;

max_power_utrip32;max_power_utrip33;max_power_utrip34;max_power_utri
p35;max_power_utrip36;max_power_utrip37;max_power_utrip38;max_power_
utrip39;

max_power_utrip40;max_power_utrip41;max_power_utrip42;max_power_utri
p43;max_power_utrip44;max_power_utrip45;max_power_utrip46;max_power_
utrip47;

max_power_utrip48;max_power_utrip49;max_power_utrip50;max_power_utri
p51;max_power_utrip52];


figure (1);
stem(UDDS_parameters(:,2),'r');
title ('Comparing drive cycle features');
hold on
plot(UDDS_parameters(:,6),'b');
xlabel('microtrip');
ylabel('drive cycle feature');
legend('Max. speed (m/s)','Average speed (m/s)');
hold off


figure (2);
stem(UDDS_parameters(:,3),'r');
title ('Comparing drive cycle features');
hold on
plot(UDDS_parameters(:,7),'b');
xlabel('microtrip');
ylabel('drive cycle feature');
legend('Max. acceleration (m/s^2)','Average acceleration (m/s^2)');
hold off
```

```
figure (3);
stem(UDDS_parameters(:,5),'r');
title ('Comparing drive cycle features');
hold on
plot(UDDS_parameters(:,10),'b');
xlabel('microtrip');
ylabel('drive cycle feature');
legend('Max. jerk (m/s^3)','Average Jerk (m/s)^3');
hold off

figure (4);
stem(maxpower_drive_cycle,'r');
title ('Comparing drive cycle features');
hold on
plot(avpower_drive_cycle,'b');
xlabel('microtrip');
ylabel('drive cycle power in W');
legend('Max Power(W)','Av. Power (W)');
hold off
```

APPENDIX C

Electric Bicycle with Supercapacitors as Peak Power Buffer

This work implements a smart boost converter to enable an electric bicycle to be powered by a battery/supercapacitor hybrid combination. A 36V, 250W front hub motor was retrofitted onto a normal geared bike powered by a 36V; 12Ah lithium ion phosphate battery pack. A 16.2V, 58F supercapacitor module was connected in parallel to the battery pack via a custom made microcontroller-based boost converter which arbitrates power between the battery and supercapacitor. The control algorithm for the boost converter was developed using a practical approach by using various sensor inputs (battery/supercapacitor current and voltage, bike speed) and comparing the robustness of control scheme. Also energy efficient components were used in designing the boost converter to ensure maximum power transfer efficiency. Based on the implemented system experimental results show an improvement in the up-hill acceleration of the bicycle as a direct result of the boost converter being responsive enough to harvest the extra current from the high power complementary supercapacitor module avoiding deep discharges from the battery. This enhanced battery life. The maximum speed remained unchanged while the improvement in range per charge was subjective to the terrain i.e. flat land; not significant improvement, hilly terrain; significant. However, recharging the supercapacitor via regenerative braking proved to be an arduous task since the boost converter was not designed to be bi-directional.

I. INTRODUCTION.

For much of the world; especially places like China, India, and Sweden etc. bicycles have been a transportation mainstay because the work place and housing areas in most of these densely populated cities are within walking or cycling distance. This reliable yet overlooked form of transportation has evolved over the years from simple utility bicycles to powerful geared mountain bikes and now electric assisted bicycles or pedelecs. Environmental concerns in terms of emissions and depleting fuel reserves has revived the electric vehicle industry and research community. China has produced 21 million of bicycles within nine years (1997-2005). In 2005 itself, China has produced 10 million of bicycles (Alan Parker[1]).

Electric assisted bicycles still retain the characteristics of a conventional bicycle with an added advantage of extra power, say when riding up a hill. This enables the elderly or not so physically fit people to still enjoy riding a bicycle up a slope.

Batteries are the weak leak at the moment for any electrically propelled vehicle including the bicycle. The lack of a single reasonably priced energy storage device that can simultaneously provide high power density and high energy density has been the main stumbling block to the acceptance of

electric propulsion as the main form of private and public transportation (Manoj *et al*[2], Schneuwly *et al*[5])Presently the only viable solution to this problem is to combine a high energy storage device such as an electrochemical battery or fuel cell with a high power device such as an Electric Double Layer Capacitor (EDLC) or ultracapacitor or more often called a supercapacitor (Ortuzar *et al*[3]). Usually, some form of dc to dc converter executing an energy management control algorithm is used to interface the battery bank and supercapacitor array to the load bus (Payman *et al*[8]). It is the aim of this project to design a smart boost converter with a heuristic based energy management algorithm which will optimize the power flow from the battery pack to the load.

As the name implies, a supercapacitor is a capacitor with capacitance greater than any other, usually in excess of up to 4000 Farad. Supercapacitors do not have a traditional dielectric material like ceramic, polymer films or aluminum oxide to separate the electrodes instead a physical barrier made of activated carbon. A double electric field which is generated when charged, acts a dielectric. The surface area of the activated carbon is large thus allowing for the absorption of large amount of ions (Dougal *et al*[4]).

Advantages of Supercapacitors

I. Cell voltage determined by the circuit application not limited by cell chemistry
II. Very high cell voltages possible
III. High power density
IV. Can withstand extreme temperatures
V. Simple charging methods
VI. Very fast charge and discharge
VII. Overcharging not possible
VIII. Long life cycle
IX. Low impedance

Disadvantages/Shortcomings

I. Linear discharge voltage characteristic prevents use in some applications
II. Power only available for very short duration (short bursts of power)
III. Low capacity
IV. Low energy density
V. Voltage balancing required when banking
VI. High self discharge rate

Despite the fact that Lithium-ion batteries are the superior most power sources as compared to other battery systems, the performance of the Li-ion battery is greatly affected when utilized under high current discharges. Lithium ion batteries have a high energy density of about 105 J/kg; however the power density is only around 100W/kg. As a result, the Li-ion battery cannot yield to high power demands. The addition of super capacitors in parallel to the battery can greatly augment the utilization of the battery especially at higher rates of discharge because of the high power density of super capacitors (~106 W/kg). So during high power demands, the supercapacitor aids in supplying

the power instantly while it gets recharged by the battery and thus the run time of the battery super capacitor hybrid is increased and higher utilization can be ensured.

Li-ion and supercapacitors are at opposite ends of the spectrum i.e. high energy density and high power density respectively. A combination of both technologies could bring about very desirable effects in terms of battery features. A Direct connection of the supercapacitor across the battery terminals does reduce transient currents in and out of the battery. However, the best way to utilize the supercapacitor bank is to be able control its energy content through a power converter (Pay & Baghzouz[5]). Usually, a static bi-directional buck-boost converter is used to interface the supercapacitor bank (connected to the boost side) with the battery pack (connected to the buck side) because batteries work at relatively constant voltage levels while capacitors voltage is directly related to its state-of-charge (Dixon & Ortuzar[6]).

A. Outline

The objective of this project is to design and build a Pulse Width Modulated (PWM) DC/DC boost converter with the following ideal specifications:

- Input Voltage: 12 - 16.2 VDC
- Output Voltage: 36 - 39 VDC
- Output Power: 200 – 300 W
- Switching Frequency: 20 – 100 kHz

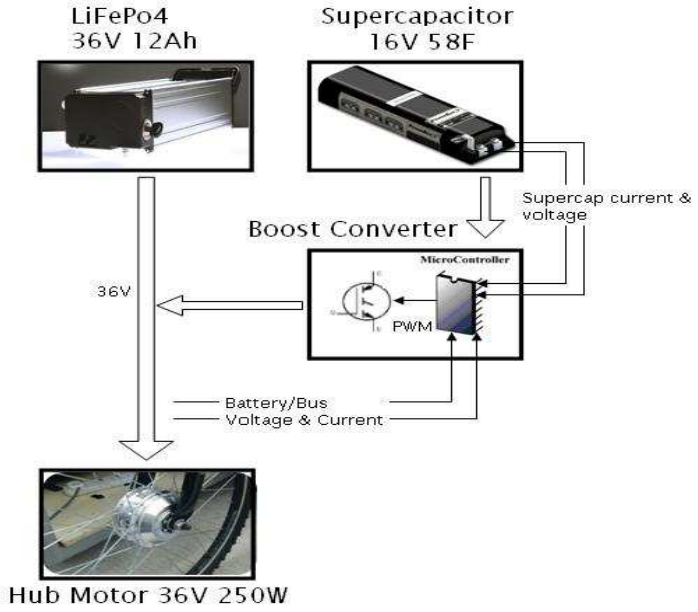

Figure 1: Overview of the proposed system

Figure 1 above shows the block diagram of the proposed system. The main power source consists of a 36V~40V, 12Ah lithium ion Phosphate (LiFePo4) battery pack with cell balancing circuitry which weighs 5.5kg. This can comfortably provide a continuous discharge current of 12A. The supercapacitor consists of a 0.5kg POWERBUSRT© 16V, 58F module to be connected in parallel with

the battery pack via a boost converter which is designed to harvest the maximum energy from it. The propulsion device consists of a state of the art front hub motor rated at 250W (Golden Motors[11]), eliminating the need for transmission and the losses associated with it.

Section 2 describes the sizing and design of the boost converter based on the specific energy requirements of the previously mentioned electric assisted bicycle. Section 3 discusses the results obtained from the implemented system using a portable data logger.

II. BOOST CONVERTER DESIGN

In order to size the boost converter appropriately, the electric bicycle was powered with the 36V 12Ah LiFePo4 batteries initially, and certain figures were collected. The track used was a mixture of flat terrain, uphills and downhills. This is shown in the table below.

TABLE I. E-bikes performance with battery

Maximum Voltage	40.69 V
Maximum Current	18.38 A
Average Voltage	39.0 V
Average Current	8.2 A
Max. Voltage Drop	3.31 V
Maximum Power	693.0 W
Average Power	315.0 W

From the table above, the maximum voltage is 40.69V. This voltage is actually equivalent to the total batteries voltage at full charge. Even though the datasheet mentions that each battery is only supplied 36V, however there is some tolerance in battery which causes each battery to go up to 40V. When the motor is running at maximum load (i.e. uphill), the maximum current drawn from the battery is 18.38A whereas when the motor is running at constant load (usually on a flat terrain) the average current is 8.2A. Thus, the supercapacitor is required to supply at least 10.18A to ensure that batteries only supplies average current.

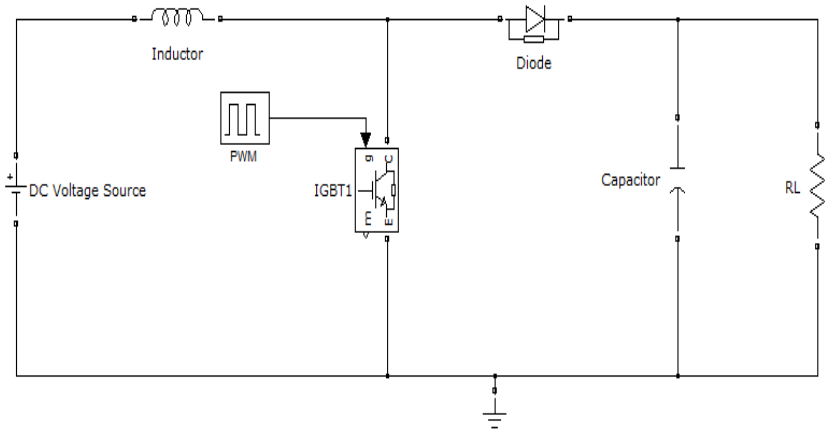

Figure 2: Conventional PWM Boost Converter

The conventional boost converter is shown in figure 2 above. It can be operated in two modes which are continuous current mode (CCM) and discontinuous current mode (DCM. This converter functions based on pulse width modulation (PWM); PWM is sent from a microcontroller/driver in order to control the IGBT to switch on or switch off (Farzanehfard & Beyragh[9]).

During on time, IGBT will be turned on by setting the PWM to high. During the on time, current from the voltage source will flow through inductor and IGBT. This results in positive voltage across the inductor, thus inductor current is linearly increases. The capacitor will discharge through the load resistance in order to provide continuous supply to the load.

During off time, current through the inductor cannot change instantaneously. It will try to oppose any drop in current by reversing its electromotive force (EMF) or polarity. Thus, the inductor will be treated as another voltage source which is in series with the input voltage. Energy stored in the inductor will add extra voltage to the input voltage. The current will flow into the capacitor to charge up the capacitor as well. In short, output voltage will be boosted with extra voltage from the inductor.

A. Supercapacitor Energy Analysis

Total Energy $E_T = \frac{1}{2}CV^2$ (1)

$E_T = \frac{1}{2} \times 58 \times 16^2 = 7.424KJ\ (2.1Wh)$

Assume the minimum voltage can drop to 10V, maximum voltage is 16V

Usable Energy; $E_u = \left(1 - \frac{V^2_{min}}{V^2_{max}}\right) E_T$ (2)

E_u = 4.524 KJ (1.26Wh)

Thus 452.4W (28.28A @ 16V) can be supplied for a period of 10seconds or 226.2W (14.14A @ 16V) for 20 seconds. This is more than sufficient for an uphill acceleration keeping in mind that the battery is able to supply an average power. However the boost converter is required to output a voltage of between 38V~40V depending on the battery pack voltage leading to a lower output current.

Assuming a 90% converter efficiency,

$$P_{output} = 0.9\ P_{input} \quad (3)$$

$$0.9 * V_{input} * \mathrm{I}_{input} = V_{output} * \mathrm{I}_{output} \quad (4)$$

I_{output} = 12.89A @ V_{input} =16V

I_{output} = 8.06A @ V_{input} =10V

B. Component Sizing

The converter must be designed such that it is able to handle the worst case scenario. Thus, input voltage used in the design calculation will be the minimum whereas the output voltage will be the maximum. The design specifications are showed as below:

$f = 100kHz$ (Arbitrarily chosen)

Duty cycle can be calculated by using the formula as follows:

$$D = 1 - \frac{V_{in}}{V_{out}} \quad (5)$$

$$D = 1 - \frac{10}{41}$$

$$D = 0.756$$

Since the output power is 500W and voltage is 39V, the resistive load can be calculated as

$$R = \frac{V^2}{P}$$

$$R = \frac{39^2}{500} = 3.042\Omega$$

Therefore, the minimum inductor value can be calculated by substitute the value as followed:

$$L_{min} = \frac{D(1-D)^2 R}{2f} \quad (6)$$

$$L_{min} = \frac{0.756 \times (1 - 0.756)^2 \times 3.042}{2 \times 100 \times 10^3}$$

$$L_{min} = 0.6846\mu H$$

The inductor must be selected such that it is able to handle input current. The converter is assumed to be 90% efficient, thus the output power will be nine-tenth of the input power.

$$I_{in} = \frac{P_{out}}{0.9V_{in}} = 14.25A$$

The selected inductor is J. Bournes and Miller 8121-RC which has 1mH inductance with maximum current of 20A.The output capacitance reduces the output ripple voltage. The filtering capacitance is selected by assuming the ripple voltage, ΔV_{out} is equaled to 10% of the output voltage.

$$C_{min} = \frac{1}{\Delta V_o} \times \frac{V_o}{R} \times DT \quad (7)$$

$$C_{min} = \frac{1}{0.05 \times 39} \times \frac{39}{3.042} \times 0.756 \times \frac{1}{100 \times 10^3}$$

$$C_{min} = 50\mu F$$

The selected output capacitance is 100µH. Capacitors with higher capacitance will actually reduce the ripple voltage, but higher capacitance will have a slower response time [6]. Table II below shows the list of other components used in this design.

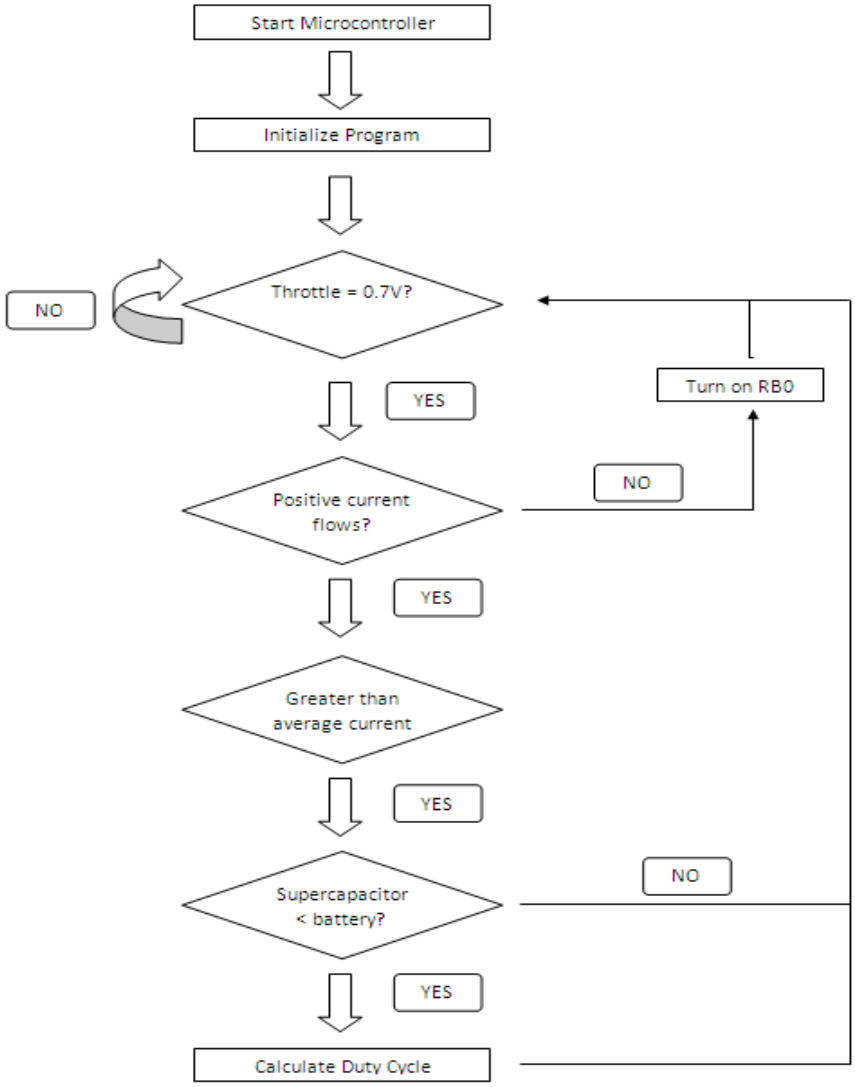

Figure 3: Control strategy for Boost Converter

TABLE II. Components for boost converter

	Component	Function
1	PIC16F877A Microcontroller	Generate PWM signals based on input sensors
2	HCPL 3120 Optocoupler	Gate driver for switching device
3	IKP15N60T IGBT (20A)	Switching device for converter
4	Vishay Schottky diode (30A)	Prevent reverse current
5	LTS-25NP LEM current sensor	Sense load current give input to MCU

C. Control Algorithm

Figure 3 above describes the simple control strategy adopted for calculating the duty cycle of the PWM pulse which is required to turn on the IGBT for the boost converter. Inputs from a Hall Effect speed sensor and current sensors are required to turn on the converter. This ensures that the E-bike is on and ready for an impending acceleration and also prevents unnecessary usage of the supercapacitor's limited energy. Voltage transducer circuits at the input side (supercapacitor) and output side (battery/converter out) feed input signals to the microcontroller. By comparing these two signals, the duty cycle can be appropriately adjusted. Figure 4 below shows the boost converter along with its control circuit (a PIC16f877a microcontroller) while figure 5 shows the complete system retrofitted onto a conventional bicycle.

Figure 4: Boost Converter with control circuit.

Figure 5: Ebike with battery supercapacitor hybrid via a boost converter.

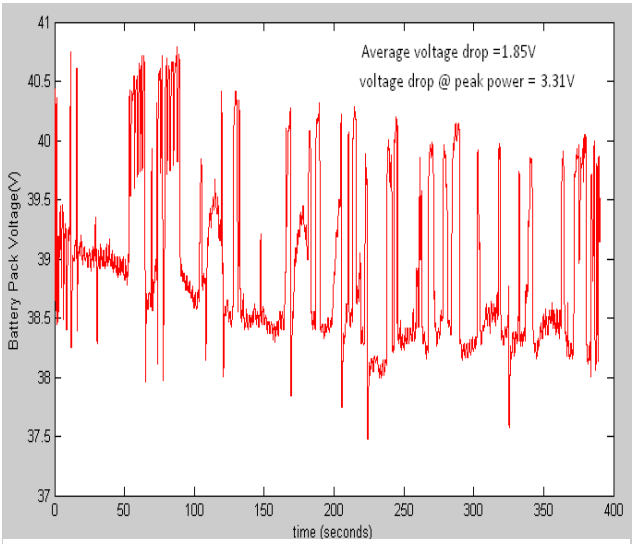

Figure 6: Battery pack voltage of E-bike with only LiFePo4 as power source

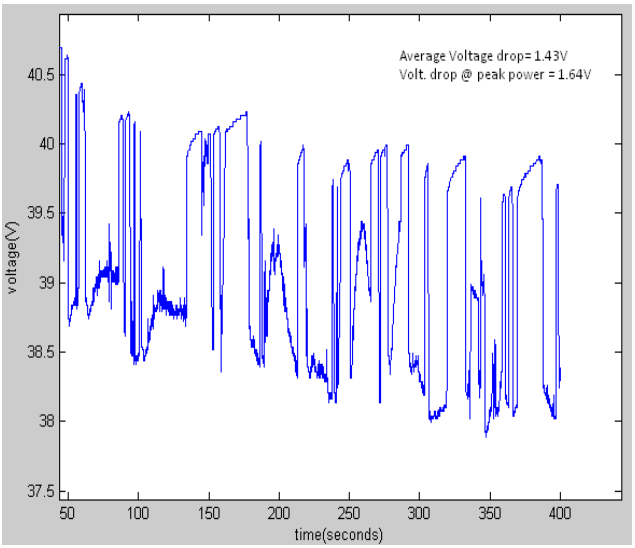

Figure 9: Battery pack voltage of E-bike with hybrid power source

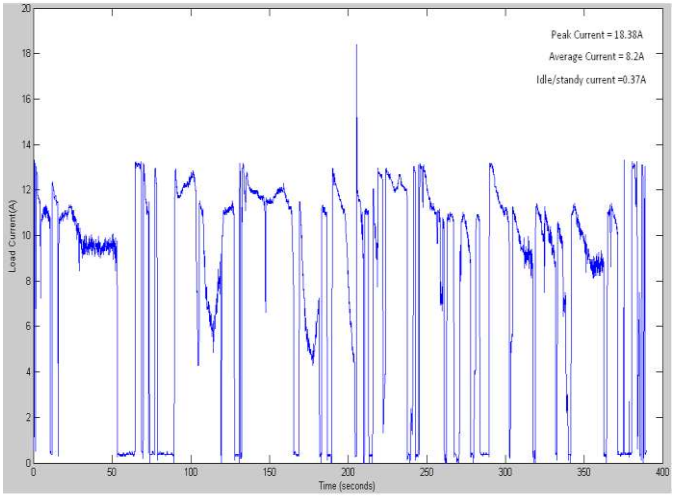

Figure 7: Current drawn from LiFePo4 only

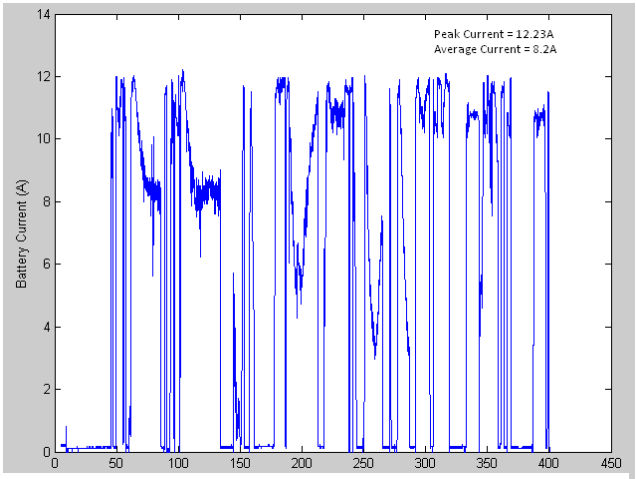

Figure 10: Current drawn from LiFePo4 battery with hybrid power source

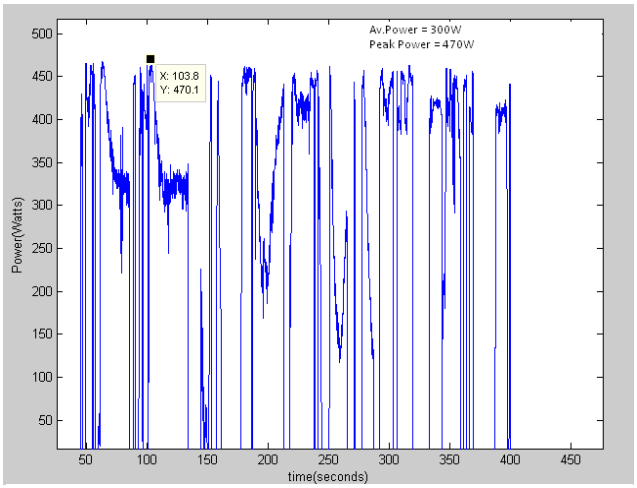

Figure 8: Power Output from LiFePo4 battery

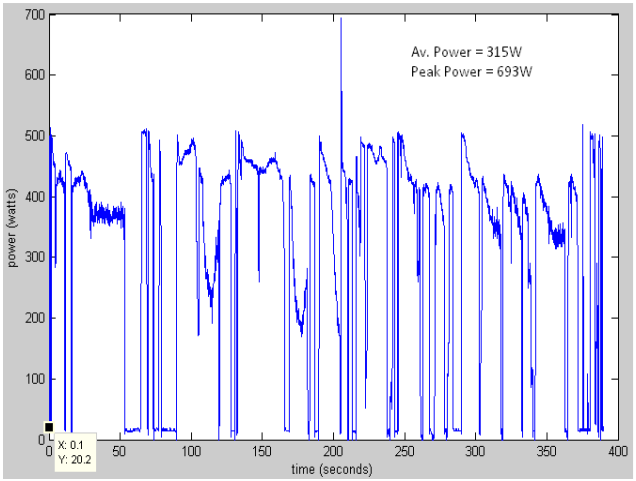

Figure 11: Power Output from LiFePo4 battery with hybrid power source

III. RESULTS AND DISCUSSION.

A portable data logging device was used to collect sensor data of bike speed, battery voltage and current, supercapacitor voltage and current. This was used to evaluate the performance of the electric assisted bicycle in terms of maximum speed, voltage drop of battery pack, peak current drawn from battery pack and up-hill acceleration. Figure 6 to figure 8 shows the battery parameters when the E-bike was powered solely by the battery pack. An average voltage drop of 1.85V was recorded while riding on flat terrain while a maximum voltage drop of 3.31V was recorded when riding uphill. A peak current of 18.38A was recorded uphill. This is potentially dangerous for the battery as it only able to handle a maximum of 15A continuous discharge. An Average Power of 315W and peak of 693W was subsequently recorded. Figure 9 to figure 11 plots the battery parameters when the E-bike was powered by hybrid battery/supercapacitor power source. A significant reduction in the maximum voltage drop from 3.31V to 1.64V occurred. This was a direct result of the supercapacitor being able to attend to the peak power requests from the load. Peak current from the battery pack reduced to 12.23A which was observed in figure 10. As a result, peak power reduced to 470W. Table III below summarizes the results.

Battery Parameter @ Peak conditions	LiFePo4 only	LiFePo4 + Supercap
Volt. Drop	3.31V	1.64V
Current	18.38A	12.23A
Power	693W	470W
Max Speed from GPS Speed sensor	28Km/h	28.8Km/h

TABLE III. Summary of Results with Battery + Supercapacitor

For every instance in time, the current drawn from the *battery-only* power source is always greater than the current drawn from the *battery + supercapacitor* power source. However, there appears to be certain discrepancies which is caused by variation in driving pattern although data collection for both instances where taken by following exactly the same route. The voltage profile of the hybrid power source is smoother with less variations than the profile of the battery only power source. Since the voltage of the supercapacitor is always tied to the battery pack (direct parallel connection), we cannot fully unravel its true potential which is its ability to charge and discharge very fast. A simple efficiency analysis shows that only 23% of the total energy of the supercapacitor was used up. The remaining 77% cannot be utilized due to the direct parallel configuration. The parallel hybrid power source has no significant effect on the maximum speed achievable over a drive cycle except that the rider felt an improvement in uphill acceleration as compared to battery alone.

This test was just part of comprehensive tests that was scheduled to be carried out in near future to optimize supercapacitor integration with an electric vehicle. Significant amount of engineering work still remains for the optimization especially the “smart” control algorithm for the

supercapacitor to be switched “on” and “off” at most appropriate driving pattern. This would enable a wider range of usage of the supercapacitor’s energy of up to 75%.

IV. CONCLUSION.

In conclusion, this work has successfully implemented a battery/supercapacitor hybrid power source for an electric assisted bicycle using state of the art hub motor technology. A boost converter was designed and implemented based on the energy requirements of the system.

Based on the implemented system experimental results show an improvement in the up-hill acceleration of the bicycle as a direct result of the boost converter being responsive enough to harvest the extra current from the high power complementary supercapacitor module avoiding deep discharges from the battery. This enhanced battery life. The maximum speed remained unchanged. The main battery pack was shielded from high discharge currents which would eventually enhance its life cycle.

ACKNOWLEDGEMENTS

The author of the work would like to thank MOSTI (Ministry of Science Technology and Innovation Grant No: 01-02-12-SF0095) Malaysia and Sahz holdings.

REFERENCES

[1] Alan. A Parker, *Electric Power-Assisted Bicycles Reduce Oil Dependence and Enhance the Mobility of the Elderly electric power assisted bicycle*. Presented at 29th Australian Transport Research Forum.

[2]Manoj Embrandiri, Dino Isa and Roselina Arelhi, 2011. *An Electric Vehicle Conversion using Batteries and Ultracapacitors: Preliminary Performance Investigation Journal of Asian Electric Vehicles*. 9(2), 1521-1527

[3] Ortuzar, M, Moreno J, Dixon, J; “Ultracapacitor-Based Auxiliary Energy System for an Electric Vehicle: Implementation and Evaluation," *Industrial Electronics, IEEE Transactions,* vol.54, no.4, pp.2147-2156, Aug. 2007

[4] R. Dougal, L. Gao, and S. Liu, “Ultracapacitors model with automatic order selection and capacity scaling for dynamic system simulation,” *Journal of Power Sources*, vol. 126, pp. 250–257, February 2004

[5]Adrian Schneuwly, Bobby Maher, Juergen Auer. “*Ultracapacitors, the New Thinking in the Automotive World*”. Maxwell Technologies Inc (2004).

[6]Pay, S.; Baghzouz, Y.; , "Effectiveness of battery-supercapacitor combination in electric vehicles," *Power Tech Conference Proceedings, 2003 IEEE Bologna* , vol.3, no., pp. 6 pp. Vol.3, 23-26 June 2003

[7]Dixon, J.W.; Ortuzar, M.E.; "Ultracapacitors + DC-DC converters in regenerative braking system," *Aerospace and Electronic Systems Magazine, IEEE* , vol.17, no.8, pp. 16- 21, Aug 2002

[8]Alireza Payman, Serge Pierfederici, Farid Meibody-Tabar, *Energy control of supercapacitor/fuel cell hybrid power source*, Energy Conversion and Management, Volume 49, Issue 6, June 2008, Pages 1637-1644, ISSN 0196-8904, 10.1016/j.enconman.2007.11.012.

[9]H.Farzanehfard and D.S Beyragh (2007), *A Bidirectional soft switched ultracapacitor interface circuit for hybrid electric vehicles*. Energy Conversion Management 49(2008) 3578-3584.

[10]Michael George and Sam Choi (2003), *Contrasting Hybrid Electric Bicycles and Electric Bicycle*. Inter-Professional Project 315 Spring 2003 p20-25.

[11]Golden motor (2008), Testing Report, Last retrieved: http://www.goldenmotor.com/hubmotors/Mini%20Front%2036V200W%20Performance.pdf on 8 March 2010.

[12]Farnell, *EPCOS - B82506W0000A007 - CHOKE, I CORE, 0.2MH, 40A*, Last retrieved:http://my.farnell.com/epcos/b82506w0000a007/choke-i-core-0-2mh-0a/dp/1644743 on 10 March 2010.

[13]Farnell, *BOURNS JW MILLER - 8121-RC - INDUCTOR, COMMON MODE, 1MH*, Last retrieved: http://my.farnell.com/bourns-jw-miller/8121-rc/inductor-common-mode-1mh/dp/1692691 on 10 March 2010.

[14]C.Blake and C.Bull, *IGBT or MOSFET: Choose Wisely*. Last Retrieved: http://www.irf.com/technical-info/whitepaper/choosewisely.pdf on 22 Sept 2009.

[15]W. A Giovino(2002),*Microcontrollers and DSPs-Will the Two World Intersects?* Last Retrieved: http://www.microcontroller.com/Embedded.asp?did=61 on 24 Sept 2009.

[16]Rüdiger Bürkel and Michel Friot (1997), *ASIC Based Close-Loop Transducers from 6A to 25A Nominal*, Last Retrieved: http://pccorot15.obspm.fr/COROT-ETC/Files/lts.pdf on 16 March 2010.

[17] Don Tuite ,"*Get the Lowdown on Ultracapacitors",* Technology report electronic design online , November 2007.

[18]Croydon Cycling Campaign (2008), *Electric-Assist Cycles*, Last retrieved: http://www.croydon-lcc.org.uk/info/electric.htm on 13 March 2010.